Volume 69A
Number 2
Mar.–Apr. 1965

Physics and Chemistry

U.S. DEPARTMENT OF COMMERCE

SECTION A

JOURNAL OF RESEARCH

NATIONAL BUREAU OF STANDARDS

Journal of Research

of the

National Bureau of Standards

A. Physics and Chemistry

Mar.–Apr. • 1965

VOLUME • 69A

NUMBER • 2

Editor: C. W. Beckett

Associate Editors: D. D. Wagman
J. M. Richardson

Publication dates:
Feb. 1, Apr. 1, June 1, Aug. 1, Oct. 1, Dec. 1, 1965

JOURNAL OF RESEARCH

The National Bureau of Standards Journal of Research reports research and development in the fields of activity shown at right. Also included from time to time are survey articles on topics closely related to the Bureau's scientific and technical program.

The Journal is published in four separate sections as follows:

A. Physics and Chemistry

Contains papers of interest primarily to scientists working in these fields. Issued six times a year. Annual subscription: domestic, $4.00; foreign, $4.75. Single copy, 70c.

B. Mathematics and Mathematical Physics

Presents studies and compilations designed mainly for the mathematician and the theoretical physicist. Issued quarterly. Annual subscription: domestic, $2.25; foreign, $2.75. Single copy, 75c.

C. Engineering and Instrumentation

Reports research and development results of interest chiefly to the engineer and the applied scientist. Issued quarterly. Annual subscription: domestic, $2.25; foreign, $2.75. Single copy, 75c.

D. Radio Science (formerly Radio Propagation)

Published in cooperation with U.S. National Committee of URSI. Presents papers in radio propagation, communications, and radio science generally. Issued monthly. Annual subscription: domestic, $9.00; foreign, $11.50. Single copy, $1.00.

The National Bureau of Standards is a principal focal point in the Federal Government for assuring maximum application of the physical and engineering sciences to the advancement of technology in industry and commerce. Its responsibilities include development and maintenance of the national standards of measurement, and the provisions of means for making measurements consistent with those standards; determination of physical constants and properties of materials; development of methods for testing materials, mechanisms, and structures, and making such tests as may be necessary, particularly for government agencies; cooperation in the establishment of standard practices for incorporation in codes and specifications; advisory service to government agencies on scientific and technical problems; invention and development of devices to serve special needs of the Government; assistance to industry, business and consumers in the development and acceptance of commercial standards and simplified trade practice recommendations; administration of programs in cooperation with United States business groups and standards organizations for the development of international standards of practice; and maintenance of a clearinghouse for the collection and dissemination of scientific, technical, and engineering information.

Institute for Basic Standards. Electricity. Metrology. Heat. Radiation Physics. Mechanics. Applied Mathematics. Atomic Physics. Physical Chemistry. Laboratory Astrophysics.* Radio Standards Laboratory: Radio Standards Physics; Radio Standards Engineering.** Office of Standard Reference Data.

Institute for Materials Research. Analytical Chemistry. Polymers. Metallurgy. Inorganic Materials. Reactor Radiations. Cryogenics.** Office of Standard Reference Materials.

Central Radio Propagation Laboratory.** Ionosphere Research and Propagation. Troposphere and Space Communications. Radio Systems. Upper Atmosphere and Space Physics.

Institute for Applied Technology. Textiles and Apparel Technology Center. Building Research. Industrial Equipment. Information Technology. Performance Test Development. Instrumentation. Transport Systems. Office of Technical Services. Office of Weights and Measures. Office of Engineering Standards. Office of Industrial Services.

*NBS Group, Joint Institute for Laboratory Astrophysics at the University of Colorado.
**Located at Boulder, Colo.

U.S. DEPARTMENT OF COMMERCE
John T. Connor Secretary

NATIONAL BUREAU OF STANDARDS
A. V. Astin, Director

Order all publications from the Superintendent of Documents
U.S. Government Printing Office, Washington, D.C., 20402

Use of funds for printing this publication approved by the Director of the Bureau of the Budget (June 19, 1961).

JOURNAL OF RESEARCH of the National Bureau of Standards—A. Physics and Chemistry
Vol. 69A, No. 2, March–April 1965

Radiolysis of $N^{15}N^{14}O$*

R. Gorden, Jr., and P. Ausloos

(December 15, 1964)

The gas-phase gamma-ray radiolysis of $N^{15}N^{14}O$ has been investigated as a function of dose, concentration, and temperature (−80 to 376 °C). Around 40 °C the ratios N_2^{30}/N_2^{29} and $N^{15}O/N^{14}O$ are 0.1 and 0.4, respectively, independent of dose and concentration. In the radiolysis of $N^{14}N^{14}O$-$N^{15}O$ mixtures it was found that the ion pair yield of N^{14} was 0.5. The ion pair yield of N_2^{29} in the radiolysis of $N^{15}N^{14}O$ increases with temperature from 2.6 at 50 °C to 21.7 at 376 °C. On the other hand, the yield of N_2^{30} is, within experimental error, not affected by a change in temperature, indicating that only the "molecular" nitrogen increases with an increase in temperature. The occurrence of dissociative electron attachment processes is consistent with the experimental observations. The yields of N_2^{29} and N_2^{30} increase when a potential difference is applied during radiolysis at the saturation plateau. The latter increase can be accounted for by an enhancement of neutral excited molecule decompositions. Addition of xenon and krypton enhances the decomposition of nitrous oxide. The results indicate that N atoms play a relatively less important role in the inert gas-induced decomposition than in the direct radiolysis.

1. Introduction

The radiolytic decomposition of nitrous oxide has been investigated on several occasions[1] using alpha-particles,[2,3,4] accelerated electrons,[5] X-rays[6,7] or gamma rays.[8,9]

At pressures around 1 atmosphere the number of N_2O molecules which undergo decomposition per ion pair is rather high (~4) and has been shown to increase as a result of (a) the effect of an applied field,[3,4,6] (b) a decrease in pressure from 200 mm to 50[6] mm and (c) an increase in temperature[1] from 18 to 220 °C.

As a result of some of these observations, it has been suggested[3,4,6] that neutral excited molecule decomposition may play an important role in the radiolysis of N_2O.

The present study was undertaken with the expectation that, by irradiating $N^{15}N^{14}O$, it might be possible to obtain a better insight of the radiolysis mechanism. Although not all of the results presented in this communication can be interpreted as yet, they are considered to be of sufficient interest to be reported, especially if one considers that N_2O has occasionally been proposed as a suitable gas-phase dosimeter.[8,9]

*This research was supported by the U.S. Atomic Energy Commission.

[1] For a review see: S. C. Lind, Radiation Chemistry of Gases (Reinhold Publishing Corp., New York, 1961), p. 243.
[2] E. Wourtsel, Le Radium **11,** 342 (1919); J. Phys. Radium **1,** 77 (1920).
[3] H. Essex and A. D. Koluban, J. Chem. Phys. **8,** 450 (1940).
[4] H. Essex and N. T. Williams, J. Chem. Phys. **16,** 1153 (1948).
[5] G. Gedye, J. Chem. Soc., 3016 (1931).
[6] B. P. Burtt and J. F. Kircher, Rad. Res. **9,** 1 (1958).
[7] G. R. A. Johnson, Proc. Chem. Soc., p. 213, June 1960.
[8] P. Harteck and S. Dondes, Nucleonics **14,** 66 (1956).
[9] R. W. Hummel and J. A. Hearne, Nature 188, 734 (1960).

2. Experimental Procedure

2.1. Materials

$N^{15}H_4N^{14}O_3$ was obtained from Isomet Corporation and had a stated purity of 95.3 percent N^{15} as labeled. Nitrous oxide was obtained by heating the ammonium nitrate until decomposition occurred. Purification was effected by thorough repeated outgassing at −195 °C followed by distillation from −130 to −195 °C.

The mass spectrum (Consolidated 21–101, 70 eV), given below,

14	6.56	31	2.59
15	5.68	32	0.07
16	4.71	44	5.42
28	0.70	45	100.
29	10.4	46	0.42
30	30.4	47	.2

indicates that the labeled nitrous oxide contained approximately 5.4 percent $N^{14}N^{14}O$ and 0.4 percent $N^{15}N^{15}O$. The cracking pattern indicates that at least 93 percent of the $N_2^{14,15}O$ consisted of $N^{15}N^{14}O$.[10]

$N_2{}^{28}O$ was obtained from Matheson Company, Incorporated and treated in exactly the same way as $N^{15}N^{14}O$.

$N^{15}O$ from Isomet contained 2.5 percent $N^{14}O$. Chemical impurities were removed by outgassing the nitric oxide at −210 °C followed by distillation from a low temperature distillation column maintained at −185 °C. $N^{14}O$ obtained from Matheson Company, Incorporated was treated in a similar fashion.

[10] This estimate is based on the ratio of mass 31 to mass 30 as an upper limit of the impurity, because mass 31 can also be produced by a decomposition of $N^{15}N^{14}O^+$. The fact that the ratio $N_2^{15,15}O/N_2^{14,15}O$ is not much higher than expected from the natural abundance of N^{15}, also suggests that labeling of the center nitrogen atom of nitrous oxide is negligible.

Labeled oxygen obtained from Isomet was as stated, 95.2 percent O_2^{18}.

Phillips research grade ethylene was degassed at −195 °C.

Krypton and Xenon were assayed reagents from Airco.

2.2. Irradiation Procedure

The geometry of the gamma-ray sources was identical to that previously described.[11] The source used in this work had an intensity of 3000 esu/cm³/sec in December of 1961.

Most radiolysis experiments were carried out in 300 cm³ Pyrex vessels, which were equipped with a break seal and were heated close to the melting point of Pyrex prior to being filled. The vessels could be heated during radiolysis by a cylindrical furnace controlled by a Variac. In one experiment, capillary tubing (3 mm i.d.) attached to a break seal was used to contain the solid nitrous oxide which was irradiated at −195 °C.

Accurate values of the ion pair yields were based on the measurement of the ion current in the saturation region. For this purpose, a cylindrical cell (500 cm³ volume) was constructed with an outer steel wall (6.65 cm i.d.) as the anode, and a centrally located inner electrode (1.62 cm o.d.) as the cathode. The two electrodes were joined through glass to metal seals and a grounded guard ring. The dead space required a 4 percent correction. Taking a value of 30 eV for W, the energy absorbed by nitrous oxide was 60×10^{17} eV M^{-1} sec^{-1} in the stainless steel vessel. Additional applied field experiments were carried out in a 200 cm³ graphite coated Pyrex cell which was similar in design to that used by Back et al.[12]

The light source for a few $Hg(^3P_1)$ sensitized experiments, which were carried out in connection with this study, was a flat-spiral, low pressure mercury arc obtained from Hanovia. A Corning 7–54 filter was used to eliminate wavelengths below 2200 Å.

2.3. Analysis

The products analyzed were nitrogen, oxygen, and nitric oxide. Nitrogen and oxygen were distilled from a trap at −210 °C by means of a Toepler pump. Nitric oxide was removed from a modified Ward still held at −185 °C. After measurement in a gas burette, they were further analyzed in a Consolidated 21–101 mass spectrometer.

No attempt was made to determine the yield of NO_2. Also, it was assumed that some portion of the NO_2 was converted to nitric oxide through reaction with mercury in the analysis system, thus contributing to the yield of the latter product.

[11] P. Ausloos and R. Gorden, Jr., J. Chem. Phys. **36,** 5 (1962).

[12] R. A. Back, T. W. Woodward, and K. A. Laughlan, Can. J. Chem. **40,** 1380 (1962).

3. Results

The results reported in tables 1, 2, and 3 have been expressed in rates per mole of nitrous oxide, rather than in ion pair yields, because the experiments were carried out in ordinary Pyrex vessels in which the saturation current could not be measured. Because all experiments were carried out at the same dose rate, approximate ion pair yields in the pure nitrous oxide experiments can be estimated by dividing the rates by the constant factor 2.01×10^{17}. This factor is based on the assumption that the ion pair yield of nitrogen is the same in the stainless steel vessel used for the dosimetry experiments as in the Pyrex vessel under otherwise identical experimental conditions. The ion pair yields (M/N) of N_2^{29} given in table 3 are only approximate calculated values based on the W-values [1] of Xe and Kr. In addition to the results given in the tables, the following information should be reported:

3.1. $Hg(^3P_1)$ Sensitized Photolysis

A few $Hg(^3P_1)$ sensitized experiments were carried out at a concentration of $N^{15}N^{14}O$ of 1.8×10^{-6} mole/cm³ from 30 to 250 °C. The isotopic distribution of the product nitrogen agrees within experimental error with what is to be expected considering the mass spectrum of the $N^{15}N^{14}O$ used in this investigation (i.e., 5.4:100:0.4 for N_2^{28}, N_2^{29}, and N_2^{30} respectively).

In these experiments, the yield of oxygen is within 5 percent one-half the total nitrogen at all temperatures. NO is a very minor product. Even at 250 °C, the yield of nitric oxide is only about 2 percent of the nitrogen. The formation of oxygen is completely quenched by 2.6 percent of ethylene.

3.2. Radiolysis—Effect of Dose

It should be noted that in the tables "N_2^{30} corr" is equal to the measured yield of N_2^{30} minus $0.004 \times N_2^{29}$. The latter term essentially represents the N_2^{30} formed by elimination from the 0.4 percent $N_2^{30}O$ present in the nitrous oxide.

At 30 °C, the ion pair yield of N_2^{28} produced in the radiolysis of $N_2^{28}O$ at 5 and 14.9 cm pressure was 3.37 and 3.21 respectively. The conversion in these experiments as well as in all of those reported in the tables was 0.1 percent or less. These ion pair yield values are in rather poor agreement with the room temperature values of 4.74 and 3.72 reported by Burtt and Kircher[6] for pressures of 5 and 20 cm respectively, but are in good correspondence with the value of 3.36 ± 0.1 reported by Harteck and Dondes[8] for an unspecified temperature. Experiments carried out with $N^{15}N^{14}O$ gave, within experimental error, the same ion pair yield for $N_2^{29} + N_2^{30} + N_2^{28}$ as is observed for N_2^{28} with $N_2^{28}O$. At 40 °C and a pressure of 5 cm in these experiments, a value of 0.10 is obtained for the ratio N_2^{30}/N_2^{29} and a value of 0.45 for the ratio $N^{15}O/N^{14}O$.

The values for these ratios are independent of conversion from 0.03 to 3 percent but show a slight

(5%) decrease with increase in pressure from 5 cm to 20 cm. After correcting for the N_2^{28} produced from the radiolysis of the 5.4 percent $N_2^{28}O$ in $N^{15}N^{14}O$, the value of the ratio N_2^{28}/N_2^{29} becomes approximately 0.04. At the low conversions used in this work, the latter value is however necessarily less accurate than the values of N_2^{30}/N_2^{29} which are not affected by the presence of traces of N_2^{28} which may be released from the wall of the reaction vessel during irradiation or introduced in the system in the course of the analytical procedure.

The analysis of NO and O_2 is, in most cases, not quantitative for reasons enumerated by Burtt and Kircher.[6] However, secondary reactions of the type mentioned by these authors should not affect the isotopic distributions.

TABLE 1. *Effect of nitric oxide and oxygen*

Nitrous Oxide mole/cm³×10⁶	Additive percent	Time minutes	Rates, molecules M⁻¹sec⁻¹×10⁻¹⁷				N_2^{30}corr/N_2^{29}
			N_2^{28}	N_2^{29}	N_2^{30}	$N^{14}O$	
$N^{14}N^{14}O$	$N^{15}O$						
2.71		60	5.85			1.26	
2.68	0.25	6	6.13	0.92	0.232	4.42	
2.70	0.25	15	5.58	0.80	0.296	2.99	
2.67	5.7	60	4.9	1.06	0.207		
$N^{15}N^{14}O$	$N^{14}O$						
2.73		15	0.5	5.35	0.56		0.100
2.74	1.6	15	0.72	5.2	0.46		0.085
2.70	7.9	60	1.0	5.1	0.35		0.065
2.75	26.0	60	1.3	5.15	0.305		0.055
$N^{15}N^{14}O$	O_2^{18}						
2.67	4.0	60	0.7	4.99	0.603		0.117

TABLE 2. *Effect of temperature* *

T °C	Rates, molecules M⁻¹sec⁻¹×10⁻¹⁷						N_2^{30}corr/N_2^{29}	$N^{15}O/N^{14}O$
	N_2^{28}	N_2^{29}	N_2^{30}	O_2	$N^{14}O$	$N^{15}O$		
−195 (solid)	0.6	9.72	0.148	2.6	0.53	0.34	0.011	0.64
−80		4.94	.482	.56	.81	.33	.094	.41
40	.5	5.35	.56	.67	1.11	.51	.10	.46
83	1.15	5.9	.64	<.01	2.2	1.2	.105	.54
150	1.61	13.6	.92		9.36	6.15	.064	.66
250	3.17	26.7	1.03		24.0	19.0	.034	.79
310	3.71	34.5	1.00		31.0	26.1	.025	.84
376	5.36	43.7	1.11		39.3	33.4	.021	.85
50[a]		4.45	0.477				.103	
150[a]		6.38	.582				.087	.54
275[a]		14.7	.60				.037	
277[b]		11.9	.457		3.91	2.65	.034	
165[c]		3.73	.223	.219			.056	

* The concentration of $N^{15}N^{14}O$ in all gas-phase experiments was 2.7×10^{-6} mole/cm³.
[a] 2.3 percent ethylene was added.
[b] 11.4 percent ethylene was added.
[c] 40 percent I_2 added.

TABLE 3. *Effect of inert gases*

Inert/$N^{15}N^{14}O$	$N^{15}N^{14}O$ mole/cm³×10⁶	T°C	Rates, molecules M⁻¹ sec⁻¹×10⁻¹⁷						N_2^{30} corr/N^{29}
			N_2^{28}	N_2^{29}	N_2^{30}	O_2	$N^{14}O$	$N^{15}O$	
Xenon/$N^{15}N^{14}O$:									
4.13	1.08	50	5.18	35.2 (2.4)	2.57	11.9	4.2	1.64	0.069
4.18	1.05	200	15.5	84.4 (5.65)	4.44	<1.0	66.3	47.8	.049
4.02[a]	1.08	50	7.58	27.0 (1.9)	0.656	<1.0			.020
4.05[b]	1.07	50	5.3	26.5 (1.85)	0.688	<1.0			.022
9.7	1.07	50	10.8	79.4 (2.45)	4.61	22.3			.054
Krypton/$N^{15}N^{14}O$:									
5.66	1.13	50	4.35	36.0 (2.65)	2.73	4.38			.072
12.3	1.07	50	8.3	66.6 (2.4)	4.84	11.2			.069

Values given in parentheses are M/N values.
[a] 2.0 percent $N^{14}O$ added.
[b] 6.9 percent $N^{14}O$ added.

3.3. Effect of Nitric Oxide and Oxygen

In table 1, it is seen that N_2^{29} is an important product in the radiolysis of $N^{15}O$—$N^{14}N^{14}O$ mixtures. An increase in the added percentage of $N^{15}O$ from 0.25 to 5.7 raises the yield of N_2^{29} only slightly. Addition of 0.25 percent $N^{15}O$ to $N^{14}N^{14}O$ also results in appreciable increase of the measured product, $N^{14}O$. This can be ascribed to the fact that, under these conditions, oxygen will mainly react with the added $N^{15}O$ to produce $N^{15}O_2$, instead of reacting with the product $N^{14}O$ which is present at a relatively smaller concentration. The decrease of $N^{14}O$ with increase in conversion (table 1) can thus be attributed to the increased probability for oxygen to react with $N^{14}O$. It can be noticed that N_2^{30} is a minor product in all $N_2^{14}O$—$N^{15}O$ experiments.

Addition of O_2^{18} to $N^{15}N^{14}O$ did not appreciably affect the rate of formation of N_2^{29} and N_2^{30}, but did lead to the production of appreciable yields of $N^{14}O^{18}$ and $N^{15}O^{18}$. A value of 0.44 was obtained for the ratio $(N^{15}O^{16}+N^{15}O^{18})/(N^{14}O^{16}+N^{14}O^{18})$ which is comparable to the values for the ratio $N^{15}O/N^{14}O$ obtained in the radiolysis of $N^{15}N^{14}O$. These observations indicate that oxygen reacts with nitric oxide to form NO_2 of which a certain fraction is reconverted to NO prior to or during analysis. The latter reaction does apparently not affect the ratio $N^{15}O/N^{14}O$.

3.4. Effect of Temperature

Table 2 and figure 1 are mainly concerned with the effect of temperature at constant concentration of $N^{15}N^{14}O$. One solid phase experiment, carried out at −195 °C, has been included in the table. The most striking features of the solid phase radiolysis are (a) the low relative yield of N_2^{30} and (b) the high measured yield of O_2.

In the gas phase at temperatures from −80° to 376°, there is a marked increase of N_2^{29}, $N^{14}O$, and $N^{15}O$, as well as of the product ratio $N^{15}O/N^{14}O$. On the other hand, the ratio N_2^{30}/N_2^{29} goes through a maximum and the yield of N_2^{30} increases only very slightly especially at the higher temperatures. It can be seen that the effect of temperature is much less pronounced when 2.3 percent C_2H_4 has been added to $N^{15}N^{14}O$. A further increase in the percentage of ethylene from 2.3 to 11.4 has only a minor effect on the product yields. The addition of iodine quenches the formation of nitrogen.

Blank experiments, carried out up to 400 °C, under identical conditions to those in the experiments listed in table 2, except for the actual irradiation, did not show any detectable products.

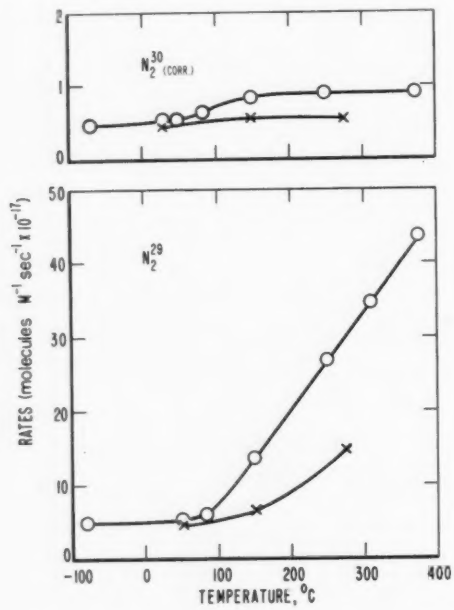

FIGURE 1. *Effect of temperature on the γ-radiolysis of* $N^{15}N^{14}O$.
×, 2.3% C_2H_4 added.

3.5. Effect of Inert Gases

Several $N^{15}N^{14}O$—Xe mixtures were irradiated and the results are given in table 3. Ion pair yields of N_2^{29} are given in parentheses. It can be noted that in the inert gas sensitized radiolysis, oxygen is a more important product than in the direct radiolysis, although the analytical procedure was the same in both cases. A rise in temperature from 50 to 200 °C shows qualitatively the same enhancing effect on the product yields as in the direct radiolysis.

3.6. Effect of Applied Field

In figure 2, the ion current and the ion pair yields

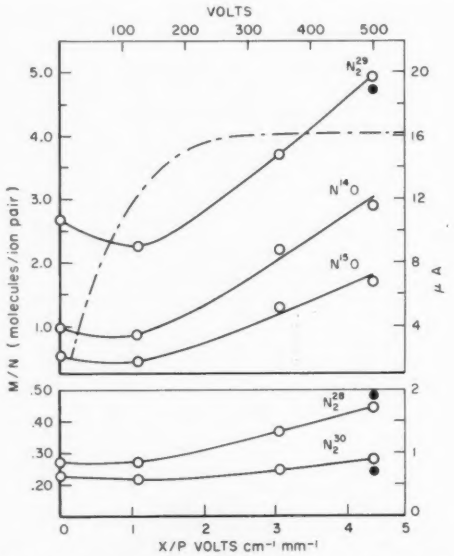

FIGURE 2. *Effect of electric fields on the γ-radiolysis of* $N^{15}N^{14}O$.
●, 2.5% C_2H_4 added. ——— ion current in μA.

of the products formed when an electrical field is applied during the radiolysis are given. These experiments were carried out in a graphite coated cell. It may be noted that in this reaction vessel, even in the absence of an applied field, the yields of $N^{15}O$ and $N^{14}O$ were larger than in an ordinary Pyrex vessel (table 2). Also, oxygen could not be detected as a product. It may thus be surmised that oxygen disappears on the wall of the reaction vessel. The addition of 2.5 percent ethylene to nitrous oxide at the highest field strength reduced the yield of N_2^{29} by only 4 percent.

4. Discussion

From the cracking pattern of $N^{15}N^{14}O$, it can be deduced that, at 70 eV, only about 35 percent of the parent ions decompose. The major modes of fragmentation of the positive parent ion at 70 eV are as follows:

$$N^{15}N^{14}O^+ \rightarrow N^{14}O^+ + N^{15} \quad 50.4\% \quad (1)$$

$$\rightarrow N^{15}O^+ + N^{14} \quad 4.3\% \quad (2)$$

$$\rightarrow O^+ + N^{15}N^{14} \quad 7.8\% \quad (3)$$

$$\rightarrow N^{15+} + N^{14}O \quad 9.4\% \quad (4)$$

$$\rightarrow N^{14+} + N^{15}O \quad 10.9\% \quad (5)$$

$$\rightarrow N^{15}N^{14+} + O \quad 17.2\% \quad (6)$$

Besides the formation of the positive ions dissociative electron attachment has to be considered[13, 14] as well. In the case of $N^{15}N^{14}O$, the latter process can be represented thus:

$$N^{15}N^{14}O + e^- \rightarrow N^{15}N^{14} + O^-. \quad (7)$$

In addition to the production of ions in the initial events the formation and decomposition of neutral excited molecules may also be of importance. It is obvious that on the basis of data reported in this paper, a detailed discussion of the different reaction mechanisms is unwarranted. An attempt will, however, be made to account for some of the processes which lead to the formation of N atoms and N_2 molecules.

4.1. Evaluation of G(N)

Although the results provide a rather accurate estimate of the relative yield of N_2^{30} produced in the radiolysis of $N^{15}N^{14}O$, one cannot immediately deduce a value of $G(N^{15})$. It is indeed known that ground state N atoms do not readily react with nitrous oxide,[15] but will undergo a fast reaction with the product nitric oxide to form a nitrogen molecule [16]

$$N + NO \rightarrow N_2 + O. \quad (8)$$

This is supported by the results given in table 1. For instance, the relatively large yield of N_2^{29} in the radiolysis of $N^{14}N^{14}O$—$N^{15}O$ mixtures, containing only 0.25 percent $N^{15}O$, clearly demonstrates the importance of reaction 8. From these results it would follow that about 20 percent of the total nitrogen is formed by this reaction. At 40 °C this would correspond to a value of $M/N = 0.5$ in good agreement with an earlier estimate by Harteck and Dondes.[8]

If N_2^{30} in the radiolysis of $N^{15}N^{14}O$ is entirely formed by the reaction

$$N^{15} + N^{15}O \rightarrow N_2^{30} + O \quad (9)$$

it may be expected that, at short conversions, small amounts of added $N^{14}O$ should prevent the formation of N_2^{30} in the radiolysis of $N^{15}N^{14}O$ by way of reaction 10.

$$N^{15} + N^{14}O \rightarrow N_2^{29} + O. \quad (10)$$

Consequently, the fact that, in mixtures containing up to 26 percent $N^{14}O$, N_2^{30} is still an important product indicates that besides reaction 9, one or more as yet unidentified processes involving a nitrous oxide molecule must contribute to the formation of N_2^{30}. The presence of electronically excited N atoms, N^+ or N_2O^+, may have to be considered as possible participants.

If we assume that all N atoms which are produced in the radiolysis of $N^{15}N^{14}O$ react with $N^{15}O$ and $N^{14}O$ at the same rate, then a value of 0.38 can be deduced for the ion pair yield of N^{15} after correcting the yield of N_2^{30} for the residual yield of N_2^{30} observed in the $N^{15}N^{14}O$—$N^{14}O$ experiments. Because the latter value is considerably larger than the ion pair yield of 0.18 estimated from the mass spectrum pattern, it may be concluded that other processes besides 1 must contribute to the formation of N^{15} atoms. As will be shown later, decomposition of neutral excited nitrous oxide formed by electron impact or by neutralization of the parent ion may be an additional source of N^{15} atoms. Recent photochemical studies by Doering and Mahan [17] have indeed shown that the process

$$N^{15}N^{14}O^* \rightarrow N^{15} + N^{14}O \quad (11)$$

is of importance at wavelengths ranging from 1236 to 1830 Å.

[13] R. K. Curran and R. E. Fox, J. Chem. Phys. **34,** 1590 (1961).
[14] G. J. Schulz, J. Chem. Phys. **34,** 1778 (1961).
[15] G. B. Kistiakowski and G. G. Volpi, J. Chem. Phys. **27,** 1141 (1957).
[16] (a) John T. Herron, J. Research NBS **65A,** 411 (1961). (b) R. A. Back and J. Y. Mui, J. Phys. Chem. **66,** 1362 (1962).
[17a] J. P. Doering and B. H. Mahan, J. Chem. Phys. **34,** 1617 (1961).
[17b] J. P. Doering and B. H. Mahan, Ibid **36,** 1682 (1962).

4.2. Formation of "Molecular" Nitrogen

N_2^{29} can be eliminated as a molecule from $N^{15}N^{14}O$ in several different ways. Besides initial events such as neutral excited molecule decompositions [17] or dissociative electron attachment,[13, 14] secondary reactions such as [18, 6]

$$N_2O+O(^1S)\rightarrow O_2+N_2 \quad (12)$$

$$N_2O+O^-\rightarrow O_2^-+N_2 \quad (13)$$

may also lead to the formation of this product.

The effect of temperature provides us with probably the most interesting information about at least one mode of formation of "molecular" nitrogen. It should first be noted that the observed increase in the yield of nitrogen from −80 to 376 °C (tables 2, 3, fig. 1) which cannot be due to the pyrolysis of nitrous oxide under our experimental conditions up to 400 °C (see Results) can also not be explained by an increase in neutral excited molecule decomposition for the following reasons:

(1) There is, within experimental error, no increase in the yield of "N_2^{29} corr" from 150 to 376 °C[19] indicating the non-enhancement of process 11 which, as shown recently [17] should occur when highly excited nitrous oxide molecules decompose independent of the degree of excitation.

(2) Lower excited nitrous oxide molecules such as those produced in the $Hg(^3P_1)$ sensitized decomposition do not eliminate an N atom but do produce an O atom in the ^3P or ^1D state which does not react any further with nitrous oxide even up to 250 °C (see Results). The results of table 2, however, show that the yield of nitric oxide increases as fast as that of N_2^{29} indicating that, if a neutral O atom is produced at high temperatures, it does react readily with nitrous oxide and so cannot be in the ^3P or ^1D state.

By the process of elimination we suggest the occurrence of the negative ion reactions proposed before by other investigators [3, 4, 6]

$$N^{15}N^{14}O+e^-\rightarrow N_2^{29}+O^- \quad (14)$$

$$O^-+N^{15}N^{14}O\rightarrow \begin{cases} N^{14}O+N^{15}O^- & (15)\\ N^{15}O+N^{14}O^- & (16)\\ N_2^{29}+O_2^- & (17)\end{cases}$$

which, at elevated temperatures, must be followed by a reaction which regenerates O^- in order to account for the temperature effect. Processes such as 18 and 19 may be considered

$$NO^-+N_2O\rightarrow NO+N_2+O^- \quad (18)$$

$$O_2^-+N_2O\rightarrow O_2+N_2+O^-. \quad (19)$$

Reaction 19 must be of less importance than reaction 18 because at the highest temperature the material balance N_2/NO approaches the value 0.5, indicating that O_2 can only be formed in small yields. The following observations favor the proposed negative ion chain reaction:

(1) An electron trap such as iodine effectively reduces the yield of N_2^{29} to a value which is lower than that obtained at −80 °C.

(2) As may be expected from the above mechanism, the effect of temperature is not related to the manner by which the secondary electrons are produced. This is demonstrated by the fact that an increase in temperature in the xenon-induced decomposition of $N^{15}N^{14}O$ affects the product yields in very much the same way as in the direct radiolysis although there are considerable differences in the initial radiolytic processes occurring in the two systems at 40 °C.

(3) Small amounts of ethylene suppress the yield of N_2^{29}. Such an effect would not be expected to occur if neutral excited molecules are involved. This has been corroborated by a few experiments carried out in our laboratory at 1236 Å, and by the negligible effect of ethylene in the applied field experiments (see Results). Ethylene may, however, be expected to intercept O^- or NO^-, thus reducing the yield of N_2^{29}.

(4) At the highest temperatures, $N^{15}O$ becomes equal to $N^{14}O$.

In view of the foregoing, it may be concluded that nitrous oxide can only be recommended as a dosimeter provided the temperature is carefully controlled. The absence of a temperature effect up to 200 °C, mentioned in an earlier study,[8] is inconsistent with the present data.

In the solid phase radiolysis experiment the relatively low yield of N_2^{30} and the high yield of O_2 indicates that the dissociation of $N^{15}N^{14}O$ into N_2^{29} and $O(^3P)$ or $O(^1D)$ occurs with a relatively higher probability than in the gas phase.

4.3. Effect of Applied Field

The effects of applied field on the product yields from $N^{15}N^{14}O$ are very similar (fig. 2) to those reported by Burtt and Kircher [6] for $N_2^{28}O$.

As previously suggested,[6] ion recombination can account for the initial decrease in the yields of nitrogen and nitric oxide with increasing X/P (field strength/unit pressure in mm). Woodward and Back [20] came to a similar conclusion regarding the decrease in the yield of hydrogen from hycrocarbons irradiated in the presence of increasing electric field.

As the field strength is increased in the region of current saturation there is a pronounced increase in the yield of nitric oxide, N_2^{29}, and to a lesser degree N_2^{30} without an accompanying increase in the ion pair production. The negligible effect of ethylene (see Results) indicates that the increase of N_2^{29} cannot be accounted for by the same negative ion mechanism as has been proposed to account for the effect of temperature. Excitation of $N^{15}N^{14}O$ by the accelerated electrons followed by a reaction mechanism analogous to that observed in the vacuum

[19] M. Zelikoff and L. M. Aschenbrand, J. Chem. Phys. **22**, 1680 (1959).
[19] The slight increase in "N_2^{30} corr" from 150 to 376 °C can be entirely accounted for by the increase of the ratio $N^{15}O/N^{14}O$ which enhances the reaction of N^{15} with $N^{15}O$.

[20] T. W. Woodward and R. A. Back, Can. J. Chem. **41**, 1463 (1963).

u.v. photolysis[17] is the most likely explanation for the observed increase in ion pair yields [3, 4, 6]. A similar effect of electrical fields is found to play an important role in the decomposition of hydrocarbons.[21]

4.4. Inert Gas Induced Decomposition of Nitrous Oxide

The Xe-$N_2^{29}O$ experiments show (table 3) that energy is transferred efficiently from xenon to nitrous oxide although the appearance potential of N_2O^+ (12.63 eV)[14] is above that of the xenon ion in the $^3P_{3/2}$ state which is considered to be the major ion produced by electron impact. The M/N values of N_2^{29} are, however, somewhat lower than in the direct radiolysis.

The major differences between the product distributions in the xenon induced and direct radiolysis are: (a) the lower values of the ratio N_2^{30}/N_2^{29}, both in the presence and absence of $N^{14}O$ and (b) the higher yield of O_2. The first observation can readily be accounted for by the fact that the parent ion decomposition according to process 1 will be of less importance in the xenon induced decomposition. The higher yield of O_2 implies a low yield of NO and can tentatively be ascribed to the formation of O atoms in the low lying ^1D or ^3P levels. Very similar conclusions can be drawn from the krypton experiments except that, as may be expected in this case, the relative yield of O_2 is lower than in the xenon induced decomposition. It may be noted that the dissociative process 1 accounted for only 11 percent of the total ionization[22] in the charge transfer mass spectrum between Kr^+ and N_2O.

(Paper 69A2–330)

[21] P. Ausloos and R. Gorden, Jr., J. Chem. Phys. **41**[1278 (1964).
[22] E. Lindholm, Z. Naturforsch. **9a**, 535 (1954).

JOURNAL OF RESEARCH of the National Bureau of Standards—A, Physics and Chemistry
Vol. 69A, No. 2, March–April, 1965

Oscillator Strengths for Lines of Ni I

Charles H. Corliss

(November 10, 1964)

Relative intensities and oscillator strengths for 888 lines of Ni I between 2800 and 9900 Å from several investigations have been reduced to the absolute scale of Corliss and Bozman and critically compared. New observations of faint lines in the visible and infrared portions of the spectrum are included.

1. Introduction

Since nickel is more abundant in the solar system than any other element having a complex spectrum except iron, it is important to have a good description of the wavelengths and line strengths in the nickel spectrum. Accurate wavelengths of the Ni I lines are available in the work of Burns and Sullivan [1947, 1948]. They were able to classify most of the observed lines by use of the energy levels found earlier by Russell [1929]. Although hundreds of additional lines could be observed with modern light sources, few of them would be of practical interest in the laboratory or in astrophysics.

The situation with regard to the measurement of line strengths is not as satisfactory as with wavelengths. Numerous investigations have been published, especially for the near ultraviolet, but the various results need to be reduced to the same entity, adjusted to a uniform scale, and critically compared. By the process of intercomparing results, obvious errors can be discovered, and the defective values can be rejected or in some cases corrections can be applied. Furthermore, new measurements need to be made in regions of the spectrum not yet adequately studied. In this paper I have assembled the published data for Ni I in the manner suggested above and have added to them new measurements that I have made in the visible and infrared.

Measurements of oscillator strengths in Ni I are beset with difficulties arising from the peculiar distribution of lines in the spectrum. The circumstances can best be appreciated by examining the table of nickel lines in the NBS Tables of Spectral-Line Intensities by Meggers, Corliss, and Scribner [1961]. The strong lines arising from the low levels lie in the near ultraviolet between 2900 and 4000 Å. Then there is a gap in the spectrum, occupied by only the faintest lines. Finally there is a group of lines of moderate intensity in the region from 4400 to 8000 Å which arise from high levels. It is difficult to put the measurements from different groups onto the same scale because the observations require different techniques and there are usually no lines in common between sets of observations of the different groups.

2. Published Data

A summary of the previously published data on the strength of spectrum lines in Ni I is given in table 1. Because of the different entities reported and the different scales adopted, it is in most cases impossible to make direct comparisons of the results. The entities reported are either intensities or oscillator strengths. The intensities are usually observed at different effective temperatures and must be reduced to a common temperature if they are to be compared. Apart from a factor λ^3, the oscillator strength is proportional to the intensity from a source at an infinite temperature. I have chosen to convert all reported quantities to log gf, which is widely used in astrophysical work.

Most of the scales on which the data are reported are arbitrary and different from one another.

TABLE 1. *Previously published data on intensities and oscillator strengths in the first spectrum of nickel*

Reference	Date	Wavelength range	No. of lines	No. accepted	Method of observation	Entity reported	Temperature	Reference symbol
		Å					°K	
Ornstein and Bouma	(1930)	2419–3858	140	106	Spark emission	Intensity	6400	OBS
Ornstein and Bouma	(1930)	2798–4201	304	190	Arc emission	Intensity	4300	OBA
van Driel	(1935)	3232–3858	52	48	Arc emission	Intensity	6400	vD
King	(1948)	3012–3912	134	132	Furnace absorption	gf	1600–2700	K
Heid and Dieke	(1954)	3359–5893	478	244	Arc emission	Intensity	5000	HD
Parchevsky and Penkin	(1954)	3050–3807	47	46	Furnace hooks	f	2300–2800	PP
Allen and Asaad	(1957)	3315–3973	40	40	Arc emission	log gf	4300	AA
Mitrofanova	(1960)	3722–5155	77	----------	Arc emission	log gf	5160	M
Corliss and Bozman	(1962)	2289–8862	242	216	Arc emission	log gf	5100	CB

760–594—65——2

Parchevsky and Penkin [1954], however, have reported their f-values on King's arbitrary scale. But the time is past when it can be considered satisfactory to report oscillator strengths on arbitrary relative scales. There is enough knowledge now for most common spectra for us to adopt a reasonably accurate absolute scale for reporting relative measurements. Allen and Asaad [1957] and also Corliss and Bozman [1962] have attempted to report their measurements on absolute scales but the scales differ by a factor of two. The values of log gf are derived here on the basis of the absolute scale of Corliss and Bozman. Their scale is especially convenient for this purpose since their measurements cover the entire range of wavelengths of the published data. The accuracy of the scale is discussed in section 2.1.

To convert the data from arc sources that have been reported as intensitites (I), to oscillator strengths, I have generally compared them with I_{NBS}, the intensities reported by Meggers, Corliss, and Scribner [1961], as follows:

1. Plot log I versus log I_{NBS} for lines of about the same excitation potential.

2. If the points above a certain value of I fall below a 45° straight line, all lines with values of I above this critical value are self-absorbed and should be rejected (or corrected).

3. Plot I/I_{NBS} versus wavelength for lines of about the same excitation potential to find out if the intensity scale has been properly calibrated as a function of wavelength. Introduce a correction if there is significant variation.

4. Plot log I/I_{NBS} versus E, the upper energy level in kaysers, and determine the temperature of the light source from the equation

$$\frac{1}{T}=\frac{1}{T_{\text{NBS}}}-\frac{1}{0.625}\left(\frac{\Delta \log I/I_{\text{NBS}}}{\Delta E}\right) \qquad (1)$$

where T_{NBS} is 5100 °K, the temperature of the NBS copper arc, and the factor in parentheses is the slope of the plot.

5. Calculate a preliminary value of log gf, by assuming a Boltzmann distribution, from the equation

$$\log gf=\log I+3 \log \lambda+\frac{0.625E}{T}. \qquad (2)$$

6. Plot log gf/gf_{CB} versus E to determine the departure from a Boltzmann distribution at high levels.

7. Add the function determined in 6 to the preliminary log gf to obtain the final absolute scale.

By this process I have tried to select the most reliable parts of each set of intensity data, introduce corrections where they are obviously necessary, and derive oscillator strengths which lie as closely as possible on the absolute scale.

The data reported as oscillator strengths were compared with CB for evidence of variation with wavelength and then adjusted to the CB scale by adding the mean difference between the scales to the reported values.

2.1. Data of Corliss and Bozman [1962]

The "Experimental Transition Probabilities for Spectral Lines of Seventy Elements" by Corliss and Bozman [1962] is based on "Tables of Spectral-Line Intensities" by Meggers, Corliss, and Scribner [1961]. Corliss and Bozman have derived values of log gf on an absolute scale for 242 lines of Ni I between 2300 and 8900 Å. The intensities of the 26 lines below 2500 Å grow progressively too weak at short wavelengths because the calibration made by Meggers, Corliss, and Scribner was applicable only at longer wavelengths and, for lack of a better method, was extrapolated from 2500 to 2000 Å. These lines have therefore been omitted from the present list. The remaining values are entered in column 6 of table 2.

A test of the intensity calibration between 3000 and 4000 Å can be made by comparing CB with K. The method of total absorption used by King does not depend on a calibration of intensity versus wavelength. This does not, of course, preclude other wavelength dependent sources of error from affecting the observations. In figure 1, where we plot the ratio K/CB against wavelength, we find no systematic variation.

The accuracy of Corliss and Bozman's values of log gf is discussed at length in section 8 of the introduction to their tables. From a study of the internal consistency of the data they found that the standard deviation of an individual determination taken as a relative value of log gf within a spectrum increased from 0.13 for lines with upper levels at 15000 K to 0.17 for lines with upper levels at 50000 K. Taken as absolute values, they found that the corresponding values of standard deviation were 0.24 and 0.29. Comparisons of the relative values of K and PP with CB are shown in figures 2 and 3. Allen and Corliss [1963] compared the CB scale with a scale determined by Allen [1960] based on the f-sum rule. They found in the case of Ni I that the f-sum scale values of log gf were larger than those of the CB scale by 0.05.

2.2. Data of Allen and Asaad [1957]

Allen and Asaad at the University of London Observatory measured the intensities of 40 nickel lines between 3315 and 3974 Å. The spectrum was excited in a 3 amp d-c arc between electrodes of copper containing 0.05 percent and less of nickel, a concentration which assures freedom from self-absorption. From measurements in similar arcs of copper containing Fe, Co, Ni, Cr, and Mn, they deduced an effective arc temperature of 4300 °K, based on King's temperature scale. They reported their values of log gf on an absolute scale determined by comparing their relative scale with experimental and theoretical absolute values for seven spectra from the group that they studied. Although their absolute scale was determined in the same way as that of Corliss and Bozman, it is based on less than a third as many determinations, and is probably

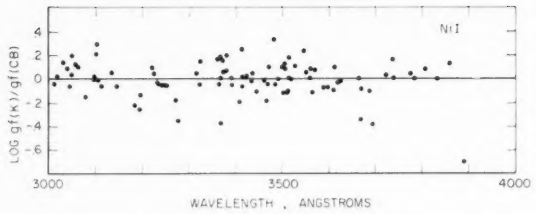

FIGURE 1. *Log ratio of* gf*-values from King (1948) to those of Corliss and Bozman (1962) as a function of wavelength.*

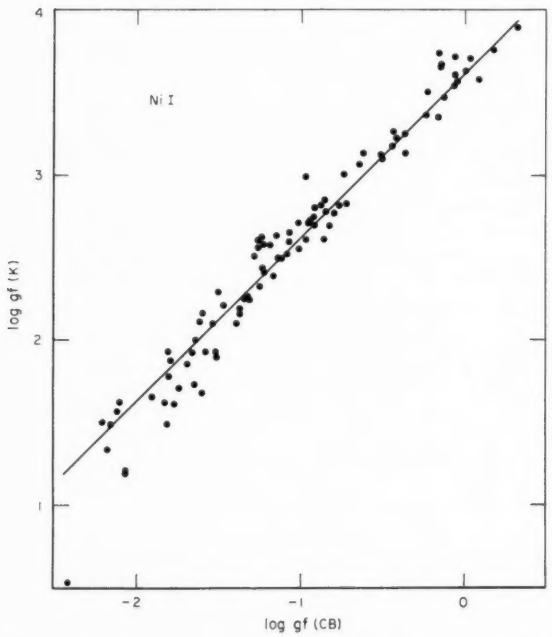

FIGURE 2. *Comparison of log* gf*-values from King (1948) with those from Corliss and Bozman (1962).*

not as accurate. Their absolute scale for Ni I has therefore been adjusted to that of CB by adding 0.30 to their log *gf*. The results are given in column 9 of table 2. A graphical comparison of AA with K is given by Goldberg, Müller, and Aller [1960, p. 104].

2.3. Data of Ornstein and Bouma [1930]

Ornstein and Bouma [1930] at Utrecht published relative intensities for about 300 lines of Ni I observed between 2800 and 4200 Å in the spectrum from a 0.45 ampere arc between nickel electrodes. About 20 percent of the values, those of intensity 40 or more on the OBA scale, are affected by self-absorption. These lines have all been measured subsequently by others and no attempt is made here to derive oscillator strengths from them. The OBA intensity scale declines progressively from 2800 to 3800 Å by about a factor of three and it has been adjusted to conform to the NBS scale. The values

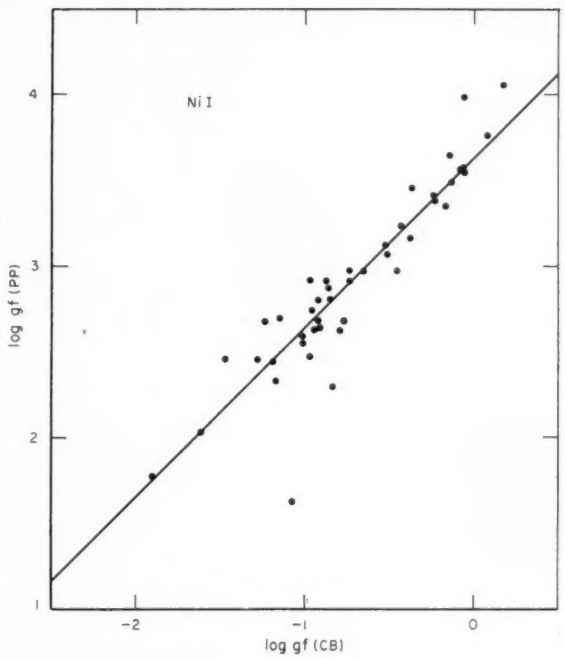

FIGURE 3. *Comparison of log* gf*-values from Parchevsky and Penkin (1954) with those from Corliss and Bozman (1962).*

of log *gf* were derived by using a temperature of 4300 °K. Earlier, King [1948] attempted to derive *gf*-values from the OBA measurements. He noticed the self-absorption, but was unable to determine an arc temperature for the remaining lines because of the small range of excitation potential (less than one volt) for lines observed in his furnace spectra and the large random errors in the OBA data. In the present work a range of more than four volts was available for the temperature determination.

Ornstein and Bouma also published intensities for about 230 lines observed in a condensed spark between nickel electrodes. About 140 of these lines are classified in Ni I. About 120 of these lines, with intensities less than 15, appear to be free from self-absorption. Their intensity scale is correctly calibrated below 3400 Å but declines gradually at longer wavelengths.

The population distribution over the energy levels of atoms in an arc departs from a Boltzmann distribution at high levels in a particular way which is illustrated in figure 5 of the introduction to Corliss and Bozman. Since that normalization curve is not likely to apply to sparks, it did not seem appropriate to determine the spark temperature by comparison of the spark intensities with the NBS arc intensities, the method outlined earlier in this section for determination of arc temperatures. Instead a plot of $\log I\lambda^3/gf_{CB}$ against energy of upper levels was made and an effective spark temperature of 6400 °K was derived from the slope. The linearity of the plot

indicated the existence of a nearly exponential decline in the population of the upper energy levels in the range between 30 and 60 kK. The departure from a Boltzmann distribution in a spark apparently takes place only at much higher levels than in the arc. For this reason, the oscillator strengths for the lines observed in Ornstein and Bouma's spark were calculated directly from a Boltzmann distribution at 6400 °K and adjusted to the absolute scale of CB with a constant factor independent of excitation potential.

The values of log *gf* derived from Ornstein and Bouma's arc observations (OBA) are entered in table 2 in column 10; those from their spark observations (OBS) are entered in column 11.

2.4. Data of van Driel [1935]

In 1935 H. van Driel completed a Thesis at the University of Utrecht in which he measured relative intensities for 50 lines of Ni I between 3230 and 3860 Å. He made his observations in 2.0–2.4 amp arcs between various alloys of nickel and at pressures between 18 and 77 mm Hg. Van Driel studied the question of self-absorption carefully and his intensities, when plotted against the NBS intensities show no trace of self-absorption. He finally adopted a carbon arc with a hollow carbon electrode containing a mixture of carbon powder and nickel sulfate. The arc was operated at 2.4 amperes and at an ambient pressure of 32 mm Hg. He measured an effective temperature of 6400 °K for this arc from the intensity distribution in the CN band at 3883 Å. His intensities are here reduced to log *gf* by using his temperature and the resulting relative values are normalized to the absolute scale of Corliss and Bozman. The results are entered in column 8 of table 2 for wavelengths less than 3800 Å. For longer wavelengths this column is used for a different set of measurements.

2.5. Data of King [1948]

In 1948 R. B. King at the California Institute of Technology measured relative *gf*-values for 134 lines of Ni I between 3012 and 3912 Å. The observations were made by the method of total absorption in a tube furnace operated at temperatures between 1600 and 2700 °K. A comparison of his values with those of CB is shown in figure 2. King's values (K) were adjusted to the CB scale by adding −3.63 to his log *gf* and are tabulated in column 7 of table 2. Figure 1 shows that, within the range of King's observations, there is no wavelength-dependent variation between K and CB.

2.6. Data of Heid and Dieke [1954]

Heid and Dieke at Johns Hopkins University measured the relative intensities of 478 lines of Ni I between 3359 and 5893 Å. The light source was a 2 amp d-c arc 3 mm long struck between nickel rods in air. Light was taken from a section about 0.5 mm long at the center of the arc and measured with a photomultiplier tube at the focal curve of a 21-foot Wadsworth spectrograph. Lines closer than about 0.6 Å were not resolved. Corrections were made for background intensity and for self-reversal. When the values corrected for self-reversal are plotted against the NBS intensities of Meggers, Corliss, and Scribner, it is evident that some self-absorption remains. All lines with background-corrected intensities greater than 450 which lie shortward of 4700 Å are self-absorbed and have been omitted from our tabulation. All the lines lying longward of 4700 are free of self-absorption. I have also omitted the blended lines. There remain about 350 lines whose intensities seem to be suitable for reduction to oscillator strengths.

When the ratio of Heid and Dieke's intensities to the NBS intensities is plotted against wavelength, a sudden rise by nearly a factor of two is noted at 4700 Å.

The temperature of Heid and Dieke's arc was determined to be 5000 °K. Separate determinations were made for the two wavelength regions above and below 4700 Å to avoid any systematic error. The values obtained were 4950 °K below 4700 Å and 5020 °K at longer wavelengths. Finally, a separate normalization function was determined and applied to each of the two wavelength regions.

The values of log gf calculated as described above are entered in column 12 and have been averaged into the "Best" value only at wavelengths longer than 4200 Å. At shorter wavelengths they do not agree well with the other determinations.

2.7. Data of Parchevsky and Penkin [1954]

In 1954 Parchevsky and Penkin at the University of Leningrad measured relative oscillator strengths for 47 lines of Ni I by means of the hook method. These lines lie between 3050 and 3807 Å. A comparison of their values with those of CB is shown in figure 3. In a recent paper reviewing all of his work, Penkin [1964] has made very slight revisions to 16 of his values for Ni I. The recent values are used here and are reduced to the scale of Corliss and Bozman by adding −3.66 to Penkin's log *gf*. The results are entered in column 13 of table 2. It will be seen in the table that his value for 3612.74 Å is too small by a factor of ten and it has not been used in making the reduction to the common scale or in taking the best value.

2.8. Data of Mitrofanova [1960]

Mitrofanova at the Pulkovo Observatory reported oscillator strengths for 77 lines of Ni I between 3722 and 5155 Å. They were measured in the spectrum emitted from a 2.3 ampere a-c arc. Her data show insufficient correlation with the other data and have not been listed here.

3. New Observations

Reference to table 1 indicates that although a considerable amount of work has been done in the near ultraviolet, much remains to be done in the visible and especially in the infrared. To help fill this need, I have made three sets of observations; at Imperial College, London (IC), at University of London Observatory (ULO) and at the National Bureau of Standards (CHC).

3.1. Data From Imperial College [1963]

The work at Imperial College was carried out in connection with the measurement of oscillator strengths in Fe I in the region from 4000 to 10000 Å. These observations are reported by Corliss and Warner [1964]. While making the plates for iron, I made a similar set for nickel, using the methods of observation and reduction described in detail in the paper by Corliss and Warner.

The plates were made on the Eagle spectrographs at Imperial College with a 4 amp d-c arc between nickel rods as the source. Intensity calibration was provided by a rotating step-sector placed at the horizontal focus of the spectrograph. The intensity measurements were made using the ratio of the step openings to determine intensity ratios of lines visually matched in different steps of the sectored spectrograms. The wavelength response of the observing equipment was determined as outlined in section 2. In the region from 4000 to 4400 Å, where the nickel spectrum is deficient in lines, the response curve was determined from the iron spectrum. The temperature, obtained as described in section 2, was 4480 °K, which is substantially the same as that determined earlier for the iron arc. The derived values of log *gf*, adjusted to the CB scale, are entered in column 14 of table 2 under the symbol IC.

3.2. Data From ULO [1963]

During the academic year 1962–1963, I obtained at the University of London Observatory a set of spectrograms of the nickel arc with their ten foot Eagle spectrograph. This instrument is equipped with a 600 lines/mm Rowland grating and yields a (reciprocal) dispersion of 5.5 Å/mm. The intensity information was impressed on the lines by mounting a step wedge at Sirk's stigmatic position in front of the slit. A 2.9 ampere arc, 8 mm long, struck between two $\frac{3}{8}$ inch nickel rods, was focused on the grating by a lens at the step wedge. The plates were measured and reduced at the Observatory, the intensity versus wavelength and the temperature calibrations being carried out by comparison with the NBS Intensity Tables. The values of log *gf* were adjusted to the CB scale. The results cover the wavelength range 5424 to 6533 Å and are reported in the column 10, headed ULO.

3.3. Data From National Bureau of Standards [1964]

Because of conflicting results in the region between 3800 and 5000 Å, I made a new set of observations using a different light source, a spark in air between two nickel rods. The power was drawn from a capacitor of 0.007 microfarads through an inductor of 14 microhenries and passed through a 2 mm gap between the electrodes. The spectrograms were made in the second order of a 600 line/mm concave grating in a Wadsworth stigmatic mounting at a reciprocal dispersion of 2.4 Å/mm between 3800 and 4400Å. Further observations were made in the first order of the same instrument at 5 Å/mm in the region from 3800 to 5050 Å. Because of the scarcity of nickel lines in the NBS Intensity Tables in this region, the response of the apparatus was determined by using iron and cobalt sparks. The temperature of the spark was determined by plotting log $I\lambda^3/gf_{CB}$ versus upper energy level value for those nickel lines in this region which are also found in Corliss and Bozman. An independent study of similar sparks in cobalt and iron shows that there is no detectable departure from a Boltzmann distribution in these sparks up to 55000 K. On this basis I calculated oscillator strengths for Ni I lines observed in the spark in this region, assuming a Boltzmann distribution at 6170 °K. The resulting values (CHC) are adjusted to the CB scale and entered in column 8.

4. Results

The various values of log *gf*, obtained as described in the two preceding sections, have been entered in columns 6 through 14 in table 2. Except for about a dozen lines in the infrared that are taken from Meggers and Kiess [1932], the wavelengths are taken from Burns and Sullivan [1947, 1948] and rounded off to the nearest 0.01 Å. The classifications are taken from the same authors, and the numerical values of the energy levels are given to the nearest kayser (cm^{-1}) in columns 2 and 3. The lower excitation potential in electron volts has been calculated by multiplying the lower energy level in column 2 by 0.00012398 and the result, rounded off to two decimal places, is entered in column 4. The multiplet numbers in column 5 are those assigned by Moore [1945, 1952] in her Multiplet Tables.

The recommended or "best" value of log *gf*, given in column 15, is the unweighted mean of the individual values in the preceding columns, with the exception of the HD values below 4200 Å, which have been rejected. If the maximum and minimum values for any line differ by more than 0.4, no best value is recommended unless there is an obviously discrepant value. No best value has been recommended for about 10 percent of the lines. Most of these lines are faint lines in the region from 3800 to 4200 Å, where the discordance amongst individual determinations is extraordinarily bad.

Log $gf\lambda$ and log gA/λ have been computed from the best value and are given in the last two columns. Log $gf\lambda$ is useful in dealing with curves of growth in absorption spectra and log gA/λ in determining temperatures from intensities in emission spectra. Also, it may be noted that the line strength, S, is equal to $gf\lambda/304$, or log S=log $gf\lambda-2.48$.

5. Discussion of the Absolute Scale

There have been a number of attempts, by both theoretical and experimental methods, to determine absolute oscillator strengths for selected lines of Ni I. The first was by Estabrook (1950), who determined the total absorption of three resonance lines of nickel, using a quartz cell containing nickel vapor in a wire-wound electric furnace operated at about 1300 °C. His values are now generally agreed to be too low. (See e.g., Goldberg, Müller, and Aller (1960), pp. 98–107.) They are smaller than the values in table 2 by a factor of ten. Lawrence, Link, and King (1965), using new vapor pressure data, have raised Estabrook's values by a factor of two but they are still too low.

Hinnov and Kohn (1957) determined the absolute oscillator strength of Ni I 3524.55 Å in a flame. They found a lower limit for log gf of 0.12 which compares with the value in table 2 of 0.13.

Goldberg, Müller, and Aller, using the f-sum rule, computed absolute values of log gf for two groups of lines in Ni I; one in the region 3300 to 3700 Å and the other from 4800 to 5700 Å. For the first group of 20 lines their values of log gf averaged 0.20 larger than those in table 2, while for the second group of 29 lines their values averaged 0.05 larger than the ones in table 2.

King, Lawrence, and Link (1964) have determined absolute values for six resonance lines of Ni I using the atomic beam method. On the average, their values of log gf are smaller than the ones in table 2 by 0.22.

It seems reasonable to conclude from the above comparisons that the scale of values in table 2 does not depart from the absolute scale by more than the uncertainty with which the absolute scale for Ni I is known, and that this uncertainty is about 0.2 in log gf.

I would like to acknowledge my obligation to W. R. S. Garton who invited me to spend a year at Imperial College, to Professor C. W. Allen who extended to me the hospitality of the London Observatory, to W. R. Bozman and C. R. Drew who helped prepare the tables on IBM equipment and to Ruth Peterson who helped make the tables and put them on punched cards.

6. References

Allen, C. W. (1960) Monthly Notices Roy. Astron. Soc. **121,** 299.
Allen, C. W., and Asaad, A. S. (1957) ibid. **117,** 36.
Allen, C. W., and Corliss, C. H. (1963) ibid. **126,** 37.
Burns, K. and Sullivan, F. (1947) Science Studies St. Bonaventure College **13,** 4; (1948) ibid. **14,** 2.
Corliss, C. H., and Bozman, W. R. (1962) Experimental Transition Probabilities for Spectral Lines of Seventy Elements, NBS Mono. No. 53 [Washington: Government Printing Office].
Corliss, C. H., and Warner, B. (1964) Astrophys. J. Suppl. Ser. **8,** 395, No. 83.
Estabrook, F. B. (1951) Astrophys. J. **113,** 684.
Goldberg, L., Müller, E. A., and Aller, L. H. (1960) Astrophys. J. Supplement Series No. 45.
Heid, R. L., and Dicke, G. H. (1954) J. Opt. Soc. Am. **44,** 402.
Hinnov, E., and Kohn, H. (1957) J. Opt. Soc. Am. **47,** 156.
King, R. B., 1948, Astrophys. J. **108,** 87.
Lawrence, G. M., Link, J. K., and King, R. B. (1965) Astrophys. J. **141,** 293.
Meggers, W. F., Corliss, C. H., and Scribner, B. F. (1961) Tables of Spectral-Line Intensities, NBS Mono. No. 32, Washington.
Meggers, W. F., and Kiess, C. C. (1932) BS J. Res. **9,** 309.
Mitrofanova, L. A. (1960) Publ. Pulkovo Obs. **21,** 185.
Moore, C. E. (1945) A Multiplet Table of Astrophysical Interest, Contr. Princeton U. Obs. No. 20.
Moore, C. E. (1952) An Ultraviolet Multiplet Table, NBS Circ. 488, Section 2.
Ornstein, L. S., and Bouma, T. (1930) Phys. Rev. **36,** 679.
Parchevskii, G. F., and Penkin, N. P. (1954) Vestnik Leningrad State University **11,** 113. Translated by J. Tech in Astron. Papers Trans. from the Russian, No. II (1964) Smithsonian Astrophys. Obs., Cambridge, Mass.
Penkin, N. P. (1964) J. Quant. Spectr. Radiative Transfer **4,** 41. Translated by J. Tech in Astron. Papers Trans. from the Russian, No. II (1964) Smithsonian Astrophys. Obs., Cambridge, Mass.
Russell, H. N. (1929) Phys. Rev. **34,** 821.
van Driel, H. (1935) Thesis, University of Utrecht, also published in King (1948).

TABLE 2.—*Oscillator Strengths for Ni* I

Wave-length	Energy Levels		Lower e.p.	Mult. No.	CB	K	vD	AA	OBA	OBS	HD	PP	IC	Best	Log gfλ	Log gA/λ
Å	K		Volts													
(1)	(2)	(3)	(4)	(5)	(6)	(7)	(8)	(9)	(10)	(11)	(12)	(13)	(14)	(15)	(16)	(17)
2798.65	880 –	36601	0.11	UV26	−1.18				−1.06	−1.14				−1.13	2.32	4.35
2803.14	13521 –	49185	1.68	UV69					−0.47					−0.47	2.98	5.01
2805.08	0 –	35639	0.00	UV 1					−1.89	−2.20				−2.04	1.41	3.44
2814.35	27261 –	62783	3.38	UV79					−0.17					−0.17	3.28	5.31
2821.29	205 –	35639	0.03	UV25	−1.07				−1.06	−1.13				−1.09	2.36	4.38
2834.55	1332 –	36601	0.17	UV 2					−1.78	−1.54				−1.66	1.79	3.81
2838.95	13521 –	48735	1.68	UV68					−0.52					−0.52	2.93	4.94
2849.82	15610 –	50689	1.93	UV77					−0.69					−0.69	2.76	4.77
2865.50	1713 –	36601	0.21	UV26	−1.63				−1.44	−1.59				−1.55	1.91	3.90
2868.74	15610 –	50458	1.93	UV76					−0.45					−0.45	3.01	5.00
2905.75	15734 –	50139	1.95	UV74					−0.73					−0.73	2.73	4.70
2907.46	2217 –	36601	0.27	UV 2	−1.51				−1.33					−1.42	2.04	4.01
2914.01	1332 –	35639	0.17	UV 1	−2.03				−1.79	−2.15				−1.99	1.47	3.44
2916.85	28542 –	62815	3.54						−0.49					−0.49	2.97	4.94
2917.53	28542 –	62808	3.54						−0.49					−0.49	2.98	4.94
2930.91	25754 –	59863	3.19	UV78					−0.28					−0.28	3.19	5.14
2943.91	205 –	34163	0.03	UV24	−0.89					−0.90				−0.90	2.57	4.52
2958.28	15610 –	49403	1.93	UV74					−0.64					−0.64	2.83	4.77
2969.19	15734 –	49403	1.95	UV74					−0.40	−0.29				−0.34	3.13	5.07
2973.73	13521 –	47139	1.68	UV66					−1.17					−1.17	2.30	4.23
2981.64	880 –	34409	0.11	UV24	−0.78					−0.78				−0.78	2.69	4.62
2983.43	13521 –	47030	1.68	UV66					−0.30					−0.30	3.17	5.10
2984.13	0 –	33501	0.00	12	−1.26				−1.22	−1.18				−1.22	2.25	4.18
2991.11	2217 –	35639	0.27	UV 1					−2.20					−2.20	1.28	3.20
2992.59	205 –	33611	0.03	25	−0.94					−0.99				−0.96	2.52	4.44
2994.45	205 –	33590	0.03	27	−0.64					−0.79				−0.72	2.76	4.67
3002.48	205 –	33501	0.03	UV24	−0.04									−0.04	3.44	5.35
3003.62	880 –	34163	0.11	UV24	−0.21									−0.21	3.27	5.18
3012.00	3410 –	36601	0.42	41	0.31	0.27								0.29	3.77	5.68
3017.95	15610 –	48735	1.93	UV74					−1.06					−1.06	2.42	4.32
3019.14	0 –	33112	0.00	11	−1.14	−1.12				−1.08				−1.11	2.37	4.27
3029.29	15734 –	48735	1.95	UV74					−0.75					−0.75	2.73	4.63
3031.87	0 –	32973	0.00	11	−1.60	−1.46			−1.36	−1.55				−1.49	1.99	3.89
3037.93	205 –	33112	0.03	25	−0.44	−0.35				−0.54				−0.44	3.04	4.94
3045.01	1332 –	34163	0.17	12	−1.37	−1.43			−1.21	−1.45				−1.36	2.12	4.01
3050.82	205 –	32973	0.03	25	−0.15	0.05						0.03		−0.02	3.46	5.35
3054.31	880 –	33611	0.11	25	−0.43	−0.39				−0.51		−0.42		−0.44	3.04	4.93
3057.64	1713 –	34409	0.21	UV24	−0.24	−0.11						−0.27		−0.21	3.28	5.16
3064.62	880 –	33501	0.11	UV24	−0.92	−0.82				−0.89		−1.01		−0.91	2.58	4.45
3066.44	27261 –	59863	3.38						−0.10					−0.10	3.39	5.26
3080.75	1713 –	34163	0.21	UV24	−0.86	−1.01				−0.97				−0.95	2.54	4.41
3097.12	1332 –	33611	0.17	11	−1.12	−1.12			−1.08	−1.27				−1.15	2.34	4.20
3099.11	1332 –	33590	0.17	13	−1.22	−1.20			−1.18	−1.39				−1.25	2.24	4.10
3101.56	880 –	33112	0.11	25	−0.17	0.04								−0.06	3.43	5.29
3101.88	3410 –	35639	0.42	40	−0.17	0.12				−0.28				−0.11	3.38	5.24
3105.46	2217 –	34409	0.27	12	−1.09	−1.10			−1.00	−1.25				−1.11	2.38	4.24
3107.71	1332 –	33501	0.17	12		−2.67			−2.55					−2.61	0.88	2.74
3114.12	880 –	32982	0.11	24	−1.17	−1.23				−1.28		−1.32		−1.25	2.24	4.09
3116.72	25754 –	57829	3.19	95					−0.38					−0.38	3.11	4.96
3129.30	2217 –	34163	0.27	12		−1.99			−1.85	−2.19				−2.01	1.49	3.33
3134.10	1713 –	33611	0.21	25	−0.07	−0.01						−0.09		−0.06	3.44	5.28
3145.11	0 –	31786	0.00	7		−3.48			−3.28					−3.38	0.12	1.95
3145.70	1332 –	33112	0.17	11	−1.84	−1.90			−1.72					−1.82	1.68	3.51
3154.58	15734 –	47425	1.95	78					−0.92					−0.92	2.58	4.41
3159.52	1332 –	32973	0.17	11		−3.03			−2.88					−2.96	0.54	2.37
3164.16	15734 –	47329	1.95	79					−1.15					−1.15	2.35	4.17
3165.50	205 –	31786	0.03	21		−3.04			−2.98					−3.01	0.49	2.31
3170.72	15610 –	47139	1.93	78					−1.16					−1.16	2.34	4.16
3176.29	15734 –	47208	1.95	77					−1.03					−1.03	2.47	4.29
3181.74	15610 –	47030	1.93	78	−0.11				−0.18					−0.14	3.36	5.18

TABLE 2.—*Oscillator Strengths for Ni* I—Continued

Wavelength Å	Energy Levels K		Lower e.p. Volts	Mult. No.	CB	K	vD	AA	OBA	OBS	HD	PP	IC	Best	Log gfλ	Log gA/λ
(1)	(2)	(3)	(4)	(5)	(6)	(7)	(8)	(9)	(10)	(11)	(12)	(13)	(14)	(15)	(16)	(17)
3183.02	16017 –	47425	1.99	78					−0.69					−0.69	2.81	4.63
3183.25	15734 –	47139	1.95	78					−0.36					−0.36	3.14	4.96
3184.37	2217 –	33611	0.27	11	−1.51	−1.73			−1.56					−1.60	1.90	3.71
3191.86	28542 –	59863	3.54	125					−0.29					−0.29	3.21	5.02
3195.57	2217 –	33501	0.27	12	−1.77	−2.02			−1.89					−1.89	1.61	3.42
3197.11	1713 –	32982	0.21	24	−1.39	−1.52			−1.46	−1.43				−1.45	2.05	3.86
3200.42	205 –	31442	0.03	23		−2.45			−2.46					−2.46	1.05	2.85
3202.14	25754 –	56974	3.19	94	0.55				0.58					0.56	4.07	5.87
3206.95	27415 –	58588	3.40	94					−0.29					−0.29	3.22	5.02
3209.91	26666 –	57810	3.31	94					0.33					0.33	3.84	5.63
3213.41	27415 –	58526	3.40	91					0.10					0.10	3.61	5.40
3214.06	25754 –	56858	3.19	93	1.05				0.92	0.84				0.94	4.45	6.24
3216.82	26666 –	57744	3.31	93					0.50	0.85				0.68	4.19	5.98
3217.82	25754 –	56821	3.19	91	1.05				1.13	1.06				1.08	4.59	6.38
3219.79	27944 –	58993	3.46	94					0.02					0.02	3.53	5.32
3221.27	30923 –	61958	3.83	185	0.94				0.69	1.27				0.97	4.48	6.27
3221.65	0 –	31031	0.00	8	−1.61	−1.51			−1.45	−1.42		−1.62		−1.52	1.99	3.78
3223.53	25754 –	56767	3.19	94					0.21					0.21	3.72	5.51
3225.02	3410 –	34409	0.42	39	−1.07	−1.02			−0.87	−0.95		−1.10		−1.00	2.51	4.30
3226.98	0 –	30980	0.00	7		−2.15			−2.04	−1.76		−2.00		−1.99	1.52	3.31
3232.93	0 –	30923	0.00	7	−0.77	−0.80	−0.49			−0.78		−0.97		−0.76	2.75	4.54
3233.94	15610 –	46523	1.93	77					−0.86					−0.86	2.65	4.43
3234.65	880 –	31786	0.11	21	−1.25	−1.29			−1.35	−1.28				−1.29	2.22	4.00
3235.75	2217 –	33112	0.27	11		−2.82			−2.65					−2.74	0.77	2.55
3243.04	205 –	31031	0.03	22	−1.01	−1.06	−0.98			−0.97		−1.11		−1.03	2.48	4.26
3245.38	28068 –	58873	3.48	108					−0.27					−0.27	3.24	5.02
3248.46	205 –	30980	0.03	21	−1.80	−1.85			−1.77	−1.71				−1.78	1.73	3.51
3249.44	2217 –	32982	0.27	10		−2.17			−2.07	−1.66				−1.97	1.54	3.32
3250.74	3410 –	34163	0.42	39	−1.32	−1.37			−1.18	−1.21				−1.27	2.24	4.02
3268.96	27944 –	58526	3.46	91					−0.67					−0.67	2.84	4.61
3271.11	880 –	31442	0.11	23	−1.74	−1.92			−1.74	−1.80				−1.80	1.71	3.48
3273.45	28578 –	59118	3.54	108					−0.38					−0.38	3.14	4.90
3277.19	27944 –	58449	3.46	90					−0.37					−0.37	3.15	4.91
3281.88	28578 –	59040	3.54	106					0.16					0.16	3.68	5.44
3282.69	1332 –	31786	0.17	7	−1.60	−1.95			−1.83	−1.76				−1.78	1.74	3.50
3282.83	28068 –	58521	3.48	106						0.41				0.41	3.93	5.69
3284.42	26666 –	57104	3.31	96					0.02					0.02	3.54	5.29
3286.94	205 –	30619	0.03	19		−2.11			−2.02	−2.08				−2.07	1.45	3.20
3293.63	27415 –	57768	3.40	90					0.04					0.04	3.56	5.31
3296.26	27415 –	57744	3.40						−0.38					−0.38	3.14	4.89
3304.94	27580 –	57829	3.42	108					0.31	0.38				0.34	3.86	5.61
3307.01	27580 –	57810	3.42	107					−0.23					−0.23	3.29	5.04
3310.20	3410 –	33611	0.42	38		−2.44			−2.25					−2.34	1.18	2.92
3312.32	27580 –	57762	3.42	106					0.89	0.89				0.89	4.41	6.15
3312.99	29013 –	59189	3.60	106					0.32	0.81				0.56	4.08	5.82
3315.66	880 –	31031	0.11	22	−0.95	−0.90	−1.21	−0.94		−0.89		−1.02		−0.98	2.54	4.28
3320.26	1332 –	31442	0.17	9	−1.19	−1.04	−1.07	−1.00		−1.04		−1.21		−1.09	2.43	4.17
3322.31	3410 –	33501	0.42	39	−0.97	−1.01	−0.98			−0.99		−1.18		−1.03	2.49	4.23
3326.67	28578 –	58630	3.54	108					0.09	0.28				0.18	3.70	5.44
3327.39	26666 –	56711	3.31	90					0.20					0.20	3.72	5.46
3328.71	880 –	30913	0.11	20		−2.93			−2.90					−2.92	0.60	2.34
3337.01	205 –	30163	0.03	17		−3.69			−3.40					−3.54	−0.02	1.71
3338.76	13521 –	43464	1.68	54					−2.07					−2.07	1.45	3.18
3339.05	28578 –	58518	3.54	104					0.09					0.09	3.61	5.34
3351.05	0 –	29833	0.00	3		−4.23								−4.23	−0.70	1.02
3359.10	28068 –	57829	3.48	108					0.64	0.52	0.26			0.58	4.11	5.83
3361.55	880 –	30619	0.11	19	−1.28	−1.11	−1.10	−1.13		−1.05		−1.20		−1.14	2.39	4.10
3362.80	1713 –	31442	0.21	23		−2.47			−2.42	−2.37	−2.08			−2.42	1.11	2.82
3363.60	28068 –	57790	3.48	105					0.26		−0.05			0.26	3.79	5.50
3364.58	27261 –	56974	3.38	107					0.51		0.06			0.51	4.04	5.75

TABLE 2.—*Oscillator Strengths for Ni* I—Continued

Wavelength Å	Energy Levels K		Lower e.p. Volts	Mult. No.	CB	K	vD	AA	OBA	OBS	HD	PP	IC	Best	Log gfλ	Log gA/λ
(1)	(2)	(3)	(4)	(5)	(6)	(7)	(8)	(9)	(10)	(11)	(12)	(13)	(14)	(15)	(16)	(17)
3365.76	3410 –	33112	0.42	38	−0.97	−1.01	−0.93			−0.91				−0.96	2.57	4.28
3366.16	1332 –	31031	0.17	8	−1.23	−1.04	−1.04	−1.15		−1.08				−1.11	2.42	4.13
3366.80	27261 –	56954	3.38	108	0.69				1.12	1.06	0.73			0.96	4.49	6.20
3367.88	205 –	29888	0.03	20	−2.06	−2.43			−2.29		−1.98			−2.26	1.27	2.98
3369.56	0 –	29669	0.00	6	−0.45	−0.44	−0.28	−0.47				−0.68		−0.46	3.07	4.78
3371.99	1332 –	30980	0.17	7	−1.15	−0.99	−0.76	−1.11		−1.05		−0.96		−1.00	2.53	4.24
3374.22	205 –	29833	0.03	17	−1.47	−1.41	−1.32		−1.49	−1.37		−1.20		−1.38	2.15	3.86
3374.64	27261 –	56885	3.38	106	0.99				1.52	1.02				1.18	4.71	6.42
3375.55	29013 –	58630	3.60	108					0.22		−0.33			0.22	3.75	5.46
3376.32	28068 –	57678	3.48	104					0.41		0.05			0.41	3.94	5.65
3380.57	3410 –	32982	0.42	37	0.02	0.09	0.03	0.17						0.08	3.61	5.32
3380.89	2217 –	31786	0.27	7	−1.26	−1.06			−1.61	−0.81				−1.18	2.35	4.06
3387.46	880 –	30392	0.11	17		−3.69			−3.45		−3.30			−3.57	−0.04	1.66
3391.04	0 –	29481	0.00	5	−0.80	−0.85	−0.75	−0.82		−0.79		−1.03		−0.84	2.69	4.39
3392.98	205 –	29669	0.03	20	−0.38	−0.37	−0.17	−0.40				−0.49		−0.36	3.17	4.87
3396.18	29084 –	58521	3.60	122					0.30	0.70	0.03			0.50	4.03	5.73
3401.16	27580 –	56974	3.42	107					0.78	0.57	0.40			0.68	4.21	5.91
3403.43	27580 –	56954	3.42	108					0.84	0.77	0.45			0.80	4.33	6.03
3409.58	0 –	29321	0.00	5	−1.82	−2.01			−1.99	−1.89	−1.88			−1.93	1.60	3.30
3413.48	1332 –	30619	0.17	5	−1.26	−1.01			−1.41	−1.01				−1.17	2.36	4.05
3413.94	880 –	30163	0.11	17	−1.31	−1.37				−1.35				−1.34	2.19	3.88
3414.76	205 –	29481	0.03	19	0.00	0.02	0.09	−0.04						0.02	3.55	5.24
3420.73	2217 –	31442	0.27	9		−2.61			−2.75		−2.28			−2.68	0.85	2.54
3421.34	28542 –	57762	3.54	122					0.89	0.73	0.52			0.81	4.34	6.03
3422.32	28578 –	57790	3.54	105					0.37		−0.02			0.37	3.90	5.59
3422.87	29833 –	59040	3.70	122					0.66		0.17			0.66	4.19	5.88
3423.71	1713 –	30913	0.21	20	−0.52	−0.49	−0.42	−0.51		−0.53		−0.53		−0.50	3.03	4.72
3433.56	205 –	29321	0.03	19	−0.51	−0.52	−0.39	−0.48				−0.58		−0.50	3.04	4.72
3435.48	13521 –	42621	1.68	53					−1.42		−1.35			−1.42	2.12	3.80
3437.28	0 –	29084	0.00	3	−0.96	−0.91	−0.81	−1.03		−0.70		−0.91		−0.89	2.65	4.33
3442.04	27580 –	56625	3.42	104					0.47					0.47	4.01	5.68
3442.59	29833 –	58873	3.70	124					0.17					0.17	3.71	5.38
3443.03	28068 –	57104	3.48						−0.16					−0.16	3.38	5.05
3444.25	30163 –	59189	3.74	122					0.48		0.12			0.48	4.02	5.69
3446.26	880 –	29888	0.11	20	−0.17	−0.27	−0.13	−0.28				−0.30		−0.23	3.31	4.98
3452.88	880 –	29833	0.11	17	−0.74	−0.61	−0.50	−0.68		−0.63		−0.68		−0.64	2.90	4.57
3458.46	1713 –	30619	0.21	19	−0.06	−0.05	0.01	−0.06				−0.11		−0.05	3.49	5.16
3461.66	205 –	29084	0.03	17	−0.24	−0.25	−0.08	−0.27				−0.24		−0.22	3.32	4.99
3464.13	32973 –	61832	4.09						0.08					0.08	3.62	5.29
3467.50	1332 –	30163	0.17	3	−1.52	−1.70	−1.64		−1.54	−1.65				−1.61	1.93	3.59
3469.48	2217 –	31031	0.27	8	−1.32	−1.36	−1.53		−1.29	−1.31				−1.36	2.18	3.84
3472.55	880 –	29669	0.11	20	−0.65	−0.55	−0.40	−0.62		−0.61		−0.68		−0.58	2.96	4.62
3476.62	29833 –	58588	3.70	123					0.20		−0.20			0.20	3.74	5.40
3477.88	29084 –	57829	3.60	124					−0.12					−0.12	3.42	5.08
3478.32	29889 –	58630	3.70	173					0.20					0.20	3.74	5.40
3479.26	28068 –	56802	3.48	105					0.25		−0.16			0.25	3.79	5.45
3480.17	29084 –	57810	3.60	123					0.19		−0.12			0.19	3.73	5.39
3483.77	2217 –	30913	0.27	6	−0.97	−0.63	−0.80			−0.75		−0.73		−0.78	2.76	4.42
3485.11	29833 –	58518	3.70	118							−0.03					
3485.88	1713 –	30392	0.21	17	−1.66	−1.70	−1.87		−1.69	−1.88				−1.76	1.78	3.44
3488.30	29084 –	57744	3.60	121					0.20		−0.35			0.20	3.74	5.40
3492.96	880 –	29501	0.11	18	−0.14	−0.14	−0.03	−0.23				−0.16		−0.14	3.40	5.05
3496.35	29084 –	57678	3.60	118					0.49		0.13			0.49	4.03	5.68
3498.19	0 –	28578	0.00	2		−4.23								−4.23	−0.69	0.96
3500.85	1332 –	29888	0.17	6	−1.01	−0.91	−0.96	−1.16		−0.91		−1.06		−1.00	2.54	4.19
3502.60	0 –	28542	0.00	3	−2.18	−2.29			−2.42	−2.31	−2.13			−2.30	1.24	2.89
3507.69	1332 –	29833	0.17	3	−2.10	−2.01			−2.10	−1.97	−1.85			−2.04	1.51	3.15
3510.33	1713 –	30192	0.21	18	−0.37	−0.48	−0.51	−0.43				−0.20		−0.40	3.15	4.79
3511.61	29321 –	57790	3.63	152						0.56				0.56	4.11	5.75
3511.91	30163 –	58630	3.74	124					0.24					0.24	3.79	5.43

TABLE 2.—*Oscillator Strengths for Ni* I—Continued

Wave-length	Energy Levels		Lower e.p.	Mult. No.	CB	K	vD	AA	OBA	OBS	HD	PP	IC	Best	Log gfλ	Log gA/λ
Å	K		Volts													
(1)	(2)	(3)	(4)	(5)	(6)	(7)	(8)	(9)	(10)	(11)	(12)	(13)	(14)	(15)	(16)	(17)
3513.93	1713 –	30163	0.21	17	−1.37	−1.47	−1.64		−1.51					−1.50	2.05	3.69
3515.05	880 –	29321	0.11	19	−0.08	−0.07	0.08	−0.13				−0.07		−0.09	3.46	5.10
3516.22	28542 –	56974	3.54	123					1.15	0.90	0.70			1.02	4.57	6.21
3518.63	28542 –	56954	3.54	124					0.97	0.70	0.59			0.84	4.39	6.02
3519.76	2217 –	30619	0.27	5	−0.92	−0.92	−1.09			−1.05		−0.80		−0.96	2.59	4.22
3523.07	3410 –	31786	0.42	34		−2.81			−1.95					−2.81	0.74	2.37
3523.44	205 –	28578	0.03	16		−2.06			−2.04					−2.05	1.50	3.13
3524.55	205 –	28569	0.03	18	−0.07	0.11	0.13	0.13				0.33		0.13	3.68	5.31
3526.53	29481 –	57829	3.65	155					0.63		0.28			0.63	4.18	5.81
3527.98	1332 –	29669	0.17	6	−1.81	−1.70	−1.91		−1.80	−1.81				−1.81	1.74	3.37
3528.88	29481 –	57810	3.65	154					0.41					0.41	3.96	5.59
3529.62	15610 –	43933	1.93	76					−1.15		−1.13			−1.15	2.40	4.03
3530.59	28542 –	56858	3.54	121					0.56		0.23			0.56	4.11	5.74
3537.24	29481 –	57744	3.65	153					0.12					0.12	3.67	5.30
3537.62	28542 –	56802	3.54	120					0.22					0.22	3.77	5.40
3542.03	28542 –	56767	3.54	119					0.10		−0.38			0.10	3.65	5.28
3545.16	15734 –	43933	1.95	76					−1.34		−1.26			−1.34	2.21	3.84
3548.18	2217 –	30392	0.27	3	−1.24	−1.00	−1.28	−1.05		−1.21		−0.98		−1.13	2.42	4.04
3548.18	1713 –	29889	0.21	20		−1.18	−1.33	−1.05						−1.19	2.36	3.98
3551.53	1332 –	29481	0.17	5	−2.12	−2.06			−2.19	−2.04	−1.89			−2.10	1.45	3.07
3553.48	880 –	29013	0.11	16		−2.33			−2.74	−2.09	−2.16			−2.33	1.22	2.84
3559.92	28542 –	56625	3.54	118					0.24		−0.13			0.24	3.79	5.41
3561.75	0 –	28068	0.00	2	−2.21	−2.12			−2.18	−2.07	−2.00			−2.14	1.41	3.03
3566.37	3410 –	31442	0.42	36	0.08	−0.03	0.02	−0.05				0.11		0.03	3.58	5.20
3571.86	1332 –	29321	0.17	5	−0.88	−0.80	−0.82	−0.92		−0.77		−0.74		−0.82	2.73	4.35
3575.93	29833 –	57790	3.70	120					0.29		−0.55			0.29	3.84	5.45
3577.23	2217 –	30163	0.27	3		−3.31			−3.18		−2.99			−3.24	0.31	1.92
3587.93	205 –	28068	0.03	16	−1.90	−1.97	−2.06		−1.99	−2.21		−1.88		−2.00	1.55	3.16
3597.70	1713 –	29501	0.21	18	−0.73	−0.79	−0.85	−0.80		−0.73		−0.74		−0.77	2.79	4.39
3599.54	29084 –	56858	3.60	121					0.18		−0.45			0.18	3.74	5.34
3602.28	1332 –	29084	0.17	3		−1.70	−1.78		−1.67	−1.66		−2.21		−1.70	1.86	3.45
3604.26	29084 –	56822	3.60								−0.63					
3606.85	29084 –	56802	3.60	120					0.31		−0.13			0.31	3.87	5.46
3609.31	880 –	28578	0.11	16		−1.69	−1.72		−1.69	−1.47				−1.64	1.92	3.51
3610.46	880 –	28569	0.11	18	−0.83	−0.92	−0.85	−0.80		−0.74		−1.35		−0.83	2.73	4.32
3611.43	29084 –	56767	3.60	119							0.06					
3611.54	1332 –	29013	0.17	2		−3.80								−3.80	−0.24	1.35
3612.74	2217 –	29888	0.27	6	−1.07	−0.97	−1.15	−1.10		−0.93		−2.03		−1.04	2.52	4.11
3619.39	3410 –	31031	0.42	35	0.17	0.15	0.27	0.18				0.40		0.19	3.75	5.34
3624.73	0 –	27580	0.00	2	−1.95	−1.96			−1.94	−1.79				−1.91	1.65	3.24
3629.90	30980 –	58521	3.84	182					0.26		−0.12			0.26	3.82	5.40
3634.95	3410 –	30913	0.42	33		−2.11			−2.12		−1.88			−2.12	1.44	3.02
3641.64	2217 –	29669	0.27	6		−3.03			−3.28		−2.82			−3.16	0.40	1.98
3642.38	16017 –	43464	1.99	75					−1.46		−1.63			−1.46	2.10	3.68
3643.94	29669 –	57104	3.68	174							−0.64					
3656.54	29481 –	56822	3.65								−0.91					
3657.70	31786 –	59118	3.94	183							−0.65					
3661.95	1713 –	29013	0.21	16		−2.47			−2.59		−2.31			−2.53	1.03	2.60
3664.09	2217 –	29501	0.27	4	−1.53	−1.52		−1.48	−1.64	−1.47				−1.53	2.03	3.60
3668.21	31786 –	59040	3.94	182					0.45		−0.23			0.45	4.01	5.58
3669.24	1332 –	28578	0.17	2	−1.81	−2.14			−2.06		−1.94			−2.00	1.56	3.13
3670.43	1332 –	28569	0.17	4	−1.69	−1.77		−1.87	−1.90	−1.59				−1.76	1.80	3.37
3674.06	205 –	27415	0.03	15		−2.37	−1.80		−1.59							
3674.15	3410 –	30619	0.42	32	−1.65	−1.23	−1.48	−1.5		−1.31						
3688.41	2217 –	29321	0.27	5	−1.59	−1.69			−1.76	−1.82				−1.76	1.81	3.36
3693.93	880 –	27944	0.11	15	−2.06	−2.44			−2.48		−2.27			−2.46	1.11	2.66
3696.91	29669 –	56711	3.68	172					0.24		−0.28			0.24	3.81	5.36
3705.10	3410 –	30392	0.42	30							−3.85					
3713.70	15734 –	42654	1.95	74					−1.47					−1.47	2.10	3.64
3715.50	30923 –	57829	3.83	183					0.20		−0.61			0.20	3.77	5.31

TABLE 2.—*Oscillator Strengths for Ni* I—Continued

Wave-length	Energy Levels		Lower e.p.	Mult. No.	CB	K	CHC	AA	OBA	OBS	HD	PP	IC	Best	Log gfλ	Log gA/λ
Å	K		Volts													
(1)	(2)	(3)	(4)	(5)	(6)	(7)	(8)	(9)	(10)	(11)	(12)	(13)	(14)	(15)	(16)	(17)
3722.49	1713 –	28569	0.21	18	−1.79	−1.75			−1.81	−1.84				−1.80	1.77	3.31
3724.82	30923 –	57762	3.83	182					0.32		−0.19			0.32	3.89	5.43
3728.92	30980 –	57790	3.84	181					0.22		−0.62			0.22	3.79	5.33
3730.75	2217 –	29013	0.27	2		−2.95			−3.00		−2.76			−2.98	0.59	2.13
3736.81	3410 –	30163	0.42	30	−1.50	−1.33			−1.23	−1.47				−1.38	2.19	3.73
3739.23	1332 –	28068	0.17	2	−2.15	−2.14			−2.11	−1.98				−2.10	1.47	3.01
3739.79	31786 –	58518	3.94	180					1.14					1.14	4.71	6.25
3744.56	30980 –	57678	3.84	180					0.66		−0.07			0.66	4.23	5.76
3749.05	0 –	26666	0.00	1		−2.73			−2.69		−2.49			−2.71	0.86	2.39
3762.62	22102 –	48672	2.74						−0.32		−0.76			−0.32	3.26	4.78
3772.53	1713 –	28213	0.21	15		−2.84			−2.90		−2.66			−2.87	0.71	2.22
3775.57	3410 –	29888	0.42	33	−0.92	−0.87		−0.95		−0.85		−0.97		−0.91	2.67	4.18
3778.06	205 –	26666	0.03	15		−3.00			−3.01		−2.80			−3.00	0.58	2.09
3783.53	3410 –	29833	0.42	30	−0.85	−0.84		−0.99		−0.79		−0.85		−0.86	2.72	4.23
3792.34	2217 –	28578	0.27	2		−2.71			−2.62		−2.48			−2.67	0.91	2.42
3793.60	2217 –	28569	0.27	4		−2.34			−2.26		−2.12			−2.30	1.28	2.79
3807.14	3410 –	29669	0.42	33	−0.86	−0.77	−0.84	−0.89		−0.64		−0.78		−0.79	2.79	4.29
3811.28	1713 –	27944	0.21	15		−3.67			−3.84		−3.51			−3.76	−0.18	1.32
3831.69	3410 –	29501	0.42	31	−1.64	−1.63	−1.60	−1.65	−1.52					−1.61	1.97	3.46
3832.87	1332 –	27415	0.17	1		−2.96	−2.85		−2.99		−2.72			−2.93	0.65	2.14
3844.26	28569 –	54575	3.54	137			−0.61		0.21							
3844.56	31786 –	57790	3.94	181			−0.57		0.24							
3854.68	30923 –	56858	3.83				−0.34									
3855.84	33112 –	59040	4.10				−0.45									
3858.30	3410 –	29321	0.42	32	−0.62	−0.48	−0.66	−0.65		−0.38				−0.56	3.03	4.50
3863.06	30923 –	56802	3.83	181			0.11		0.53		−0.10					
3871.59	30980 –	56802	3.84	181			−0.38				−0.78					
3885.87	2217 –	27944	0.27	1		−3.71								−3.71	−0.12	1.35
3889.67	1713 –	27415	0.21	15	−2.41	−3.10	−2.16		−2.81		−2.60					
3908.92	29084 –	54660	3.60	117			−0.44		0.44		−0.16					
3912.29	30619 –	56173	3.80	151					0.34		−0.16					
3912.97	205 –	25754	0.03	15		−3.48	−3.20		−3.83		−3.24					
3941.84	30913 –	56275	3.83	171					0.07		−0.62					
3944.11	29321 –	54668	3.63	151					0.57		0.11					
3954.53	29481 –	54761	3.65						−0.03		−0.51					
3962.13	31031 –	56263	3.85	199					0.09		−0.45					
3970.48	29481 –	54660	3.65	151			−0.24		0.53		0.09					
3972.16	3410 –	28578	0.42	29	−2.19		−2.34		−2.42		−2.30			−2.32	1.28	2.71
3973.55	3410 –	28569	0.42	31	−1.71		−1.88	−1.75	−1.97		−1.82			−1.82	1.78	3.21
3974.64	31031 –	56184	3.85	198			−0.16		0.63		−0.01					
3984.14	29669 –	54761	3.68	171			−0.39		0.29		−0.07		−0.68			
3986.36	25754 –	50832	3.19										−2.03			
3993.93	29669 –	54700	3.68	170					−0.01		−0.34		−0.83			
3996.12	33501 –	58518	4.15										−1.40			
3999.03	29669 –	54668	3.68										−1.31			
4002.51	33611 –	58588	4.17										−1.10			
4009.98	29321 –	54251	3.63	150			−0.80		−1.19		−1.11		−1.22			
4012.58	33611 –	58526	4.17										−1.10			
4017.44	29888 –	54773	3.70	171			−0.45		0.18		−0.20		−0.68			
4019.07	15610 –	40484	1.93	72			−1.99		−2.05		−2.19		−2.40			
4022.05	32973 –	57829	4.09	241			−0.34				−0.95		−0.79			
4024.00	29889 –	54732	3.70	170							−0.53		−0.82			
4025.10	32973 –	57810	4.09	240			−0.46						−0.84	−0.65	2.95	4.36
4025.42	29833 –	54668	3.70	117					0.00				−1.04			
4027.66	31442 –	56263	3.90								−0.39		−0.63			
4028.49	32973 –	57790	4.09										−1.24			
4039.03	15610 –	40361	1.93										−3.07			
4045.38	25754 –	50466	3.19				−0.98									
4046.75	32973 –	57678	4.09								−1.25		−0.99			
4051.18	33112 –	57790	4.10	239									−0.99			

TABLE 2.—*Oscillator Strengths for Ni* I—Continued

Wavelength Å	Energy Levels K		Lower e.p. Volts	Mult. No.	CB	K	CHC	AA	OBA	OBS	HD	PP	IC	Best	Log gfλ	Log gA/λ
(1)	(2)	(3)	(4)	(5)	(6)	(7)	(8)	(9)	(10)	(11)	(12)	(13)	(14)	(15)	(16)	(17)
4057.27	26666 –	51306	3.31	89			−1.08		−0.30		−1.16		−1.28			
4059.66	27415 –	52041	3.40										−1.90			
4064.37	30980 –	55577	3.84	179			−0.23		−0.22		−0.50		−0.58	−0.34	3.27	4.66
4069.15	29669 –	54237	3.68				−0.88						−1.26			
4072.86	31031 –	55577	3.85	197					−0.92		−1.22		−1.40			
4074.90	3410 –	27944	0.42	28					−4.45		−4.24		−4.05			
4093.03	34163 –	58588	4.23				−0.24						−1.29			
4103.57	34163 –	58526	4.23										−1.29			
4112.44	33501 –	57810	4.15										−1.64			
4115.98	33501 –	57790	4.15	255			0.06		−0.23		−0.48		−0.38			
4121.98	29501 –	53754	3.66										−1.39			
4123.79	33501 –	57744	4.15								−1.04		−0.94			
4130.52	29501 –	53704	3.66										−1.98			
4131.17	33590 –	57790	4.16										−1.23			
4138.49	33611 –	57768	4.17	237			−0.31		−0.82		−0.94		−0.91			
4142.16	31442 –	55577	3.90	212									−1.10			
4142.96	32973 –	57104	4.09								−0.78		−0.92			
4148.73	27944 –	52041	3.46	89									−1.42			
4150.37	31786 –	55874	3.94	178			−0.32		−0.40		−0.63		−0.77			
4158.53	34409 –	58449	4.26								−1.34		−1.26			
4161.33	25754 –	49778	3.19	86							−1.61		−1.88			
4164.64	3410 –	27415	0.42	28			−3.21		−4.37		−3.68		−4.15			
4165.44	32973 –	56974	4.09										−2.08			
4166.96	33112 –	57104	4.10				−0.30		−0.53		−0.75		−0.82			
4184.47	27415 –	51306	3.40	89			−0.75		−0.42		−0.66		−0.91			
4188.97	29889 –	53754	3.70										−1.81			
4193.70	30923 –	54761	3.83										−1.72			
4195.52	32973 –	56802	4.09	239			0.25		0.17		−0.09		−0.05	0.12	3.74	5.08
4200.45	26666 –	50466	3.31	89			−0.40		−0.18		−0.29		−0.64			
4201.71	32973 –	56767	4.09	238			0.26		0.35				−0.03	0.19	3.81	5.14
4202.14	31786 –	55577	3.94	179									−0.96	−0.96	2.66	3.99
4217.78	28569 –	52272	3.54										−2.24	−2.24	1.39	2.71
4221.68	26666 –	50346	3.31	86			−0.99				−1.13		−1.37	−1.16	2.47	3.79
4226.39	33112 –	56767	4.10										−0.91	−0.91	2.72	4.04
4229.49	31031 –	54668	3.85										−1.62	−1.62	2.01	3.33
4231.03	28569 –	52197	3.54	136			−0.42				−0.29		−0.71			
4235.29	34163 –	57768	4.23								−1.36			−1.36	2.27	3.58
4236.37	33112 –	56711	4.10	237							−0.72		−0.66	−0.69	2.94	4.25
4246.76	30163 –	53704	3.74										−2.02	−2.02	1.61	2.92
4252.02	30192 –	53704	3.74	136							−1.13		−1.44	−1.28	2.35	3.66
4260.92	28578 –	52041	3.54										−2.14	−2.14	1.49	2.80
4284.68	25754 –	49086	3.19	86			−0.59				−0.29		−0.61	−0.50	3.13	4.43
4285.18	27415 –	50745	3.40	86									−1.74	−1.74	1.89	3.19
4287.99	30923 –	54237	3.83	178			0.40				0.44		0.39	0.41	4.04	5.34
4290.26	27415 –	50717	3.40										−1.94	−1.94	1.69	2.99
4295.88	30980 –	54251	3.84	178			0.04				0.06		−0.06	0.01	3.64	4.93
4296.97	33501 –	56767	4.15								−1.14		−1.14	−1.14	2.49	3.78
4298.51	30980 –	54237	3.84	178			−0.51						−0.77	−0.64	2.99	4.28
4298.76	3410 –	26666	0.42	28									−4.59	−4.59	−0.96	0.33
4302.09	28068 –	51306	3.48	102									−1.64	−1.64	1.99	3.28
4307.28	33501 –	56711	4.15				−0.31				−0.72		−0.84			
4322.94	27580 –	50706	3.42										−1.74	−1.74	1.90	3.18
4325.36	29084 –	52197	3.60	116			−0.93						−0.75	−0.84	2.80	4.08
4325.60	26666 –	49778	3.31	86			−0.32						−0.36	−0.34	3.30	4.58
4330.70	30619 –	53704	3.80	149			−0.50				−0.46		−0.73	−0.56	3.08	4.35
4331.64	13521 –	36601	1.68	52			−1.38				−1.20		−1.52	−1.37	2.27	3.54
4333.19	33112 –	56184	4.10										−1.03	−1.03	2.61	3.88
4341.45	29013 –	52041	3.60										−1.73	−1.73	1.91	3.18
4355.90	29321 –	52272	3.63	149			−0.56				−0.38		−0.73	−0.56	3.08	4.35
4357.85	34163 –	57104	4.23	256							−1.82		−1.79	−1.80	1.84	3.11

TABLE 2.—*Oscillator Strengths for Ni* I—Continued

Wavelength Å	Energy Levels K		Lower e.p. Volts	Mult. No.	CB	K	CHC	AA	ULO	OBS	HD	PP	IC	Best	Log gfλ	Log gA/λ
(1)	(2)	(3)	(4)	(5)	(6)	(7)	(8)	(9)	(10)	(11)	(12)	(13)	(14)	(15)	(16)	(17)
4359.58	27415 –	50346	3.40	86			−0.17				0.06		−0.26	−0.09	3.55	4.82
4367.33	27944 –	50834	3.46	88							−1.42		−1.84			
4368.31	27580 –	50466	3.42	102			−0.66				−0.69		−1.01	−0.79	2.85	4.11
4370.04	29321 –	52197	3.63	149			−0.95				−0.72		−1.04	−0.90	2.74	4.00
4382.70	27944 –	50754	3.46										−1.84	−1.84	1.80	3.06
4382.87	31442 –	54251	3.90								−0.82		−1.10	−0.96	2.68	3.94
4384.53	27944 –	50745	3.46	86			−0.46				−0.22		−0.50	−0.39	3.25	4.51
4386.46	30913 –	53704	3.83	168			−0.54				−0.71		−1.05			
4389.86	27944 –	50717	3.46	87			−0.80				−0.55		−0.91	−0.75	2.89	4.15
4390.32	29501 –	52272	3.66	136							−0.69		−1.03	−0.86	2.78	4.04
4396.92	28569 –	51306	3.54								−1.49		−1.79	−1.64	2.00	3.25
4398.62	28578 –	51306	3.54	102							−1.00		−1.16	−1.08	2.56	3.81
4399.60	31031 –	53754	3.85	196			−0.20				−0.29		−0.46	−0.32	3.32	4.57
4400.87	29481 –	52197	3.65	149			−0.27				−0.15		−0.50	−0.31	3.33	4.58
4401.54	25754 –	48467	3.19	86	0.83		0.81						0.93	0.86	4.50	5.75
4410.52	26666 –	49333	3.31	88			−0.50				−0.27		−0.67	−0.48	3.16	4.41
4422.43	26666 –	49272	3.31										−2.38	−2.38	1.27	2.51
4422.99	29669 –	52272	3.68	168							−0.73		−1.17			
4424.84	33590 –	56184	4.16	262							−1.41		−1.94			
4431.03	33611 –	56173	4.17										−1.24	−1.24	2.41	3.64
4433.82	34163 –	56711	4.23										−1.80	−1.80	1.85	3.08
4435.35	29501 –	52041	3.66								−1.31		−1.59	−1.45	2.20	3.43
4436.97	28213 –	50745	3.50	86			−0.14				−0.06		−0.38	−0.19	3.46	4.69
4437.57	29669 –	52197	3.68	168			−0.40				−0.31		−0.71	−0.47	3.18	4.41
4441.44	26666 –	49175	3.31								−1.28		−1.69			
4442.43	28213 –	50717	3.50	87			−0.64				−0.57		−0.94	−0.72	2.93	4.16
4444.55	26666 –	49159	3.31										−2.56	−2.56	1.09	2.32
4450.10	31786 –	54251	3.94	178									−1.28	−1.28	2.37	3.60
4450.21	33112 –	55577	4.10	236									−1.28	−1.28	2.37	3.60
4459.03	26666 –	49086	3.31	86	0.78		0.69				0.82		0.76	0.76	4.41	5.64
4462.45	27944 –	50346	3.46	86	0.23		0.23				0.44		0.31	0.30	3.95	5.18
4463.42	28068 –	50466	3.48	102			−0.75				−0.63		−0.87	−0.75	2.90	4.12
4466.38	29889 –	52272	3.70	168									−0.78	−0.78	2.87	4.09
4470.48	27415 –	49778	3.40	86	0.67		0.51				0.68		0.51	0.59	4.24	5.46
4480.56	31442 –	53754	3.90	211							−0.52		−0.76	−0.64	3.01	4.23
4481.24	29889 –	52197	3.70	168							−1.18		−1.55	−1.36	2.29	3.51
4484.49	29013 –	51306	3.60	102							−1.80		−1.93	−1.86	1.79	3.01
4490.53	28569 –	50832	3.54	134							−0.59		−0.94	−0.76	2.89	4.11
4492.33	28578 –	50832	3.54								−1.56		−1.98	−1.77	1.88	3.10
4501.67	29833 –	52041	3.70	115							−1.37		−1.63	−1.50	2.15	3.36
4506.30	28569 –	50754	3.54	133							−1.22		−1.44	−1.33	2.32	3.53
4508.10	28578 –	50754	3.54										−2.30	−2.30	1.35	2.56
4512.99	29889 –	52041	3.70	163			−0.37				−0.50		−0.64	−0.50	3.15	4.36
4513.32	35639 –	57790	4.42										−1.32	−1.32	2.33	3.54
4513.88	28569 –	50717	3.54	131									−2.31	−2.31	1.34	2.55
4517.84	28578 –	50706	3.54	103							−1.76		−1.94	−1.85	1.80	3.01
4519.98	13521 –	35639	1.68	51			−2.08				−2.04		−2.25	−2.12	1.54	2.74
4521.87	30163 –	52272	3.74	116							−1.51		−1.68	−1.60	2.06	3.26
4523.70	28578 –	50678	3.54	99									−2.18	−2.18	1.48	2.68
4528.53	33501 –	55577	4.15										−0.45	−0.45	3.21	4.41
4542.24	34163 –	56173	4.23										−1.44	−1.44	2.22	3.41
4546.93	33590 –	55577	4.16	261			0.72						0.48	0.60	4.26	5.45
4547.22	29321 –	51306	3.63	146			0.05						−0.25	−0.10	3.56	4.75
4551.23	33611 –	55577	4.17	236			0.09				−0.31		−0.14	−0.12	3.54	4.73
4553.17	29501 –	51457	3.66	135							−0.68		−0.75	−0.72	2.94	4.13
4559.93	28542 –	50466	3.54	115							−0.76		−0.81	−0.78	2.88	4.07
4565.15	27415 –	49314	3.40	88									−2.27	−2.27	1.39	2.58
4567.41	28578 –	50466	3.54	102							−1.43		−1.36	−1.40	2.26	3.44
4569.64	30163 –	52041	3.74										−1.84	−1.84	1.82	3.00
4573.98	27415 –	49272	3.40	87							−1.67		−1.63	−1.65	2.01	3.19

TABLE 2.—*Oscillator Strengths for Ni* I—Continued

Wavelength Å	Energy Levels K		Lower e.p. Volts	Mult. No.	CB	K	CHC	AA	ULO	OBS	HD	PP	IC	Best	Log gfλ	Log gA/λ
(1)	(2)	(3)	(4)	(5)	(6)	(7)	(8)	(9)	(10)	(11)	(12)	(13)	(14)	(15)	(16)	(17)
4580.60	29481 –	51306	3.65	146							−0.85		−0.76	−0.80	2.86	4.04
4581.42	29013 –	50834	3.60										−1.34	−1.34	2.32	3.50
4592.53	28578 –	50346	3.54	98	0.57		0.48				0.60		0.61	0.56	4.22	5.40
4595.94	27580 –	49333	3.42	101							−0.39		−0.57	−0.48	3.18	4.36
4597.65	27415 –	49159	3.40										−2.01	−2.01	1.65	2.83
4600.36	29013 –	50745	3.60	98	0.30		0.19				0.38		0.26	0.28	3.94	5.12
4604.99	28068 –	49778	3.48	98	0.77		0.58				0.73		0.85	0.73	4.39	5.56
4606.22	29013 –	50717	3.60	100	0.30		−0.15				−0.01		0.06	−0.03	3.63	4.80
4609.92	32973 –	54660	4.09										−0.85	−0.85	2.81	3.98
4614.58	29013 –	50678	3.60	99							−1.30		−1.27	−1.28	2.38	3.55
4617.96	30392 –	52041	3.77	115							−0.89		−0.83	−0.86	2.80	3.97
4620.39	29669 –	51306	3.68	163							−1.59		−1.51	−1.55	2.11	3.28
4629.54	27580 –	49175	3.42										−1.35	−1.35	2.32	3.48
4641.56	27415 –	48953	3.40										−1.98	−1.98	1.69	2.84
4647.43	29321 –	50832	3.63	148									−1.11	−1.11	2.56	3.71
4648.65	27580 –	49086	3.42	98	0.78		0.73				0.89			0.80	4.47	5.62
4655.65	29833 –	51306	3.70	115							−0.43		−0.38	−0.40	3.27	4.42
4666.98	30619 –	52041	3.80	146			−0.03				−0.17		−0.20	−0.13	3.54	4.69
4667.76	29889 –	51306	3.70	163			0.06				0.03		0.08	0.06	3.73	4.88
4668.62	34163 –	55577	4.23								−1.11		−1.01	−1.06	2.61	3.76
4674.76	29321 –	50706	3.63								−0.57		−0.69	−0.63	3.04	4.18
4675.60	29084 –	50466	3.60	115							−0.84		−0.93	−0.88	2.79	3.93
4681.04	29321 –	50678	3.63	143									−1.80	−1.80	1.87	3.01
4686.21	29013 –	50346	3.60	98	0.39		0.26				0.38		0.23	0.32	3.99	5.13
4698.39	32973 –	54251	4.09	235			−0.03				−0.29		−0.20	−0.17	3.50	4.64
4701.35	28068 –	49333	3.48	101									−0.61	−0.61	3.06	4.20
4701.53	32973 –	54237	4.09	235			0.52						0.54	0.53	4.20	5.34
4703.81	29501 –	50754	3.66	133			0.04				−0.06		0.34	0.11	3.78	4.92
4705.51	28068 –	49314	3.48	101									−1.22	−1.22	2.45	3.59
4705.92	29501 –	50745	3.66	128									−0.77	−0.77	2.90	4.04
4710.05	29481 –	50706	3.65										−1.34	−1.34	2.33	3.46
4712.06	29501 –	50717	3.66	131							−0.76		−0.44	−0.60	3.07	4.20
4714.42	27261 –	48467	3.38	98	0.84		1.02				0.84			0.90	4.57	5.70
4715.76	28578 –	49778	3.54	98	0.26		0.45				0.28		0.62	0.40	4.07	5.20
4723.88	29669 –	50832	3.68	167							−1.83		−1.53	−1.68	1.99	3.12
4727.84	29321 –	50466	3.63	146							−1.19		−0.84	−1.01	2.66	3.79
4728.40	30163 –	51306	3.74	115							−1.48		−1.02			
4729.28	33112 –	54251	4.10	235							−1.01		−0.55			
4731.80	30913 –	52041	3.83	163			0.07				−0.29		0.00	−0.07	3.61	4.73
4732.47	33112 –	54237	4.10	235			0.29				−0.21		0.20	0.09	3.77	4.89
4736.51	28068 –	49175	3.48	99							−1.68		−1.43	−1.56	2.12	3.24
4740.17	28068 –	49159	3.48	99							−1.16		−1.02	−1.09	2.59	3.71
4752.12	29669 –	50706	3.68	165			−0.27						−0.42	−0.35	3.33	4.44
4752.42	29501 –	50537	3.66	132			−0.06						0.15	0.04	3.72	4.83
4754.75	29321 –	50346	3.63	141			−0.14				−0.39		−0.15	−0.23	3.45	4.56
4756.51	28068 –	49086	3.48	98	0.39		0.48				0.35		0.63	0.46	4.14	5.25
4758.42	31031 –	52041	3.85	193							−1.42		−1.29	−1.36	2.32	3.43
4762.63	15610 –	36601	1.93	71			−1.71				−1.87		−1.70	−1.76	1.92	3.03
4763.94	29481 –	50466	3.65	146	0.17		0.15				−0.08		0.12	0.09	3.77	4.88
4772.86	29889 –	50834	3.70	162							−0.99		−0.83	−0.91	2.77	3.88
4773.41	29889 –	50832	3.70	167							−0.93		−0.89	−0.91	2.77	3.88
4786.28	13521 –	34409	1.68	50									−2.33	−2.33	1.35	2.45
4786.54	27580 –	48467	3.42	98	0.47		0.53							0.50	4.18	5.28
4790.97	15734 –	36601	1.95	71							−2.77		−2.73	−2.75	0.93	2.03
4791.24	29889 –	50754	3.70										−1.32	−1.32	2.36	3.46
4793.43	29889 –	50745	3.70	158							−1.67		−1.40	−1.54	2.14	3.24
4795.81	29501 –	50346	3.66	128							−1.85		−1.66	−1.76	1.92	3.02
4799.42	31442 –	52272	3.90										−1.46	−1.46	2.22	3.32
4799.80	29889 –	50717	3.70	161									−0.72	−0.72	2.96	4.06
4806.99	29669 –	50466	3.68	163	0.34						0.00		0.24	0.19	3.87	4.97

TABLE 2.—*Oscillator Strengths for Ni* I—Continued

Wavelength Å	Energy Levels K		Lower e.p. Volts	Mult. No.	CB	K	CHC	AA	ULO	OBS	HD	PP	IC	Best	Log gfλ	Log gA/λ
(1)	(2)	(3)	(4)	(5)	(6)	(7)	(8)	(9)	(10)	(11)	(12)	(13)	(14)	(15)	(16)	(17)
4808.54	28542 –	39333	3.54	114									−2.23	−2.23	1.45	2.55
4808.89	29889 –	50678	3.70	160									−0.74	−0.74	2.94	4.04
4811.98	29501 –	50276	3.66	130							−0.87		−0.64	−0.76	2.92	4.02
4812.90	32982 –	53754	4.09								−1.30		−1.05	−1.18	2.50	3.60
4814.60	29013 –	49778	3.60	98							−1.04		−0.87	−0.96	2.72	3.82
4815.93	28569 –	49328	3.54	131							−1.17		−1.03	−1.10	2.58	3.68
4817.82	33501 –	54251	4.15	254							−0.56		−0.21	−0.38	3.30	4.40
4819.18	28569 –	49314	3.54										−1.79	−1.79	1.89	2.99
4821.12	33501 –	54237	4.15	254							−0.56		−0.15			
4829.02	28569 –	49271	3.54	131	0.25		0.29				0.33		0.34	0.30	3.98	5.07
4831.17	29084 –	49778	3.60	100	0.24		0.38				0.26		0.35	0.31	3.99	5.08
4832.69	30619 –	51306	3.80	146			0.07				−0.29		−0.13	−0.12	3.56	4.65
4836.28	30163 –	50834	3.74	114							−1.37		−1.41	−1.39	2.29	3.38
4836.85	30163 –	50832	3.74										−1.59	−1.59	2.09	3.18
4838.64	33590 –	54251	4.16	260			0.43						0.09	0.26	3.94	5.03
4841.68	29889 –	50537	3.70	164									−1.65	−1.65	2.03	3.12
4841.97	33590 –	54237	4.16	260							−1.23		−1.03	−1.13	2.56	3.64
4843.16	13521 –	34163	1.68	50							−2.60		−2.73	−2.66	1.03	2.11
4843.51	33611 –	54251	4.17	235									−0.53	−0.53	3.16	4.24
4845.17	29833 –	50466	3.70	115							−1.44		−1.71	−1.58	2.11	3.19
4852.55	28569 –	49171	3.54	130			−0.38				−0.39		−0.52	−0.43	3.26	4.34
4853.78	28578 –	49175	3.54	99							−0.86		−1.03	−0.94	2.75	3.83
4855.41	28569 –	49159	3.54	130	0.55		0.54				0.57		0.53	0.55	4.24	5.32
4857.39	30163 –	50745	3.74	111			0.04				−0.23		−0.23	−0.14	3.55	4.62
4863.93	30163 –	50717	3.74	113									−0.40	−0.40	3.29	4.36
4864.27	30192 –	50745	3.74	128									−0.54	−0.54	3.15	4.22
4866.27	28542 –	49086	3.54	111	0.42		0.42				0.37		0.47	0.42	4.11	5.18
4870.83	30192 –	50717	3.74	131			−0.12				−0.23		−0.22	−0.19	3.50	4.57
4873.25	30163 –	50678	3.74	112									−0.66	−0.66	3.03	4.10
4873.44	29833 –	50346	3.70	111	0.25		0.30				0.23		0.22	0.25	3.94	5.01
4874.79	28578 –	49086	3.54	98							−0.83		−0.82	−0.82	2.87	3.94
4886.71	29889 –	50346	3.70	158									−1.11	−1.11	2.58	3.65
4886.98	29321 –	49778	3.63	141							−0.50		−0.53	−0.52	3.17	4.24
4890.44	30392 –	50834	3.77	114							−1.86		−1.92	−1.89	1.80	2.87
4900.97	28068 –	48467	3.48	98							−1.04		−1.05	−1.04	2.65	3.71
4904.41	28569 –	48953	3.54	129	0.48		0.46				0.49		0.36	0.45	4.14	5.20
4912.02	30392 –	50745	3.77	111			−0.02				−0.21		−0.17	−0.13	3.56	4.62
4913.97	30192 –	50537	3.74	132			0.00				−0.03		0.03	0.00	3.69	4.75
4918.36	30980 –	51306	3.84	177	0.43		0.54						0.56	0.51	4.20	5.26
4918.71	30392 –	50717	3.77	113			−0.02						−0.41	−0.22	3.47	4.53
4925.56	29481 –	49778	3.65	141			−0.10				−0.19		−0.24	−0.18	3.51	4.57
4930.80	31031 –	51306	3.85	193							−0.76		−0.72	−0.74	2.95	4.01
4935.83	31786 –	52040	3.94	177	0.26		0.50				0.25		0.28	0.32	4.01	5.06
4937.35	29084 –	49333	3.60	114			0.00				0.12		−0.06	0.02	3.71	4.76
4945.44	30619 –	50834	3.80	145									−0.47	−0.47	3.22	4.27
4946.03	30619 –	50832	3.80	148									−0.90	−0.90	2.79	3.84
4952.28	29084 –	49272	3.60	113							−0.71		−1.00	−0.86	2.83	3.88
4953.21	30163 –	50346	3.74	111			0.15				−0.01		−0.03	0.04	3.73	4.78
4965.17	30619 –	50754	3.80	147							−0.65		−0.87	−0.76	2.94	3.98
4967.53	30619 –	50745	3.80	141							−1.00		−1.08	−1.04	2.66	3.70
4971.34	36601 –	56711	4.54	274			0.73				0.22		0.65			
4974.36	30619 –	50717	3.80										−1.52	−1.52	2.18	3.21
4976.13	29084 –	49174	3.60	112									−0.85	−0.85	2.85	3.88
4976.32	13521 –	33611	1.68	49									−2.59	−2.59	1.11	2.14
4976.70	34163 –	54251	4.23	254									−1.00	−1.00	2.70	3.73
4980.17	29084 –	49158	3.60	112	0.52		0.61				0.61		0.50	0.56	4.26	5.29
4984.11	30619 –	50678	3.80	143	0.64		0.72				0.70		0.66	0.68	4.38	5.41
4995.65	29321 –	49333	3.63	145							−0.99		−1.27	−1.13	2.57	3.60
4996.84	29321 –	49328	3.63	144							−0.39		−0.54	−0.41	3.29	4.32
4998.22	29084 –	49086	3.60	111			0.05				−0.09		−0.14	−0.06	3.64	4.67

TABLE 2.—*Oscillator Strengths for Ni* I—Continued

Wavelength Å	Energy Levels K		Lower e.p. Volts	Mult. No.	CB	K	CHC	AA	ULO	OBS	HD	PP	IC	Best	Log gfλ	Log gA/λ
(1)	(2)	(3)	(4)	(5)	(6)	(7)	(8)	(9)	(10)	(11)	(12)	(13)	(14)	(15)	(16)	(17)
5000.34	29321 –	49314	3.63	145	0.07		0.34				0.20		0.13	0.18	3.88	4.91
5003.74	13521 –	33501	1.68	50							−2.53		−2.66	−2.60	1.10	2.13
5010.02	30392 –	50346	3.77	111			0.00				−0.38		−0.38	−0.25	3.45	4.47
5010.94	29321 –	49272	3.63	144			−0.06				−0.23		−0.39	−0.23	3.47	4.49
5012.44	29833 –	49778	3.70	111	0.18		0.32				0.06		0.09	0.16	3.86	4.88
5014.22	35639 –	55577	4.42								−0.26		−0.01	−0.14	3.56	4.58
5017.58	28542 –	48467	3.54	111	0.53		0.67				0.58		0.58	0.59	4.29	5.31
5018.29	30913 –	50834	3.83	162			0.27				0.12		−0.05	0.11	3.81	4.83
5026.48	29889 –	49778	3.70	158							−1.71		−1.57	−1.64	2.06	3.08
5032.73	31442 –	51306	3.90	207							−0.65		−0.54	−0.60	3.10	4.12
5035.36	29321 –	49175	3.63	143	0.90		0.80						0.71	0.80	4.50	5.52
5035.96	29481 –	49333	3.65	145			0.01						−0.18	−0.08	3.62	4.64
5038.59	30913 –	50754	3.83	166			0.14				0.01		−0.08	0.02	3.72	4.74
5039.36	29321 –	49159	3.63	142							−0.52		−0.57	−0.54	3.16	4.18
5041.03	30913 –	50745	3.83	158							−0.41		−0.29	−0.35	3.35	4.37
5042.18	29501 –	49328	3.66	131			0.11				0.01		0.02	0.05	3.75	4.77
5048.06	30913 –	50717	3.83	161							−0.41		−0.44	−0.42	3.28	4.29
5048.84	31031 –	50832	3.85	195	0.20		0.30				0.17		0.22	0.22	3.92	4.93
5051.51	29481 –	49272	3.65	144							−0.35		−0.36	−0.36	3.34	4.35
5053.31	30923 –	50706	3.83								−1.50		−1.28	−1.39	2.31	3.32
5057.99	29321 –	49086	3.63	141							−0.69		−0.63	−0.66	3.04	4.05
5067.79	30619 –	50346	3.80	141							−1.02		−0.78	−0.90	2.80	3.81
5068.79	31031 –	50754	3.85								−0.78		−0.65	−0.72	2.98	3.99
5075.30	30980 –	50678	3.84										−1.10	−1.10	2.61	3.61
5076.33	29481 –	49175	3.65	143							−0.79		−0.61	−0.70	3.01	4.01
5079.96	14729 –	34409	1.83	60									−2.00	−2.00	1.71	2.71
5080.53	29481 –	49158	3.65	143	0.91								0.91	0.91	4.62	5.62
5081.11	31031 –	50706	3.85	194	0.82						0.91		0.90	0.88	4.59	5.59
5082.36	29501 –	49171	3.66	130							0.08		0.06	0.07	3.78	4.78
5084.09	29669 –	49333	3.68	162	0.32						0.54		0.51	0.46	4.17	5.17
5085.49	29501 –	49159	3.66	130							−0.54		−0.61	−0.58	3.13	4.12
5088.53	31031 –	50678	3.85	190									−0.40	−0.40	3.31	4.30
5088.96	29669 –	49314	3.68	162									−0.60	−0.60	3.11	4.10
5094.41	30913 –	50537	3.83	164							−0.50		−0.47	−0.48	3.23	4.22
5096.86	30163 –	49778	3.74	111							−0.30		−0.19	−0.24	3.47	4.46
5099.31	29481 –	49086	3.65	141	0.15						0.18		0.28	0.20	3.91	4.90
5099.93	29669 –	49271	3.68	161	0.32						0.45		0.41	0.39	4.10	5.09
5102.96	13521 –	33112	1.68	49							−2.28		−2.41	−2.34	1.37	2.36
5115.39	30923 –	50466	3.83	177	0.32						0.53		0.70	0.52	4.23	5.22
5121.56	31786 –	51306	3.94	177							−0.46		−0.34	−0.40	3.31	4.30
5125.23	29669 –	49175	3.68	160							−0.09		−0.20	−0.14	3.57	4.55
5126.82	29833 –	49333	3.70										−2.02	−2.02	1.69	2.67
5128.09	29833 –	49328	3.70	113							−1.18		−1.14	−1.16	2.55	3.53
5129.37	29669 –	49159	3.68	159	0.16						0.03		−0.02	0.06	3.77	4.75
5130.37	30980 –	50466	3.84	177							−0.64		−0.53	−0.58	3.13	4.11
5131.77	29833 –	49314	3.70	114							−0.36		−0.37	−0.36	3.35	4.33
5137.07	13521 –	32982	1.68	48	−1.66						−1.41		−1.55	−1.54	2.17	3.15
5139.25	29501 –	48953	3.66	129							−0.38		−0.39	−0.38	3.33	4.31
5142.78	29888 –	49328	3.70	161	0.29						0.35		0.25	0.30	4.01	4.99
5146.48	29888 –	49314	3.70	162	0.51						0.53		0.44	0.49	4.20	5.18
5148.67	29669 –	49086	3.68	158							−1.15		−1.08	−1.12	2.59	3.57
5155.12	31442 –	50834	3.90	206							−0.05		−0.08	−0.06	3.65	4.63
5155.76	31442 –	50832	3.90	210	0.63						0.48		0.50	0.54	4.25	5.23
5157.98	29084 –	48467	3.60	111							−0.84		−0.78	−0.81	2.90	3.88
5168.66	29833 –	49175	3.70	112	0.11						0.13		0.13	0.13	3.84	4.81
5176.56	31442 –	50754	3.90	209	0.15						0.10		0.03	0.06	3.77	4.74
5179.12	31442 –	50745	3.90	202							−0.96		−0.90	−0.93	2.78	3.75
5182.74	32982 –	52272	4.09										−1.27	−1.27	2.44	3.41
5184.56	29889 –	49171	3.70	159							−0.21		−0.34	−0.28	3.43	4.40
5186.55	31442 –	50717	3.90	205							−0.74		−0.71	−0.72	2.99	3.96

TABLE 2.—*Oscillator Strengths for Ni* I—Continued

Wave-length	Energy Levels	Lower e.p.	Mult. No.	CB	K	CHC	AA	ULO	OBS	HD	PP	IC	Best	Log gfλ	Log gA/λ
Å	K	Volts													
(1)	(2) (3)	(4)	(5)	(6)	(7)	(8)	(9)	(10)	(11)	(12)	(13)	(14)	(15)	(16)	(17)
5187.82	29889 – 49159	3.70	159							−1.29		−1.20	−1.24	2.47	3.44
5192.49	29833 – 49086	3.70	111							−0.69		−0.64	−0.66	3.06	4.02
5197.16	31442 – 50678	3.90	204							−0.61		−0.53	−0.57	3.15	4.11
5200.35	32973 – 52197	4.09										−1.64	−1.64	2.08	3.04
5216.48	30163 – 49328	3.74	113							−0.68		−0.79	−0.74	2.98	3.93
5217.94	33112 – 52272	4.10										−1.70	−1.70	2.02	2.97
5220.29	30163 – 49314	3.74	114							−0.66		−0.67	−0.66	3.06	4.01
5235.50	31442 – 50537	3.90	208							−0.48		−0.51	−0.50	3.22	4.17
5243.80	29889 – 48953	3.70								−1.66		−1.62	−1.64	2.08	3.02
5245.62	32982 -- 52041	4.09								−1.62		−1.43	−1.52	2.20	3.14
5248.38	31786 – 50834	3.94								−1.39		−1.36	−1.38	2.34	3.28
5249.04	31786 – 50832	3.94								−1.54		−1.54	−1.54	2.18	3.12
5259.48	30163 – 49171	3.74								−1.31		−1.39	−1.35	2.37	3.31
5262.83	30163 – 49159	3.74										−2.04	−2.04	1.68	2.62
5265.71	29481 – 48467	3.65	141							−1.11		−0.96	−1.13	2.59	3.53
5268.33	36601 – 55577	4.54	273							−0.48		−0.12	−0.30	3.42	4.36
5281.66	33112 – 52041	4.10	231							−0.85		−0.71	−0.78	2.94	3.88
5328.72	30192 – 48953	3.74	129							−2.06		−1.93	−2.00	1.73	2.64
5347.71	30619 – 49314	3.80	145							−1.39		−1.38	−1.38	2.35	3.26
5353.39	15734 – 34409	1.95	70							−2.18		−2.13	−2.16	1.57	2.48
5371.33	35639 – 54251	4.42								−0.17		0.12	−0.02	3.71	4.61
5386.36	31786 – 50346	3.94										−1.95	−1.95	1.78	2.68
5388.34	15610 – 34163	1.93	70							−2.93		−2.89	−2.91	0.82	1.72
5392.33	33501 – 52041	4.15	250							−0.77		−0.61	−0.69	3.04	3.94
5411.22	32982 – 51457	4.09	222							−0.23		−0.09	−0.16	3.57	4.46
5424.54	33611 – 52041	4.17	231									0.02	0.02	3.75	4.64
5424.64	15734 – 34163	1.95	70					−1.95		−2.12		−2.02	−2.03	1.70	2.59
5428.86	30913 – 49328	3.83	161					−1.45		−1.73		−1.66	−1.61	2.12	3.01
5430.37	30923 – 49333	3.83						−0.96		−1.31		−1.40			
5435.86	16017 – 34409	1.99	70	−1.89				−1.78		−1.94		−1.94	−1.89	1.85	2.73
5452.82	30980 – 49314	3.84						−1.01				−1.24	−1.12	2.62	3.49
5453.24	32973 – 51306	4.09	231					−0.69				−0.70	−0.70	3.04	3.91
5462.49	31031 – 49333	3.85	192					−0.07		−0.38		−0.32	−0.25	3.49	4.36
5463.92	31031 – 49328	3.85						−1.67				−1.67	−1.67	2.07	2.94
5468.10	31031 – 49314	3.85	192					−0.70		−1.01		−0.78	−0.83	2.91	3.78
5476.90	14729 – 32982	1.83	59	−0.68						−0.48			−0.58	3.16	4.03
5480.78	31031 – 49272	3.85	191					−0.74		−0.99		−0.82	−0.85	2.89	3.76
5494.49	30980 – 49175	3.84										−1.49	−1.49	2.25	3.11
5494.88	33112 – 51306	4.10	231					−0.30		−0.55		−0.37	−0.41	3.33	4.19
5499.41	30980 – 49159	3.84	176					−1.40		−1.70		−1.55	−1.55	2.19	3.05
5504.10	30923 – 49086	3.83	175					−0.82		−1.10		−0.86	−0.93	2.81	3.67
5510.01	31031 – 49175	3.85	190	−0.19				−0.12		−0.35		−0.26	−0.23	3.51	4.37
5514.80	31031 – 49159	3.85	189					−1.12		−1.39		−1.12	−1.21	2.53	3.39
5520.76	34163 – 52272	4.23						−1.45					−1.45	2.29	3.15
5521.43	30980 – 49086	3.84	175					−1.44		−1.76		−1.57	−1.59	2.15	3.01
5537.11	31031 – 49086	3.85	188					−1.24		−1.70		−1.48			
5553.69	15610 – 33611	1.93	69					−2.54		−2.63		−2.56	−2.58	1.16	2.01
5578.72	13521 – 31442	1.68	47	−2.30				−2.20		−2.27		−2.27	−2.26	1.49	2.32
5587.86	15610 – 33501	1.93	70	−1.90				−1.83		−1.89		−1.85	−1.87	1.88	2.71
5589.36	31442 – 49328	3.90	205					−0.44		−0.53		−0.44	−0.47	3.28	4.11
5592.15	34163 – 52041	4.23	250									0.03	0.03	3.78	4.61
5592.26	15734 – 33611	1.95	69	−1.73				−1.66				−1.96	−1.78	1.97	2.80
5593.74	31442 – 49314	3.90	206					−0.14		−0.25		−0.18	−0.19	3.56	4.39
5600.02	32982 – 50834	4.09	219					−0.34		−0.52		−0.40	−0.42	3.33	4.16
5607.00	31442 – 49272	3.90	205					−1.25		−1.58		−1.27	−1.37	2.38	3.21
5614.78	33501 – 51306	4.15	250	0.14				0.13		−0.03		0.18	0.10	3.85	4.68
5625.32	32982 – 50754	4.09	221	−0.14				0.02		−0.17		−0.07	−0.09	3.66	4.48
5628.35	32982 – 50745	4.09	215					−0.57		−0.74		−0.53	−0.61	3.14	3.96
5637.12	32982 – 50717	4.09	218					−0.18		−0.41		−0.27	−0.29	3.46	4.28
5637.68	32973 – 50706	4.09						−1.13				−1.24	−1.18	2.57	3.39

TABLE 2.—*Oscillator Strengths for Ni* I—Continued

Wavelength Å	Energy Levels K		Lower e.p. Volts	Mult. No.	CB	K	CHC	AA	ULO	OBS	HD	PP	IC	Best	Log gfλ	Log gA/λ
(1)	(2)	(3)	(4)	(5)	(6)	(7)	(8)	(9)	(10)	(11)	(12)	(13)	(14)	(15)	(16)	(17)
5638.75	31442 –	49171	3.90	203					−0.93		−1.16		−0.92	−1.00	2.75	3.57
5641.12	33112 –	50834	4.10	230					−1.14		−1.22		−1.10	−1.15	2.60	3.42
5641.88	33112 –	50832	4.10	234					−0.27		−0.50		−0.30	−0.36	3.39	4.21
5642.61	31442 –	49159	3.90	203					−1.09				−1.08	−1.08	2.67	3.49
5643.08	33590 –	51306	4.16	259					−0.54				−0.43	−0.48	3.27	4.09
5649.70	33611 –	51306	4.17	231	−0.22				−0.29		−0.47		−0.30	−0.32	3.43	4.25
5663.99	36601 –	54251	4.54	272	0.08				0.08		−0.25		0.05	−0.01	3.74	4.55
5666.80	33112 –	50754	4.10	233					−1.34		−1.73		−1.26			
5669.95	34409 –	52041	4.26	250					−0.34		−0.57		−0.36	−0.42	3.33	4.14
5682.20	33112 –	50706	4.10	232	0.22				0.25		0.10		0.24	0.20	3.95	4.76
5691.48	33112 –	50678	4.10	228					−1.26		−1.59		−1.11			
5694.98	32982 –	50537	4.09	220	0.04				0.08		−0.06		0.11	0.04	3.80	4.60
5703.69	31786 –	49314	3.94						−1.09		−1.49		−1.13			
5709.55	13521 –	31031	1.68	46	−1.76				−1.96		−1.79		−1.74	−1.81	1.95	2.74
5711.89	15610 –	33112	1.93	69	−1.86				−1.98		−1.90		−1.80	−1.88	1.88	2.67
5715.07	32973 –	50466	4.09	231	0.16				0.21		0.15		0.31	0.21	3.97	4.76
5748.35	13521 –	30913	1.68	45					−2.74		−2.82		−2.67	−2.74	1.02	1.81
5749.29	31786 –	49175	3.94	176					−1.13		−1.42		−1.14	−1.23	2.53	3.32
5754.66	15610 –	32982	1.93	68	−1.69				−1.52		−1.72		−1.63	−1.64	2.12	2.90
5760.83	33112 –	50466	4.10	231	0.05				−0.06		−0.18		0.03	−0.04	3.72	4.50
5780.73	32982 –	50276	4.09	217					−1.28		−1.74		−1.28			
5796.08	15734 –	32982	1.95	68					−3.04		−3.18		−3.04	−3.09	0.67	1.44
5798.23	33590 –	50832	4.16						−1.05		−1.30		−1.02	−1.12	2.64	3.41
5805.22	33611 –	50832	4.17	234					0.02		−0.11		0.06	−0.01	3.75	4.52
5820.22	33501 –	50678	4.15						−1.81				−1.53	−1.67	2.09	2.86
5831.60	33611 –	50754	4.17	233					−0.26		−0.39		−0.33	−0.32	3.45	4.21
5831.74	34163 –	51306	4.23	250									−1.09	−1.09	2.68	3.44
5847.00	13521 –	30619	1.68	44					−2.93		−2.95		−3.03	−2.97	0.80	1.55
5857.75	33611 –	50678	4.17	228	0.21				0.13		0.09		0.09	0.13	3.90	4.65
5863.93	34409 –	51457	4.26	253					−1.15		−1.35		−1.07	−1.19	2.58	3.33
5892.87	16017 –	32982	1.99	68	−1.83				−1.77		−1.73		−1.84	−1.79	1.98	2.72
5906.50	33611 –	50537	4.17						−1.12				−1.08	−1.10	2.67	3.41
5923.94	33590 –	50466	4.16	259					−1.07				−0.91	−0.99	2.78	3.52
5925.80	13521 –	30392	1.68	42					−4.43					−4.43	−0.66	0.08
5996.74	34163 –	50834	4.23	249					−0.57				−0.51	−0.54	3.24	3.95
5997.59	34163 –	50832	4.23	252					−0.77				−0.65	−0.71	3.07	3.78
5998.85	33112 –	49778	4.10	226					−1.96				−1.50			
6007.31	13521 –	30163	1.68	42					−3.08				−2.78	−2.93	0.85	1.56
6025.76	34163 –	50754	4.23	251					−1.28				−1.12	−1.20	2.58	3.28
6039.30	34163 –	50717	4.23	248					−1.58				−1.35	−1.46	2.32	3.02
6053.69	34163 –	50678	4.23	247					−0.57				−0.43	−0.50	3.28	3.98
6086.28	34409 –	50834	4.26	249					−0.24				0.04	−0.10	3.68	4.37
6095.34	35639 –	52041	4.42						−1.86				−1.41			
6105.76	34163 –	50537	4.23						−1.59				−1.32	−1.46	2.33	3.01
6108.12	13521 –	29888	1.68	45	−2.16				−2.53				−2.20	−2.30	1.49	2.17
6111.07	32973 –	49333	4.09	230					−0.51				−0.47	−0.49	3.30	3.98
6116.18	32982 –	49328	4.09	218					−0.12				0.01	−0.06	3.73	4.40
6118.10	32973 –	49314	4.09	230					−1.82				−1.51	−1.66	2.13	2.80
6119.76	34409 –	50745	4.26	244					−1.01				−0.66	−0.84	2.95	3.62
6128.98	13521 –	29833	1.68	42					−3.14				−2.92	−3.03	0.76	1.43
6130.13	34409 –	50717	4.26	248					−0.54				−0.36	−0.45	3.34	4.01
6133.97	32973 –	49272	4.09	229					−1.42				−1.30	−1.36	2.43	3.10
6142.03	33501 –	49778	4.15	244					−1.67				−1.42	−1.54	2.25	2.92
6163.42	33112 –	49333	4.10	230					−0.26				−0.36	−0.31	3.48	4.14
6165.25	33112 –	49328	4.10	229									−1.58	−1.58	2.21	2.87
6170.58	32973 –	49175	4.09	228					−0.99				−0.81	−0.90	2.89	3.55
6175.36	32982 –	49171	4.09	217					−0.11				−0.03	−0.07	3.72	4.38
6176.81	32973 –	49158	4.09	228	0.16				0.16				0.23	0.18	3.97	4.63
6177.24	14729 –	30913	1.83	58					−3.42				−3.05	−3.28	0.51	1.17
6177.55	34163 –	50346	4.23	244									−1.15	−1.15	2.64	3.30

TABLE 2.—*Oscillator Strengths for Ni* I—Continued

Wavelength Å	Energy Levels K		Lower e.p. Volts	Mult. No.	CB	K	CHC	AA	ULO	OBS	HD	PP	IC	Best	Log gfλ	Log gA/λ
(1)	(2)	(3)	(4)	(5)	(6)	(7)	(8)	(9)	(10)	(11)	(12)	(13)	(14)	(15)	(16)	(17)
6179.99	32982 –	49159	4.09	214									−1.29	−1.29	2.50	3.16
6180.16	15610 –	31786	1.93	65					−3.60				−3.84	−3.72	0.07	0.73
6183.10	27944 –	44112	3.46						−2.63				−2.21			
6183.85	33611 –	49778	4.17	226					−1.49				−1.24	−1.36	2.43	3.09
6186.72	33112 –	49272	4.10	229					−0.46				−0.43	−0.44	3.35	4.01
6191.18	13521 –	29669	1.68	45	−2.17				−2.12				−2.12	−2.14	1.65	2.31
6198.63	34409 –	50537	4.26										−1.52	−1.52	2.27	2.93
6204.61	32973 –	49086	4.09	226					−0.68				−0.49	−0.58	3.21	3.87
6223.99	33112 –	49175	4.10	228					−0.55				−0.46	−0.50	3.29	3.94
6230.09	33112 –	49159	4.10	227					−0.85				−0.64	−0.74	3.05	3.70
6256.36	13521 –	29501	1.68	43	−2.08				−2.14				−2.19	−2.14	1.66	2.29
6258.59	33112 –	49086	4.10	226					−0.90				−0.76	−0.83	2.97	3.60
6259.60	32982 –	48953	4.09	216					−0.96				−0.82	−0.89	2.91	3.54
6271.78	26666 –	42606	3.31						−2.00				−2.04	−2.02	1.78	2.41
6272.64	34409 –	50346	4.26	244					−1.14				−1.13	−1.14	2.66	3.29
6300.34	34409 –	50276	4.26	246					−1.40				−1.43	−1.42	2.38	3.01
6314.66	15610 –	31442	1.93	67	−1.93				−1.76				−1.92	−1.87	1.93	2.55
6316.58	33501 –	49328	4.15	248					−1.34				−1.31	−1.32	2.48	3.10
6322.17	33501 –	49314	4.15	249					−0.69				−0.58	−0.64	3.16	3.78
6327.60	13521 –	29321	1.68	44					−2.80				−2.79	−2.80	1.00	1.62
6339.12	33501 –	49272	4.15	248					−0.10				−0.07	−0.08	3.72	4.34
6350.49	33590 –	49333	4.16						−1.25				−1.37	−1.31	2.49	3.11
6360.81	33611 –	49328	4.17	229					−0.55				−0.60	−0.58	3.22	3.83
6364.58	15734 –	31442	1.95	67					−3.56				−3.51	−3.54	0.26	0.87
6366.48	33611 –	49314	4.17	230					−0.32				−0.42	−0.37	3.43	4.04
6370.35	28569 –	44263	3.54	127					−1.21				−1.23	−1.22	2.58	3.19
6375.23	33590 –	49272	4.16						−1.45				−1.41	−1.43	2.37	2.98
6378.26	33501 –	49175	4.15	247					−0.22				−0.17	−0.20	3.60	4.21
6381.11	35639 –	51306	4.42						−1.49				−1.27	−1.38	2.42	3.03
6384.67	33501 –	49159	4.15	246					−0.38				−0.39	−0.38	3.43	4.03
6414.59	33501 –	49086	4.15	244					−0.27				−0.43	−0.35	3.46	4.05
6421.52	33590 –	49159	4.16	258					−0.28				−0.51	−0.40	3.41	4.00
6424.86	33611 –	49171	4.17	227					−0.60				−0.81	−0.70	3.11	3.70
6432.00	28569 –	44112	3.54	126					−1.97				−1.96	−1.96	1.85	2.44
6451.56	33590 –	49086	4.16	257					−1.24				−1.12	−1.18	2.63	3.21
6452.70	32973 –	48467	4.09	226									−1.38	−1.38	2.43	3.01
6482.80	15610 –	31031	1.93	66					−2.08				−2.17	−2.12	1.69	2.27
6502.21	27415 –	42790	3.40						−1.89				−1.78	−1.84	1.97	2.54
6516.08	33611 –	48953	4.17						−1.31				−1.31	−1.31	2.50	3.07
6532.88	15610 –	30913	1.93	64					−2.72				−2.78	−2.75	1.07	1.63
6580.22	35639 –	50832	4.42	265									−0.59	−0.59	3.23	3.78
6586.31	15734 –	30913	1.95	64									−2.25	−2.25	1.57	2.12
6592.51	34163 –	49328	4.23	248									−0.47	−0.47	3.35	3.90
6598.60	34163 –	49314	4.23	249									−0.34	−0.34	3.48	4.03
6610.82	42621 –	57744	5.28										−0.86	−0.86	2.96	3.50
6617.09	34163 –	49272	4.23	248									−1.86	−1.86	1.96	2.50
6621.14	29013 –	44112	3.60	97									−1.86	−1.86	1.96	2.50
6635.13	35639 –	50706	4.42	264									−0.19	−0.19	3.63	4.17
6643.64	13521 –	28569	1.68	43	−1.86								−1.85	−1.86	1.96	2.50
6661.33	34163 –	49171	4.23	246									−0.96	−0.96	2.86	3.39
6666.71	34163 –	49159	4.23										−1.76	−1.76	2.06	2.59
6690.77	29321 –	44263	3.63	140									−1.76	−1.76	2.07	2.59
6700.90	34409 –	49328	4.26	248									−1.62	−1.62	2.21	2.73
6711.59	16017 –	30913	1.99										−3.81	−3.81	0.02	0.53
6716.14	15734 –	30619	1.95										−3.90	−3.90	−0.07	0.44
6733.75	27944 –	42790	3.46										−2.44	−2.44	1.39	1.90
6742.59	35639 –	50466	4.42										−1.19	−1.19	2.64	3.15
6759.44	34163 –	48953	4.23	245									−1.52	−1.52	2.31	2.81
6767.77	14729 –	29501	1.83	57	−1.58								−1.64	−1.61	2.22	2.72
6772.32	29501 –	44263	3.66	127	−0.17								−0.20	−0.18	3.65	4.15

TABLE 2.—*Oscillator Strengths for Ni* I—Continued

Wave-length	Energy Levels		Lower e.p.	Mult. No.	CB	K	CHC	AA	ULO	OBS	HD	PP	IC	Best	Log gfλ	Log gA/λ
Å	K		Volts													
(1)	(2)	(3)	(4)	(5)	(6)	(7)	(8)	(9)	(10)	(11)	(12)	(13)	(14)	(15)	(16)	(17)
6782.50	43090 –	57829	5.34										−0.23	−0.23	3.60	4.10
6798.43	36601 –	51306	4.54										−1.28	−1.28	2.55	3.05
6813.62	43090 –	57762	5.34	288									0.04	0.04	3.87	4.36
6842.04	29501 –	44112	3.66	126									−0.56	−0.56	3.28	3.76
6850.38	29669 –	44263	3.68	157									−1.63	−1.63	2.21	2.69
6861.24	43259 –	57829	5.36	293									−0.06	−0.06	3.78	4.25
6870.15	43259 –	57810	5.36										−0.10	−0.10	3.74	4.21
6876.69	28068 –	42606	3.48	97									−1.25	−1.25	2.59	3.06
6902.80	42621 –	57104	5.28										−0.20	−0.20	3.64	4.11
6914.56	15734 –	30192	1.95	62	−1.79								−1.68	−1.74	2.10	2.56
6928.19	29833 –	44263	3.70	110									−1.55	−1.55	2.29	2.75
6955.03	29889 –	44263	3.70	157									−0.86	−0.86	2.98	3.44
6973.49	42768 –	57104	5.30										−0.38	−0.38	3.46	3.91
7001.54	15610 –	29889	1.93	64									−2.94	−2.94	0.91	1.35
7004.19	44315 –	58588	5.49										−0.34	−0.34	3.51	3.95
7023.68	36601 –	50834	4.54										−0.48	−0.48	3.37	3.80
7024.87	36601 –	50832	4.54	271									−0.02	−0.02	3.83	4.26
7028.54	29889 –	44112	3.70										−1.43	−1.43	2.42	2.85
7028.96	15610 –	29833	1.93	61									−3.02	−3.02	0.83	1.26
7030.01	28569 –	42790	3.54	126									−0.96	−0.96	2.89	3.32
7034.38	28578 –	42790	3.54	97									−1.16	−1.16	2.69	3.12
7037.35	44315 –	58521	5.49	288									−0.07	−0.07	3.78	4.21
7049.61	42585 –	56767	5.28										−0.48	−0.48	3.37	3.80
7062.95	15734 –	29889	1.95	64									−2.92	−2.92	0.93	1.36
7063.55	36601 –	50754	4.54	270									−0.43	−0.43	3.42	3.85
7067.45	42621 –	56766	5.28	277									−0.44	−0.44	3.41	3.84
7095.37	42621 –	56711	5.28	276									−0.09	−0.09	3.76	4.18
7101.94	36601 –	50678	4.54										−0.92	−0.92	2.93	3.35
7110.90	15610 –	29669	1.93	64	−1.99								−2.54	−2.36	1.49	1.91
7122.20	28569 –	42606	3.54	126	0.29								0.42	0.36	4.21	4.63
7126.68	28578 –	42606	3.54	97									−1.63	−1.63	2.22	2.64
7129.16	44565 –	58588	5.52										−0.36	−0.36	3.49	3.90
7166.98	30163 –	44112	3.74	109									−0.94	−0.94	2.92	3.32
7170.08	42768 –	56711	5.30	282									−0.34	−0.34	3.52	3.92
7173.73	36601 –	50537	4.54	269									−0.71	−0.71	3.15	3.55
7181.97	30192 –	44112	3.74	126	−0.11								−0.07	−0.09	3.77	4.17
7197.02	15610 –	29501	1.93	62	−2.00								−2.08	−2.04	1.82	2.21
7220.76	43259 –	57104	5.36	294									−0.06	−0.06	3.80	4.19
7225.04	45281 –	59118	5.61										−0.26	−0.26	3.60	3.99
7261.93	15734 –	29501	1.95	62	−1.99								−2.10	−2.04	1.82	2.20
7266.20	45281 –	59040	5.61	288									0.20	0.20	4.06	4.44
7286.55	30392 –	44112	3.77	109									−1.40	−1.40	2.46	2.84
7290.88	43090 –	56802	5.34	287									0.21	0.21	4.07	4.45
7291.45	15610 –	29321	1.93	63	−2.06								−2.42	−2.42	1.44	1.82
7297.68	45419 –	59118	5.63	293									−0.10	−0.10	3.76	4.13
7309.57	43090 –	56767	5.34										−0.40	−0.40	3.46	3.83
7327.65	30619 –	44263	3.80	140									−1.05	−1.05	2.81	3.18
7351.40	43259 –	56858	5.36										−0.34	−0.34	3.53	3.88
7381.92	43259 –	56802	5.36	292									0.46	0.46	4.33	4.68
7385.24	22102 –	35639	2.74	84	−1.34								−1.40	−1.37	2.50	2.85
7386.20	43090 –	56625	5.34	286									0.69	0.69	4.56	4.91
7393.60	29084 –	42606	3.60	109	0.14								0.25	0.20	4.07	4.42
7401.14	43259 –	56767	5.36	291									0.36	0.36	4.23	4.58
7409.35	30619 –	44112	3.80	139	0.33								0.36	0.34	4.21	4.55
7414.51	16017 –	29501	1.99	62	−1.96								−2.05	−2.00	1.87	2.21
7419.29	44315 –	57790	5.49	287									−0.11	−0.11	3.76	4.10
7422.28	29321 –	42790	3.63	139	0.31								0.32	0.32	4.19	4.53
7433.46	43655 –	57104	5.41	280									−0.07	−0.07	3.80	4.14
7481.48	44315 –	57678	5.49	286									0.18	0.18	4.05	4.38
7488.70	30913 –	44263	3.83	157									−1.44	−1.44	2.43	2.76

TABLE 2.—*Oscillator Strengths for Ni* I—Continued

Wavelength Å	Energy Levels K		Lower e.p. Volts	Mult. No.	CB	K	CHC	AA	ULO	OBS	HD	PP	IC	Best	Log gfλ	Log gA/λ
(1)	(2)	(3)	(4)	(5)	(6)	(7)	(8)	(9)	(10)	(11)	(12)	(13)	(14)	(15)	(16)	(17)
7521.03	44475 –	57768	5.51	282									−0.15	−0.15	3.73	4.05
7522.76	29501 –	42790	3.66	126	0.09								0.08	0.08	3.96	4.27
7525.12	29321 –	42606	3.63	139	−0.09								−0.03	−0.06	3.82	4.13
7545.50	45281 –	58530	5.61	287									−0.13	−0.13	3.75	4.06
7552.52	45281 –	58518	5.61	286									0.06	0.06	3.94	4.25
7555.60	31031 –	44263	3.85	187	0.45								0.50	0.48	4.36	4.67
7559.66	44565 –	57790	5.52	292									0.08	0.08	3.96	4.27
7574.05	30913 –	44112	3.83	156	0.03								0.12	0.08	3.96	4.27
7586.04	44565 –	57744	5.52										−0.29	−0.29	3.59	3.89
7616.98	29481 –	42606	3.65	139	0.32								0.42	0.37	4.25	4.55
7619.21	29669 –	42790	3.68	156	−0.05								−0.05	−0.05	3.83	4.13
7624.74	45419 –	58530	5.63	292									−0.06	−0.06	3.82	4.12
7657.26	43655 –	56711	5.41	278									0.04	0.04	3.92	4.21
7714.32	15610 –	28569	1.93	62	−1.53								−1.65	−1.59	2.30	2.57
7715.58	29833 –	42790	3.70	109	−0.28								−0.33	−0.30	3.59	3.86
7727.61	29669 –	42606	3.68	156	0.27								0.31	0.29	4.18	4.45
7748.89	29889 –	42790	3.70	156	0.30								0.28	0.29	4.18	4.45
7788.94	15734 –	28569	1.95	62	−1.71								−1.81	−1.76	2.13	2.39
7797.59	31442 –	44263	3.90	201	0.31								0.42	0.36	4.25	4.51
7826.76	29833 –	42606	3.70	109									−1.05	−1.05	2.84	3.09
7855.14	36601 –	49328	4.54	267									−0.54	−0.54	3.36	3.60
7861.05	29889 –	42606	3.70	156									−1.13	−1.13	2.77	3.01
7863.79	36601 –	49314	4.54	268									−0.22	−0.22	3.68	3.92
7890.15	31442 –	44112	3.90	200									−1.20	−1.20	2.70	2.93
7917.44	30163 –	42790	3.74	109	−0.67								−0.60	−0.64	3.26	3.49
7953.03	36601 –	49171	4.54	266									−0.89	−0.89	3.01	3.23
8012.93	31786 –	44263	3.94										−1.45	−1.45	2.45	2.66
8417.19	30913 –	42790	3.83	156									−1.09	−1.09	2.84	2.96
8501.80	31031 –	42790	3.85	186									−0.73	−0.73	3.20	3.31
8606.38	42621 –	54237	5.28	275									0.28	0.28	4.21	4.30
8637.00	31031 –	42606	3.85	186									−0.89	−0.89	3.05	3.12
8770.68	22102 –	33501	2.74	82									−2.18	−2.18	1.76	1.81
8809.42	31442 –	42790	3.90	200	−0.53								−0.53	−0.53	3.41	3.46
8862.55	32982 –	44263	4.09	214	0.33								0.34	0.34	4.29	4.32
8877.01	44315 –	55577	5.49	285									0.47	0.47	4.42	4.45
8954.65	31442 –	42606	3.90	200									−1.52	−1.52	2.43	2.45
8965.96	33112 –	44263	4.10	225									−0.07	−0.07	3.88	3.90
8968.14	43090 –	54237	5.34	284									0.60	0.60	4.55	4.57
8982.35	32982 –	44112	4.09	213									−1.35	−1.35	2.60	2.61
9005.14	44475 –	55577	5.51										0.00	0.00	3.95	3.96
9078.70	44565 –	55577	5.52										−0.35	−0.35	3.61	3.60
9085.25	31786 –	42790	3.94										−1.27	−1.27	2.69	2.68
9106.40	43259 –	54237	5.36	289									0.16	0.16	4.12	4.11
9196.18	22102 –	32973	2.74										−3.19	−3.19	0.77	0.74
9385.62	33611 –	44263	4.17	225									−0.88	−0.88	3.09	3.03
9447.29	43655 –	54237	5.41										−0.02	−0.02	3.96	3.88
9520.06	33611 –	44112	4.17	224									−0.03	−0.03	3.95	3.86
9898.90	34163 –	44263	4.23	243									−0.22	−0.22	3.78	3.62

(Paper 69A2–331)

JOURNAL OF RESEARCH of the National Bureau of Standards—A. Physics and Chemistry
Vol. 69A, No. 2, March–April, 1965

More Wavelengths From Thorium Lamps

William F. Meggers and Robert W. Stanley*

(December 13, 1964)

For the purpose of supplementing or superseding the spectroscopic secondary standards of wavelength derived since 1910 from an iron arc, Meggers and Stanley, in 1958, reported the first interferometric determinations of wavelengths emitted by a thorium lamp. Those determinations were restricted to 222 intense radiations of thorium with wavelengths ranging from 3288.7356 Å to 6991.5839 Å. Now the same, and additional, interference spectrograms have been measured to provide improved wavelengths for 510 radiations ranging in wavelength from 3269.6089 Å to 7020.504 Å. The present list includes many lines of lower intensity than those previously published and fills most of the large intervals in our first report. The accuracy in relative wavelength values of 163 classified thorium lines is tested by the combination principle which indicates that the average error is less than 1 part in 20 to 40 million. Similar measurements of wavelengths emitted by iron-halide lamps have errors that are 3 to 5 times greater.

1. Introduction

After forty years of intermittent effort to extend and improve the international standards of wavelengths used in spectroscopy, Meggers [1][1] suggested, in 1955, that secondary standards, superior in sharpness and distribution, could be obtained by replacing the standard iron arc with a modern thorium lamp as a light source. Such improvement was demonstrated by Meggers and Stanley [2] who first measured the wavelengths of 222 intense radiations emitted by a thorium-iodide lamp. Those wavelengths extended from 3288.7356 Å to 6991.5839 Å in vacuum; they were measured interferometrically relative to wavelengths emitted by a Meggers mercury 198 lamp. In the meantime, those measurements have found favor among all spectroscopists who specialize in making accurate descriptions of complex spectra, especially of chemical elements whose atoms are more massive than those of iron. Moreover, those spectroscopists have suggested that more wavelengths of thorium radiations be accurately measured to increase the range of intensity and decrease the average interval, thus removing handicaps on account of overexposure and/or expanded dispersion in modern photographic spectrograms. Consequently, the same, and additional, interference spectrograms have been measured to provide improved values of wavelengths for 510 thorium radiations (including 222 reported earlier) ranging in value from 3263.6089 Å to 7020.504 Å in vacuum. The purpose of this paper is to present a new list of thorium wavelengths including many lines of lower intensity than those previously published [2] and also to reduce the average interval between standards. Because of the increase in the number of carefully measured wavelengths, the combination principle is applied as an internal test of the accuracy in relative value of a considerable fraction of them.

2. Experiments

In our first paper [2], full details concerning light sources, interferometers, spectrograph, measurements, and computations were given for the first determinations of thorium wavelengths from Fabry-Perot etalons. Briefly, the thorium radiations were emitted by a small electrodeless lamp containing a few milligrams of thorium iodide and several torr of helium. The wavelengths of selected thorium lines were measured relative to adopted standards emitted by a similar lamp containing 1 mg of mercury-198 and 3 torr of argon. Both lamps were excited by magnetrons generating 2450 Mc/s. One lamp was imaged in the other and both simultaneously illuminated a Fabry-Perot etalon interferometer to avoid errors usually entailed by alternate exposures to different light sources.

The enclosed and evacuated Fabry-Perot interferometer consisted of two flat plates of crystalline quartz whose facing surfaces were coated with thin aluminum films and separated by invar etalons of 25, 40, or 50 mm length. The 25 and 40 mm spacers were relied upon to insure the correct integral order of interference for any given line, assuming that available values of the wavelength obtained from diffraction-grating spectrograms had no errors greater than ± 0.02 Å.

The interference patterns (Haidinger fringes) were photographed with a concave grating of 22 feet radius in a (stigmatic) Wadsworth mounting. The spectral range 4400 Å to 7000 Å was photographed in the first-order spectrum with a slit width of 0.30 mm and plate factor of 5 Å/mm. Because

*Present address, Purdue University, Lafayette, Ind.
[1] Figures in brackets indicate the literature references at the end of this paper.

of a greater density of thorium lines in the unltraviolet, the region from 3250 Å to 4500 Å was recorded in the second-order grating spectrum with a plate factor of 2.5 Å/mm and slit width of 0.15 mm. In each wavelength range, several spectrograms were made with different times of exposure, and with slightly different spacing of the interferometer plates to alter the interference configurations or fractional orders for all spectral lines. The green (5462.2705 Å) and violet (4047.7144 Å) lines of Hg^{198} were chosen as standards, respectively, for the long- and short-wave interference spectrograms described above. The wavelengths of Hg^{198} radiations used for the calibration of etalons were previously measured [3] relative to red radiation (6438.4696 Å) of cadmium, the primary standard of wavelength prior to 1960.

In our first report [2] ,the fractional order at the center of an interference pattern was determined from measurements of five interference fringes for each line and least-squares calculations according to the formula

$$\epsilon=\frac{2(3D_1+2D_2^2+D_3^2-D_5^2)}{-2D_1^2-D_2^2+D_4^2+2D_5^2},$$

first discussed by Rolt and Barrell [4]. After taking squares from a table, all computations were by mental arithmetic except the final quotient which was obtained from a desk calculator. About 12,000 interference fringes were thus used to derive the wavelengths of 222 intense radiations in thorium spectra, 172 from Th I and 50 from Th II.

The results reported in the present paper were obtained by Meggers from spectrograms made by Stanley in 1956 and described jointly in 1958 [2]. In addition, several spectrograms that were overexposed, and, therefore, unsuitable for measurement of the stronger lines, were salvaged by dissolving the dense background in solutions of sodium thiosulphate and potassium ferricyanide, thereby making them ideal for measurement of the weaker lines.

In this series of measurements, the diameters of six interference circles (Haidinger fringes) were determined from readings of the distances between twelve fringes for each line. In most cases, two readings were made on each fringe and the mean was recorded. Since the fringes on 510 thorium lines and several mercury 198 lines were measured on two to six spectrograms, the average being four, it appears that more than 40,000 readings were made. The recorded readings were transferred to IBM cards in a punch machine and transmitted to an electronic computer that calculated wavelengths after determining the fractional and integral orders of interference for each line in a given interferometer.

The fractional order, ϵ, at the center of an interference pattern was calculated from 6 diameters according to the formula:

$$\epsilon=\frac{5}{3}\left(\frac{11D_1^2+8D_2^2+5D_3^2+2D_4^2-D_5^2-4D_6^2}{-5D_1^2-3D_2^2-D_3^2+D_4^2+3D_5^2+5D_6^2}\right).$$

The final calculations of wavelength, λ, were made from the relation $\lambda=2t/(p+\epsilon)$, where t is the separation of the interferometer plates, p is the integral order, and ϵ the fractional order of interference at the center of a pattern. In this series of measurements, the wavelengths of 510 thorium radiations were determined relative to Hg^{198} wavelengths (5462.2706 Å, 4359.5625 Å, and 4047.7147 Å) which in turn were measured by Kaufman [5] in terms of the new primary standard of length, 6057.80211 Å, radiated by Kr^{86}.

3. Results

Our latest measurements of vacuum wavelengths for 510 radiations from thorium lamps are presented in table 1. The vacuum values in column 1 were converted to appropriate values in standard air, column 2, by using the Table of Wavenumbers of Coleman, Bozman, and Meggers [6]. The estimated relative intensities, column 3, and assignment to spectrum, Th I or Th II, are quoted from a *New Description of Thorium Spectra* by Zalubas [7]. Table 1 contains data for 510 radiations, 395 from Th I and 115 from Th II. Wavelength values given to 8 figures have estimated errors less than 0.0005 Å, 34 given to 7 figures are included to suggest that they are suitable for further refinement.

Although the Kr^{86} wavelength (6057.80211 Å in vacuum) was derived from the Cd wavelength (6438.46960 Å, in air), the wavelengths of identical Hg^{198} lamps (3 torr Ar) measured relative to the former are slightly greater (0.0001 to 0.0003 Å) than those derived from the latter. Consequently, the wavelengths of 222 thorium radiations reported in our first paper [2] have now increased by 0.0001 Å on the average. We are unable to explain the source of this small discrepancy. Fortunately for spectroscopic use as standards, the absolute values of thorium wavelengths are less important than their relative values for calibrating spectrograms.

Because the number of independent determinations of each thorium wavelength is, in general, too small to yield a true probable error, we have extensively applied the combination principle as a rigid test of the accuracy of measured wavelengths in relative value. Two radiations resulting from combinations of a highly excited atomic (or ionic) level with two low-energy levels will exhibit in their wavenumbers the energy difference of the low levels. Any other high levels that combine with the same low levels will exhibit the same difference within the accuracy of measurement. In table 2, we present typical examples of 21 low-energy differences, 20 involving wavenumber differences between designated low-energy levels for Th I [8], and 1 for Th II [9]. The total number of line pairs in table 2 is 111 but, since some radiations participate two or three times in pairing with others, only 163 different lines are involved. However, these are randomly distributed throughout the list and comprise nearly 63 percent of the classified Th I wavelengths given to 8 figures.

We may expect, therefore, that the remainder will satisfy these tests when other wavelengths are measured and the present partial analyses of these spectra are greatly extended.

The critical test of our thorium wavelengths is shown in the last two columns of table 2, where recurring wavenumber differences and their deviations from the mean are listed.

The deviations of the measured level separations from the mean range from 0 to ±4 m K (milli-Kayser $= 10^{-3}$ cm^{-1}). The average deviation of all tested pairs of lines is ±0.0012 K, and if we assume the errors are shared equally by all lines, the individual average error is 0.0006 K, or one part in 20 to 40 million, depending on the spectral region. These tests indicate that our thorium wavelengths qualify as Class A standards defined as having accuracy of 0.001 K according to a suggestion by Littlefield [10]. Calculated probable errors, as well as atomic energy intervals, for similar measurements of wavelengths from iron-halide lamps [11] indicate that the relative values are uncertain by 1 part in 7 or 8 million.

Recently, additional measurements of thorium wavelengths have been reported by Littlefield and Wood [12], by Davison, Giacchetti, and Stanley [13], and by Giacchetti, Gellarado, Garavaglia, Gonzalez, Valero, and Zakowicz [14]. The first [12] used a hollow-cathode light source and reflection-echelon interferometer to measure the wavelengths of 484 thorium radiations ranging from 2566.3615 Å to 9050.7361 Å; the results have been reported in the Transactions of the I A U but no further experimental details have been published. The others, [13, 14], used electrodeless thorium lamps and Fabry-Perot interferometers similar to ours. Davison et al. [13] published the wavelengths of 68 radiations ranging from 2651.3722 Å to 3394.9671 Å, and Giacchetti et al. [14] gave 129 values from 2687.9304 Å to 4596.7088 Å. Unfortunately, none of the above-mentioned observers tested their results by means of the combination principle; there are many serious discrepancies between values reported by two or more observers and it will be important to seek the source of the larger differences.

The senior author gladly and gratefully acknowledges the assistance of Mrs. John B. Peterson who transferred written readings to punched cards, and thanks Victor Kaufman for presenting these data to an electronic computer that produced wavelengths by using a code previously prepared by Karl G. Kessler.

Washington, D.C., November 2, 1964

TABLE 1. *Wavelengths of thorium lines*

λvac	λair	Relative intensity	Spectrum
Å	Å		
3263.6089	3262.6682	3000	II
3272.9913	3272.0482	800	I
3274.8374	3273.8938	600	II
3276.011	3275.067	400	II
3286.6984	3285.7518	900	I
3288.7358	3287.7887	1600	II
3292.6868	3291.7387	3000	II
3293.4688	3292.5205	3000	II
3302.207	3301.256	600	II
3305.1895	3304.2382	3000	I
3310.3178	3309.3652	800	I
3314.022	3313.068	400	I
3321.4317	3320.4763	400	I
3325.7088	3324.7523	2000	II
3326.0767	3325.1201	3000	II
3331.4345	3330.4765	1800	I
3334.0872	3333.1285	1000	I
3338.8297	3337.8698	2000	II
3349.7310	3348.768	3000	I
3352.1912	3351.2279	2500	II
3359.5667	3358.6015	2000	II
3368.7860	3367.8185	1200	II
3375.9440	3374.9747	1600	I
3379.5433	3378.5730	400	II
3381.8300	3380.8592	900	I
3386.5031	3385.5311	800	II
3393.0082	3392.0345	6000	II
3397.7023	3396.7274	1400	I
3399.5201	3398.5447	1600	I
3406.5348	3405.5576	1400	I
3413.9919	3413.0128	1800	I
3422.1909	3421.2097	2500	I
3424.9714	3423.9895	1600	I
3434.9827	3433.9983	3000	II
3438.2923	3437.3070	2500	I
3443.5653	3442.5787	800	I
3452.6909	3451.7019	900	I
3458.0588	3457.0685	800	I
3463.8419	3462.8501	2000	II
3469.2125	3468.2193	2000	II
3480.1683	3479.1723	800	II
3487.5248	3486.5269	3500	II
3494.5176	3493.5179	2000	II
3499.6217	3498.6207	900	I
3504.7880	3503.7857	500	I
3512.1610	3511.1568	1000	I
3519.4096	3518.4035	1000	I
3522.0660	3521.0592	500	I
3531.5236	3530.5144	500	II
3532.4595	3531.4501	1000	I
3540.3335	3539.3220	800	II
3540.5985	3539.5870	4000	II
3545.0303	3544.0176	1500	I
3550.6096	3549.5955	1200	I
3552.4160	3551.4014	1000	I
3556.0284	3555.0129	1500	I
3560.4658	3559.4491	2500	II
3564.3930	3563.3753	800	I
3568.2824	3567.2637	1200	I
3573.4119	3572.3919	1000	II

TABLE 1. *Wavelengths of thorium lines*—Continued

λvac	λair	Relative intensity	Spectrum
Å	Å		
3577.5785	3576.5574	1000	I
3585.1986	3584.1756	800	I
3592.4771	3591.4522	1000	I
3593.8042	3592.7790	2000	I
3599.1464	3598.1198	2000	I
3605.711	3604.683	800	I
3606.222	3605.194	500	I
3609.4067	3608.3774	1200	I
3613.4576	3612.4273	1400	I
3616.1634	3615.1324	2000	II
3623.8281	3622.7951	800	I
3626.6612	3625.6275	500	II
3633.8656	3632.8300	1000	I
3636.9796	3635.9432	1900	I
3643.2867	3642.2487	2200	I
3650.7746	3649.7346	1200	I
3657.7354	3656.6936	1000	I
3662.6653	3661.6223	500	II
3669.1843	3668.1396	1000	I
3671.0138	3669.9686	750	I
3672.5853	3671.5397	700	I
3676.6136	3675.5670	1000	II
3683.5345	3682.4861	1000	I
3691.6742	3690.6237	1000	I
3693.6172	3692.5662	1200	I
3699.1584	3698.1059	1300	I
3702.0314	3700.9782	300	I
3707.8219	3706.7672	2400	I
3712.3597	3711.3038	600	II
3720.4927	3719.4347	3000	I
3728.9626	3727.9024	800	I
3734.0467	3732.9852	500	I
3734.7340	3733.6723	500	I
3742.2464	3741.1828	3000	II
3743.9873	3742.9232	1100	I
3748.6040	3747.5387	900	II
3753.6352	3752.5686	3500	II
3758.7620	3757.6941	1000	I
3764.0030	3762.9337	1200	I
3771.1268	3770.0557	1300	I
3772.4419	3771.3704	1500	I
3777.3435	3776.2708	600	I
3782.0398	3780.9659	350	I
3786.6751	3785.5999	1000	II
3790.2449	3789.1688	1500	I
3796.4632	3795.3855	500	II
3804.1547	3803.0750	4000	I
3808.9554	3807.8745	1200	II
3814.1499	3813.0676	1200	II
3819.7690	3818.6853	500	I
3829.4708	3828.3845	3200	I
3831.8604	3830.7735	800	I
3838.9638	3837.8751	2000	I
3840.7835	3839.6943	2500	I
3843.0499	3841.9601	1200	II
3853.2278	3852.1354	600	I
3855.6037	3854.5106	1200	II
3860.9341	3859.8396	500	II
3864.5011	3863.4057	1200	II
3870.7604	3869.6634	600	I

TABLE 1. *Wavelengths of thorium lines*—Continued

λvac	λair	Relative intensity	Spectrum
A	Å		
3875.9602	3874.8618	1800	I
3876.4723	3875.3738	500	I
3880.7435	3879.6439	1000	I
3885.9251	3884.8241	400	II
3896.5229	3895.4192	400	I
3904.2082	3903.1025	1500	I
3905.169	3904.063	1000	II
3906.2923	3905.1860	1500	II
3913.0171	3911.9091	600	I
3917.5266	3916.4174	500	I
3920.1336	3919.0239	800	I
3924.9106	3923.7995	400	I
3926.2046	3925.0932	1000	I
3930.7818	3929.6692	2500	II
3934.0244	3932.9109	1400	I
3938.1548	3937.0402	400	II
3944.5112	3943.3950	400	II
3950.0814	3948.9637	1000	II
3953.8796	3952.7609	500	I
3960.4204	3959.3000	1000	I
3968.5146	3967.3921	2000	I
3973.2783	3972.1546	1400	I
3974.3200	3973.1960	1100	I
3981.2151	3980.0893	1100	I
3988.3509	3987.2232	600	I
3991.6206	3990.4921	800	I
3995.6788	3994.5492	1200	I
4002.1893	4001.0580	800	I
4003.0253	4001.8938	150	I
4009.3433	4008.2102	1600	I
4010.190	4009.057	1600	I
4013.6295	4012.4952	2000	I
4019.2344	4018.0987	400	I
4020.2649	4019.1289	1200	II
4028.1470	4027.0089	1000	I
4031.4314	4030.2925	200	I
4031.9815	4030.8424	1800	I
4037.1879	4036.0475	1800	I
4037.7056	4036.5650	400	II
4044.5369	4043.3946	800	I
4052.0315	4050.8872	800	I
4054.6727	4053.5277	1000	I
4060.3994	4059.2529	1000	I
4064.5547	4063.4071	800	II
4065.4793	4064.3315	400	I
4068.5994	4067.4508	400	I
4070.3508	4069.2017	750	II
4070.6098	4069.4606	400	I
4073.7787	4072.6287	400	I
4076.6536	4075.5029	400	I
4082.5200	4081.3677	800	I
4087.6742	4086.5206	1600	II
4089.8815	4088.7273	400	I
4090.2920	4089.1377	400	I
4095.9029	4094.7471	1600	II
4098.9042	4097.7476	800	I
4101.4985	4100.3413	1100	I
4109.5792	4108.4198	800	II
4110.4832	4109.3236	400	I
4113.9150	4112.7545	700	I

TABLE 1. *Wavelengths of thorium lines*—Continued

λvac	λair	Relative intensity	Spectrum
Å	Å		
4116. 9203	4115. 7590	800	I
4117. 8754	4116. 7139	600	II
4128. 5761	4127. 4118	1000	I
4132. 1675	4131. 0022	800	I
4133. 9192	4132. 7535	600	II
4141. 4028	4140. 2351	400	II
4151. 1570	4149. 9868	800	II
4159. 7076	4158. 5351	800	I
4166. 9496	4165. 7662	1000	I
4171. 7090	4170. 5334	500	I
4179. 2377	4178. 0601	3000	II
4185. 3170	4184. 1378	500	I
4194. 1984	4193. 0169	900	I
4196. 1178	4194. 9358	350	I
4203. 0308	4201. 8469	500	II
4210. 0764	4208. 8907	3000	I
4211. 9511	4210. 7649	400	I
4212. 1096	4210. 9234	200	I
4214. 2542	4213. 0674	400	I
4216. 0158	4214. 8285	200	I
4221. 253	4220. 064	750	I
4228. 5780	4227. 3874	400	I
4231. 6184	4230. 4271	600	I
4236. 6565	4235. 4638	600	I
4249. 1853	4247. 9893	400	II
4251. 511	4250. 314	1200	I
4254. 7362	4253. 5388	800	I
4258. 6948	4257. 4963	700	I
4259. 719	4258. 520	500	I
4261. 5322	4260. 3327	800	I
4271. 1445	4269. 9428	200	I
4274. 5603	4273. 3577	1000	II
4278. 5178	4277. 3141	1200	II
4283. 2464	4282. 0415	2000	II
4293. 0177	4291. 8102	400	I
4298. 5155	4297. 3066	400	I
4301. 0492	4299. 8396	600	I
4308. 3879	4307. 1764	700	I
4316. 4680	4315. 2543	400	I
4319. 6302	4318. 4157	700	I
4321. 3414	4320. 1265	300	II
4330. 1329	4328. 9156	400	I
4332. 0619	4330. 8441	300	I
4338. 4971	4337. 2777	900	I
4343. 4765	4342. 2557	300	II
4345. 5479	4344. 3266	300	II
4347. 6587	4346. 4368	500	I
4350. 2950	4349. 0724	400	I
4354. 6724	4353. 4487	500	I
4360. 5972	4359. 3719	600	I
4367. 1575	4365. 9305	600	I
4371. 1038	4369. 8758	200	I
4375. 3536	4374. 1244	600	I
4379. 4071	4378. 1769	500	I
4383. 0917	4381. 8605	900	I
4392. 3443	4391. 1107	3000	II
4394. 2084	4392. 9743	400	I
4402. 8178	4401. 5814	400	I
4404. 1639	4402. 9272	400	I
4410. 1211	4408. 8828	600	I

TABLE 1. *Wavelengths of thorium lines*—Continued

λvac	λair	Relative intensity	Spectrum
Å	Å		
4415. 7260	4414. 4862	400	I
4423. 2900	4422. 0482	350	I
4434. 2077	4432. 9640	600	II
4440. 370	4439. 124	400	II
4442. 114	4440. 867	400	II
4446. 5562	4445. 3083	300	I
4447. 1495	4445. 9014	200	I
4453. 8148	4452. 5650	200	I
4459. 2531	4458. 0018	600	I
4462. 4933	4461. 2412	600	I
4466. 5940	4465. 3408	300	II
4470. 7800	4469. 5257	400	I
4483. 4270	4482. 1694	300	I
4488. 1563	4486. 8974	200	I
4494. 5943	4493. 3337	1200	I
4500. 2022	4498. 9401	800	I
4501. 2459	4499. 9836	500	I
4506. 4799	4505. 2162	400	I
4511. 7910	4510. 5259	800	II
4516. 3845	4515. 1182	300	I
4522. 489	4521. 221	500	I
4531. 5895	4530. 3192	160	I
4536. 5265	4535. 2549	300	I
4542. 2720	4540. 9988	300	I
4547. 1900	4545. 9155	350	I
4557. 0903	4555. 8132	500	I
4562. 6266	4561. 3481	500	I
4572. 2528	4570. 9717	500	I
4589. 7124	4588. 4267	400	I
4593. 953	4592. 666	400	I
4596. 7082	4595. 4207	600	I
4604. 461	4603. 171	175	I
4622. 4565	4621. 1621	200	I
4633. 0585	4631. 7613	300	II
4641. 344	4640. 045	500	II
4652. 857	4651. 555	500	II
4664. 5080	4663. 2025	200	I
4669. 4785	4668. 1717	700	I
4671. 2916	4669. 9843	400	I
4674. 9693	4673. 6611	600	I
4687. 5060	4686. 1944	400	I
4696. 3520	4695. 0380	400	I
4705. 3063	4703. 9900	500	I
4713. 7713	4712. 4528	500	I
4719. 9363	4718. 6162	200	II
4730. 4507	4729. 1278	250	I
4741. 8552	4740. 5293	400	II
4753. 7432	4752. 4141	500	II
4762. 4415	4761. 1101	400	II
4767. 9332	4766. 6003	200	I
4779. 6300	4778. 2940	300	I
4790. 7256	4789. 3867	300	I
4809. 4775	4808. 1336	350	I
4810. 9583	4809. 6140	300	I
4824. 2027	4822. 8549	300	I
4828. 0490	4826. 7002	300	I
4832. 4710	4831. 1210	350	I
4842. 195	4840. 843	400	I
4849. 7168	4848. 3623	250	I
4859. 6895	4858. 3323	300	II

TABLE 1. *Wavelengths of thorium lines*—Continued

λvac	λair	Relative intensity	Spectrum
Å	Å		
4864. 5305	4863. 1720	1000	II
4866. 8363	4865. 4772	350	I
4880. 0955	4878. 7329	200	I
4896. 3218	4894. 9549	350	I
4908. 5795	4907. 2093	150	I
4921. 1892	4919. 8157	600	II
4929. 1564	4927. 7808	140	I
4941. 0208	4939. 6420	350	I
4946. 8387	4945. 4584	140	I
4967. 1169	4965. 7312	250	I
4981. 5757	4980. 1862	600	I
4986. 7636	4985. 3727	300	I
4990. 7005	4989. 3085	200	I
5003. 4924	5002. 0970	400	I
5018. 6541	5017. 2547	500	II
5030. 0586	5028. 6562	400	II
5040. 6359	5039. 2307	200	I
5046. 1263	5044. 7196	400	I
5051. 2040	5049. 7960	400	I
5061. 2716	5059. 8609	200	I
5069. 3870	5067. 9741	900	I
5086. 411	5084. 994	150	I
5097. 9046	5096. 4842	200	I
5102. 0426	5100. 6210	200	I
5116. 4702	5115. 0448	250	I
5127. 3781	5125. 9498	150	I
5129. 9184	5128. 4894	125	I
5136. 1764	5134. 7458	150	I
5145. 3493	5143. 9162	200	I
5153. 0472	5151. 6121	400	II
5155. 6791	5154. 2433	400	I
5160. 0414	5158. 6044	700	I
5164. 8968	5163. 4585	300	I
5178. 4026	5176. 9607	400	I
5183. 9704	5182. 5270	200	II
5197. 2605	5195. 8136	400	I
5200. 6116	5199. 1638	800	I
5212. 6816	5211. 2306	400	I
5220. 5630	5219. 1099	500	I
5232. 6161	5231. 1598	900	I
5234. 6822	5233. 2253	350	II
5249. 1148	5247. 6541	400	II
5259. 8240	5258. 3604	300	I
5268. 1760	5266. 7102	200	I
5278. 9688	5277. 5001	400	II
5297. 7529	5296. 2792	200	I
5299. 2158	5297. 7417	250	I
5308. 9423	5307. 4657	300	II
5313. 4795	5312. 0016	400	I
5326. 6264	5325. 1450	300	II
5328. 4577	5326. 9758	400	I
5345. 0677	5343. 5814	500	I
5352. 6146	5351. 1263	120	I
5361. 6410	5360. 1503	250	I
5370. 773	5369. 280	200	I
5374. 1973	5372. 7033	200	I
5388. 1085	5386. 6107	300	I
5396. 2608	5394. 7609	400	I
5409. 1571	5407. 6537	200	I
5412. 2733	5410. 7691	180	I

TABLE 1. *Wavelengths of thorium lines*—Continued

λvac	λair	Relative intensity	Spectrum
Å	Å		
5418. 9918	5417. 4858	200	I
5427. 1864	5425. 6782	250	II
5432. 6214	5431. 1118	300	I
5437. 4039	5435. 8930	400	II
5450. 9935	5449. 4790	150	II
5453. 7341	5452. 2188	250	I
5465. 7236	5464. 2051	75	I
5472. 2790	5470. 7588	100	I
5494. 168	5492. 642	100	I
5500. 7831	5499. 2553	250	I
5505. 8312	5504. 3020	160	I
5511. 5245	5509. 9938	300	I
5516. 4051	5514. 8731	160	I
5526. 1178	5524. 5832	100	I
5540. 8005	5539. 2620	400	I
5549. 7170	5548. 1761	300	I
5558. 5886	5557. 0453	200	I
5559. 8863	5558. 3427	400	I
5572. 7389	5571. 1919	300	I
5574. 9017	5573. 3541	350	I
5580. 9078	5579. 3586	300	I
5588. 5781	5587. 0268	500	I
5596. 6168	5595. 0634	200	I
5603. 1587	5601. 6035	150	I
5613. 6262	5612. 0682	100	I
5616. 8788	5615. 3200	350	I
5631. 8595	5630. 2967	60	I
5641. 3117	5639. 7463	250	II
5659. 4958	5657. 9256	100	I
5666. 7532	5665. 1810	140	I
5676. 561	5674. 986	120	I
5686. 7695	5685. 1920	150	I
5702. 4993	5700. 9176	150	II
5708. 6868	5707. 1034	150	II
5721. 2097	5719. 6230	200	I
5721. 7704	5720. 1835	400	I
5726. 9767	5725. 3884	250	I
5750. 3347	5748. 7402	150	I
5754. 6225	5753. 0268	100	I
5762. 1489	5760. 5512	600	I
5765. 1270	5763. 5285	80	I
5769. 7813	5768. 1816	150	I
5775. 5478	5773. 9465	150	I
5791. 2500	5789. 6445	200	I
5794. 0363	5792. 4301	150	I
5797. 6759	5796. 0687	150	I
5802. 4380	5800. 8295	175	I
5805. 7507	5804. 1414	300	I
5814. 5842	5812. 9725	150	I
5817. 0346	5815. 4222	175	II
5833. 9875	5832. 3706	125	I
5854. 3043	5852. 6820	200	I
5855. 7424	5854. 1197	100	I
5861. 2904	5859. 6662	140	II
5869. 9996	5868. 3731	125	I
5887. 3330	5885. 7018	120	I
5893. 0838	5891. 4511	70	I
5907. 2068	5905. 5703	100	I
5916. 3095	5914. 6706	140	I
5927. 8744	5926. 2324	100	I

TABLE 1. *Wavelengths of thorium lines*—Continued

λvac	λair	Relative intensity	Spectrum
Å	Å		
5940.4706	5938.8252	140	I
5946.2946	5944.6476	75	II
5975.3199	5973.6652	250	I
5976.7203	5975.0652	250	I
5990.7034	5989.0445	150	II
5995.7897	5994.1295	200	I
6008.7362	6007.0725	180	I
6011.8253	6010.1608	90	I
6022.7038	6021.0364	140	I
6039.3697	6037.6978	140	I
6050.7257	6049.0507	100	I
6055.0569	6053.3808	300	I
6074.7856	6073.1042	50	II
6079.554	6077.871	75	I
6087.0596	6085.3749	100	I
6089.7162	6088.0308	125	I
6104.2840	6102.5947	90	I
6114.5300	6112.8379	125	II
6123.1031	6121.4087	75	I
6126.178	6124.483	75	I
6153.6960	6151.9934	125	I
6163.0585	6161.3534	50	I
6166.1856	6164.4797	75	I
6171.5299	6169.8226	500	I
6180.1417	6178.4320	100	I
6184.3331	6182.6223	400	I
6189.8381	6188.1258	160	I
6193.6189	6191.9056	100	I
6199.9380	6198.2230	80	I
6205.2095	6203.4931	100	I
6208.9377	6207.2203	160	I
6226.2496	6224.5276	100	I
6236.5804	6234.8556	200	I
6259.1550	6257.4241	100	I
6263.1498	6261.4179	180	I
6275.8522	6274.1169	100	II
6292.9314	6291.1915	30	I
6304.9940	6303.2508	40	I
6328.117	6326.368	60	II
6329.0285	6327.2789	180	I
6339.3728	6337.6204	40	I
6344.6140	6342.8602	300	I
6350.4928	6348.7374	40	I
6357.6686	6355.9113	40	I
6370.9008	6369.1409	120	I
6373.7056	6371.9440	50	I
6378.6942	6376.9313	350	I
6389.1624	6387.3967	50	I
6390.583	6388.817	40	I
6408.2173	6406.4464	75	I
6413.6720	6411.8997	250	I
6415.3879	6413.6151	200	I
6426.5890	6424.8132	30	II
6439.5405	6437.7612	50	I
6448.5530	6446.7713	50	I
6459.0677	6457.2832	500	I
6464.4002	6462.6142	400	II
6492.5315	6490.7380	120	I
6494.9922	6493.1980	75	I
6514.1635	6512.3642	75	I

TABLE 1. *Wavelengths of thorium lines*—Continued

λvac	λair	Relative intensity	Spectrum
Å	Å		
6523.8458	6522.0439	40	II
6533.1470	6531.3426	400	I
6555.9711	6554.1605	100	I
6579.0336	6577.2168	50	I
6585.7251	6583.9065	200	I
6590.3598	6588.5400	200	I
6593.3058	6591.4852	100	I
6595.7612	6593.9399	200	I
6607.2410	6605.4167	30	II
6621.7752	6619.9470	20	II
6640.7452	6638.9119	100	I
6646.488	6644.653	30	II
6660.5164	6658.6777	50	I
6664.1092	6662.2696	250	I
6676.5400	6674.6970	30	I
6680.5511	6678.7071	30	I
6715.824	6713.969	100	I
6729.3159	6727.4587	200	I
6758.3180	6756.4530	250	I
6780.183	6778.312	80	I
6782.285	6780.414	140	I
6793.110	6791.236	80	I
6826.561	6824.678	100	I
6830.9202	6829.0357	150	I
6836.8112	6834.9251	75	I
6913.1336	6911.2270	400	I
6945.5265	6943.6112	600	I
6991.5839	6989.6562	900	I
7002.735	7000.804	300	I
7020.504	7018.568	200	I

TABLE 2. *Test of thorium wavelengths*

Line pair	Wavelength	Wavenumber	Wavenumber difference	Deviaiton from mean
	Å	K	K	mK
1	5164.8968	19361.471	177.487	0
	5212.6816	19183.984		
2	5345.0677	18708.837	177.487	0
	5396.2608	18531.350		
3	5975.3199	16735.506	177.487	0
	6039.3697	16558.019		
4	6514.1635	15351.165	177.487	0
	6590.3598	15173.678		
5	3288.7358	30406.821	338.043	0
	3325.7088	30068.778		
6	5990.7034	16692.531	338.044	0
	6114.5300	16354.487		
7	5472.2790	18273.922	689.244	0
	5686.7695	17584.678		
8	5574.9017	17937.536	689.245	+1
	5797.6759	17248.291		

TABLE 2. *Test of thorium wavelengths*—Continued

Line pair	Wavelength	Wavenumber	Wavenumber difference	Deviation from mean
	Å	K	K	mK
9	5769. 7813 6008. 7362	17331. 679 16642. 435	689. 244	0
10	3960. 4204 4089. 8815	25249. 844 24450. 586	799. 258	+3
11	5775. 5478 6055. 0569	17314. 375 16515. 121	799. 254	−1
12	5940. 4706 6236. 5804	16833. 683 16034. 428	799. 255	0
13	6208. 9377 6533. 1470	16105. 815 15306. 559	799. 256	+1
14	6373. 7056 6715. 824	15689. 460 14890. 206	799. 254	−1
15	3413. 9919 3512. 1610	29291. 224 28472. 499	818. 725	−3
16	3519. 4096 3623. 8281	28413. 857 27595. 128	818. 729	+1
17	3585. 1986 3693. 6172	27892. 458 27073. 731	818. 727	−1
18	4379. 4071 4542. 2720	22834. 141 22015. 414	818. 727	−1
19	4664. 5080 4849. 7168	21438. 488 20619. 761	818. 727	−1
20	5136. 1764 5361. 6410	19469. 736 18651. 006	818. 730	+2
21	5465. 7236 5721. 7704	18295. 839 17477. 108	818. 731	+3
22	5765. 1270 6050. 7257	17345. 672 16526. 943	818. 729	+1
23	6184. 3331 6514. 1635	16169. 892 15351. 165	818. 727	−1
24	5558. 5886 5887. 3330	17990. 178 16985. 620	1004. 558	+1
25	6492. 5315 6945. 5265	15402. 313 14397. 757	1004. 556	−1
26	5432. 6214 5791. 2500	18407. 320 17267. 429	1139. 891	−2
27	5750. 3347 6153. 6960	17390. 292 16250. 397	1139. 895	+2
28	5976. 7203 6413. 6720	16731. 584 15591. 692	1139. 892	−1
29	6193. 6189 6664. 1092	16145. 650 15005. 757	1139. 893	0
30	4488. 1563 4767. 9332	22280. 864 20973. 448	1307. 416	−1
31	4880. 0955 5212. 6816	20491. 402 19183. 984	1307. 418	+1

TABLE 2. *Test of thorium wavelengths*—Continued

Line pair	Wavelength	Wavenumber	Wavenumber difference	Deviation from mean
	Å	K	K	mK
32	5040. 6359 5396. 2608	19838. 767 18531. 350	1307. 417	0
33	5232. 6161 5616. 8788	19110. 899 17803. 482	1307. 417	0
34	5097. 9046 5580. 9078	19615. 903 17918. 232	1697. 671	+3
35	5259. 8240 5775. 5478	19012. 043 17314. 375	1697. 668	0
36	5396. 2608 5940. 4706	18531. 350 16833. 683	1697. 667	−1
37	5616. 8788 6208. 9377	17803. 482 16105. 815	1697. 667	−1
38	6039. 3697 6729. 3159	16558. 019 14860. 352	1697. 667	−1
39	3585. 1986 3875. 9602	27892. 458 25800. 059	2092. 399	−1
40	3728. 9626 4044. 5369	26817. 110 24724. 710	2092. 400	0
41	4098. 9042 4483. 4270	24396. 764 22304. 367	2092. 397	−3
42	4687. 5060 5197. 2605	21333. 306 19240 906	2092. 400	0
43	4842. 1950 5388. 1085	20651. 791 18559. 389	2092. 402	+2
44	5003. 4924 5588. 5781	19986. 040 17893. 639	2092. 401	+1
45	5136. 1764 5754. 6225	19469. 736 17377. 334	2092. 402	+2
46	5465. 7236 6171. 5299	18295. 839 16203. 438	2092. 401	+1
47	5765. 1270 6555. 9711	17345. 672 15253. 270	2092. 402	+2
48	3691. 6742 4076. 6536	27087. 980 24529. 924	2558. 056	−1
49	3804. 1547 4214. 2542	26287. 049 23728. 991	2558. 058	+1
50	5762. 1489 6758. 3180	17354. 637 14796. 581	2558. 056	−1
51	3592. 4771 3974. 3200	27835. 946 25161. 537	2674. 409	0
52	3764. 0030 4185. 3170	26567. 460 23893. 053	2674. 407	−2
53	4828. 0490 5549. 7170	20693. 347 18018. 937	2674. 410	+1
54	5313. 4795 6193. 6189	18820. 059 16145. 650	2674. 409	0

TABLE 2. *Test of thorium wavelengths*—Continued

Line pair	Wavelength	Wavenumber	Wavenumber difference	Deviation from mean
	Å	K	K	mK
55	5345.0677 6236.5804	18708.837 16034.428	2674.409	0
56	5361.6410 6259.1550	18651.006 15976.597	2674.409	0
57	3310.3178 3657.7354	30208.580 27339.320	2869.260	0
58	3331.4345 3683.5345	30017.099 27147.839	2869.260	0
59	3458.0588 3838.9638	28917.958 26048.696	2869.262	+2
60	3599.1464 4013.6295	27784.366 24915.105	2869.261	+1
61	3643.2867 4068.5994	27447.744 24578.483	2869.261	+1
62	3840.7835 4316.4680	26036.354 23167.090	2869.264	+4
63	4113.9150 4664.5080	24307.746 21438.488	2869.258	−2
64	4251.5110 4842.195	23521.049 20651.791	2869.258	−2
65	4375.3536 5003.4924	22855.296 19986.040	2869.256	−4
66	4494.5943 5160.0414	22248.949 19379.689	2869.260	0
67	4946.8387 5765.1270	20214.930 17345.672	2869.258	−2
68	5127.3781 6011.8253	19503.145 16633.883	2869.262	+2
69	5603.1587 6676.5400	17847.076 14977.818	2869.258	−2
70	4483.4270 5220.5630	22304.367 19155.022	3149.345	0
71	5588.5781 6782.285	17893.639 14744.293	3149.346	0
72	3512.1610 4019.2344	28472.499 24880.360	3592.139	+2
73	3920.1336 4562.6266	25509.335 21917.200	3592.135	−2
74	4596.7082 5505.8312	21754.698 18162.562	3592.136	1
75	3305.1895 3764.0030	30255.451 26567.460	3687.991	+4
76	3424.9714 3920.1336	29197.324 25509.335	3687.989	+2
77	3829.4708 4459.2531	26113.269 22425.280	3687.989	+2

TABLE 2. *Test of thorium wavelengths*—Continued

Line pair	Wavelength	Wavenumber	Wavenumber difference	Deviation from mean
	Å	K	K	mK
78	3831.8604 4462.4933	26096.984 22408.997	3687.987	0
79	4003.0253 4696.3520	24981.106 21293.122	3687.984	−3
80	4101.4985 4832.4710	24381.333 20693.347	3687.986	−1
81	4113.9150 4849.7168	24307.746 20619.761	3687.985	−2
82	4212.1096 4986.7636	23741.073 20053.086	3687.987	0
83	4338.4971 5164.8968	23049.456 19361.471	3687.985	−2
84	4516.3845 5418.9918	22141.605 18453.617	3687.988	+1
85	4779.6300 5802.4380	20922.122 17234.135	3687.987	0
86	4896.3218 5975.3199	20423.494 16735.506	3687.988	+1
87	4946.8387 6050.7257	20214.930 16526.940	3687.990	+3
88	5046.1263 6199.9380	19817.181 16129.194	3687.987	0
89	3458.0588 3991.6206	28917.958 25052.481	3865.477	+4
90	4258.6948 5097.9046	23481.373 19615.903	3865.470	−3
91	4330.1329 5200.6116	23093.979 19228.508	3865.471	−2
92	4338.4971 5212.6816	23049.456 19183.984	3865.472	−1
93	4371.1038 5259.8240	22877.517 19012.043	3865.474	+1
94	4896.3218 6039.3697	20423.494 16558.019	3865.475	+2
95	3532.4595 4261.5321	28308.888 23465.739	4843.149	+1
96	4216.0158 5297.7529	23719.076 18875.928	4843.148	0
97	4350.2950 5511.5245	22986.947 18143.800	4843.147	−1
98	3381.8300 4110.4832	29569.789 24328.040	5241.749	0
99	3438.2923 4194.1984	29084.206 23842.458	5241.748	0
100	3349.7310 4116.9203	29853.143 24290.001	5563.142	0

TABLE 2. *Test of thorium wavelengths*—Continued

Line pair	Wavelength	Wavenumber	Wavenumber difference	Deviation from mean
	Å	*K*	*K*	*mK*
101	3599.1464 4500.2022	27784.366 22221.224	5563.142	0
102	4258.6948 5580.9078	23481.373 17918.232	5563.141	+1
103	4371.1038 5775.5478	22877.517 17314.375	5563.142	0
104	4705.3063 6373.7056	21252.602 15689.460	5563.142	0
105	4896.3218 6729.3159	20423.494 14860.352	5563.142	0
106	3305.1895 4185.3170	30255.451 23893.053	6362.398	+2
107	4037.1879 5432.6214	24769.717 18407.320	6362.397	+1
108	4101.4985 5549.7170	24381.333 18018.937	6362.396	0
109	4330.1329 5976.7203	23093.979 16731.584	6362.395	−1
110	4371.1038 6055.0569	22877.517 16515.121	6362.396	0
111	4705.3063 6715.824	21252.602 14890.206	6362.396	0

4. References

[1] W. F. Meggers, Trans. I.A.U. **9,** 225–226 (1955).
[2] W. F. Meggers and R. W. Stanley, J. Res. NBS **61,** 95–103 (1958).
[3] K. G. Kessler and W. F. Meggers, J. Opt. Soc. Am. **45,** 902 (1955).
[4] F. H. Rolt and H. Barrell, Proc. Roy. Soc. **A 122,** 131–133 (1929).
[5] V. Kaufman, J. Opt. Soc. Am. **52,** 866–870 (1962).
[6] C. D. Coleman, W. R. Bozman and W. F. Meggers, Table of Wavenumbers, 2000 A to 7000 A, NBS Monograph 3, Vol. 1, 500 pp. (1960).
[7] R. Zalubas, NBS Monograph 17, 103 pp. (1960).
[8] R. Zalubas, J. Res. NBS **63A,** 275–278 (1959).
[9] G. W. Charles, Compilation of Data on Some Spectra of Thorium, ORNL 2319, May 8, 1958, 162 pp.
[10] T. A. Littlefield, Trans. I.A.U. **11 B,** 212 (1961).
[11] R. W. Stanley and W. F. Meggers, J. Res. NBS **58,** 41–49 (1957).
[12] T. A. Littlefield and W. A. Wood, Trans. I.A.U. **11A,** 105–108 (1961). I.A.U. Agenda and Draft Reports, p. 142 (1964).
[13] A. Davison, A. Giacchetti and R. W. Stanley, J. Opt. Soc. Am. **52,** 447–451 (1962).
[14] A. Giacchetti, M. Gallardo, M. J. Garavaglia, Z. Gonzalez, F. P. J. Valero, and E. Zakowicz, J. Opt. Soc. Am. **54,** 957–959 (1964).

(Paper 69A2-332)

JOURNAL OF RESEARCH of the National Bureau of Standards—A. Physics and Chemistry
Vol. 69A, No. 2, March–April, 1965

Phase Equilibria in the System Vanadium Oxide-Niobium Oxide

J. L. Waring and R. S. Roth

(December 14, 1964)

The phase diagram for the pseudo-binary system V_2O_5—Nb_2O_5 was constructed from fusion characteristics and x-ray diffraction data. Three compounds were postulated for the system. The compound VNb_9O_{25} and $V_3Nb_{23}O_{62}$ were found to melt incongruently at about 1290 °C and 1322 °C respectively. The third compound occurring at about 93 to 94 mole percent Nb_2O_5 melted incongruently at approximately 1332 °C. Apparently, Nb_2O_5 accepted up to 5 mole percent V_2O_5 in solid solution, however, V_2O_5 did not accept any appreciable Nb_2O_5 in solid solution.

In addition, the Nb_2O_5 rich portions of the following binary systems were reinvestigated: ZnO—Nb_2O_5, NiO—Nb_2O_5, Al_2O_3—Nb_2O_5, TiO_2—Nb_2O_5, and ZrO_2—Nb_2O_5. In each case an Nb_2O_5 solid solution had been reported previously in excess of 90 mole percent Nb_2O_5. However, subsequent data indicated that these Nb_2O_5 solid solutions contained discrete compounds which are related to those found in the pseudo-binary V_2O_5—Nb_2O_5.

1. Introduction

In a number of previously reported phase studies of the general type M_xO_y—Nb_2O_5, the existence of Nb_2O_5-rich solid solutions were postulated. These include TiO_2—Nb_2O_5, ZrO_2—Nb_2O_5 [1],[1] Al_2O_3—Nb_2O_5 [3, 4], ZnO—Nb_2O_5 [2] and NiO—Nb_2O_5 [3, 4].

When selected compositions in these systems were examined they were found to give x-ray powder diffraction patterns with marked similarity one to the other as well as to the stable high temperature form of Nb_2O_5.

However, it seemed unlikely that a solid solution with oxygen deficiencies could account for the differences in the x-ray pattern. In an attempt to determine whether these phases were solid solutions or discrete compounds the system V_2O_5—Nb_2O_5 was selected to be studied, as cations of similar ionic radii and the same valence might be most expected to form a solid solution.

Goldschmidt [3] surveyed and reported the existence of two intermediate phases in the system: $\beta'(Nb, V)_2O_5$ and a phase with a rutile-type structure, a=4.633 Å, c=3.021 Å. However, no systematic attempt to study the phase equilibrium relationships in air has been previously reported.

X-ray diffraction data, together with the determination of the melting points of the compounds and the solidus and liquidus temperatures at various compositions across the system have supplied data from which an equilibrium diagram has been constructed.

[1] Figures in brackets indicate the literature references at the end of this paper.

2. Sample Preparation and Test Methods

High purity grade niobium and vanadium pentoxides were used. Spectrographic analysis indicated less than 0.1 percent Si, 0.01 percent Fe, Sn, and Ti and 0.001 percent Ca and Mg in the former and less than about 0.01 percent Si, 0.001 percent Ca and Cr and 0.0001 percent Ag, Ca, Mg and Mn in the latter. Cu was not determined in Nb_2O_5 because of Nb interference.

Mixtures of V_2O_5 and Nb_2O_5 were weighed to the nearest ± 0.1 mg in sufficient quantities to yield 2 g batches. No corrections were made for percent purity except loss on ignition. Each batch was mixed in a mechanical shaker for 15 min. The mixtures were then pressed into a disk in a $\frac{5}{8}$ in. diameter mold at 10^4 lb in^{-2}. The disks were placed on setters fabricated from platinum foil and calcined in air at 500 °C for 10 hr. Following this preliminary heat treatment specimens ranging in composition from 5 to 55 mole percent Nb_2O_5 were recalcined at 600 °C for 168 hr in sealed Pt tubes. Specimens ranging in composition from 90 to 99 mole percent Nb_2O_5 received an additional calcination of 1000 °C for 5 hr.

Since V_2O_5 was found to be volatile only to the extent of about 0.46 percent when heated to about 1000 °C for 6 hr, no correction other than loss on ignition was applied. However, to minimize possible volatility at higher temperatures, sealed platinum tubes were employed for all succeeding experiments unless otherwise stated. At this point it should be noted that platinum tubes approximately 2 cm long were used to contain the specimen. About one-third

of the volume was occupied by the specimen and the remainder of the tube was flattened prior to sealing. At elevated temperatures the expansion of the flattened portion of the tube provided the necessary additional volume for expansion of the vapors without rupture.

Sub-solidus and melting point values were obtained by quenching specimens sealed in platinum tubes and examining them at room temperature. An electrically heated vertical tube resistance furnace was used for quenching which had a primary winding of 60% Pt-40% Rh and a secondary or booster winding of 80% Pt-20% Rh. An a-c controller utilizing the furnace primary as one arm of a Wheatstone bridge served to control the furnace temperature to ±2 °C for extended periods of time. The secondary was regulated with a variable autotransformer.

Temperatures were measured with a Pt versus Pt 10 percent Rh thermocouple which was calibrated

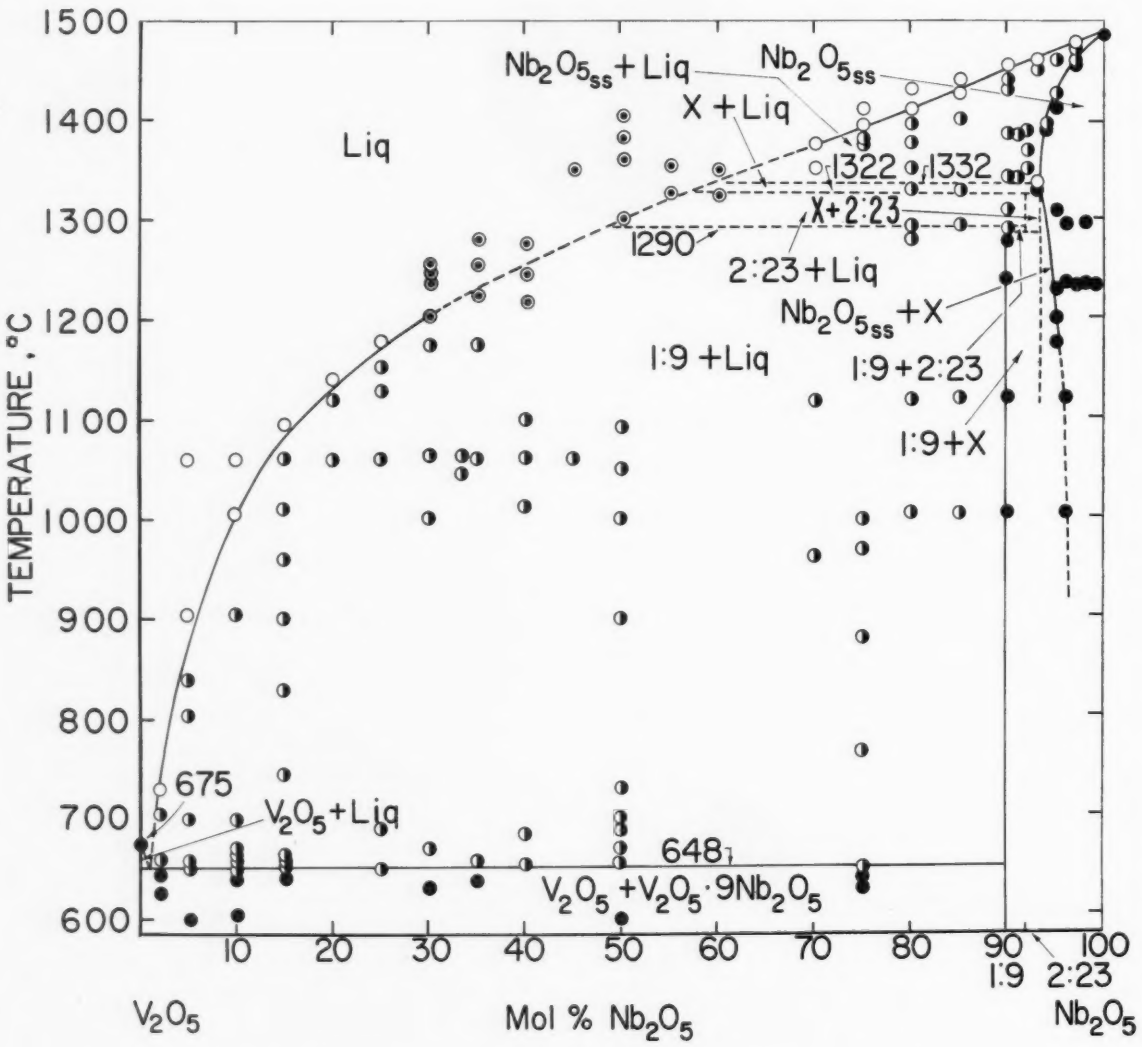

FIGURE 1. *Phase equilibrium diagram for the system vanadium oxide-niobium-oxide.*

●—no melting.
◑—partial melting.
○—complete melting.
◉—cannot be interpreted from fusion characteristics.
Liq.—liquid.
X—unknown phase.
Nb_2O_{5ss}—Nb_2O_5 solid solution.
For clarity, not all experimental data appearing in table 4 are plotted on this diagram.

several times during the course of the work against the reported values of NaCl (800.5 °C) [6], Au (1063 °C) [5] and barium disilicate (1420 °C) [7].

Liquidus values were established in the following manner: (a) In the region from 2 to 5% Nb_2O_5, the formation of a concave meniscus established the liquidus. (b) In the region from 5 to 30% Nb_2O_5, specimens when quenched from above the liquidus and examined at room temperature were glass. (c) In the region from 30 to 70% Nb_2O_5, no criteria could be employed to establish the liquidus since any given composition between these limits gave the same physical appearance over a range of about a hundred degrees, and this portion (fig. 1) of the curve was dashed. (d) In the region from 70 to 100% Nb_2O_5 (fig. 1) the formation of a concave meniscus and the abrupt change in x-ray diffraction pattern established the liquidus.

The first sign of glazing of the specimen's surface, together with a marked color change established the solidus in the 0–90 mole percent Nb_2O_5 compositional range. This interpretation seemed reasonably valid since most specimens showed abrupt changes in x-ray diffraction patterns when partially melted. Unfortunately, compositions in the Nb_2O_5 rich portion of the system 90–99% Nb_2O_5, did not provide a definitive picture of partial melting, and the approximate solidus values were delineated by data obtained from changes in the x-ray diffraction powder patterns of the quenched specimens and the solidus (figs. 1 and 2) in this region is dashed. The precision of the temperature measurement for the experimental data points is about ±2 °C and the overall accuracy of the reported temperature is about ±5 °C.

Equilibrium is generally considered to have been obtained when x-ray diffraction patterns of specimens successively heated for longer times and/or at higher temperatures show no change. However, as this system does not appear to be binary at high temperatures this criteria could not always be applied without interpretation. (See sec. 4 and table 4.) X-ray diffraction powder patterns were made using a high angle recording Geiger counter diffractometer and nickel-filtered copper radiation, with the Geiger counter traversing the specimen at 1/4°2θ/min and radiation being recorded on the chart at 1°2θ/in. The unit cell dimensions reported can be considered accurate to about ±5 in the last decimal place listed.

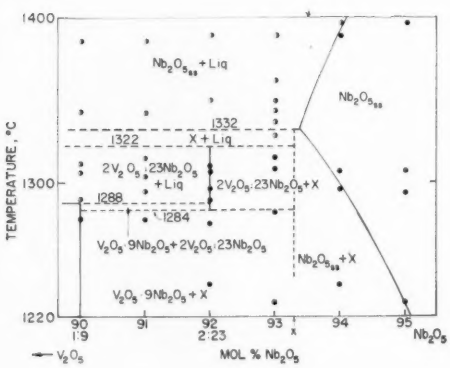

FIGURE 2. *Expanded view of the high* Nb_2O_5 *region of the phase diagram for the system vanadium oxide-niobium oxide.*

●—no melting.
◑—partial melting.
Liq.—liquid.
X—unknown phase
Nb_2O_{5ss}—Nb_2O_5 solid solution.

3. Compounds in the Pseudo-Binary System V_2O_5—Nb_2O_5

3.1. V_2O_5

Holtzberg et al. [8] concluded from x-ray diffraction and differential thermal analyses data that V_2O_5 has only one stable form. These results were later independently verified by Levin and McDaniel [9] by high temperature x-ray diffraction analysis. The structure of V_2O_5 was described by Byström et al. [10] as having the space group Pmmn with two molecules per unit cell, and the indexed x-ray powder diffraction pattern was reported by Swanson et al. [11] a=11.51 Å, b=3.559 Å, c=4.371 Å. The melting point of 675 ±5 °C was established for V_2O_5 by C. L. McDaniel of this laboratory [12].

3.2. Compound V_2O_5·$9Nb_2O_5$

The compound V_2O_5·$9Nb_2O_5$ was found to occur in the present study and to be stable to the incongruent melting point at about 1290 °C. Goldschmidt [3] reported a solid solution phase $\beta'(Nb,V)_2O_5$ which had a nominal composition $Nb_{1.8}V_{0.2}O_5$. He reported the unindexed x-ray diffraction pattern of β' $(Nb,V)_2O_5$. In the present study, the x-ray diffraction powder pattern of V_2O_5·$9Nb_2O_5$ was found to be essentially the same as that previously reported. The compound V_2O_5·$9Nb_2O_5$ (table 1) which was indexed on the basis of a body-centered tetragonal cell a=15.72 Å, c=3.821 Å was found to be isostructural with a series of phases of the general type M_2O_5·$9M'_2O_5$ [13] and apparently with Ta_2O_5·$2Nb_2O_5$ which was previously reported by Holtzberg and Reisman [14] as being cubic, and by Mohanty et al. [15] as being tetragonal.

3.3. Compound $V_2Nb_{23}O_{62}$

A compound was found to occur in the system at the ratio $2V_2O_5$:$23Nb_2O_5$ which exists from about 1284 °C, depending on the length of heating time, to the incongruent melting point at 1322 °C. The indexed x-ray diffraction powder pattern given in table 2 has a marked similarity to that of the high temperature form of Nb_2O_5. However, this phase could not be indexed as a solid solution of the high temperature modification Nb_2O_5. Roth and Wadsley [16] have shown from a single crystal structure determination that a phase TiO_2·$12Nb_2O_5$ occurs in the system TiO_2—Nb_2O_5 and is a member of a series

$M_{3n+1}O_{8n-2}$ with $n=8$. The composition $2V_2O_5 \cdot 23Nb_2O_5$ was found to have an x-ray diffraction powder pattern which is apparently isostructural with $TiO_2 \cdot 12Nb_2O_5$ which could be indexed on the basis of a monoclinic cell $a=29.77$ Å, $b=3.823$ Å, $c=21.05$ A and $\beta=95°1.6'$.

The composition $2V_2O_5 \cdot 23Nb_2O_5$ has the general formula $M_{50}O_{125}$. However, the structural formula $M_{3n+1}O_{8n-2}$ (referring to one-half the unit cell) requires the composition to be $M_{50}O_{124}$. From the above considerations it is likely that 1 out of 125 oxygen ions are lost and that the system is not binary.

TABLE 1. *X-ray diffraction powder data for the compound* $V_2O_5 \cdot 9Nb_2O_5$ (CuKα *radiation*)

d Obs Å	I/I_0[a]	$1/d^2$ obs Å^{-2}	$1/d^2$ calc. Å^{-2}[b]	hkl[b]
11.340	1	0.0080	0.0081	110
7.82	1	.0163	.0162	200
5.54	1	.0326	.0325	220
4.96	25	.0407	.0406	310
3.92	3	.0652	.0649	400
3.70	35	.0729	.0726	101
3.490	100	.0815	.0811	420
3.353	12	.0889	.0888	211
3.076	1	.1057	.1055	510
2.868	30	.1216	.1213	312
2.696	15	.1376	.1375	411
2.482	15	.1623	.1622	620
2.426	5	.1700	.1699	501
2.318	5	.1862	.1862	521
2.222	1	.2025	.2028	710
2.177	1	.2110	.2109	640
2.139	5	.2186	.2186	611
2.062	21	.2353	.2353	730
1.996	1	.2510	.2510	631
1.962	2	.2597	.2596	800
1.910	12	.2742	.2742	002

[a] Relative intensity.
[b] Based on tetragonal cell, $a=15.72$ Å, $c=3.821$ Å.

TABLE 2. *X-ray diffraction powder data for the compound* $V_2Nb_{21}O_{62}$ (CuKα *radiation*)

d Obs	I/I_0[a]	$1/d^2$ obs Å^{-2}	$1/d^2$ calc Å^{-2}	hkl
Å				
10.48	4	0.0091	0.0092	002
9.04	3	.0125	.0125	$\bar{2}02$
6.81	3	.0216	.0216	401
5.25	3	.0364	.0364	004
5.09	30	.0387	.0387	$\bar{2}04$
4.70	20	.0450	.0449	601
3.74	43	.0716	.0716	$\bar{1}11$
3.60	100	.0772	.0773	801
3.469	80	.0831	.0831	$\bar{2}06$
3.348	17	.0892	.0892	$\bar{1}13$
			.0893	$\bar{6}05$
			.0895	312
3.273	5	.0933	.0933	406
3.213	5	.0969	.0966	313
			.0969	510
3.068	5	.1061	.1062	605
2.839	23	.1241	.1242	710
2.761	17	.1312	.1313	315
2.700	20	.1372	.1372	712
2.620	3	.1459	.1456	008
			.1457	$\bar{2}08$
2.528	27	.1565	.1564	$\bar{1}0\ 0\ 5$
2.467	16	.1643	.1642	607
			.1645	912
2.310	17	.1874	.1872	516
2.066	37	.2343	.2344	$\bar{4}\ 0\ 10$
2.039	38	.2404	.2403	609
1.913	33	.2734	.2736	020

[a] Relative intensity.
[b] Based on monoclinic cell $a=29.77$ Å, $b=3.823$ Å, $c=21.05$ Å and $\beta=95°1.6'$.

3.4. Compound X

A new phase was found to occur in the system at approximately 93 to 94 mole percent Nb_2O_5 and to melt incongruently at about 1332 °C. The partially indexed x-ray diffraction powder pattern is given in table 3. The x-ray pattern of this phase has the greatest similarity to the high temperature polymorph of Nb_2O_5 of any of the phases which occur in the system. However, the low angle x-ray diffraction lines, which should shift the least in 2θ for a solid solution, actually are shifted more than many high angle lines. Therefore, the pattern cannot be indexed on the basis of an Nb_2O_5 solid solution or as a solid solution of $V_2Nb_{25}O_{62}$.

TABLE 3. *X-ray diffraction powder data for the unknown phase X occurring at about 93 to 94 mole percent* Nb_2O_5 (CuKα *radiation*)

hkl[a]	d_{calc}	d_{obs}	I/I_0[b]
	Å	Å	
002	15.85	16.00	5
003	10.57	10.57	10
$20\bar{1}$	10.53		
$10\bar{3}$	10.53		
201	9.09	9.11	6
004	7.93	7.92	6
$20\bar{3}$	6.57	6.55	6
$10\bar{5}$	6.54		
006	5.28	5.27	7
$40\bar{2}$	5.27		
$20\bar{6}$	5.26		
$40\bar{1}$	5.26		
400	5.11	5.12	35
107	4.68	4.68	17
402	4.54	4.54	5
404	3.88	3.88	5
$30\bar{8}$	3.87		
010	3.83	3.83	6
110	3.76	3.75	65
$11\bar{1}$	3.76		
306	3.75		
502	3.74		
$\bar{1}09$	3.63	3.63	83
112	3.63		
211	3.53	3.53	10
$50\bar{3}$	3.53		
009	3.52	3.51	13
$60\bar{3}$	3.51		
$30\bar{9}$	3.51		
$21\bar{3}$	3.492	3.477	100
$60\bar{1}$	3.483		
$11\bar{4}$	3.464		
$60\bar{4}$	3.461		
208	3.419	3.418	15
		3.290	5
		3.190	7
		3.076	8
		2.953	8
		2.834	23
		2.771	32
		2.707	33
		2.626	4
		2.549	13
		2.536	33
		2.514	4
		2.473	27
		2.451	5
		2.335	9
		2.314	16
		2.273	4
		2.259	4
		2.202	4
		2.171	7
		2.102	4
		2.085	21
020		2.040	25
		1.9161	31

[a] This pattern was tentatively indexed only after approximate a, c, and β unit cell constants were provided by Mr. A. Perloff from $h0l$ single crystal precession data. The unit cell constants derived from this data are $a=21.12$A, $b=3.831$A, $c=32.75$ Å and $\beta=104°5'$. With the exception of the (020) Miller indexes are not reported for reflections with d values less than 3.419 Å because of the relatively large size of the monoclinic cell.
[b] Relative intensity.

3.5. Rutile Type Phase

Goldschmidt [3] reported a phase with a rutile type structure and an approximate composition ranging from $90V_2O_5$:$10Nb_2O_5$ to about $75V_2O_5$:$25Nb_2O_5$. According to Goldschmidt this rutile phase formed from specimens fused in a carbon arc furnace in an atmosphere of argon and was not present when the specimens were annealed at 800 °C in air. In the present study no rutile phase was found to occur in the system in an air environment. However, the composition $75V_2O_5$:$25Nb_2O_5$ heated to about 1300 °C in a flowing stream of argon contained a rutile type phase.

From the above discussion it can probably be concluded the rutile phase is a reduced phase which occurs in the V-Nb-O system.

3.6. Nb_2O_5

The phase equilibrium relations of the polymorphs of Nb_2O_5 have been discussed by various workers [17], [18], [19], [20]. Since it has been concluded by [17], [20], [21] that the high temperature polymorph of Nb_2O_5 is the stable form and since V_2O_5 has no catalytic action on the various modifications of Nb_2O_5 no phase transition has been indicated. The unit cell dimensions were reported previously by one of the present authors [21].

4. Discussion of Phase Equilibria

Although the V_2O_5-Nb_2O_5 system does not appear to be binary, a pseudo-binary phase diagram can be constructed from the experimental data listed in table 4. The appearance of the pseudo-binary diagram might well be changed by different environmental and/or time-temperature experimental conditions and only a complete study of the ternary diagram V-Nb-O could be expected to elucidate the true equilibrium relations. As constructed, the pseudo-binary system contains three intermediate compounds, all melting incongruently. The indexed x-ray diffraction powder pattern and unit cell dimensions of the first, $V_2O_5{\cdot}9Nb_2O_5$, are given in table 1 and those of the second, $V_2Nb_{23}O_{62}$, in table 2. The *d*-spacings for the third, a compound of unknown symmetry occurring at about 93 to 94 mole percent Nb_2O_5, are given in table 3.

TABLE 4. *Experimental data for compositions in the system vanadium oxide-niobum oxide*

Composition		Heat treatment [a]		Results	
V_2O_5	Nb_2O_5	Temp.	Time	Physical observation	X-ray diffraction analysis [b]
Mole %	*Mole %*	*°C*	*hr*		
98	2	627	1	Not melted	V_2O_5+$V_2O_5{\cdot}9Nb_2O_5$+unknown [c]
		649	0.08	Partially melted	$V_2O_{5_{ss}}$ [d]+$V_2O_5{\cdot}9Nb_2O_5$
		661	.08	do	
		707	.25	do	$V_2O_{5_{ss}}$ [d]+unknown [c]
		730	.33	Completely melted	Do.
95	5	600	.3	Not melted	V_2O_5+L−Nb_2O_5 [e]
		602	.5	do	Do.
		652	19	Partially melted	$V_2O_5{\cdot}9Nb_2O_5$+$V_2O_{5_{ss}}$ [d]
		658	.5	do	Do.
		700	.5	do	Do.
		804	.5	do	$V_2O_{5_{ss}}$ [d]
		841	.5	do	Do.
		904	.5	Completely melted	Glass
		1060	1	do	Do.
90	10	605	.5	Not melted	
		640	.33	do	V_2O_5+$V_2O_5{\cdot}9Nb_2O_5$
		650	20	Partially melted	
		652	.33	do	
		658	.33	do	$V_2O_{5_{ss}}$ [d]+$V_2O_5{\cdot}9Nb_2O_5$
		662	.33	do	
		664	67	do	$V_2O_{5_{ss}}$ [d]+$V_2O_5{\cdot}9Nb_2O_5$
		666	.33	do	Do.
		673	.08	do	
		700	.5	do	$V_2O_{5_{ss}}$ [d]+$V_2O_5{\cdot}9Nb_2O_5$
		904	.5	do	$V_2O_{5_{ss}}$ [d]+$V_2O_5{\cdot}9Nb_2O_5$+unknown [c]
		1006	.5	Completely melted	Glass
		1060	1	do	Do.
85	15	[f] 640	.33	Not melted	V_2O_5+$V_2O_5{\cdot}9Nb_2O_5$+unknown [c]
		[f] 652	.33	Partially melted	$V_2O_{5_{ss}}$ [d]+$V_2O_5{\cdot}9Nb_2O_5$+unknown [c]
		658	21	do	Do.
		665	.33	do	Do.
		[f] 666	16	Partially melted	$V_2O_{5_{ss}}$ [d]+$V_2O_5{\cdot}9Nb_2O_5$
		670	.5	do	
		674	.5	do	
		688	.5	do	$V_2O_{5_{ss}}$ [d]+$V_2O_5{\cdot}9Nb_2O_5$
		746	.5	do	$V_2O_{5_{ss}}$+$V_2O_5{\cdot}9Nb_2O_5$
		828	1	do	Do.
		902	1	do	Do.
		961	4	do	Do.
		1011	.5	do	Do.
		1061	1	do	Glass
		1096	.5	Completely melted	Do.

See footnotes at end of table.

TABLE 4. *Experimental data for compositions in the system vanadium oxide-niobium oxide*—Continued

Composition		Heat treatment [a]		Results	
V_2O_5	Nb_2O_5	Temp.	Time	Physical observation	X-ray diffraction analysis [b]
Mole %	*Mole %*	*°C*	*hr*		
80	20	1061	1	Partially melted	$V_2O_5{}^{d}{}_{ss}+V_2O_5{\cdot}9Nb_2O_5$
		1119	.75	do	Glass
		1140	.5	Completely melted	Do.
75	25	[f] 650	1	Partially melted	
		[f] 690	16	do	$V_2O_5{}^{d}{}_{ss}+V_2O_5{\cdot}9Nb_2O_5$
		1061	1	Partially melted	Do.
		1130	.5	do	Do.
		1154	.5	do	Glass+$V_2O_5{\cdot}9Nb_2O_5$
		1180	.33	Completely melted	Glass
70	30	632	168	Not melted	$V_2O_5+V_2O_5{\cdot}9Nb_2O_5$+unknown [c, e]
		[f] 670	.5	Partially melted	
		1064	.33	do	$V_2O_5{}^{d}{}_{ss}+V_2O_5{\cdot}9Nb_2O_5$
		1175	.5	do	$V_2O_5{}^{d}{}_{ss}+V_2O_5{\cdot}9Nb_2O_5$+glass
		1204	.5	Melted [b]	Glass+unknown [c]
		1235	.5	do	Do.
		1246	.17	do	Do.
		1257	.5	do	Do.
66.67	33.33	1045	3	Partially melted	$V_2O_5{}^{d}{}_{ss}+V_2O_5{\cdot}9Nb_2O_5$+unknown [e]
		1064	.66	do	$V_2O_5{}^{d}{}_{ss}+V_2O_5{\cdot}9Nb_2O_5$
65	35	[g] 637	.5	Not melted	$V_2O_5+V_2O_5{\cdot}9Nb_2O_5$
		[g] 658	.5	Partially melted	
		1062	24	do	$V_2O_5{}^{d}{}_{ss}+V_2O_5{\cdot}9Nb_2O_5$
		1175	.5	do	Do.
		1225	.5	Melted [b]	Do.
		1255	.75	do [b]	Do.
		1279	.5	do	Do.
		1280	.75	do	Do.
60	40	[f] 654	1	Partially melted	
		[f] 684	60	do	$V_2O_5{\cdot}9Nb_2O_5+V_2O_5{}^{d}{}_{ss}$
		[f] 1014	60	do	Do.
		[f] 1062	24	do	Do.
		[f] 1100	65	do	Do.
		[f] 1219	.5	Melted [b]	$V_2O_5{\cdot}9Nb_2O_5+V_2O_5{}^{d}{}_{ss}$
		[f] 1246	.17	do	$V_2O_5{\cdot}9Nb_2O_5+V_2O_5{}^{d}{}_{ss}$+unknown [e]
		[f] 1277	.08	do	$V_2O_5{\cdot}9Nb_2O_5+V_2O_5{}^{d}{}_{ss}$
55	45	1060	60	Partially melted	Do.
		1352	.17	Completely melted	
50	50	600	6	Not melted	$V_2O_5{\cdot}9Nb_2O_5+V_2O_5$
		657	3	Partially melted	
		[f] 670	.5	do	$V_2O_5{\cdot}9Nb_2O_5+V_2O_5{}^{d}{}_{ss}$
		[f] 688	.5	do	
		703	1	do	
		730	1	do	$V_2O_5{\cdot}9Nb_2O_5+V_2O_5{}^{d}{}_{ss}$
		901	1	do	Do.
		999	16	do	Do.
		1049	22	do	Do.
		1092	1.5	do	Do.
		1300	.08	Melted [b]	Do.
		1358	.17	do	
		1382	.17	do	
		1402	.17	do	$V_2O_5{\cdot}9Nb_2O_5+V_2O_5{}^{d}{}_{ss}$
45	55	1325	.1	do	
		1352	.1	do	
40	60	1324	.1	Melted [b]	
		1349	.1	do [b]	
30	70	963	.08	Partially melted	$V_2O_5{\cdot}9Nb_2O_5+V_2O{}^{d}{}_{ss}$
		1119	.08	do	Do.
		1350	.08	Melted [b]	$M-Nb_2O_5{}^{t,e}$
		1375	.08	do [b]	Do.
25	75	629	.25	Not melted	$M-Nb_2O_5{}^{t}+L\ Nb_2O_5$
		642	.33	do	
		649	.5	Partially melted	$V_2O_5{\cdot}9Nb_2O_5+V_2O_5{}^{d}{}_{ss}$ +unknown [e]
		[f] 767	.3	do	$V_2O_5{\cdot}9Nb_2O_5+V_2O_5{}^{d}{}_{ss}$
		880	16	do	Do.
		970	2	do	Do.
		[g] 1375	.08	do	
		[g] 1382	.08	do	
		[g] 1395	.08	Completely melted	
		[g] 1410	.25	do	$L-Nb_2O_5{}^{l}$

See footnotes at end of table.

TABLE 4. *Experimental data for compositions in the system vanadium oxide-niobium oxide*—Continued

Composition		Heat treatment [a]		Results	
V_2O_5	Nb_2O_5	Temp.	Time	Physical observation	X-ray diffraction analysis [b]
Mole %	*Mole %*	*°C*	*hr*		
20	80	≤ 1006	24	Partially melted	$V_2O_5 \cdot 9Nb_2O_5 + V_2O_{5ss}$ [d]
		≤ 1121	16	do	Do.
		≤ 1280	65	do	Do.
		≤ 1294	2	do	Do.
		≤ 1329	168	do	$V_2O_5 \cdot 9Nb_2O_5 + V_2Nb_{22}O_{62}$
		≤ 1352	.66	do	$V_2O_5 \cdot 9Nb_2O_5$
		≤ 1377	2	do	$V_2O_5 \cdot 9Nb_2O_5 + V_2Nb_{22}O_{62}$
		≤ 1394	.5	do	
		≤ 1410	.25	Completely melted	$M - Nb_2O_5$ [i]
		≤ 1430	.25	do	Do.
15	85	≤ 1006	65	Partially melted	$V_2O_5 \cdot 9Nb_2O_5$
		≤ 1121	16	do	Do.
		≤ 1294	25	do	Do.
		≤ 1329	168	do	$V_2Nb_{22}O_{62}$
		≤ 1400	1.5	do	$V_2Nb_{22}O_{62} + Nb_2O_{5ss}$
		≤ 1426	1.5	Completely melted	Do.
		≤ 1440	1.5	do	Do.
10	90	≤ 1000	65	Not melted	$V_2O_5 \cdot 9Nb_2O_5$
		≤ 1122	16	do	Do.
		≤ 1240	72	do	Do.
		≤ 1278	72	do	Do.
		≤ 1290	72	Partially melted	$V_2O_5 \cdot 9Nb_2O_5 + V_2Nb_{22}O_{62}$
		≤ 1306	.08	do	Do.
		≤ 1311	72	do	$V_2Nb_{22}O_{62} + V_2O_5 \cdot 9Nb_2O_5$
		≤ 1311	72	do	$V_2Nb_{22}O_{62}$
		≤ 1342	22	do	$V_2O_5 \cdot 9Nb_2O_5$ [k]
		≤ 1385	46	do	Nb_2O_{5ss}
		≤ 1431	.33	do	$V_2Nb_{22}O_{62} + Nb_2O_{5ss}$
		≤ 1441	2	do	$M - Nb_2O_5$ [j]
		≤ 1455	1	Completely melted	Nb_2O_{5ss}
		≤ 1458	.33	do	$M - Nb_2O_5$ [j] + L Nb_2O_5
		≤ 1471	.08	do	
	91	≤ 1122	20	do	$V_2O_5 \cdot 9Nb_2O_5$ [k]
		≤ 1175	88	do	Do.
		≤ 1201	72	do	$V_2O_5 \cdot 9Nb_2O_5 + X$ [l]
		≤ 1278	72	do	Do.
		≤ 1295	22	Partially melted	$V_2O_5 \cdot 9Nb_2O_5$
		≤ 1304	60	do	$V_2Nb_{22}O_{62} + V_2O_5 \cdot 9Nb_2O_5$
		≤ 1315	70	do	Do.
		≤ 1342	22	do	$V_2O_5 \cdot 9Nb_2O_5$
		≤ 1385	46	do	$Nb_2O_{5ss} + V_2Nb_{22}O_{62}$
8	92	≤ 1006	65	Not melted	$V_2O_5 \cdot 9Nb_2O_5 + X$ [l]
		≤ 1121	65	do	Do.
		≤ 1240	72	do	Do.
		≤ 1276	91	do	Do.
		≤ 1290	72	do	$V_2Nb_{22}O_{62}$
		≤ 1297	25	do	$(V_2O_5 \cdot 9Nb_2O_5 + X + V_2Nb_{22}O_{62} + Nb_2O_{5ss}^{m})$ [e]
		≤ 1307	90	do	$V_2O_5 \cdot 9Nb_2O_5 + (X + V_2Nb_{22}O_{62})$ [e]
		≤ 1311	72	do	$V_2Nb_{22}O_{62}$
		≤ 1350	24	Partially melted	$V_2O_{5ss} \cdot 9Nb_2O_5 + V_2Nb_{22}O_{62} + Nb_2O_{5ss}$
		≤ 1389	19	do	$Nb_2O_5 + V_2Nb_{22}O_{62}$
7	93	≤ 1006	65	Not melted	$(V_2O_5 \cdot 9Nb_2O_5 + M - Nb_2O_5^{i})$ [e]
		≤ 1175	88	do	$(X + Nb_2O_{5ss}^{m} + V_2Nb_{22}O_{62})$ [e]
		≤ 1201	72	do	$(X + V_2O_5 \cdot 9Nb_2O_5 + Nb_2O_{5ss}^{m})$ [e]
		≤ 1229	72	do	Do.
		≤ 1283	4	do	$X + V_2O_5 \cdot 9Nb_2O_5$
		≤ 1309	72	do	$X + V_2Nb_{22}O_{62}$
		≤ 1316	.5	do	$(V_2Nb_{22}O_{62} + X + Nb_2O_{5ss}^{m})$ [e]
		≤ 1323	1	Partially melted	
		≤ 1323	72	do	$V_2Nb_{22}O_{62} + V_2O_5 \cdot 9Nb_2O_5$
		≤ 1329	168	do	$V_2Nb_{22}O_{62} + X$ [l]
		≤ 1337	16	do	$V_2O_5 \cdot 9Nb_2O_5 + Nb_2O_{5ss} + V_2Nb_{22}O_{62}$
		≤ 1450	.25	do	
		≤ 1460	1	Completely melted	$Nb_2O_{5ss} + X$ [l]
		≤ 1464	1	do	$Nb_2O_{5ss} + X$ [l] $+ V_2Nb_{22}O_{62}$
6	94	≤ 1006	16	Not melted	$(V_2O_5 \cdot 9Nb_2O_5 + Nb_2O_{5ss}^{m})$ [e]
		≤ 1121	65	do	$(V_2O_5 \cdot 9Nb_2O_5 + X + V_2Nb_{22}O_{62})$ [e]
		≤ 1240	72	do	$Nb_2O_{5ss}^{m} + X$ [l]
		≤ 1297	25	do	$(Nb_2O_{5ss}^{m} + V_2Nb_{22}O_{62})$ [e]
		≤ 1308	70	do	$Nb_2O_{5ss}^{m} + X$ [l]
		≤ 1389	.06	do	
		≤ 1397	17	Partially melted	Nb_2O_{5ss}
		≤ 1403	.06	do	

See footnotes at end of table.

TABLE 4. *Experimental data for compositions in the system vanadium oxide-niobum oxide*—Continued

Composition		Heat treatment [a]		Results	
V_2O_5	Nb_2O_5	Temp.	Time	Physical observation	X-ray diffraction analysis
Mole X	*Mole* X	°C	*hr*		
5	95	[e] 1006	65	Not melted	(M−$Nb_2O_5^i$+V_2O_5·9Nb_2O_5)[c]
		[e] 1175	88	do	V_2O_5·9Nb_2O_5+X[i]
		[e] 1201	72	do	V_2O_5·9Nb_2O_5+X[i]
		[e] 1229	72	do	$Nb_2O_{5_{ss}}$[m]
		[e] 1295	2	do	Do.
		[e] 1308	70	do	Do.
		[e] 1397	16	do	Do.
		[e] 1412	.25	do	
		[e] 1427	.25	Partially melted	
		[e] 1460	.25	do	$Nb_2O_{5_{ss}}$+X[i]
4	96	[e] 1006	65	Not melted	L−Nb_2O_5+$Nb_2O_{5_{ss}}$[m]
		[e] 1121	65	do	$Nb_2O_{5_{ss}}$[m]
		[e] 1236	115	do	Do.
		[e] 1296	25	do	Do.
		[e] 1308	70	do	Do.
3	97	[e] 1233	72	do	Do.
		[e] 1405	.25	do	
		[e] 1420	.16	do	
		[e] 1455	.16	do	
		[e] 1457	.16	Partially melted	
		[e] 1472	.06	do	
		[e] 1477	.16	Completely melted	
2	98	[e] 1236	115	Not melted	$Nb_2O_{5_{ss}}$[m]
		[e] 1296	25	do	Do.
1	99	[e] 1233	72	do	Do.

[a] All specimens were preheated to 500 °C for 10 hr. Rate of heating and cooling was approximately 3°/min. Specimens were heated in sealed Pt tubes and quenched from temperature indicated.

[b] The phases identified are given in the order of the amount present (greatest amount first) at room temperature. These phases are not necessarily those present at the temperature to which the specimen was heated.

[c] Unknown—a small amount of an unknown metastable phase with x-ray diffraction lines occurring at the following 2θ values: 22.22°, 27.27°, 30.28°, 37.84°, 44.78°, 45.22°, 47.34°, and 49.70°.

[d] Specimen contained metastable "V_2O_5 type solid solution" when quenched from above the solidus and examined at room temperature.

[e] The interpretation of the x-ray diffraction pattern is inconsistent with the phase diagram and is considered to be non-equilibrium due to differences in time and/or temperature of heat treatment.

[f] Second heat treatment was 600 °C for 168 hr in sealed Pt tubes. Rate of heating and cooling was approximately 3°/min.

[g] Second heat treatment was 1000 °C for 5 hr. Rate of heating and cooling was approximately 3° min.

[h] Criteria could not be established to determine complete melting (see sec. 2).

[i] Specimen contained (nonequilibrium) M-type Nb_2O_5 [29].

[j] Specimen contained (nonequilibrium) low temperature form of Nb_2O_5 when quenched from above the liquidus and examined at room tenperature.

[k] The presence of a second phase was detected with a petrographic microscope.

[l] Unknown phase occurring at about 93 to 94 mole percent Nb_2O_5.

[m] Specimen contained a phase interpreted as Nb_2O_5 solid solution, however; other discrete phases may be present which are not detected by the present experimental methods.

4.1. Description of Phase Diagram

The liquidus falls sharply from the melting point of V_2O_5 (675 °C) to a eutectic at about 1 mole percent Nb_2O_5 and 648 °C. The exact eutectic composition was not determined because of the relatively small amount of Nb_2O_5 involved and the liquidus lines defining the eutectic composition are dashed. The liquidus is also dashed from 30 to 70 mole percent Nb_2O_5 (see sec. 2) and is indicated as rising smoothly from the eutectic composition to a peritectic at about 48 mole percent Nb_2O_5 and 1290 °C which corresponds to the incongruent melting temperature of the compound V_2O_5·9Nb_2O_5. There is no apparent solid solution on either side of this compound, as indicated by the similarity of unit cell dimensions in the two phase regions adjacent to the 1:9 composition. The liquidus again rises smoothly to another peritectic at about 57 mole percent Nb_2O_5 and 1322 °C which represents the incongruent melting temperature of the compound $V_2Nb_{23}O_{62}$.

A two phase area should separate the compounds $V_2Nb_{23}O_{62}$ and V_2O_5·9Nb_2O_5. This small area, represented in figures 1 and 2 as extending in width from 90 to 92 mole percent Nb_2O_5, was not found experimentally and is dashed. The liquidus rises again from approximately 60 mole % Nb_2O_5 and 1332 °C, the incongruent melting point of the phase occurring at some composition apparently between 93 and 94 mole percent Nb_2O_5 to the melting point of Nb_2O_5.

A narrow two phase area was found to occur from about 92 to 94 mole percent Nb_2O_5 separating the X compound and the $2V_2O_5$·23Nb_2O_5 compound. Another two phase area, of less than 1 mole percent width just below the solidus, separates the X compound and Nb_2O_5 ss field. About 5 mole percent V_2O_5 is apparently accepted by Nb_2O_5 in solid solution. Since the unit cell dimensions of the Nb_2O_5 solid solution did not change significantly with composition, the solid solution area was delineated by the disappearing phase method. In addition, it should again be emphasized at this

point, that the x-ray diffraction patterns for $2V_2O_5$:$23Nb_2O_5$ and the X compound bear a marked similarity to one another and to the high temperature form of Nb_2O_5. Furthermore, it is not impossible that other discrete phases may exist which are below the limit of detection of the experimental conditions employed.

Since V_2O_5 did not stabilize the low temperature form of Nb_2O_5 and since temperatures below 1200 °C were not sufficient to attain equilibrium, the lines delineating the areas represented on figure 1 from 90 to 99 mole percent Nb_2O_5 (below 1200 °C) were dashed.

The liquidus rises again from 1332 °C and 60 mole percent Nb_2O_5, the peritectic for the X compound to the melting point of Nb_2O_5. This 1485 °C melting point was determined previously by the authors [22] and was not redetermined for this study.

4.2. Reversibility, Oxidation, and Reduction

Relatively long periods of time at temperatures above the apparent minimum decomposition temperature of 1288 °C were required in order to form the $2V_2O_5$:$23Nb_2O_5$ compound. This apparent minimum decomposition was delineated from data obtained by heating the compound at successively higher temperatures.

To establish reversibility, it is necessary to decompose the compound into the same two phases previously seen below the apparent minimum decomposition temperature. Both the 92 and 93 mole percent Nb_2O_5 compositions were reheated at lower temperatures in sealed and unsealed Pt tubes and these results are given in table 5. The composition 8 mole percent V_2O_5:92 mole percent Nb_2O_5 when heated to 1307 °C for 90 hr in a sealed Pt tube formed the compound $V_2Nb_{23}O_{62}$. This compound when reheated in a closed Pt tube at 1222 °C for 70 hr as outlined in table 5 was not reversed to V_2O_5·$9Nb_2O_5$+X phase, but formed only the X phase at the expense of some $V_2Nb_{23}O_{62}$. This X phase apparently exists at some composition between 93 and 94 mole percent Nb_2O_5. A portion of the same specimen previously heated 1222 °C for 70 hr was again reheated to 1298 °C for 68 hr in a sealed Pt tube and further reduction apparently took place. Some of the $V_2Nb_{23}O_{62}$ was still present but the X phase could no longer be detected. Another more reduced phase occurred which was found from x-ray diffraction data to be apparently isostructural with the compound $Ti_2Nb_{10}O_{29}$ reported by Wadsley [23].

The situation, however, is quite different when the same composition received a similar heat treatment in unsealed Pt tubes. When the compound $V_2Nb_{23}O_{62}$, previously formed by heating to 1307 °C for 90 hr was reheated at 1222 °C for 70 hr in an unsealed tube, the x-ray diffraction powder pattern data indicated that the specimen apparently contained a non-equilibrium mixture of three phases, the X phase, V_2O_5·$9Nb_2O_5$, and $V_2Nb_{23}O_{62}$. Apparently it was approaching binary equilibrium and tending to reverse into V_2O_5·$9Nb_2O_5$+X phase. A portion of this material previously heated at 1222 °C for 70 hr unsealed was again reheated to 1298 °C for 68 hr in an open tube. The x-ray diffraction pattern of this material showed the presence of 2 phases $2V_2O_5$·$23Nb_2O_5$ and X phase. It has apparently changed composition slightly due to volatilization.

In view of the foregoing discussion of an open versus closed system, it can probably be concluded that in the V_2O_5-Nb_2O_5 system, specimens when

TABLE 5. *Experimental data for reversibility of phases in the system vanadium oxide-niobium oxide*

Composition Mole %		Initial heat treatment		X-ray [a]	Final heat treatment		X-ray [a]
V_2O_5	Nb_2O_5	Temp.	Time	Identification	Temp.	Time	Identification
		°C	hr		°C	hr	
		500	10				
7	93	1000	5				
		[b] 1323	72	X [c]+V_2O_5·$9Nb_2O_5$	[b] 1235	72	X [c]
		500	10				
		1000	5				
		[b] 1323	72	X [c]+V_2O_5·$9Nb_2O_5$	[b] 1219	144	X [c]+V_2O_5·$9Nb_2O_5$
		500	10				
8	92	[b] 1307	90	$2V_2O_5$·$23Nb_2O_5$	[b] 1298	168	$2V_2O_5$·$23Nb_2O_5$
		500	10				
		[b] 1307	90	$2V_2O_5$·$23Nb_2O_5$	[b] 1222	70	$2V_2O_5$·$23Nb_2O_5$+X [c]
		500	10				
		[b] 1307	90				
		[b] 1222	70	$2V_2O_5$·$23Nb_2O_5$+X [c]	[b] 1298	68	$2V_2O_5$·$23Nb_2O_5$+$(V,Nb)_{12}O_{29}$ [d]
		500	10				
		[b] 1307	90	$2V_2O_5$·$23Nb_2O_5$	[c] 1222	70	X [c]+V_2O_5·$9Nb_2O_5$+$2V_2O_5$·$23Nb_2O_5$
		500	10				
		[c] 1307	90				
		[c] 1222	70	X [c]+V_2O_5·$9Nb_2O_5$+$2V_2O_5$·$23Nb_2O_5$	[c] 1298	68	$2V_2O_5$·$23Nb_2O_5$

[a] The phases identified are given in the order of amount present (greatest amount first) at room temperature. The phases are not necessarily those present at the temperature to which the specimens were heated.

[b] Specimen heated in sealed Pt tube and quenched.

[c] Unknown phase occurring in the system at approximately 93 to 94 mole percent Nb_2O_5.

[d] A reduced phase apparently isostructural with the monoclinic form of $2TiO_2$·$5Nb_2O_5$ [23].

[c] Specimen heated in open Pt tube and quenched.

heated in a closed or oxygen deficient environment tended to reduce with time and those heated in an open or oxygen rich environment tended to reverse and approach binary equilibrium. Since the experimental evidence apparently did not validate reversibility in the closed or restricted oxygen situation, the line indicating a minimum decomposition for the compound $V_2Nb_{23}O_{62}$ was dashed.

5. Nb_2O_5-Type "Solid Solution"

A re-examination of selected compositions in the systems ZnO-Nb_2O_5; NiO-Nb_2O_5; Al_2O_3-Nb_2O_5; TiO_2-Nb_2O_5; and ZrO_2-Nb_2O_5, has shown that phases reported previously as "Nb_2O_5 solid solution" are, in fact, discrete compounds. Several of the compounds in the V_2O_5-Nb_2O_5 pseudo-binary system (VNb_9O_{25}, $V_2Nb_{23}O_{62}$ and $(V, Nb)_{12}O_{29}$) have apparently analogous structures in other mixed oxide systems.

All of these phases are grouped in table 6 into five general formula types according to the cation to anion ratio.

It is worth noting that in this investigation no phase was detected in the V_2O_5-Nb_2O_5 pseudo-binary system with either of the cation to anion ratios 11:27 or 3:7.

Goldschmidt [3] reported the existence of Nb_2O_{5ss} in the Al_2O_3-Nb_2O_5 system. Thereafter, Layden [24] postulated from the Norin and Magneli [25] formulae that compounds should occur at the compositions Al_2O_3·$9Nb_2O_5$, Al_2O_3·$25Nb_2O_5$ and Al_2O_3·$49Nb_2O_5$ but found only the first two. Roth, Wadsley & Gatehouse [26] reported the compound $Al_2Nb_{24}O_{62}$ (1:49) and indicated, from structural considerations, that the 1:25 compound should have the composition $AlNb_{21}O_{54}$. Andersson and Roth [27] from single crystal data found the compound occurring around the 1:9 composition to have the actual formula Al_2O_3·$11Nb_2O_5$.

6. Summary

The system V_2O_5-Nb_2O_5 was studied and the phase diagram was constructed from fusion characteristics, and x-ray diffraction data.

From structural considerations and from experimental evidence this system does not appear to be binary.

There seemed to be no evidence for equilibrium solid solution of Nb_2O_5 in V_2O_5 and a eutectic occurred at approximately 1 mole percent Nb_2O_5 and 648 °C.

The existence of three intermediate compounds was postulated. The first, V_2O_5·$9Nb_2O_5$ melted incongruently at about 1290 °C and the second $V_2Nb_{23}O_{62}$ melted incongruently at about 1322 °C. The third compound which melted incongruently at about 1332 °C was found to exist at some composition between about 93 and 94 mole percent Nb_2O_5. Up to about 5 mole percent V_2O_5 was apparently accepted by Nb_2O_5 in solid solution lowering the melting point of Nb_2O_5 from 1485 to 1332 °C.

The possibility of other discrete phases which cannot be identified by the experimental techniques employed in the study must not be excluded in the region from 90 to 99 mole percent Nb_2O_5. In addition the Nb_2O_5 rich portions of the following binary systems were reinvestigated: ZnO-Nb_2O_5, NiO-Nb_2O_5, Al_2O_3-Nb_2O_5, TiO_2-Nb_2O_5, and ZrO_2-Nb_2O_5. Solid solution of M_xO_y with Nb_2O_5 was previously reported in all cases in excess of 90 mole percent Nb_2O_5. Subsequent data (table 6) has shown that in each of these systems discrete compounds could be identified in compositions previously reported as being Nb_2O_5 solid solution. The compound $V_2Nb_{23}O_{62}$ is apparently isostructural with $TiNb_{24}O_{62}$ and $Al_2Nb_{24}O_{62}$. The highly reduced compound $(V,Nb)_{12}O_{29}$ is apparently isostructural with $Ti_2Nb_{10}O_{29}$, $Nb_{12}O_{29}$, $AlNb_{11}O_{29}$, $NiNb_{11}O_{29}$, and $ZnNb_{11}O_{29}$.

TABLE 6. *Apparently isostructural phases in mixed oxide systems of* Nb_2O_5 *or* Ta_2O_5

Composition	Valence of cation additions to Nb_2O_5 and/or Ta_2O_5			
Cation: Anion	M_2O_5–M'_2O_5	MO_2–M'_2O_5	M_2O_3–M'_2O_5	MO–M'_2O_5
2:5	Nb_2O_5 $V\,Nb_9O_{25}$ [a] [13] $P\,Nb_9O_{25}$ [13] $As\,Nb_9O_{25}$ [13] $Ta_{2\,1/3}Nb_{6\,2/3}O_{25}$ [13] $P\,Ta_9O_{25}$ [13] $As\,Ta_9O_{25}$ [13] $V\,Ta_9O_{25}$ [13]	GeO_2·$9Nb_2O_5$ [b] [13]		
25:62	$V_2Nb_{23}O_{62}$ [c] $+\frac{1}{2}O$	$TiNb_{24}O_{62}$ [d] [1, 16] $ZrNb_{24}O_{62}$ [d] [1]	$Al_{1.2}Nb_{24\,1/2}O_{62}$ [26]	
11:27	$[NbO_{2.46}]$ [25] $[NbO_{2.467}]$ [28] $[NbO_{2.454}]$ [26]		Al_2O_3·$25Nb_2O_5$ [24] $Al_{1/2}Nb_{10\,1/2}O_{27}$ [26]	
12:29	$(V,Nb)_{12}O_{29}+O$ [c]	$Ti_2Nb_{10}O_{29}$ [23]	$AlNb_{11}O_{29}$ [26] [27]	$Ni_{2/3}Nb_{11\,1/3}O_{29}$ [26] $Zn_{2/3}Nb_{11\,1/3}O_{29}$ [e]
3:7	$TiNb_2O_7$ [23]			

[a] This phase was previously reported as solid solution [3] (see sect. 3).

[b] Ge^{+4} is accepted into the structure and would seem to indicate that either the cation/anion ratio is varying or that minor differences exist in the packing of cation coordination polyhedra.

[c] This phase has not been previously reported in the binary system.

[d] This phase was originally reported as solid solution [1] but later described as a compound by one of the authors [16].

[e] This phase previously unreported is apparently isostructural with the high temperature polymorph of $Ti_2Nb_{10}O_{29}$ and has the following unit cell dimensions: $a=15.57$ Å, $b=3.826$ Å, $c=20.5$ Å and $\beta=113°41'$.

7. References

[1] R. S. Roth and L. W. Coughanour, J. Res. NBS **55** [4] 209–213 (1955).
[2] A. J. Pollard, J. Am. Ceram. Soc. **44** [12] 630 (1961).
[3] H. J. Goldschmidt (1960), Metallurgia **62,** 241.
[4] A. Burdese, M. Borlera, Ric. Sci. Rend. Sez. **A3** [7] 1025 (1963).
[5] H. F. Stimson, J. Res. NBS **65A,** 139–145 (1960).
[6] H. S. Roberts, Phys. Rev. **23,** 386–95 (1924).
[7] R. S. Roth and E. M. Levin; J. Research NBS **62** [5] 193–200 (1959).
[8] F. Holtzberg, A. Reisman, M. Berry, and M. Berkenblit; J. Amer. Chem. Soc. **78** [7] 1536–1540 (1956).
[9] E. M. Levin and C. L. McDaniel; NBS personal communication.
[10] A. Bystrom, K. A. Wilhelmi, and O. Brotzen, Act. Chem. Sci. 1119–1130 (1950).
[11] H. E. Swanson, N. T. Gilfrich, M. I. Cook, R. S. Stinchfield, and P. C. Parks, NBS Cir. 539 [8] 66–67 (1959).
[12] C. L. McDaniel, personal communication.
[13] J. L. Waring and R. S. Roth, Acta Cryst. **17** [4] 455–456 (1964).
[14] F. Holtzberg and A. Reisman, J. Phys. Chem. **65** 1193 (1961).
[15] G. P. Mohanty, L. J. Fiegel and J. H. Healy, Acta Cryst. **15** 1190 (1962).
[16] R. S. Roth and A. D. Wadsley, Acta Cryst. (accepted for publication).
[17] F. Holtzberg, A. Reisman, and M. Berry, J. Am. Chem. Soc. **79** 2039–2043 (1957).
[18] M. W. Shafer and R. Roy, Z. Krist. **110** [3] 241–244 (1958).
[19] H. J. Goldschmidt, J. Inst. Metals **87** 235–239 (1958–59).
[20] A. Reisman and F. Holtzberg, J. Am. Chem. Soc. **81** 3182–3184 (1958).
[21] R. S. Roth, J. Research NBS **62,** 27 (1959).
[22] R. S. Roth and J. L. Waring, J. Research NBS **66A** [6] 451–463 (1962).
[23] A. D. Wadsley, Acta Cryst. **14,** 660–670 (1961).
[24] G. K. Layden, J. Amer. Cer. Soc. **46** [10] 506 (1963).
[25] R. Norin and A. Magneli, Naturwiss. **47** [15] 354–55 (1960).
[26] R. S. Roth, A. D. Wadsley, and B. M. Gatehouse, Naturwiss. **51** [11] 262–263 (1964).
[27] S. Andersson and R. S. Roth, personal communication.
[28] R. Gruehn and H. Schäfer, Naturwiss. **50** 642 (1963).
[29] G. Brauer, Z. Anorg. u. allgem. Chem. **248,** 1 (1941).

(Paper 69A2–333)

JOURNAL OF RESEARCH of the National Bureau of Standards—A. Physics and Chemistry
Vol. 69A, No. 2, March–April, 1965

Thermodynamics of the Ternary System: Water-Glycine-Potassium Chloride at 25 °C From Vapor Pressure Measurements

V. E. Bower and R. A. Robinson

(November 18, 1964)

The thermodynamic properties of the ternary system: water-glycine-potassium chloride at 25 °C have been evaluated by means of isopiestic vapor pressure measurements. The effect of added glycine on the activity coefficient of potassium chloride has been calculated and the effect of added potassium chloride on the activity coefficient of glycine. The variation of the activity coefficient of potassium chloride has been studied previously by Roberts and Kirkwood, using an entirely different method—the measurement of the emf of suitable concentration cells. The agreement between these independent measurements is shown to be excellent within the concentration ranges common to both experiments.

1. Introduction

The ternary system: water-sucrose-mannitol has been investigated [1][1] by means of isopiestic vapor pressure measurements. The immediate result of such measurements is the chemical potential, or activity, of the volatile component (water) in the ternary mixture but it was shown that, provided the solvent activity could be expressed as a function of the concentrations of sucrose and mannitol, the chemical potentials of sucrose and mannitol (or their activity coefficients) could be calculated. Similar measurements have made on the systems: water-mannitol-sodium chloride [2], water-mannitol-potassium chloride [3], water-urea-sodium chloride [4], and water-sorbitol-sodium chloride [5]. It can, furthermore, be shown that once the activity coefficients of the two solutes are known as a function of concentration, then the effect of each solute on the solubility of the other can be calculated. Comparison with experimentally determined values of the solubility of each component thus provides a test both of the underlying theory and of the accuracy of the isopiestic measurements. However, by its very nature, such a test is limited to those solutions in which at least one component has the concentration of the saturated solution. It is, therefore, desirable to make a further test of the method by comparison with data for unsaturated solutions; such data are available [6] for the system: water-glycine-potassium chloride and isopiestic vapor pressure measurements are now reported for this system.

[1] Figures in brackets indicate the literature references at the end of this paper.

Roberts and Kirkwood [6] measured the emf of the cell: Ag, AgCl | KCl (m_c) | glycine (m_B), KCl (m_c) | AgCl, Ag and calculated therefrom the effect of glycine on the activity coefficient of potassium chloride. They expressed the activity coefficient of potassium chloride as a power series in the two concentrations:

$$2 \log \gamma_c = 2 \log \gamma_c^\circ + m_B(A + Bm_c^{1/2} + Cm_c + Dm_B) \quad (1)$$

where γ_c° is the activity coefficient of potassium chloride in a solution containing no glycine. Application of the cross-differentiation relation:

$$2\left(\frac{\partial \log \gamma_c}{\partial m_B}\right)_{m_c} = \left(\frac{\partial \log \gamma_B}{\partial m_c}\right)_{m_B} \quad (2)$$

then gives the activity coefficient of glycine as:

$$\log \gamma_B = \log \gamma_B^\circ + m_c(A + \tfrac{2}{3}Bm_c^{1/2} + \tfrac{1}{2}Cm_c + 2\,Dm_B) \quad (3)$$

Thus both activity coefficients can be calculated from experiments the immediate result of which is the activity coefficient of potassium chloride. The isopiestic measurements described in this paper lead directly to a knowledge of the water activity and thence to the activity coefficients of glycine and potassium chloride. Comparison of the results, therefore, involves two different experimental techniques.

2. Method

If a solution containing glycine at a molality m_B and potassium chloride at a molality m_c is in isopiestic

or vapor-phase equilibrium with a (reference) solution of potassium chloride of molality m_{ref}, then the following relation must be true:

$$-55.51 \ln a_w = 2m_{ref}\varphi_{ref} \quad (4)$$

where a_w is the water activity of each solution and φ_{ref} is the osmotic coefficient of potassium chloride in the reference solution. Values of φ_{ref} have been tabulated [7]. A function, Δ, is defined as:

$$\Delta = -55.51 \ln a_w - m_B\varphi_B - 2m_c\varphi_c^0 \quad (5)$$

where φ_B is the osmotic coefficient of a solution containing glycine only at a molality m_B and φ_c^0 is the osmotic coefficient of a solution containing potassium chloride only at a molality m_c. An equation for φ_B as a function of m_B has been given recently [8].

If Δ can be expressed as a function of m_B and m_c of the form:

$$\Delta = m_B m_c[f(m_B) + F(m_c)], \quad (6)$$

where $f(m_B)$ is a function of m_B only and $F(m_c)$ is a function of m_c only, then it can be shown [1] that:

$$\left(\frac{\partial \ln \gamma_B}{\partial m_c}\right)_{m_B} = 2\left(\frac{\partial \ln \gamma_c}{\partial m_B}\right)_{m_c} = \frac{\Delta}{m_B m_c} = f(m_B) + F(m_c). \quad (7)$$

Even if the equation for Δ contains cross-products of m_B and m_c, the situation can still be handled [4]. Thus, if

$$\frac{\Delta}{m_B m_c} = A + Bm_B + Cm_c + Dm_B^2 + Em_c^2 + Fm_B m_c \quad (8)$$

then

$$\left(\frac{\partial \ln \gamma_B}{\partial m_c}\right)_{m_B} = 2\left(\frac{\partial \ln \gamma_c}{\partial m_B}\right)_{m_c} = A + Bm_B + Cm_c + Dm_B^2 + Em_c^2 + \frac{4}{3}Fm_B m_c \quad (9)$$

$$\ln \gamma_B = \ln \gamma_B^0 + m_c\left[A + Bm_B + \frac{1}{2}Cm_c + Dm_B^2 + \frac{1}{3}Em_c^2 + \frac{2}{3}Fm_B m_c\right] \quad (10)$$

and

$$2 \ln \gamma_c = 2 \ln \gamma_c^0 + m_B\left[A + \frac{1}{2}Bm_B + Cm_c + \frac{1}{3}Dm_B^2 + Em_c^2 + \frac{2}{3}Fm_B m_c\right] \quad (11)$$

where γ_B is the activity coefficient of glycine in a solution containing glycine only at a molality m_B and γ_c is the activity coefficient of potassium chloride in a solution containing potassium chloride only at a molality m_c.

3. Experimental Procedure

The isopiestic apparatus was that used previously [4]. The potassium chloride was a low-bromide preparation [9] used in a previous study [10]. Glycine was recrystallized twice from a mixture of equal parts of water and ethanol, and dried in a vacuum desiccator at room temperature.

TABLE 1. *The system: water-glycine-potassium chloride at 25 °C*

$m_{ref.}$	m_B	m_C	$-\frac{\Delta}{m_B m_C}$	φ_C
0.5081	0.3885	0.3073	0.161	+0.03
	.6094	.1926	.164	−.05
	.8379	.07436	.205	+.19
	.9806			
0.5087	0.2350	0.3871	0.157	+0.04
	.5007	.2486	.147	−.22
	.7070	.1430	.180	−.01
	.9821			
0.8178	0.6238	0.5042	0.101	−0.22
	.9712	.3292	.110	−.22
	1.3758	.1237	.132	−.02
	1.6133			
0.8344	0.4470	0.6107	0.110	+0.07
	.8336	.4164	.107	−.15
	1.2486	.2065	.118	−.13
	1.6491			
1.2151	0.9100	0.7731	0.0772	+0.28
	1.4412	.5116	.0722	+.02
	2.0881	.1880	.0897	+.06
	2.4548			
1.2183	0.6881	0.8838	0.0786	+0.25
	1.2700	.6001	.0739	+.16
	1.7196	.3760	.0741	−.06
	2.4619			
1.4380	0.4851	1.2052	0.0768	+0.23
	1.3494	0.7870	.0539	+.05
	2.1419	.3971	.0528	−.16
	2.9278			
1.4461	0.3441	1.2812	0.0708	0
	1.0629	0.9340	.0558	+.03
	1.6951	.6276	.0531	+.05
	2.9454			
1.6167	0.9836	1.1473	0.0477	−0.26
	2.0131	0.6521	.0436	+.10
	2.9358	.1945	.0534	−.02
	3.3151			
1.6174	0.5874	1.3383	0.0562	−0.28
	1.6586	0.8245	.0437	+.05
	2.4722	.4275	.0460	+.05

B=glycine, C=potassium chloride. $m_{ref.}$ is the molality of the reference solution of potassium chloride.

4. Results

Table 1 gives the experimental data. The first column gives the molality of potassium chloride, $m_{ref.}$, in the reference solution, the second and third columns the molalities of glycine and potassium chloride, respectively, in the mixed solution in isopiestic equilibrium with the reference potassium chloride solution. The fourth column gives values of the Δ function defined by eq (5). These values have been fitted by the method of least squares to a six-parameter, quadratic equation of the form of eq (8), the numerical values of the parameters being as follows: $A=-0.2609$, $B=0.0845$, $C=0.2794$, $D=-0.00786$, $E=-0.10826$, $F=-0.04171$. The

[2] The cubic equation is $\Delta/(m_B m_c) = -0.32499 + 0.15795\ m_B + 0.58007\ m_c - 0.04615\ m_B^2 - 0.57817\ m_c^2 - 0.16050\ m_B m_c + 0.00653\ m_B^3 + 0.20183\ m_c^3 + 0.01798\ m_B^2 m_c + 0.08523\ m_B m_c^2$.

final column of table 1 gives the percentage change in the molality of the reference solution necessary to give Δ values in complete accord with eq (8) and the above values of the six parameters. In many cases the percentage difference is considerably greater than the experimental error in the isopiestic measurements; a ten-parameter cubic equation [2] has been tried with little better fit, and it seems likely that the surface which represents $\Delta/(m_B m_c)$ as a function of m_B and m_c is a particularly difficult one to fit to any simple equation.

5. Discussion

Table 1 contains 11 sets of data in which reference solutions of potassium chloride were equilibrated with solutions of glycine only. From these isopiestic ratios there can be calculated the osmotic coefficient of glycine solutions. The results are given in table 2 where they are compared with those calculated by the equation of Ellerton, Reinfelds, Mulcahy, and Dunlop [8]. The mean difference is 0.0007, their results in general being slightly higher.

If we insert numerical values for the parameters of eq (10), the effect of potassium chloride on the activity coefficient of glycine is given by

$$\log \gamma_B/\gamma_B^0 = m_c\{-0.1133+0.03670m_B +0.06067m_c-0.00341m_B^2 -0.01567m_c^2-0.01208m_Bm_c\}. \quad (12)$$

TABLE 2. *Osmotic coefficients of aqueous glycine solutions at 25 °C.*

m_B	φ[a]	φ[b]
0.9806	0.9314	0.9326
.9821	.9311	.9324
1.6133	.9094	.9095
1.6491	.9077	.9085
2.4548	.8898	.8917
2.4619	.8895	.8917
2.9278	.8856	.8855
2.9454	.8854	.8854
3.3151	.8822	.8817

[a] Present data.
[b] Data of Ellerton, Reinfelds, Mulcahy, and Dunlop.

Some values of $-\log \gamma_B/\gamma_B^0$ are given in table 3; it will be noted that, while the effect of potassium chloride is more pronounced when the glycine concentration is low, the effect is appreciable at all concentrations. Thus when $m_B=m_c=1$, $-\log \gamma_B/\gamma_B^0=0.0471$ and as γ_B^0 is known [8] to be 0.861 at $m_B=1$, $m_c=0$, then $\gamma_B=0.773$ in 1 m potassium chloride solution. This may be compared with the effect of sodium chloride on the activity coefficient of urea. At a concentration of 1 m and in the absence of sodium chloride the activity coefficient of urea is 0.922; the addition of 1 m sodium chloride lowers it to 0.898, thus $\log \gamma_B/\gamma_B^0=-0.0113$ so that the effect is approximately four times as large with glycine.

TABLE 3. *Effect of potassium chloride on the activity coefficient of glycine in aqueous solution at 25 °C.*[a]

m_B	m_c			
	0.2	0.5	1.0	1.5
0.2	(.0191)	.0409	.0643	.0822
.5	(.0171)	.0362	.0569	.0738
1.0	.0142	.0298	.0471	(.0612)
1.5	.0116	.0243	.0390	(.0560)
2.0	.0094	.0196	(.0328)	(.0512)

[a] Values of $-\log \gamma_B/\gamma_B^0$ are tabulated. Values in parentheses are extrapolated.

The equation for the effect of glycine on the activity coefficient of potassium chloride becomes

$$\log \gamma_c/\gamma_c^0 = m_B\{-0.05665+0.00917m_B +0.06067m_c-0.00057m_B^2-0.02351m_c^2 -0.00604m_Bm_c\}. \quad (13)$$

Table 4 gives some values of $-\log \gamma_c/\gamma_c^0$ calculated by this equation. Again, the effect of glycine on the activity coefficient is large; at $m_B=m_c=1$, $-\log \gamma_c/\gamma_c^0=0.0170$ and as $\gamma_c^0=0.604$, $\gamma_c=0.581$ but the activity coefficient of sodium chloride, which is 0.657 when $m_B=0$, $m_c=1$, is reduced only to 0.650 on the addition of 1 m urea, so that $\log \gamma_c/\gamma_c^0=-0.0043$.

TABLE 4. *Effect of glycine on the activity coefficient of potassium chloride in aqueous solution at 25 °C* [a]

m_c	m_B				
	0.2	0.5	1.0	1.5	2.0
0.2	(0.0088)	(0.0208)	0.0381	0.0524	0.0638
0.5	.0064	.0146	.0266	.0363	.0444
1.0	.0038	.0090	.0170	.0242	(.0310)
1.5	.0037	.0094	(.0190)	(.0296)	(.0412)

[a] Values of $-\log \gamma_c/\gamma^\circ_c$ are tabulated. Values in parentheses are extrapolated.

Figure 1 shows the distribution of molalities of glycine and of potassium chloride at which measurements were made in this investigation. The measurements of Roberts and Kirkwood [6] were limited to concentrations 0.5 m and less in both glycine and potassium chloride, corresponding to the rectangle on the lower left side of figure 1. It would not be expected that an equation fitted to data for comparatively high concentrations could be extrapolated to the dilute range which was the subject of the work of Roberts and Kirkwood. Nor would it be expected that their equation can be extrapolated far into the region of concentrated solutions. A fair comparison would be in the region of concentration more or less common to both sets of measurements.

This comparison can be made in two ways. In the first method, we note that Roberts and Kirkwood expressed their results by the equation

$$\ln \gamma_c = \ln \gamma_c^0 - 0.2059m_B + 0.2824m_Bm_c^{1/2} +0.0247m_B^2-0.1446m_Bm_c \quad (14)$$

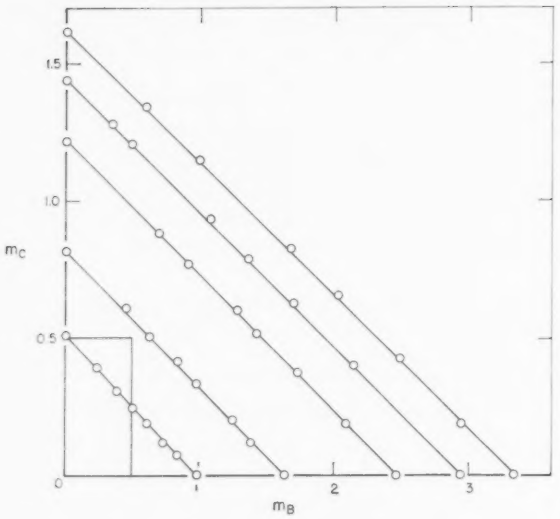

FIGURE 1. *Isopiestic measurements.*

The rectangle at the left indicates the concentration range in which the emf measurements of Roberts and Kirkwood were made.

or

$$\frac{\Delta}{m_B m_c} = 2\left(\frac{\partial \ln \gamma_c}{\partial m_B}\right)_{m_c} = -0.4118 + 0.5648 m_c^{1/2} + 0.0988 m_B - 0.2892 m_c. \quad (15)$$

We calculate Δ by this equation with the molalities of the first twelve solutions of table 1; these are recorded as Δ_2 in table 5 where Δ_1 represents the values of Δ derived from the isopiestic measurements. The column headed % (1) in table 5 gives values of % copied from table 1—they are the percentage changes in the molality of the reference solution necessary to bring our isopiestic results into complete agreement with eq (8). The column headed % (2) gives the percentage change needed to bring our results into agreement with eq (15), the equation of Roberts and Kirkwood. The average values of % (1) and % (2) for the first six entries are both 0.09; this means that for the solutions of composition closest to those used by Roberts and Kirkwood, their equation, derived from emf measurements, predicts our isopiestic data with no more error than the equation we have derived from our isopiestic data. The situation is not so favorable for the next six entries, the average value of % (1) is 0.14, that of % (2) is 0.32; however, we note that not one of the points corresponding to these solutions lies in the region studied by Roberts and Kirkwood.

A second comparison can be made by using both eq (14) and eq (13) to calculate $\log \gamma_c/\gamma_c^\circ$ at selected values of m_B and m_c. The results of such calculations are shown in table 6, where pairs of values of $-\log \gamma_c/\gamma_c^\circ$ are given, the first being calculated from the emf data of Roberts and Kirkwood and the second from the present isopiestic data. A heavy line has been drawn to enclose all pairs which agree within 0.0010 or better (the average difference in this region is 0.0004). There is excellent agreement in the concentration range more or less common to both experiments. We conclude, therefore that our results are in agreement with those of Roberts and Kirkwood insofar as comparison is possible.

TABLE 5. *Comparison of isopiestic and electromotive force data*

m_B	mc	$-\Delta_1$	$-\Delta_2$	% (1)	% (2)
0.3885	0.3073	0.0192	0.0178	+0.03	+0.15
.6094	.1926	.0192	.0187	− .05	+ .05
.8379	.07436	.0128	.0122	+ .19	+ .07
.2350	.3871	.0143	.0135	+ .04	+ .09
.5007	.2486	.0183	.0190	− .22	− .08
.7070	.1430	.0182	.0171	− .01	+ .12
0.6238	0.5042	0.0317	0.0298	−0.22	+0.13
.9712	.3292	.0350	.0277	− .22	+ .50
1.3758	.1237	.0225	.0192	− .02	+ .22
0.4470	.6107	.0299	.0281	+ .07	+ .12
.8336	.4164	.0370	.0296	− .15	+ .49
1.2486	.2065	.0305	.0235	− .13	+ .47

$\Delta_1 = -55.51 \ln a_w - m_B\varphi_B^\circ - 2 m_c\varphi_c^\circ$ as calculated from isopiestic measurements, Δ_2 from the emf data of Roberts and Kirkwood. %(1) is the percentage change in the molality of the reference solution required to give agreement with eq (8), %(2) that needed to give agreement with the results of Roberts and Kirkwood.

TABLE 6. *Effect of glycine on the activity coefficient of potassium chloride*

Comparison of electromotive force and isopiestic data

m_c	m_B				
	0.2	0.3	0.5	0.7	1.0
0.2	0.0090 .0088	0.0132 .0129	0.0209 .0208	0.0278 .0277	0.0365 .0381
0.3	0.0078 .0080	0.0113 .0115	0.0178 .0186	0.0235 0.249	0.0304 .0337
0.5	0.0064 .0064	0.0093 .0091	0.0144 .0146	0.0186 .0194	0.0234 .0266
0.7	0.0057 .0049	0.0083 .0073	0.0127 .0117	0.0163 .0157	0.0201 .0214
1.0	0.0055 .0038	0.0079 .0056	0.0121 .0090	0.0155 .0123	0.0189 .0170

$-\log \gamma_c/\gamma_c^\circ$ is tabulated. The first (upper) of each pair of figures is the value calculated from the emf data of Roberts and Kirkwood, the second (lower) that from the present isopiestic data.

6. Solubility Relations

By evaporation to dryness in vacuo at room temperature of a saturated solution of glycine in water, the solubility of glycine in water at 25 °C was found to be 3.337 mole/kg of water. McMeekin, Cohn, and Weare [11] found 2.886 mole/liter of solution or 3.331 mole/kg of water. The equation of Ellerton, Reinfelds, Mulcahy, and Dunlop [8] gives 0.7300 for the activity coefficient of glycine in water at this concentration. Hence the solubility product is 2.436 mole/kg. Putting $m_c = 0.5$ mole/kg, a short series of approximations shows that eq (10) is satisfied by $m_B = 3.437$ mole/kg, $\gamma_B = 0.7088$, $m_B\gamma_B = 2.436$ mole/kg. Thus we predict a solubility of 3.437 mole/kg in a 0.5 m potassium chloride

solution. Again by evaporation to dryness of a saturated solution of glycine in 0.5 m potassium chloride solution, we found a solubility of 3.442 mole/kg.

Our thanks are expressed to J. M. Cameron and Janace A. Speckman for their advice and assistance with the computations.

7. References

[1] R. A. Robinson and R. H. Stokes, J. Phys. Chem. **65,** 1954 (1961).
[2] F. J. Kelly, R. A. Robinson, and R. H. Stokes, J. Phys. Chem. **65,** 1958 (1961).
[3] R. A. Robinson and R. H. Stokes, J. Phys. Chem. **66,** 506 (1962).
[4] V. E. Bower and R. A. Robinson, J. Phys. Chem. **67,** 1524 (1963).
[5] V. E. Bower and R. A. Robinson, J. Phys. Chem. **67,** 1540 (1963).
[6] R. M. Roberts and J. G. Kirkwood, J. Am. Chem. Soc. **63,** 1373 (1941).
[7] R. A. Robinson and R. H. Stokes, Electrolyte solutions, p. 476 (Butterworths Scientific Publications, London, 1959).
[8] H. D. Ellerton, G. Reinfelds, D. E. Mulcahy, and P. J. Dunlop, J. Phys. Chem. **68,** 398 (1964).
[9] G. D. Pinching and R. G. Bates, J. Res. NBS **37,** 311 (1946).
[10] M. Paabo and R. A. Robinson, J. Phys. Chem. **67,** 2861 (1963).
[11] T. L. McMeekin, E. J. Cohn, and J. H. Weare, J. Am. Chem. Soc. **58,** 2173 (1936).

(Paper 69A2–334)

JOURNAL OF RESEARCH of the National Bureau of Standards—A. Physics and Chemistry
Vol. 69A, No. 2, March–April 1965

Heat of Formation of Aluminum Fluoride by Direct Combination of the Elements

Eugene S. Domalski and George T. Armstrong

(November 16, 1964)

The standard heat of formation of aluminum fluoride was calculated from the heats of combustion of Teflon and of aluminum-Teflon mixtures in fluorine. The heat measurements were made in a bomb calorimeter.

$$C_2F_4(\text{solid polymer}) + 2F_2(g) = 2CF_4(g) \quad (1)$$

$$Al(c) + 3/2F_2(g) = AlF_3(c) \quad (2)$$

For reaction (1), ΔH°_{298} was found equal to $-10{,}350.7 \pm 0.4$ Jg^{-1} (-247.43 ± 0.01 kcal monomole^{-1}), and for reaction (2) $\Delta H^\circ_{298} = \Delta H_{f298}$ was calculated to be -1507.8 ± 1.2 kJ mole^{-1} (-360.37 ± 0.29 kcal mole^{-1}). The latter uncertainties are the computed standard deviations of the means. The calculated standard heat of formation of aluminum fluoride is estimated to be accurate to within ± 6.6 kJ mole^{-1} (1.6 kcal mole^{-1}). The measurements on Teflon were combined with existing data and the heat of formation of carbon tetrafluoride was calculated to be -221.8 kcal mole^{-1}.

1. Introduction

Considerable difficulty has been encountered in determining the heat of formation of crystalline aluminum fluoride, and until about ten years ago no complete determination had been made. The most obvious procedure would have been to determine the heat of solution of $AlF_3(c)$ in an aqueous solvent, and to combine the result with the known heats of formation of $Al^{+3}(aq)$ and $F^-(aq)$. This procedure is not practicable because of the low solubility and slow rate of solution of $AlF_3(c)$ in appropriate solvents.

In the early studies by Baud [1, 2],[1] a value for the heat of formation of aluminum fluoride was calculated from heat of solution measurements on two hydrates of aluminum fluoride in conjunction with an estimate of the heat of hydration of anhydrous aluminum fluoride. Subsequent estimates of the heat of formation of $AlF_3(c)$ by von Wartenberg [3], Bichowsky and Rossini [4], Rossini et al. [5], and Brewer [6] used Baud's estimate of the heat of hydration of anhydrous aluminum fluoride as part of their calculation. Later work has shown that these estimates were in error by 25 to 50 kcal mole^{-1}.

In 1954, Gross, Hayman, and Levi [7] studied reaction (1), for which they found

$$Al(c) + \frac{3}{2}PbF_2(c) = AlF_3(c) + \frac{3}{2}Pb(c). \quad (1)$$

$\Delta H^\circ_{298} = -118.53 \pm 0.08$ kcal mole^{-1}. Using their measurement and the known heat of formation of $PbF_2(c)$, -158.5 kcal mole^{-1} [5], they reported $\Delta H^\circ_{f298}[AlF_3(c)] = -356.3 \pm 0.3$kcal mole^{-1}. In later work, Gross, Hayman, and Levi [8] measured the heat of reaction (2) to be -138.31 ± 0.12 kcal mole^{-1}.

$$3NaF(c) + Al(c) + \frac{3}{2}PbF_2(c) = Na_3AlF_6(c) + \frac{3}{2}Pb(c). \quad (2)$$

Combining this value with their value for the heat of reaction (1) and Coughlin's values [9] for the heats of formation of $NaF(c)$ and $Na_3AlF_6(c)$, they obtained $\Delta H^\circ_{f298}[AlF_3(c)] = -356.15$ kcal mole^{-1}, a value independent of the heat of formation of $PbF_2(c)$. Gross suggested [8] that since the heats of formation of all the fluorides involved in these calculations are dependent on that of hydrogen fluoride, an independent determination of the heat of formation of a metal fluoride by combustion of the metal in fluorine would be valuable.

After our work was well under way, Kolesov, Martynov, and Skuratov [10] reported a study of reaction (1). They found $\Delta H^\circ_{298} = -117.7 \pm 0.6$ kcal mole^{-1} on the basis of 24 measurements, and calculated the heat of formation of aluminum fluoride to be -357 ± 2 kcal mole^{-1}.

In view of the large discrepancy between the values calculated by Gross and his co-workers and those

[1] Figures in brackets indicate the literature references at the end of this paper.

that had been previously estimated, we undertook a determination of the heat of formation of aluminum fluoride by direct combination of the elements in a bomb calorimeter. Since investigations by Hubbard and co-workers [11] had demonstrated the feasibility of bomb calorimetry with fluorine as the oxidizer, it seemed likely that this technique would lead to an unambiguous result.

We feel our results show the substantial correctness of the measurements of Gross et al. and Kolesov et al. The agreement between their results and ours is improved by application of new information on the heat of formation of hydrogen fluoride to the auxiliary data required in their calculations. This improvement tends to substantiate a more negative value for the heat of formation of hydrogen fluoride than until recently has been accepted.

2. Preliminary Experiments

In preliminary experiments made to determine optimum reaction conditions under which aluminum metal would burn in a combustion bomb filled with fluorine, a variety of sample forms was tried including pellets, foil, and loose powder. It was found that massive samples such as pellets or large pieces of foil would either short circuit the fuse or fail to ignite from the energy supplied by the fuse. In these experiments a coiled aluminum wire was used as a fuse. Aluminum foil cut into narrow shreds (2.5 cm$\times$0.025 cm$\times$0.0025 cm) and loosely packed together, reacted very rapidly but only to about 75 percent completion. From inspection of the inner walls of the bomb after such an experiment, and from observation of reactions in a glass combustion vessel, it was evident that shortly after the combustion began, burning pieces of aluminum were thrown out of the reaction zone and quenched on contact with the cold bomb walls. It was difficult to determine the amount of unburned aluminum which was intermixed with the combustion product.

A few experiments were performed in which loose aluminum powder contained in a thermoplastic Teflon bag was burned in fluorine. Only 30 to 50 percent of the aluminum powder reacted. Considerable amounts of carbon were present in the products as the result of incomplete combustion of the Teflon bag. This technique was therefore considered to be unsatisfactory.

A sample geometry and environment were found which confined the sample to the reaction zone and provided other desirable characteristics. A mixture of finely divided aluminum powder and finely divided Teflon powder was compressed into a pellet which was supported on a stainless steel or monel plate. With this preparation, reactions were found to go essentially to completion (99 to 100 percent). The Teflon made ignition easy because of the low thermal conductivity it imparted to the pellet. In addition it acted as a moderator and maintained a temperature conducive to burning. No appreciable attack of fluorine on the bomb parts occurred when this procedure was used.

3. Materials

The aluminum used for samples was in the form of a powder and was supplied with the following analysis of metallic impurities: silicon, 0.06 percent; iron, 0.07 percent; and copper, 0.005 percent. Microscopic examination revealed that it consisted of irregularly shaped particles ranging in approximate dimensions from 10 to 160 μ; the average particle size was determined to be 26 μ by a sub-sieve sizer. Because of the small particle size and the correspondingly large surface area, the sample was tested for the presence of oxide. Investigations [12], both experimental and theoretical in nature, have estimated the thickness of the oxide layer on thin aluminum films to be 20 to 50 Å in air at room temperature. If a surface film of Al_2O_3 50 A thick were presumed to exist on smooth-surfaced cubes of aluminum 26 μ on edge, the aluminum would contain 0.28 percent Al_2O_3 by weight. Because this amount would cause a significant correction to the heat of combustion, determination of the actual amount of alumina was necessary.

The NBS Analysis and Purification Section used two methods to determine the amount of alumina. In the first method aluminum powder was heated in an atmosphere of argon until the powder melted and the oxide floated to the surface. The oxide was then treated by the method of Werner [13] in which the aluminum is dissolved by a bromine-methanol mixture leaving the Al_2O_3 as a residue.

In the second method, a stream of dry argon saturated with bromine was passed over the aluminum in a furnace. Aluminum bromide distilled off leaving an aluminum oxide residue which was weighed. The values for the Al_2O_3 content determined by the two methods were 0.46 and 0.47 percent, respectively, and the average of all the individual determinations was 0.468 percent.

The Teflon powder used was a commercial preparation designated as TFE Fluorocarbon Resin, "Teflon 5". It was composed of irregularly shaped particles which tended to adhere to one another. Particle dimensions ranged from 50 to 800 microns, as observed by examination with a microscope. The Teflon was not modified or specially treated before use.

The fluorine gas was analyzed by absorbing the fluorine in mercury and observing the residual pressure of unreacted gases [14]. The fluorine was found to be 99 percent pure. The residual gases were examined in a mass spectrometer and the impurities were found to be, in mole percent of the original sample: O_2, 0.9; N_2, 0.08; CO_2, 0.01; with smaller amounts of SiF_4, HF, fluorocarbons and other compounds that were not definitely identified.

4. Calorimetric Apparatus

An isothermal-jacket, stirred-water calorimeter was used, which was a modification of the Dickinson design [15] by Prosen and co-workers [16]. A single

motor mounted on an insulated bracket on the jacket wall was used to stir the water in both the jacket and the calorimeter vessel by a pulley arrangement. The stirrer was coupled to the motor by a pulley to minimize heat transfer from the motor to the jacket. The jacket water was maintained at a constant temperature near 30 °C with a range of 0.005 °C by a commercial thermoregulator having a temperature sensitive resistor as a sensing element.

Temperatures were measured with a G–2 Mueller bridge in conjunction with a 25-ohm platinum-resistance thermometer. The latter was immersed in the calorimeter vessel near the wall. Temperatures were read to 0.0001 °C.

Reactions were conducted in a commercially available combustion bomb shown in figures 1 and 2, which is suitable for handling fluorine as the oxidant. The bomb was fabricated from "A" nickel, and has a volume of approximately 360 cm^3. The pelleting device is shown in figure 2 along with the electrode-fuse arrangement and pellet holder used in the experiments of series I.

The standard initial calorimeter for the experiments of series I consisted of the combustion bomb with aluminum fuse supports, Chromel C fuse wire, monel pellet holder and 21 atmospheres of fluorine at 303.2 °K, the electrical heater, the resistance thermometer and the calorimeter vessel with a measured quantity of water. The mass of the calorimeter vessel, plus water, was 3700.0 g. For the experiments of series II, the standard initial calorimeter was the same as for series I except for the addition of a liner inside the bomb, slight modifications in the fuse, fuse supports, and pellet holder.

Some electrical calibration experiments were carried out using a heater of novel design. The heater consisted of an insulated Advance wire inside an annealed copper tube. The tube was flattened and coiled to fit the combustion bomb. Because of excessive thermal conduction through the heater connections to the outside, the electrical calibration experiments are not considered to be valid. However, because the results of the electrical calibration must be included in order to give an adequate description of the combustion experiments, the electrical instruments will be listed briefly.

The equipment used in measuring the power supplied to the calorimeter consisted of a Wolff-Dieselhorst potentiometer, a 0.01 ohm Reichsanstalt-type standard resistor, a volt box with a ratio of 20,000 to 20 ohms, a thermostated Weston standard (saturated) cell, and the 10.6 ohm heater. Current through the heater was turned on and off by a manually operated DPDT copper knife-switch. An electronic timer with a resolution of 10^{-5} seconds was triggered to operate by the appearance and disappearance of the voltage on the heater, and thus recorded the elapsed time of heating. The time base was the NBS standard frequency signal of 100 kc/s. A standard frequency time signal (60 c/s) was used to operate a recording clock for timing the rapid temperature rise of the calorimeter. Standard frequency time signals (one per second) were used to time the initial and final drift periods.

Procedures used in making the heat measurements have been adequately described elsewhere [17, 18].

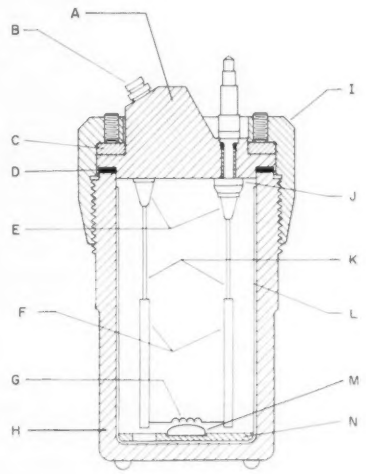

FIGURE 1. *Inner arrangement of the fluorine combustion bomb.*

A, nickel bomb head; B, needle valve; C, monel pressure plate; D, Teflon gasket; E, monel lock nut; F, aluminum electrode; G, fuse; H, bomb body; I, screw cap; J, alumina washer; K, monel rod; L, type 304 stainless steel liner; M, pellet; N, pellet holder.

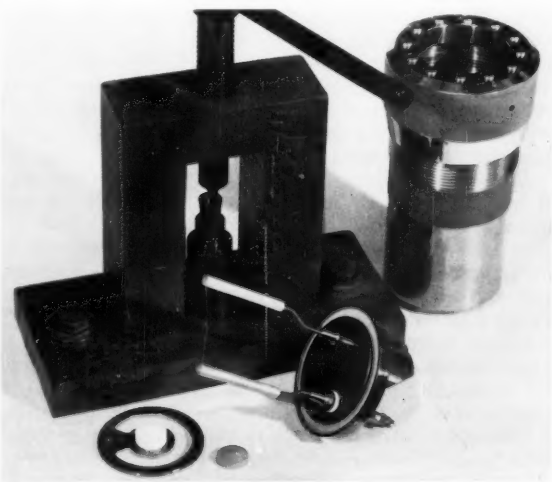

FIGURE 2. *Pellet press used in sample preparation and electrode-fuse arrangement.*

Foreground: monel pellet holder with Teflon sample, aluminum-Teflon sample nearby, bomb head showing electrode-fuse arrangement for series I experiments. Background: pellet press, die pieces, and bomb body with screw cap.

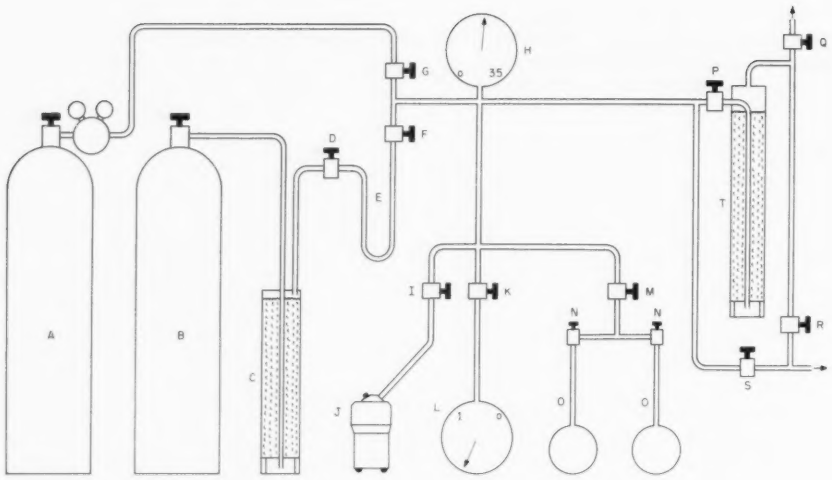

FIGURE 3. *Schematic diagram of fluorine manifold.*

A, helium; B, fluorine; C, hydrogen fluoride trap; D, fluorine valve; E, liquid nitrogen trap for fluorine; F, fluorine valve to manifold; G, helium valve to manifold; H, pressure gage (0-35 atm); I, valve to bomb; J, bomb; K, valve to vacuum gage; L, vacuum gage (0-1 atm); M, N, valves to gas-sample collector bulbs; O, gas-sample collector bulbs; P, valve to fluorine absorption tower; Q, vent valve to fume hood; R, valve to vacuum via fluorine absorption tower; S, valve direct to vacuum; T, fluorine absorption tower.

5. Fluorine Manipulation

A manifold for handling fluorine, shown in figure 3, was used with its attachments for (1) filling and emptying the combustion bomb, (2) obtaining samples of volatile products of combustions and (3) obtaining samples of fluorine for analysis. The manifold consisted of ¼ in. monel tubing (wall thickness 0.035 in.) connecting a series of commercially available packless unions, T-connectors and valves. The valves, T-connectors, and unions were made of monel or stainless steel and were silver soldered to the monel tubing. Some copper couplings were also used.

To the manifold were attached cylinders of helium, A, and fluorine, B, gas sampling bulbs, O, a fluorine absorption tower, T, a vacuum system (not shown), and two Bourdon gages, L, and H, specially constructed for fluorine service. Of the Bourdon gages, H was used for measuring pressure over the range 0 to 35 atm abs and L was for indicating rough vacuum from zero (2.5 mm Hg) to 1.0 atm. A thermocouple gage in the vacuum system was used to measure pressures below 10^{-1} mm Hg. A mechanical pump provided a sufficiently good vacuum for work with the fluorine handling system. The system was considered to be sufficiently gas-tight for use if no indication of leaks was found at internal pressures of either 35 atm or 0.005 mm Hg.

In order to fill the combustion bomb, J, with fluorine, it was attached to the manifold by a screw connector. With valves F, G, M, P, R closed and valves I, K, S, and the bomb needle valve open, the bomb was evacuated to a pressure of 10^{-2} mm Hg. When this degree of vacuum was attained, valves K and S were closed, and fluorine was introduced into the bomb by opening the fluorine tank valve, and then valves D and F. The rate of flow was regulated to allow the pressure to increase about four atm per minute. When the gage pressure was about 21 atm, valve F and the bomb needle valve were closed, then valve D and the fluorine tank valve. If the pressure in the tank was less than 21 atm, a small section of the line, E, was immersed in liquid nitrogen and fluorine was condensed in it. By allowing the condensed fluorine to evaporate and regulating the backflow through valve D, a pressure of 21 atm could be obtained in the bomb. After the bomb had been filled and valve D was closed, the residual fluorine in the manifold was diluted with helium. The gas mixture was slowly passed through valve P and into the fluorine absorption tower. The absorbent used was soda lime. The rate of flow was adjusted to reduce the pressure about 4 atm per minute until the pressure was atmospheric. Gases passing through valve Q emerged near the top of the fume hood in which the apparatus was located into the path of the up-draft. The manifold and absorption tower were filled with helium to a pressure of about 8 atm through valve G, and then valve Q was opened to release the gases. The purging procedure was performed three times. Then after valve Q was closed, valve R was opened and the system was pumped out through the absorption tower. When the pressure reached about 5 mm Hg, valve I was closed and the loaded combustion bomb was removed from the fluorine manifold.

In order to remove fluorine remaining in the bomb after an experiment, and to obtain samples of other gaseous products of combustion, the bomb was again attached to the manifold. Removal of fluorine was done using much the same procedure as described above, except that the bomb needle-valve remained open until evacuation was complete. The bomb was then filled with one atmosphere of helium and was ready to be opened.

To obtain a sample of bomb gases before completely emptying of the bomb, bulbs at O were used. If the interest was in the gaseous constituents other than fluorine, the bulb contained a little mercury which by gentle shaking absorbed the fluorine after the bulb had been filled.

6. Calibration Experiments

Each series of combustion measurements (series I and II, described later) was accompanied by an electrical calibration in which conditions were the same as in the measurements. Following the experimental measurements on Teflon and the aluminum-Teflon mixtures, two other series of calibration experiments were made.

Series III consisted of calibration experiments in which benzoic acid (Standard Sample 39h) was used as a reference material and was burned in oxygen at 30 atm pressure. The energy of combustion of benzoic acid in the standard bomb process is 26434 Jg^{-1}. Also present in the bomb were a platinum crucible to hold the sample, one ml of distilled water, and a two-cm piece of Chromel C fuse wire (diam 0.16 mm) supported over the sample by platinum wire leads. The oxygen used was of high purity (99.996 percent) and no nitric acid correction was required after a combustion experiment. This was checked by measuring the *p*H of the solution in the bomb after each experiment.

A discrepancy of about 0.17 percent between the chemical calibration and previous electrical calibrations was indicated by series III. Because of an uncertainty, mentioned in section 4, associated with the electrical calibration experiments, the calibration with benzoic acid, series III, is preferred over the electrical measurements.

Because the bomb had been changed after series I and II and before series III another electrical calibration, series IV, was carried out in order to determine accurately the correction factor to be applied to the measurements of series I and series II. For series IV the bomb, its contents, and other conditions were the same as the initial conditions of the benzoic acid calibration experiments. The heater was present in both the chemical and electrical calibration experiments.

Six experiments with benzoic acid in series III lead to a mean energy equivalent of 143,038.9 $\pm$15.6 J ohm^{-1}. The electrical calibration of series IV leads to a value of 143,276.5$\pm$16.0 J ohm^{-1} based also on six experiments. The six electrical calibration experiments of series I, adjusted by the factor 143,038.9/143,276.5 lead to an energy equivalent of 143,725.5$\pm$13.5 J ohm^{-1}. Similarly, the five electrical calibration experiments of series II, adjusted by the same factor lead to an energy equivalent of 144,097.7$\pm$14.0 J ohm^{-1}. The uncertainties cited above are the standard deviations of the means computed from the data.

The differences in the observed energy equivalent are due to small differences in the bomb and its contents which have been discussed. Each series of heat measurements was calculated using the appropriate energy equivalent.

7. Combustion Experiments

Two complete series of combustion experiments were carried out, series I and series II. Series I consisted of five combustions of Teflon (table 1), six combustions of aluminum-Teflon mixtures (table 2), and the six electrical calibration experiments previously mentioned. This series must be considered in the nature of preliminary experiments, however, it affords substantial support for the later measurements and is therefore described in detail. Series II consisted of five combustions of Teflon (table 3), five combustions of aluminum-Teflon mixtures (table 4), and five electrical calibration measurements.

TABLE 1.—*Teflon combustion experiments. Series I*

Experiment	1	2	3	4	5
(1a) m (Teflon) g	4.23389	4.24120	4.24090	4.22823	4.24161
(3) ϵ J ohm^{-1}	143,777.8	143,778.2	143,778.1	143,778.2	143,778.6
(4) ΔR_c ohms	0.305338	0.305831	0.306107	0.305673	0.306201
(5) $(\epsilon)(\Delta R_c)$ J	−43,900.8	−43,971.8	−44,011.5	−43,929.1	−44,025.2
(6) q (fuse) J	153.5	138.5	138.0	349.0	76.0
(7) q (corr.) J	30.4	30.6	30.6	30.5	30.7
(8) ΔH_{298} (Teflon) J	−43,716.9	−43,802.7	−43,842.9	−43,569.6	−43,918.5
(14) ΔH_{298}° (Teflon) Jg^{-1}	−10,325.5	−10,327.9	−10,338.1	−10,304.5	−10,354.2
(16) Mean ΔH_{298}° (Teflon)					−10,330.0 Jg^{-1}
(18) Standard deviation of the mean					8.1 Jg^{-1}

TABLE 2. *Aluminum-Teflon combustion experiments. Series I*

Experiment	1	2	3	4	5	6
(1a) m (Teflon) g	2.01775	2.13988	2.13602	2.13445	2.13814	2.13529
(1b) m (Al sample) g	0.39548	0.39914	0.40080	0.39996	0.40224	0.40190
(2) m (AlF_3 found) g	1.2209	1.2480	1.2510	1.2375	1.2375	1.2625
(3) ϵ $Johm^{-1}$	143,756.2	143,757.6	143,758.3	143,755.7	143,757.7	143,758.1
(4) ΔR_c ohms	0.299379	0.308698	0.308887	0.309101	0.309993	0.309959
(5) (ϵ) (ΔR_c) J	−43,037.6	−44,377.7	−44,405.1	−44,435.0	−44,563.9	−44,559.1
(6) q (f.use) J	170.0	370.0	195.0	226.0	221.5	308.0
(7) q (corr.) J	−49.5	−49.2	−49.4	−49.7	−50.0	−50.0
(8) $-\Delta H^\circ_{298}$ (Teflon) J	20,843.4	22,105.0	22,065.1	22,048.9	22,087.0	22,057.5
(9) ΔH°_{298} (Al) J	−22,073.7	−21,951.9	−22,194.4	−22,209.8	−22,305.4	−22,243.6
(10) ΔH°_{298} (impurities) J	42.8	43.1	43.1	43.1	43.2	43.2
(11) n (Al, corr.)	0.014569	0.014703	0.014765	0.014734	0.014818	0.014805
(12) n (AlF_3 corr.)	0.014494	0.014817	0.014853	0.014692	0.014817	0.014990
(13) ΔH°_{298} (Al corr.) J	−22,030.9	−21,908.8	−22,151.3	−22,166.7	−22,262.2	−22,200.4
(14) ΔH°_{298} (combustion), kJ (mole Al)$^{-1}$	−1512.18	−1490.09	−1500.26	−1504.46	−1502.38	−1499.52
(15) ΔH°_{298} (combustion), kJ (mole AlF_3)$^{-1}$	−1520.00	−1478.63	−1491.37	−1508.76	−1502.48	−1481.01

(16) Mean ΔH°_{298} (combustion) −1501.5kJ (mole Al)$^{-1}$; −358.87 kcal (mole Al)$^{-1}$

(17) Mean ΔH°_{298} (combustion) −1497.0kJ (mole AlF_3)$^{-1}$; −357.79 kcal (mole AlF_3)$^{-1}$

(18) Standard deviation of the mean 1.6kJ (mole Al)$^{-1}$; 0.38 kcal (mole Al)$^{-1}$

(19) Standard deviation of the mean 6.6kJ (mole AlF_3)$^{-1}$; 1.6 kcal (mole AlF_3)$^{-1}$

TABLE 3. *Teflon combustion experiments. Series II*

Experiment	1	2	3	4	5
(1a) m (Teflon) g	4.25461	4.23781	4.23486	4.22402	4.26040
(3) ϵ J ohm^{-1}	144,153.1	144,152.4	144,152.4	144,152.2	144,152.6
(4) ΔR_c ohms	0.306016	0.304855	0.304558	0.303797	0.306424
(5) $(\epsilon)(\Delta R_c)$ J	−44,113.2	−43,945.6	−43,902.8	−43,793.0	−44,171.8
(6) q (fuse) J	42.7	45.6	42.8	41.8	44.5
(7) q (corr.) J	30.8	30.5	30.5	30.5	30.8
(8) ΔH°_{298} (Teflon) J	−44,039.7	−43,869.5	−43,829.5	−43,720.7	−44,096.5
(14) ΔH°_{298} (Teflon) Jg^{-1}	−10,351.1	−10,351.9	−10,349.7	−10,350.5	−10,350.3

(16) Mean ΔH°_{298} (Teflon) −10,350.7 J g^{-1}

(18) Standard deviation of the mean 0.4 J g^{-1}

TABLE 4. *Aluminum-Teflon combustion experiments. Series II*

Experiment	1	2	3	4	5
(1a) m (Teflon) g	2.14074	2.12728	2.14192	2.13963	2.13579
(1b) m (Al sample) g	0.40028	0.39880	0.40031	0.40430	0.40278
(2) m (AlF_3 found) g	1.2311	1.2213	1.2527	1.2661	1.2600
(3) ϵ J ohm^{-1}	144,131.4	144,131.7	144,132.9	144,131.6	144,131.6
(4) ΔR_c ohms	0.308652	0.306706	0.308567	0.309709	0.308498
(5) (ϵ) (ΔR_c) J	−44,486.4	−44,206.1	−44,474.7	−44,638.9	−44,464.3
(6) q(fuse) J	49.2	49.6	50.1	50.2	49.8
(7) q (corr.) J	−49.5	−49.5	−49.6	−50.2	−50.0
(8) $-\Delta H^\circ_{298}$ (Teflon) J	22,158.2	22,018.8	22,170.4	22,146.7	22,106.9
(9) ΔH°_{298} (Al) J	−22,328.5	−22,187.2	−22,303.8	−22,492.2	−22,357.6
(10) ΔH°_{298} (impurities) J	43.1	43.0	43.1	43.4	43.2
(11) n (Al, corr.)	0.014746	0.014691	0.014747	0.014894	0.014838
(12) n (AlF_3 corr.)	0.014616	0.014499	0.014873	0.015033	0.014960
(13) ΔH°_{298} (Al, corr.) J	−22,265.4	−22,144.2	−22,260.7	−22,448.8	−22,314.4
(14) ΔH°_{298} (combustion), J (mole Al)$^{-1}$	−1511.28	−1507.33	−1509.51	−1507.24	−1503.87
(15) ΔH°_{298} (combustion), J mole AlF_3)$^{-1}$	−1524.73	−1527.30	−1496.73	−1493.29	−1491.60

(16) Mean ΔH°_{298} (combustion) −1507.8 kJ (mole Al)$^{-1}$; −360.37 kcal (mole Al)$^{-1}$

(17) Mean ΔH°_{298} (combustion) −1506.7 kJ (mole AlF_3)$^{-1}$; −360.11 kcal (mole AlF_3)$^{-1}$

(18) Standard deviation of the mean 1.2 kJ (mole Al)$^{-1}$; 0.29 kcal (mole Al)$^{-1}$

(19) Standard deviation of the mean 7.9 kJ (mole^{-1} AlF_3)$^{-1}$; 1.9 kcal (mole AlF_3)$^{-1}$

7.1. Experimental Conditions and Procedures

For the combustion of Teflon in both series I and series II, accurately weighed pellets of about 4.25 g were prepared from powdered Teflon.

For the combustion of mixtures, about 2.13 g of Teflon and 0.40 g of aluminum powder were accurately weighed for each experiment. The powders were mixed with a needle, and transferred to a pellet press for pelleting. The aluminum powder adhered to the Teflon, and thus transfer was not difficult. The pellet was also accurately weighed; a loss in weight (1.0 to 2.5 mg) on pelleting was always observed. In calculating the sample mass, we assumed that the loss of the two constituents took place in proportion to the original amount of each. The samples were weighed to 0.01 mg.

In series I, the mass of aluminum fluoride formed was determined by weighing the bomb head with the electrode-fuse system, and the bomb base with the pellet holder, before and after each experiment. A balance having a capacity of 5 kg and a readability of 0.5 mg was used for weighing the bomb parts.

The fuse system used in series I was 2-cm piece of Chromel C wire (0.015 cm diam) supported on either side by a 3-cm piece of aluminum wire (0.025-cm diam). The mass of the fuse system, i.e., aluminum wires (8 mg) and Chromel C (3 mg), was 11 mg, and its heat of combustion would be 483.5 J if it burned completely.

Inspection of the bomb after a combustion showed many small balls of melted fuse adhering to the wall. Determining the amount of melted fuse remaining was difficult because removal of the fuse from the bomb wall almost always resulted in chipping out some of the bomb material itself. Establishing the amount of unburned fuse by weighing the bomb base was also difficult because of the large mass of the bomb base (about 2 kg) compared to the spattered fuse (2 to 6 mg). The difficulty was much greater when aluminum was burned bacause fuse pieces could not be easily separated from the aluminum fluoride formed in the combustion.

The difficulties and uncertainties introduced by the fuse were a major factor in the decision to carry out an additional series of experiments on an improved fuse system. The fuse problems in series I are discussed further in section 7.2.

Series II differs in several respects from series I. A liner was inserted into the bomb base in an attempt to facilitate weighing of the aluminum fluoride product. The liner was made of type 304 stainless steel. It had a wall thickness of about 0.25 cm, weighed 177 g, and fitted snugly into the bomb with a clearance of about 0.008 cm. A different monel pellet holder was used in the liner than in the series I experiments. The mass of aluminum fluoride was determined by weighing the stainless steel liner plus monel pellet holder before and after each experiment. Aluminum fluoride deposited on parts of the bomb outside the liner was brushed into the liner for weighing.

A six-cm piece of tungsten wire (0.008 cm diam) was used for the fuse in series II. The mass of the fuse was about 5 mg, and if burned to completion, the fuse would contribute about 50 J or about 0.1 percent to the energy of combustion. The use of tungsten for the fuse wire offers the advantage that its combustion leads to a volatile substance and, therefore, any unburned fuse is easily observed. Little if any unburned fuse was observed in the aluminum-Teflon combustions, but a small residue of the ends remained after the Teflon combustions. The improved estimation of the fuse energy, and the smaller amount of fuse energy apparently are significant contributing factors in the greater precision and accuracy of the measurements of series II.

7.2. Examination of Combustion Products

The aluminum fluoride produced in the combustions was deposited as a fine white powder covering the inner surface of the bomb, and in a larger mass in the immediate area of combustion. It was examined microscopically and found to be crystalline in appearance. The particles were regularly shaped and had dimensions of three to five microns. The x-ray diffraction pattern of the powder agreed well with data reported earlier [19]. The pattern found was that for space group D_3^7–R32 #155, which is trigonal. The unit cell was hexagonal with parameters $a=4.927$Å and $c=12.445$Å, with six molecules per unit cell.

Aluminum oxide in small amounts would not be detected by the x-ray examination. However, an experiment was performed in which aluminum was burned in an equimolar mixture of fluorine and oxygen. The white powder formed as a result of the reaction was given an x-ray examination. Only aluminum fluoride was observed. Because no aluminum oxide was observed in the products of this reaction we presume that no appreciable amount of aluminum oxide would be formed by reaction of the small amount of oxygen impurity in the fluroine.

After a Teflon combustion a small amount of carbon residue was discernible (0.2 to 0.9 mg). No correction was applied for the unburned carbon. We assumed that carbon was formed in the same ratio to the amount of Teflon present in the combustion of aluminum-Teflon mixtures as in the combustion of Teflon alone, and that the error due to unburned material would tend to cancel out when the energy from the Teflon was subtracted from the total energy in the combustion of the mixtures.

Aside from the small amount of carbon formation, the combustions were complete, with CF_4 as the only significant gaseous product in both the Teflon and aluminum-Teflon experiments. Following several experiments of each kind, the gases remaining after removal of fluorine were examined in a mass spectrometer. The observed peaks could not be attributed to fluorocarbons other than CF_4 at levels of more than 0.02 percent. Oxygen, nitrogen

and other impurities except CO_2 originally present in the fluorine were still present, and the amounts were about what would have been expected if no change in them had occurred. The amount of CO_2 had increased by 0.3 to 0.5 mole percent. The source of the added CO_2 was not determined, and was found in both the Teflon and the aluminum-Teflon experiments. No correction was made for its formation.

8. Discussion and Results

8.1. Treatment of Combustion Data

The data for the experiments recorded in tables 1–4, are enumerated in such a way that the same item number, so far as possible, refers to the same quantity in all the experiments. Items (1a) and (1b) are the masses (in vacuo) of Teflon and aluminum in the sample while item (2) is the mass (in vacuo) of aluminum fluoride recovered. Neither are corrected for impurities, however, the masses of Teflon and aluminum have been adjusted for losses in pelleting. The energy equivalent of the calorimeter, the corrected temperature rise, and the total observed energy are given by items (3), (4), and (5), respectively. The contribution of the fuse, Teflon, and impurities to the total reaction energy are given by items (6), (8), and (10), respectively. No impurity corrections were made for Teflon. The quantity q (corr), item (7), includes the corrections needed to convert the observed reaction energy to that with the reactants and products in their standard states (Washburn corrections), the heat capacity corrections to convert the reaction energy from the final temperature, 30 °C, to the standard reference temperature, 25 °C, and the difference $\Delta H^\circ_{298} - \Delta E^\circ_{298}$ which converts the heat of reaction measured at constant volume to that at constant pressure. Item (9) denotes the fraction of the reaction energy contributed by the combustion of aluminum given in item (1b). Items (11) and (12) give the numbers of moles of Al and AlF_3 corrected for impurities in the aluminum and are, therefore, the most suitable measures of the quantity of reaction. Item (13) gives the reaction energy measured for the combustion of aluminum, corrected for impurities. The enthalpy change observed per mole of aluminum or per gram of Teflon introduced is listed in item (14) while the mean value is given in item (16). The corresponding values for the enthalpy change per mole based on AlF_3 recovered are listed in items (15) and (17), respectively.

It is apparent from the standard deviations of the means given in items (18) and (19) that the heat observed for the combustion is more closely correlated with the mass of aluminum introduced into the bomb than with the observed masses of the aluminum fluoride formed in both series I and series II. The calculations based on the mass of aluminum fluoride formed appear less precise in series II than in series I. We attribute this difference to the use of the liner in the calorimeter bomb in series II. The liner has more than doubled the surface area of metal exposed for fluoride film formation. This would lead to greater and perhaps more erratic increases in weight due to extraneous reactions. In addition, and perhaps more important, quantitative transfer of aluminum fluoride from the other bomb parts of the liner for weighing is difficult.

Another significant difference between series I and series II is that no dependence of the observed heat of combustion on fuse-energy correction is noted in series II, though a significant dependence is noted in series I. The use of a tungsten fuse with a low total heat of combustion in series II appears to have made a significant improvement in the experiments.

8.2. Fuse Energy Correction

Of the corrections applied in series I to the energy measurements in the combustion of both Teflon and the aluminum-Teflon mixtures, the fuse energy correction, item (6) of table 1 and table 2, is by far the largest and most uncertain. The magnitude of this correction was between 0.2 and 0.8 percent of the total energy involved in the combustion process. It was also observed that in each case the calculated energy of reaction was approximately a linear function of the fuse correction applied, and that in fact, a smaller spread of measurements would be obtained if no fuse energy correction were applied.

A least squares fit of the heat of combustion observed for Teflon (Jg^{-1}) versus the fuse energy applied, (q (fuse)), gives equation (3)

$$-\Delta H^\circ_{298}\ [\text{Teflon}]\ Jg^{-1} = 10{,}357.6 - 0.16122q\ (\text{fuse})\ J. \quad (3)$$

The standard deviation of the intercept (zero fuse energy) is 18.8 Jg^{-1} and of the slope is 0.043. The intercept bears no necessary relation to the true heat of combustion, as some fuse must have burned in order to ignite the sample. Nevertheless, the intercept is in much closer agreement with the mean of the measurements on Teflon in series II than is the mean of series I, differing by about 7 Jg^{-1}. If we assume for series I a true fuse energy of about 43.5 J (the mean of that in the Teflon experiments in series II), we obtain a value for the heat of combustion of Teflon in series I of $-10{,}350.6$ Jg^{-1}, in almost exact agreement with series II. These calculations do not justify placing any appreciable weight on the results of series I in comparison with those of series II, but do allow us to infer that the difference between series I and series II is largely attributable to the uncertainty in the values taken for the fuse energy. If the calculation of the heat of combustion of aluminum from the measurements in the aluminum-Teflon experiments is made using the heat of combustion of Teflon obtained from either series I or series II, a dependence upon the applied fuse correction is still observed. A linear correlation of the heat of formation based upon the amount of aluminum in the sample and the fuse energy leads to eq (4) when the Teflon data from series I are used and

to eq (5) when similar data from series II are applied

$$-\Delta H^{\circ}_{f298}[AlF_3]\ (\text{kJ mole}^{-1}) = 1522.06 - 0.082855q\ (\text{fuse})\ \text{J} \quad (4)$$

$$-\Delta H^{\circ}_{298}[AlF_3]\ (\text{kJ mole}^{-1}) = 1519.18 - 0.083243q\ (\text{fuse})\ \text{J}. \quad (5)$$

The standard deviation of the slope is 0.019 for both eq (4) and (5) while the standard deviation of the intercept is 11.92 for eq (4) and 12.35 for eq (5). In this case, the intercepts are further away from the results of Series II than is the mean of the unadjusted experiments of series I. If we interpolate using a fuse energy of 49.8 J (average value for series II), we find a heat of formation for AlF_3 of -1517.9 kJ mole^{-1} and -1515.0 kJ mole^{-1} as calculated from eqs (4) and (5), respectively. Here again, we feel that the uncertainty in the fuse energy is so great that little weight should be given to the experiments in series I in comparison to those in series II.

In series II, the fuse energy was essentially the same (43.5 J) in all Teflon experiments, and also essentially the same (49.8 J) in all aluminum-Teflon experiments. There seems to be no question about this small difference in fuse energy as it represents the unburned ends of the fuse found after the Teflon combustions, but not found after aluminum-Teflon combustions.

8.3. Auxiliary Data and Constants

Buoyancy corrections for the mass of aluminum and Teflon in the combustion samples were calculated using 2.702 g cm^{-3} [20] and 2.31 g cm^{-3}, respectively, for their densities. The density of Teflon was determined as part of this investigation.

The fuse energy was calculated from the masses of the fuse and the heats of formation of the fluorides formed by its combustion. For Chromel C, the calculation based on the heats of formation of FeF_3, CrF_3, and NiF_2 [5] gives 14.5 J mg^{-1}. For the aluminum fuse wire an approximate value of 55 J mg^{-1} [7] was adopted for the heat of combustion. For combustion of tungsten, the heat of formation of WF_6 (g) was taken to be -416 kcal mole^{-1} [21]. The combustion 5.25 mg of tungsten wire gives 50 J. In all cases electrical energy needed for ignition was neglected.

Washburn corrections were calculated following in general the procedure outlined by Hubbard [22] for experiments in which fluorine is an oxidant. The coefficients $\left[\frac{\partial E}{\partial P}\right] = -T\left[\frac{dB}{dT}\right]$ were found in tables based on a Lennard-Jones 6–12 potential function, as compiled by Hirschfelder, Curtiss, and Bird [23], using the appropriate force constants. The force constants used for fluorine were those determined by White, Hu, and Johnston [24], and by Douslin [25] for carbon tetrafluoride. Force constants appropriate to the mixtures of CF_4 and F_2 in the reaction products were calculated from those for the pure components. For fluorine and carbon tetrafluoride, Cv was taken to be 5.52 [26], and 12.78 [30] cal deg^{-1} mole^{-1}, respectively. Values of Cp in cal deg^{-1} g^{-1} for aluminum, Teflon, aluminum fluoride and carbon tetrafluoride were taken to be 0.217 [27], 0.28 [28], 0.215 [29], and 0.1674 [30], respectively.

Metallic impurities and aluminum oxide present in the aluminum were assumed to react completely with fluorine. For calculation of the heats of reaction of the impurities, the heats of formation of Al_2O_3, FeF_3, SiF_4, and CuF_2 in kcal mole^{-1} were taken as -400.4 [31], -235 [6], -385.98 [32], and -126.9 [5], respectively.

Atomic weights used in calculating the data were taken from the 1961 Table of Atomic Weights based on $C^{12}=12$ [33].

The unit of energy is the joule. The calorie was taken as 4.1840 J.

8.4. Sources of Error

Sources of scatter and systematic errors in the measurements applicable to Series II may be briefly reviewed. The loss of aluminum and Teflon in forming the pellet may not have been in proportion, as was assumed, to the amounts of each present. An estimated maximum error from this uncertainty is about 0.26 percent. The amount of unburned carbon remaining in all Teflon combustion experiments was measured and varied from 0.2 to 0.9 mg. No attempt was made to determine the carbon found in the combustion of an aluminum-Teflon pellet although carbon formation was assumed to occur in proportion to the mass of Teflon in the pellet. A maximum systematic error from this source is estimated to be about 0.18 percent.

The amounts of new fluoride film formation on the inner surfaces of the bomb may have varied from one experiment to another. This quantity was difficult to measure because of the small mass of fluoride formation needed for a significant heat effect, in comparison with the total mass of the bomb. In addition, the formation of some fluoride may occur before a heat measurement is actually begun, and further reaction with the walls may occur during the reaction of the sample. Aluminum fluoride, in the state in which it was formed, adheres tenaciously to the fluoride film on the bomb walls, and is difficult to remove. On the other hand, purging the bomb after an experiment may dislodge and carry away from the bomb minute amounts of finely divided aluminum fluoride. These factors in general, except for the uncertainties in weighing the original sample and in determining the amount of carbon residue, would tend to affect the scatter of the heat measurements based on the mass of aluminum fluoride more than those based on aluminum. The systematic difference between the measurements based on the mass of aluminum in the sample and those based on the aluminum fluoride formed in the combustion were taken as a measure of the uncertainty in the completeness of reaction, and found to be about 0.10 percent.

While the scatter of the measurements is probably not affected by the impurity content of the sample, the uncertainty in the energy of combustion of impurities and of the amount of impurities may lead to an error which we estimate at maximum to be 0.18 percent based upon the oxygen content of the aluminum.

The presence of extremely small pieces of melted tungsten fuse imbedded in the inner wall of the liner found after the combustion experiments of series II, indicated that combustion of the tungsten fuse was not complete. Since the imbedded fuse was impossible to remove and determine quantitatively, a resulting uncertainty in the fuse energy correction ensued which we estimate to be about 0.05 percent.

In estimating the 95 percent confidence limits for the uncertainties due to the scatter of the calibration experiments, the standard deviations of the means for series II, III, and IV were multiplied by the appropriate factors of the Student t distribution. Combining these and an uncertainty of 0.01 percent in the energy of combustion of benzoic acid, we obtain 0.05 percent for the uncertainty of the energy equivalent of the calorimeter.

The standard deviations of the means of the combustion experiments were also multiplied by the appropriate factors of the t distribution to give the 95 percent limits of uncertainty. For the aluminum-Teflon combustions, we find 0.22 percent and for the Teflon combustions 0.01 percent. Combining the various uncertainties as they would apply to aluminum, we find, as the square root of the sum of the squares, the value 0.44 percent which is equivalent to 6.6 kJ mole^{-1} (1.6 kcal mole^{-1}) uncertainty in the heat of combustion of aluminum in fluorine. We feel this is a fair estimate of the uncertainty of the heat of formation of aluminum fluoride on the basis of the present experiments.

9. Heat of Formation of Aluminum Fluoride

On the basis of the measurements and the calculations outlined in section 8, we find for the heat of reaction (6) and, hence, the heat of formation of aluminum fluoride,

$$\mathrm{Al(c)}+\frac{3}{2}\,\mathrm{F_2(g)}=\mathrm{AlF_3(c)} \qquad (6)$$

$\Delta H^\circ_{f298}[\mathrm{AlF_3(c)}]=-1507.8\pm6.6$ kJ mole^{-1} (-360.4 ± 1.6 kcal mole^{-1}).

In section 1 we outlined several previous calorimetric studies from which the heat of formation of aluminum fluoride could be determined. In that section, we listed the figures obtained by the authorities cited, which were based on data dependent upon the heat of formation of hydrogen fluoride. For this value they used the heat of formation listed in NBS Circular 500 [5], -64.2 kcal mole^{-1}. A recent reassessment of the heats of formation of HF(g) and HF(aq) by Evans [34] (see also Medvedev [35] and Feder et al. [36]) indicates that a change to a more negative value is more consistent with the available data. Evans suggests a value -64.8 kcal mole^{-1} for $\Delta H^\circ_{f298}[\mathrm{HF(g)}]$ and -79.5 kcal mole^{-1} for $\Delta H^\circ_{f298}[\mathrm{HF(aq)}]$. These values are 0.6 and 0.84 kcal mole^{-1} more negative than previously cited values.

Applying these data, or appropriately interpolated data for real aqueous solutions of HF, we recalculated from the measurements of Gross et al. [7, 8], $\Delta H^\circ_{f298}[\mathrm{AlF_3(c)}]=-358.8$ kcal mole^{-1} based on lead fluoride, and -358.0 kcal mole^{-1} based on sodium fluoride and cryolite. No assessment of the maximum dispersion of these values will be made since Gross et al. do not attempt to estimate the total uncertainty in their measurements. A corresponding treatment of the measurements of Kolesov, Martynov, and Skuratov [10] leads to $\Delta H^\circ_{f298}[\mathrm{AlF_3(c)}]=-358.0$ kcal mole^{-1} with an uncertainty which they estimate at 2.0 kcal mole^{-1}. The equilibrium data of Mashovets and Yudin [37], reduced to 298 °K using the third law of thermodynamics and then applying the revised heat of formation of HF(g) leads to $\Delta H^\circ_{f298}[\mathrm{AlF_3(c)}]=-357.7\pm0.5$ kcal mole^{-1}.

Each of the above values is still less negative than ours but with reasonable assignments of overall uncertainties, all values would fall within the assigned limits of uncertainty.

The results of this work confirm the findings of the several laboratories, whose work is mentioned above, in concluding the true enthalpy of formation of aluminum fluoride is substantially more negative than was thought until a few years ago. The improvement of the agreement between our results and those of Gross et al., Kolesov et al., and Mashovets and Yudin, upon application of a revised value for the heat of formation of HF(g) to their results, is a substantiation of the validity of the revised value.

10. Heat of Combustion of Teflon and the Heat of Formation of Carbon Tetrafluoride

The measurements of series II on Teflon lead to $\Delta H^\circ_{298}=-10350.7$ Jg^{-1} or -247.43 kcal monomole^{-1} where a monomole refers to the unit, —C_2F_4—.

$$\mathrm{C_2F_4\ (solid\ polymer)}+2\mathrm{F_2(g)}=2\mathrm{CF_4(g)}. \qquad (7)$$

Estimating the contributions to the uncertainty to be 0.01 percent from the scatter of the heat measurements on Teflon, 0.04 percent from the calibration of the calorimeter, 0.09 percent from unburned carbon and 0.02 percent from the fuse energy, we find an estimated uncertainty of 0.11 percent or 11.4 Jg^{-1} (0.27 kcal monomole^{-1}).

In a series of experiments on the combustion of Teflon in oxygen, Scott, Good, and Waddington [38] determined for reaction (8), $\Delta H^\circ_{298}=-160.3\pm0.9$ kcal mole^{-1};

$$\mathrm{C_2F_4\ (solid\ polymer)}+\mathrm{O_2(g)}+2\mathrm{H_2O(l)}=2\mathrm{CO_2(g)}+4\mathrm{HF(aq,\ 10H_2O)} \qquad (8)$$

and for reaction (9), $\Delta H^\circ_{298} = -118.8 \pm 0.5$ kcal mole^{-1},

$$C_2F_4 \text{ (solid polymer)} + O_2(g) = CO_2(g) + CF_4(g). \quad (9)$$

Using a revised value, -76.235 kcal mole^{-1} [34] for the heat of formation of $HF(aq,10H_2O)$, we calculate from their data, $\Delta H^\circ_{f298}[C_2F_4 \text{ (solid polymer)}] = -196.11$ kcal monomole^{-1}, and $\Delta H^\circ_{f298}[CF_4(g)] = -220.86$ kcal mole^{-1}.

Using the value thus calculated for C_2F_4 (solid polymer) with our results for reaction (7), we calculate $\Delta H^\circ_{f298}[CF_4(g)] = -221.77$ kcal mole^{-1}.

Here again the results are in much better agreement when the revised value for the heat of formation of hydrogen fluoride is used than if the previously accepted value had been used. The two values for $\Delta H^\circ_{f2\cdot8}[CF_4(g)]$ are in agreement within the limits of experimental error cited. However, it should be recognized that measurements based upon C_2F_4 (solid polymer) as an intermediate are subject to a possible limitation in reproducibility because Teflon is not a well defined substance. In the comparison of our results with those of Scott et al., it is therefore necessary to bear in mind the fact that different preparations of Teflon were used in the two experimental studies.

11. References

[1] Baud, E., Compt. Rend. **135,** 1103–6 (1902).
[2] Baud, E., Ann. Chim. Phys. **1,** 8–71 (1904).
[3] Wartenberg, H. v., Z. Anorg. Allgem. Chem. **151,** 326–30 (1926).
[4] Bichowsky, F. R., and Rossini, F. D., The Thermochemistry of the Chemical Substances (Reinhold Publishing Corp., New York, 1936).
[5] Rossini, F. D., Wagman, D. D., Evans, W. H., Levine, S., and Jaffa, I., Selected Values of Chemical Thermodynamic Properties, NBS Circ. 500 (U.S. Government Printing Office, Washington, 25, D.C. 1952).
[6] Brewer, L., Bromley, L. A., Gilles, P. W., and Lofgren, N., "The Thermodynamic Properties of the Halides," Paper 6, Chemistry and Metallurgy of Miscellaneous Materials: Thermodynamics, L. L. Quill, Editor, (McGraw-Hill Book Company, Inc., New York, 1950).
[7] Gross, P., Hayman, C., and Levi, D. L., Trans. Faraday Soc. **50,** 477–80 (1954).
[8] Gross, P., Hayman, C., and Levi, D. L., "The Heats of Formation of Cryolite and the Aluminum Fluorides," pp. 903–908 (Part 2). International Symposium on the Physical Chemistry of Process Metallurgy, Pittsburgh, 1959. Physical Chemistry of Process Metallurgy, G. R. St. Pierre, Editor, (Interscience Publishers, New York, 1961).
[9] Coughlin, J. P., J. Am. Chem. Soc. **80,** 1802–4 (1958).
[10] Kolesov, V. P., Martynov, A. M., and Skuratov, S. M., Zh. Neorgan. Khim. **6,** 2623–6 (1961).
[11] Hubbard, W. N., Settle, J. L., and Feder, J. M., Pure Applied Chem. **2,** 39–44 (1961).
[12] Kubaschewsky, O., and Hopkins, B. E., Oxidation of Metals and Alloys (Butterworth Scientific Publications, London, 1953), pp. 130–7, 180.
[13] Werner, O., Metall **4,** 9–12 (1950).
[14] Armstrong, G. T., and Jessup, R. S., J. Res. NBS **64A,** 49–59 (1960).
[15] Dickinson, H. C., Bul. BS **11,** 189–257 (1914).
[16] Prosen, E. J., Johnson, W. H., and Pergiel, F. Y., J. Res. Natl. Bur. Std. **62,** 43–7 (1959).
[17] Coops, J., Jessup, R. S., and Van Nes, K., "Calibration of Calorimeters for Reactions in a Bomb at Constant Volume," Chapter 3, Experimental Thermochemistry, F. D. Rossini, Editor, (Interscience Publishers, Inc., New York, 1956).
[18] Jessup, R. S., NBS Mono. 7, February 26, 1960.
[19] Staritzky, E., and Asprey, L. B., Anal. Chem. **29,** 984 (1957).
[20] Edwards, D. J., and Moorman, T. A., Chem. & Met. Eng. **24,** 61–4 (1921).
[21] Meyers, O. E., and Brady, A. P., J. Phys. Chem. **64,** 591–4 (1960).
[22] Hubbard, W. N., "Fluorine Bomb Calorimetry," Chapter 6, Experimental Thermochemistry, Vol. II, H. A. Skinner, Editor, (Interscience Publishers, Inc., New York, N.Y., 1962).
[23] Hirschfelder, J. O., Curtiss, C. F., and Bird, R. B., Molecular Theory of Gases and Liquids, (John Wiley & Sons, New York, N.Y., 1954), 1114–5.
[24] White, D., Hu, J. H., and Johnston, H. L., J. Chem. Phys. **21,** 1149–52 (1953).
[25] Douslin, D. R., "Pressure-Volume-Temperature Relations and Intermolecular Potentials for Methane and Tetrafluoromethane," Paper 11, Progress in International Research on Thermodynamic and Transport Properties, J. F. Masi and D. H. Tsai, Editors, (Academic Press, New York, N.Y., 1962).
[26] Evans, W. H., Munson, T. R., and Wagman, D. D., J. Res. NBS **55,** 147–64 (1955).
[27] Giauque, W. F., and Meads, P. F., J. Am. Chem. Soc. **63,** 1897–1901 (1941).
[28] Good, W. D., Scott, D. W., and Waddington, G., J. Phys. Chem. **60,** 1080–9 (1956).
[29] O'Brien, C. J., and Kelley, K. K., J. Am. Chem. Soc. **79,** 5616–18 (1957).
[30] Kelley, K. K., U.S. Bur. Mines Bull. 584 (1960).
[31] Mah, A. D., J. Phys. Chem. **61,** 1572–3 (1957).
[32] Wise, S. S., Margrave, J. L., Feder, H. M., and Hubbard, W. N., J. Phys. Chem. **67,** 815–821 (1963).
[33] Cameron, A. E., and Wichers, E., J. Am. Chem. Soc. **84,** 4175–97 (1962).
[34] Evans, W. H. (NBS, private communication, 1964).
[35] Medvedev, V. A., Zh. Fiz. Khim. **37** (6), 1403–6 (1963).
[36] Feder, H. M., Hubbard, W. N., Wise, S. S., and Margrave, J. L., J. Phys. Chem. **67,** 1148–50 (1963).
[37] Mashovets, V. P., and Yudin, B. F., Izv. Vysshikh Uchebn. Zavedenii, Tsvetn. Met. **5,** 95–105 (1962).
[38] Scott, D. W., Good, W. D., and Waddington, G., J. Am. Chem. Soc. **77,** 245–6 (1955).

(Paper 69A2–335)

JOURNAL OF RESEARCH of the National Bureau of Standards—A. Physics and Chemistry
Vol. 69A, No. 2, March–April 1965

Relative Enthalpy of Polytetrafluoroethylene From 0 to 440 °C[1]

Thomas B. Douglas and Ann W. Harman

(November 18, 1964)

Using a drop method and an ice calorimeter, precise measurements of enthalpy relative to 0 °C were made on a sample of granular polytetrafluoroethylene which was initially 95 percent crystalline. The measurements were at temperatures every 50 degrees from 50 to 300 °C (both before and after melting and quenching); and also at 340, 400, and 440 °C in the liquid range, where it appeared that structural equilibrium of the polymer was reached only slowly. Marked upturns in the heat capacity-temperature curves of the crystalline and quenched polymer above about 200 °C were treated as corresponding to gradual but reversible fusion of the type commonly caused by impurity components ("premelting"). Consideration was given also to the possibility of melting of thin crystals. The (total) heat of fusion could not be determined calorimetrically by the method used, but the additional assumption of three alternative approximations in all cases led to 327 °C as the crystalline melting point of the polymer, which agrees exactly with the accepted value based on direct observation. The heat capacity and relative enthalpy and entropy of the polymer derived from the data were joined smoothly with precise low-temperature values measured earlier at the Bureau on the same and two other samples of polytetrafluoroethylene, and these properties are represented by equations and tabulated as functions of temperature.

1. Introduction

Polytetrafluorethylene, $(C_2F_4)_n$, which is commercially produced under the trade name "Teflon",[2] has many properties which make it unique among known high polymers. Its crystalline melting point (327 °C), viscosity when melted, and thermal stability are especially high. It is highly resistant to chemical attack, and is insoluble in all common solvents. It has an extremely low dielectric loss and high dielectric strength. Also, it has unique non-adhesion and antifrictional characteristics. These properties suggest some of the more important practical uses of this unusual polymer.

During the past two decades numerous investigations of the properties and molecular-scale structure of polytetrafluoroethylene have been published. A comprehensive review of the subject, with numerous references, was published by Sperati and Starkweather in 1961 [1].[3]

Of the various kinds of polytetrafluoroethylene, one is the so-called "granular" polymer. It consists of spongy white particles whose porosity is confirmed by the fact that the specific surface area as determined by nitrogen adsorption is over 1000 times as great as the outer surface area of the particles observed microscopically.

The covalent chains forming the molecules of polytetrafluoroethylene are believed to be entirely "linear" (i.e., unbranched), a belief which receives support from the fact that the formation of branched chains in the polymerization of C_2F_4 would involve the breaking of C–F bonds, which are relatively strong [1]. The average number of CF_2 groups per chain has been found to vary from 3,000 for specially prepared low-molecular-weight samples to as high as 180,000 for samples similar to those of industrial interest [1], these numbers corresponding to molecular weights 50 times as great. It is considered highly probable that each molecule of the polymer contains a sulfonic or a carboxyl group at each end, depending on the type of initiator used in the polymerization [1]. Samples obtained by direct polymerization are in some cases over 95 percent crystalline, but after having been melted the degree of crystallinity is invariably decreased. Infrared absorption and x-ray diffraction studies by Thomas et al. [2] indicated that after quenched, intermediate, and slow cooling from the melt, the degree of crystallinity was approximately 50, 60, and 70 percent respectively. However, electron-microscope studies led Speerschneider and Li [3] to believe that similar variations of cooling rate led to little difference in the degree of crystallinity; they postulated alternate layers of crystalline and amorphous material in the polymer so treated. The rate of crystallization varies inversely with molecular weight. The density at room temperature varies from 2.3 g cm^{-3} for the crystalline to 2.0 g cm^{-3} for the amorphous polymer [1].

In crystalline polytetrafluoroethylene at temperatures below 19 °C the chains are arranged in helices with a 180° twist every 13 carbon atoms. As the temperature rises, at atmospheric pressure a crystal-disordering transition occurs at approximately 19°, and another much smaller one at 30 °C, with gradual untwisting and disorientation of the chain segments

[1] This paper is based on work sponsored by the Ordnance Corps, U.S. Department of the Army.
[2] Registered trademark of E. I. du Pont de Nemours and Company, Wilmington, Delaware.
[3] Figures in brackets indicate the literature references at the end of this paper.

until above 30° the preferred crystallographic direction has been lost and these segments oscillate about their long axes, with some indication of occasional complete rotations. In the amorphous regions of the polymer, glass transitions have been detected at about −97° and 127 °C, where motions of sequences of CF_2 groups are believed to set in. Eby and Sinnott [4] believed that the rise of internal friction above 240 °C in a 95-percent-crystalline sample may be the result of additional but hitherto unresolved crystalline relaxations. The generally accepted melting point of the crystalline polymer is 327 °C, where all opacity was observed to disappear on heating [5]. However, a small crystalline relaxation just below this temperature has been observed, and this is attributed to melting of crystallites. Symons [6] has recently reported that polytetrafluoroethylene, as crystallized from solution in perfluorokerosene, remained unchanged in appearance at temperatures below 327°, but showed a very gradual loss of birefringence and overall form through the range 327–347° on further heating at a rate of 0.5 deg per min. The high melting point of the polymer is attributed to the persistence of direction of the long molecular chains. A considerable amount of molecular-scale structure persists on melting. X-ray diffraction shows that in the liquid the chains are almost straight for several repeat units; Sperati and Starkweather [1] believe that the chains are folded (over long periods), as they are in other polymers. As the temperature of the melted polymer rises, pyrolysis begins to occur (by first-order reaction in the range 360–510 °C), C_2F_4 being the major gaseous decomposition product. During pyrolysis the average molecular weight and viscosity of the liquid decrease.

Most of the fundamental thermodynamic properties of different types of polytetrafluoroethylene have been measured. Data-of-state measurements include the density under various conditions (including thermal expansion to high temperatures and compressibility to high pressures), as well as the change of melting point with pressure. The standard heat of formation has been determined by fluorine-combustion calorimetry. Furukawa, McCoskey, and King [7] measured the relative enthalpy and the heat capacity of four samples (powdered, annealed, quenched, and molded) from 15 to 370 °K (i.e., up to 97 °C), estimating their heat-capacity values for a given sample to be accurate in general to ±0.2 percent. Later, Marx and Dole [8] reported measurements of the heat capacity of two samples (powdered and drawn) from −25° to 120 °C. (For the powdered form, Marx and Dole's heat capacities are, between −23° and 0 °C, about 3.5 percent lower than those of Furukawa et al., but agree much more closely above 40 °C.) These various thermodynamic data have been used by others to calculate other thermodynamic properties and to elucidate further the structure of the polymer. McGeer and Duus [9] and Lupton [10] have calculated the crystalline heat of fusion, and Starkweather and Boyd [11] have decomposed the entropy of fusion into components attributed to specific structural changes. Brandt [12] has developed an intermolecular potential function and estimated the lattice energy and the compressibility at 0 °K. Gotlib and Sochava [13] have used the method of Born and von Karman to calculate from spectroscopic data a frequency spectrum for polytetrafluoroethylene, reporting good agreement with the measured heat capacities of the polymer in the range 50–200 °K.

The present paper reports measurements by drop calorimetry of the enthalpy relative to 0 °C of polytetrafluoroethylene. The sample on which the measurements were made and that measured by Furukawa, McCoskey, and King [7] at lower temperatures and referred to by them as granular powder were actually specimens from the same batch of material. Before the sample had been melted, the heat capacities of the present work agree well with the values of Furukawa et al. on the powder, but after the sample had been melted the heat capacities became considerably higher but agreed approximately with their values on the annealed and molded forms.

2. Sample

Only one sample of polytetrafluoroethylene was used for the present enthalpy measurements. The sample was obtained from E. I. du Pont de Nemours and Company in 1951 as "Teflon TF–1", and is equivalent to their current commercial product designated as "Teflon 1 TFE fluorocarbon resin."

Recently, through the courtesy of C. A. Sperati, several tests were carried out at du Pont on a third sample of the same batch in order to characterize it more definitely in case its properties should bear a significant relation to the precise thermal results reported here. The results of these tests were summarized as indicating that the sample is of commercially available ASTM[4] Type I granular polytetrafluoroethylene (ASTM designation D–1457–62T), the particular sample having a crystalline content of 94.8 percent, a specific surface area of 2.2 $m^2\ g^{-1}$, and a standard specific gravity of 2.166. The average molecular weight, which was not measured directly, was believed to be relatively very high. As discussed in other sections of this paper, the above properties of the sample were drastically changed before the series of thermal measurements was completed, especially at the time when the sample was first heated above its melting point.

Before the thermal measurements, the sample specimen was evacuated to remove traces of moisture, and, though unsealed in its container, showed no detectable loss in mass during the subsequent periods of heating to temperatures as high as 340 °C. In the thermal measurements the sample was in a cylindrical container of pure nickel weighing about 20 g. A screw lid of the same material closed the container, but not gas-tight. Before each in-

[4] American Society for Testing Materials.

sertion into the apparatus, filled with helium at atmospheric pressure, the container with sample was evacuated and filled with the same gas.

3. Calorimetric Procedure

The apparatus and method used in measuring the enthalpy have been described in detail in a previous publication [14]. In brief, the method was as follows. The sample container was suspended in the center of a silver-core furnace until, as determined by preliminary "relaxation-time" tests [15], the sample had time to reach the constant furnace temperature within 0.01 deg C or less. The sample and container were then dropped (with almost free fall) into a precision Bunsen ice calorimeter, and the heat they delivered in cooling to 0 °C was determined by the mass of mercury entering the calorimeter because of the reduction in volume caused by the melting of ice. Similar measurements had been made on the empty container to account accurately for (a) the part of the heat which was due to the container when the sample was present, and (b) the small amount of heat lost elsewhere than to the calorimeter during the drop. The net heat contributed by the sample itself is taken as its change in enthalpy between the furnace temperature and 0 °C.

The temperature of the central portion of the furnace, which was held constant to within ± 0.01 deg C at the value desired in a particular heat measurement, was measured by a strain-free platinum resistance thermometer (ice-point resistance, about 24 ohms) and a Mueller bridge. The thermometer had been accurately calibrated on the International Temperature Scale of 1948 at the Bureau, and its ice-point resistance was periodically checked throughout the series of calorimetric measurements to guard against the occurrence of unknown significant changes in the calibration.

4. Results

Because of previous knowledge that highly crystalline polytetrafluoroethylene after being heated to the neighborhood of its melting point (about 327 °C) returns to its former thermodynamic state at lower temperatures only with great difficulty if at all, heat measurements on the sample were first made at furnace temperatures not exceeding 300 °C. The heats measured in this first series of measurements, corrected for very small deviations from the standard masses of container parts, are recorded in chronological order in table 1 (column 3). The second series of measurements on the sample was made after the sample had been heated to 340° and then cooled rapidly to 0 °C in the ice calorimeter; the results are recorded in table 2, the heats from individual runs being given for the sample plus container in column 5 and for the empty container in column 6. (The same empty-container measurements are applicable to both series involving the sample, but of course for a given furnace temperature no particular individual measurement with the empty container is to be associated with any particular one with the sample.) Because the relative enthalpy of the polymer sample as measured in this way may depend on the sample history, and actually proved to do so after melting, the lengths of time in the furnace are recorded in both tables 1 and 2, and in addition the chronological sequence of the second series of runs is indicated (table 2, column 2). The successive furnace temperatures of the second series (with the number of runs at each temperature given in parentheses) were thus (in °C) 340° (4), 400° (5), 150° (2), 400° (2), 340° (2), 400° (1), 300° (2), 50° (2), 100° (2), 200° (2), 250° (2), and 440° (4). Since the sample underwent appreciable pyrolysis at 440° (as indicated in column 4 of table 2), no measurements were attempted at higher temperatures. The first runs at 340 and 400 °C showed an upward drift well outside the measurement precision, and are parenthesized because they were not used in computing the mean enthalpy values for the sample given in the last column of the table.

TABLE 1. *Heat measurements on the sample of polytetrafluoroethylene powder before heating to 340 °C*

Furnace temperature t [a]	Time sample in furnace	Individual heat measurement (sample + container) [b]	Mean net enthalpy of sample, $H_t - H_0$ °C
°C	min	J	J g^{-1}
50.00	60	965.9	57.69
	90	966.1	
	20	966.7	
100.00	30	1877.8	108.59
	30	1879.8	
150.00	25	2828.5	162.71
	25	2828.1	
200.00	25	3816.6	220.38
	25	3816.6	
250.00	35	4846.6	281.96
	25	4847.5	
300.00	25	5944.8	350.19
	25	5943.9	

[a] International Temperature Scale of 1948.
[b] The mass of sample was 8.9382g. The corresponding individual heat measurements on the container only are recorded in table 2.

Furukawa, McCoskey, and King [7] recorded their smoothed heat capacities, relative enthalpies, and relative entropies for three of their samples of polytetrafluoroethylene at 5-deg intervals up to 92 °C (except for the transition region 7 to 37 °C). After extrapolating their enthalpies to 100 °C, the enthalpies for the intervals 0–50° and 50–100 °C obtained from the present work (tables 1 and 2, last column) were found to compare with their values as shown in table 3. The present values for the powdered sample agree with theirs within about 0.5 percent. The results after fusion ("quenched") approximate theirs on samples similarly treated, the agreement also being within about 0.5 percent when compared with their value on the annealed sample for 0–50 °C and their value on the molded sample for 50–100 °C.[5]

[5] Furukawa, McCoskey, and King [7] recorded no numerical results of their measurements on a sample that had been annealed at 350 °C and then quenched in liquid nitrogen, except over the interval 7–37 °C.

TABLE 2. *Heat measurements on the sample of polytetrafluoroethylene powder after heating to 340 °C*

Furnace temperature t [a]	Sample + container [c]				Container only	Mean net enthalpy of sample, $H_t - H_0$ [c]
	Chronological No. of run [b]	Time in furnace	Decrease in sample mass	Individual heat measurement [c]	Individual heat measurement	
°C		min	%	J	J	J g^{-1}
50.00	19	45	0	954.4	451.0	56.37
	20	60	0	954.6	450.2	
100.00	21	55	0	1887.5	908.8	109.67
	22	45	0	1889.4	907.7	
150.00	10	45	0	2862.2	1374.0	166.50
	11	60	0	2862.1	1373.9	
200.00	23	45	0	3877.5	1846.1	227.31
	24	60	0	3879.6	1847.4	
250.00	25	45	0	4943.8	2327.1	292.72
	26	60	0	4942.7	2326.6	
300.00	17	45	0	6096.4	2814.7	366.91
	18	60	0	6091.3	2814.0	
340.00	1	35	0	(7178.0)	3208.0	[f] 452.66
	2	45	0	(7187.0)	3208.8	
	3	90	0	(7193.1)	----	
	4	[d] 80	0	(7209.0)	----	
	14	180	0	7253.6	----	
	15	[e] 195	0	7255.1	----	
400.00	5	45	0.000	(8569.0)	3811.6	[f] 535.63
	6	60	.003	(8577.9)	3810.1	
	7	90	.004	(8582.0)	----	
	8	120	.001	8595.1	----	
	9	150	.002	8599.5	----	
	12	240	.017	8600.6	----	
	13	240	.017	8596.7	----	
	16	45	.000	8600.3	----	
440.00	27	45	.027	9511.9	4215.7	[f] 593.33
	28	50	.021	(9234.4)	4215.5	
	29	60	.041	9522.0	----	
	30	90	.043	9522.7	----	

[a] International Temperature Scale of 1948.
[b] Considering only the runs on the sample + container.
[c] The actual mass of sample was 8.9382 g less the aggregate loss thus far accounted for in column 4. However, for comparison small corrections (by proportion) are included in column 5 to place all the values on the basis of 8.9382 g of sample.
[d] 20 min at 400°, then 60 min at 340 °C.
[e] 45 min at 400°, then 150 min at 340 °C.
[f] Excluding the parenthesized values in column 5.

TABLE 3. *Comparison of enthalpy changes of polytetrafluoroethylene over two 50-degree temperature intervals as determined for various samples by NBS adiabatic and drop calorimetry*

Temperature interval	ΔH for the powdered sample (by adiabatic calorimetry) [b]	Deviation of ΔH from value in column 2						
		Powdered sample			Annealed sample	Quenched sample		Molded sample
		Adiabatic calorimetry (observed) [b]	Drop calorimetry (observed)	Formulated (eq 2)	Adiabatic calorimetry (observed) [b]	Drop calorimetry (observed)	Formulated (eq 5)	Adiabatic calorimetry (observed) [b]
°C	j g^{-1}	%	%	%	%	%	%	%
0–50 [a]	57.9	0.0	−0.4	----	−2.5	−2.7	----	−5.2
50–100	50.7	0	+.5	0.0	+4.0	+5.2	+4.7	+4.6

[a] Includes transition region. [b] From reference [7]. The values not so indicated are from the present paper.

An empirical equation of the form

$$H = A + BT + CT^2 + D/(E - T), \qquad (1)$$

where T is the temperature in deg K and $A \ldots E$ are constants evaluated by fitting to the data (table 1 or 2, last column), was used to represent the enthalpy H relative to that of some fixed temperature and state, for each of the forms powdered, quenched, and liquid polytetrafluoroethylene. For the liquid the term $D/(E-T)$ was omitted, giving a simple form of equation corresponding to a heat capacity varying linearly with temperature. Since mean observed sample enthalpies are available at only three temperatures in the liquid range (340, 400, and 440 °C), the data were fitted exactly. For each of the two forms powdered and quenched, the mean heat capacity over successive 50-deg intervals obviously increases with temperature at an accelerated rate in the neighborhood of 300 °C (tables 1 and 2), and the term $D/(E-T)$ was arbitrarily introduced to account for this fact. For each of these "solid" forms of the polymer, eq (1) was fit to the observed data at five temperatures (100–300 °C), so that in these cases also the fit was exact.

The enthalpy equations so derived, together with the corresponding equations for heat capacity and relative entropy obtained by differentiation and integration, are as follows. (The units are in terms of joules, grams, and deg K at T °K. Also given are the temperature ranges of applicability, derived as stated below. The subscript "0" applies to 0 °K.)

Polytetrafluoroethylene powder (346.5–573 °K)

$$H_T - H_0 = 0.54268T + 6.715(10^{-4})T^2 + 208/(603.4 - T) - 54.47 \quad (2)$$

$$C_p = 0.54268 + 1.343(10^{-3})T + 208/(603.4 - T)^2 \quad (3)$$

$$S_T - S_0 = 1.2509 \log_{10} T + 1.343(10^{-3})T + 0.34/(603.4 - T) - 0.0013 \log_{10}(603.4 - T) - 2.3954 \quad (4)$$

Quenched polytetrafluoroethylene (332.5–598.33 °K)

$$H_T - H_0 = 0.54921T + 7.2577(10^{-4})T^2 + 410.8/(608 - T) - 61.89 \quad (5)$$

$$C_p = 0.54921 + 1.45154(10^{-3})T + 410.8/(608 - T)^2 \quad (6)$$

$$S_T - S_0 = 1.2672 \log_{10} T + 1.4515(10^{-3})T + 0.676/(608 - T) - 0.0026 \log_{10}(608 - T) - 2.4663 \quad (7)$$

Liquid polytetrafluoroethylene (598.33–713 °K)

$$H_T \text{ (liquid)} - H_0 \text{ (quenched)} = 0.61488T + 5.97(10^{-4})T^2 - 12.61 \quad (8)$$

$$C_p = 0.61488 + 1.194(10^{-3})T \quad (9)$$

$$S_T \text{ (liquid)} - S_0 \text{ (quenched)} = 1.4158 \log_{10} T + 1.194(10^{-3})T - 2.6576. \quad (10)$$

The constant terms (integration constants) in the above six enthalpy and entropy equations were evaluated in the following way. First, it may be noted that the enthalpy equations fitted to the data only at higher temperatures cannot be expected to fit the 0–50 °C enthalpy increments, since in this temperature interval large heats of transition are involved. On the other hand each of eqs (2) and (5), while derived without use of the observed 50–100 °C enthalpy increment, actually fits this observed increment within its uncertainty, as seen from table 3. In fact it was found that eq (3) gives at 346.5 °K the same heat capacity for the powder as tabulated by Furukawa, McCoskey, and King [7]. Their enthalpy and entropy at this temperature, relative to 0 °K, were adopted, and the constant terms in eqs (2) and (4) were evaluated so as to satisfy these two respective values.

A similar treatment was performed for the "quenched" sample. Here the choice of a comparable state in the work of Furukawa, McCoskey, and King is not so obvious. Compared with the present "quenched" sample, their "annealed" sample was cooled more slowly whereas it seems not unlikely that their "molded" sample may be more comparable to one which has been cooled more rapidly. Because of this consideration and the fact that their values of each property are very close to each other for the annealed and molded samples at the temperatures in question, these values were averaged. Their average heat capacity is identical with that of eq (6) at 332.5 °K, and so the constant terms in eqs (5) and (7) were evaluated to give agreement with their average values for these respective properties at this temperature. (At 332.5 °K their values of $(H_T - H_0)$, C_p, and $(S_T - S_0)$ are higher for the molded than for the annealed sample by only 0.0 J g^{-1}, 0.007 J g^{-1} deg^{-1} (0.7%), and 0.002 J g^{-1} deg^{-1}, respectively.)

It is reasonable to assume that after run 7 of table 2 (when the enthalpy values ceased to drift) the quenched and liquid forms of sample cooled to the same thermodynamic state, and hence the same enthalpy, in the ice calorimeter. The further assumption was made that either the powdered or quenched sample, when heated, undergoes no *isothermal* melting but passes gradually into the liquid state. The equations for the enthalpy of the two forms relative to 0 °C give identical values at 598.33 °K. This temperature was assumed to be the actual melting point (temperature of complete conversion to liquid), and the constant terms in eqs (8) and (10) were so determined that these equations would give the same values at this temperature as eqs (5) and (7), respectively.

It may be noted that in eqs (4), (7), and (10) the entropy is expressed relative to that at 0 °K. Unlike many simple crystalline substances, polytetrafluoroethylene undoubtedly possesses some residual entropy owing to random molecular orientations. Its magnitude is unknown, but it may be small.

Values of heat capacity, relative enthalpy, and relative entropy given by eqs (2)–(10) at even temperatures are listed in tables 4 and 5. Curves of heat capacity calculated from eqs (3), (6), and (9) are compared with the results of earlier investigators in figure 1.

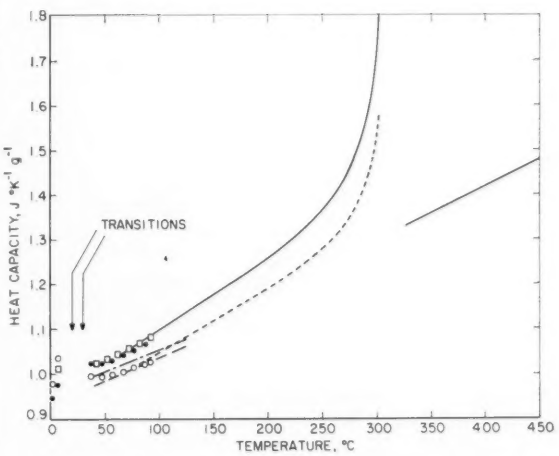

FIGURE 1. *Heat capacity of polytetrafluoroethylene.*

– – – –, powder (this work); ——, quenched and liquid (this work); 0, powder (Furukawa, McCoskey, and King [7]); ●, annealed (Furukawa, McCoskey, and King [7]); □, molded (Furukawa, McCoskey, and King [7]); — — —, powder (Marx and Dole [8]); – – – –, drawn (Marx and Dole [8]).

TABLE 4. *Heat capacity, enthalpy, and entropy of polytetrafluoroethylene powder (calculated from eqs 2–4)*

T	C_p	H_T-H_0 [a]	S_T-S_0 [b]
°K	$J\,°K^{-1}\,g^{-1}$	$J\,g^{-1}$	$J\,°K^{-1}\,g^{-1}$
350	1.016	218.6	1.255
360	1.030	228.8	1.284
370	1.043	239.1	1.312
380	1.057	249.6	1.340
390	1.071	260.3	1.368
400	1.085	271.1	1.395
425	1.120	298.6	1.462
450	1.156	327.1	1.527
475	1.193	356.4	1.591
500	1.234	386.8	1.653
525	1.282	418.2	1.714
550	1.354	451.0	1.775
575	1.573	486.9	1.839

[a] Assuming a value of 215.0 $J\,g^{-1}$ at 346.5 °K [7].
[b] Assuming a value of 1.245 $J\,°K^{-1}\,g^{-1}$ at 346.5 °K [7].

TABLE 5. *Heat capacity, enthalpy, and entropy of quenched and liquid polytetrafluoroethylene (calculated from eqs 5–10)*

T	C_p	H_T-H_0 [a]	S_T-S_0 [b]
°K	$J\,°K^{-1}\,g^{-1}$	$J\,g^{-1}$	$J\,°K^{-1}\,g^{-1}$
340	1.048	210.3	1.231
350	1.063	220.8	1.262
360	1.078	231.6	1.292
370	1.094	242.4	1.322
380	1.109	253.4	1.351
390	1.124	264.6	1.380
400	1.139	275.9	1.409
425	1.178	304.8	1.479
450	1.219	334.8	1.548
475	1.262	365.8	1.615
500	1.310	398.0	1.681
525	1.371	431.4	1.746
550	1.470	466.8	1.812
575	1.761	506.3	1.882
600[c]	1.331	571.2	1.992
625	1.361	604.9	2.047
650	1.391	639.3	2.101
675	1.421	674.4	2.154
700	1.451	710.3	2.206
725	1.480	747.0	2.258

[a] Assuming a value of 202.45 $J\,g^{-1}$ at 332.5 °K [7].
[b] Assuming a value of 1.208 $J\,°K^{-1}\,g^{-1}$ at 332.5 °K [7].
[c] The polytetrafluoroethylene was assumed to be liquid above 598.3 °K.

5. Discussion

The annealing of polytetrafluoroethylene has usually been carried out at temperatures of 350 °C or higher. From table 2 (column 5) it can be seen that the enthalpy values in individual measurements at 340 °C continued to increase steadily with time, by increments each many times the precision ordinarily obtained, during the first four runs at this temperature, and did not become constant until after four runs at 400 °C, when all subsequent values at either temperature were constant within the precision of measurement.

These drifts with time of the apparent relative enthalpy of the liquid might off-hand be attributed mainly to one of three causes: (1) The shorter times in the furnace may have been insufficient to establish thermal equilibrium; (2) the sample may in different measurements have "solidified" to different enthalpy states in the ice calorimeter; or (3) the state of the liquid may have been changing significantly. As to the first possibility, it was estimated from "relaxation-time" tests made at 100° and 150 °C that the sample + container should have had time to acquire its full enthalpy within one joule in 20 min in the furnace at either 340 or 400 °C, accounting for the absorption of the heat of fusion. In each actual measurement the time was always much greater. As to the second possibility, the rates of cooling the sample in the calorimeter were no doubt similar in different measurements, and at any rate probably varied randomly. The authors have carried out drop calorimetry on several materials having known phase diagrams which clearly predict this type of behavior, but invariably the enthalpy values obtained varied randomly with time. These arguments leave only the third possibility, which suggests that, unlike atomic and small-molecule substances, the polymer even after melting does not reach any structural equilibrium rapidly, but at a given temperature slowly absorbs still more energy in a virtual continuation of the fusion process. This is probably not surprising in view of the large number of relative positions the long polymer chains can assume even in a high state of disorder.

In contrast to the large enthalpy drifts observed at 340 and 400 °C, the two enthalpy values obtained on the powdered sample at 300 °C (table 1) show excellent agreement (to 0.03 percent). Although no measurements at lower temperatures were subsequently repeated before the sample began annealing at 340°, there is no evidence that the powdered sample underwent appreciable irreversible annealing at 300°. As pointed out in section 2, the enthalpy values at this temperature are higher by several joules per gram than would be predicted from an extrapolation of the values at and below 200 °C. This effect was treated as a reversible partial fusion.

Returning to table 2, the first enthalpy value obtained at 440 °C is appreciably lower than the last two. (The second value is assumed to involve an accidental error.) Even though the enthalpy had apparently stabilized at 340 and 400°, it is possible that some small further change in the liquid state occurred at 440 °C, a possibility that introduces some uncertainty into the slope of the heat capacity-temperature curve of the liquid. However, from 340 to 440 °C there is no correlation between weight losses and enthalpy changes which suggests such a real change.

Lupton has given an equation of state for liquid polytetrafluoroethylene (cited in reference [1]):

$$(P+a)(V-b)=B(T-c), \tag{11}$$

where $a=400$ atm, $b=0.500$ $cm^3\ g^{-1}$, $c=144$ °C,[6] and $B=0.306$ $cm^3\ atm\ g^{-1}\ deg^{-1}$. At 600 °K table 5 gives for the liquid $C_p=5.30$ $cal\ deg^{-1}\ (g\ atom)^{-1}$. Using this value, the thermodynamic relation

$$C_p-C_v=T(\partial P/\partial T)_v(\partial V/\partial T)_p, \tag{12}$$

[6] c was 156 °C for a sample of very high molecular weight.

and Lupton's equation gives C_v=4.90 cal deg^{-1} (g atom)$^{-1}$, which is 82 percent of the equipartitional value $3R$ corresponding to the limiting high-temperature three-dimensional harmonic oscillation of all the atoms in polytetrafluoroethylene. A single harmonic oscillator which gives a heat capacity at 600 °K that is 82 percent of the equipartitional value has a frequency of 650 cm^{-1}. Actually, the frequency spectrum of polytetrafluoroethylene is known to cover a wide range below and above this frequency [1], and in addition the above value of C_v may include small contributions from structural changes with temperature.

The weight losses observed at 400 and 440 °C in the present work (table 2, column 4) are at rates five to ten times smaller than those found by Madorsky and his coworkers [16, 17]. Siegel, Muus, Lin, and Larsen [18] also have recently reported rates of pyrolysis of polytetrafluoroethylene, and at 380 °C find the rate much smaller in the presence of C_2F_4 gas at a pressure of 35 mm Hg than in vacuum, as well as a weight *gain* when the partial pressure of C_2F_4 was 80 mm. These results suggest some reversibility of the decomposition reaction. Siegel et al. also used available thermodynamic data to calculate pressures of C_2F_4 in equilibrium with the polymer from 327 to 712 °C. Their equilibrium pressure at 380 °C ($\leq$0.1 mm) indicates that there should have been a gain instead of a loss of weight in the experiment at 35 mm, and suggests that either their calculated equilibrium pressures are in error by large factors or else that the volatilization reaction observed to occur at this pressure was predominantly other than that of liquid polytetrafluoroethylene to C_2F_4 gas. While the present authors have no way of knowing what the pressure of C_2F_4 was in contact with their own sample, they estimate that also in this case the pressure of the gas was probably sometimes many times the corresponding listed equilibrium pressure. The substitution of the heat capacities found in the present work for those estimated by Siegel et al. would have very little effect on the calculated equilibrium pressures. One assumption involved in their calculations is that the residual entropy ($S_{0°K}$) of the polytetrafluoroethylene powder measured by Furukawa, McCoskey, and King [7] was zero. If this was not true, the correction would *lower* the calculated equilibrium pressures of C_2F_4.

The one important piece of enthalpy data missing from the present investigation is the heat of fusion of crystalline polytetrafluoroethylene. In drop calorimetry the heat measured is that involved in *cooling* the sample; and it is evident that the powdered sample, once melted, never returned to its original state in the calorimeter. So far as is known, no one has measured the crystalline heat of fusion of this polymer calorimetrically, at least with any real accuracy. This could be done in precise heating types of calorimetry, though these are not often used at such elevated temperatures. The heat of fusion could be obtained also from the heats of combustion in fluorine of a sample that had been fused and one that had not been (together with the use of the appropriate heat-capacity data), but the heat of such a combustion is approximately 200 times the heat of fusion and hence the combustion calorimetry would need to be not only highly precise but also on entirely comparable samples.

As mentioned in section 1, the heat of fusion of polytetrafluoroethylene has been calculated using PVT data and the Clapeyron equation. The published values vary from 35 to 85 J g^{-1}, but the value of Lupton [10], 57.3 J g^{-1}, seems to be considered the best value [18].

In section 4 the simple type of temperature function $D/(E-T)$ (last term of eq (1)) was introduced to represent the accelerated increase of enthalpy with temperature (presumably as a result of partial fusion) of the two solid forms of the polymer. This function is of the form which to a good approximation represents the "premelting" of a great many low-molecular-weight substances contaminated with one or more foreign phases ("impurities") which are insoluble in the solid phase but soluble in the liquid phase of the principal component. Leaving open for the moment the question of how much justification there is in extending this interpretation to the broad melting observed for such a high polymer as polytetrafluoroethylene, it is appropriate to attempt to test empirically the validity of the $D/(E-T)$ enthalpy term, since it should account for the total heat of fusion when T reaches the observed melting point of the polymer, where fusion is complete.

According to the thermodynamic theory of dilute solutions, the heat of fusion L_f is given approximately by

$$L_f = DT_m/E\,(E-T_m), \qquad (13)$$

TABLE 6. *Values of the melting points and heats of fusion of the polytetrafluoroethylene samples calculated from the formulated results (eqs 1, 2, 4, 5, 8, 10, 13) using alternative assumptions*

Sample	Basic assumption	Calculated temperatures		Calc. heat of fusion of sample, L_f
		E	Calc. sample melting point, T_m	
		°C	°C	J g^{-1}
Powdered	Using Lupton's heat of fusion [10]	330.2	326.6	(57.3)
	Enthalpy of powdered and quenched identical at 0 °K		326.7	58
	Entropy of powdered and quenched identical at 0 °K		327.1	65
Quenched	Enthalpy at 0 °C independent of furnace temperature	334.8	325.2	41

where D and E have values as in eq (1), T_m is the actual equilibrium melting (or freezing) point of the material, and E is the corresponding temperature for the completely "pure" substance. Using the thermal results of this paper as formulated by eqs (2)—(10), eq (13) and each of several alternative assumptions described below were used to calculate values for the sample melting point and the heat of fusion, which are recorded in table 6.

The first such calculation was made assuming Lupton's value of the crystalline heat of fusion stated above. Equations (2) and (13) then give T_m= 326.6 °C. An alternative calculation can be made after assuming a definite relation between the enthalpies or entropies of different forms of the polytetrafluoroethylene sample. According to the accurate low-temperature calorimetric data of Furukawa et al. [7], the values of $(H_{310°K}-H_{0°K})$ and $(S_{310°K}-S_{0°K})$ are respectively only 0.4 and 0.2 percent different for the powdered form compared with the annealed and molded forms. If the powdered and quenched forms are assumed to have the same enthalpy at 0 °K, one can equate eqs (2) and (8) and get T_m=326.7 °C, which when substituted into eq (13) gives L_f=58 J g^{-1} (1 percent higher than Lupton's value). Or, if the entropies at 0 °K are assumed equal, one gets from eqs (4), (10), and (13) T_m=327.1 °C and L_f=65 J g^{-1} (the latter being 13 percent higher than Lupton's value). As for the *quenched* polymer, it was assumed (section 4) that its enthalpy when in the ice calorimeter was essentially identical to that of the liquid similarly cooled; this suggests equating eqs (5) and (8), which gives T_m=325.2 °C and (from eq (13)) L_f=41 J g^{-1}, or only some 70 percent of the values for the heat of fusion of the powdered form. Independent results on the polymer indicate that the quenched sample must have been much less crystalline than the powdered one, but the larger heat capacities of the former at lower temperatures may reflect further substantial contributions from the fusion process over a very wide temperature range.

It is striking that the three values in table 6 for the melting point of the powdered polymer are all 327 °C, for this is the generally accepted value based on direct observation but it was nowhere assumed in the above calculations. A simple "premelting"-type enthalpy term, then, appears to provide a satisfactory fit to the available thermodynamic data for crystalline polytetrafluoroethylene. The agreement noted lends weight to the approximate validity of eqs (2) and (5) as empirical extrapolations of the thermal data above 300 °C. Such equations may represent well the total *enthalpy* interval from 300 to 340 °C, the temperatures of the actual measurements, and the uncertainty as to how this enthalpy change is distributed over the 40-deg interval introduces but little uncertainty into the corresponding *entropy* increment (probably less than 0.002 J g^{-1} deg^{-1} in the present case). However, the *heat capacity* undoubtedly increases sharply within the interval and so is highly uncertain at many of these temperatures.

Below the melting point of a macroscopic crystal its free energy is less than that of the corresponding quantity of the pure supercooled liquid. Hence, if some fusion of the sample occurs at such a temperature, additional effects must be present which remove this free-energy inequality. In the ordinary type of premelting discussed above, a "foreign" phase can dissolve in the liquid formed and thereby lower the free energy of the latter. Incidentally, the theory of dilute solutions on which the ordinary treatment of premelting is based does not require that "chemical" impurities be present. A nominally pure substance may behave thermodynamically as a multicomponent system, and undergo broad melting, if two or more molecular forms are present which convert into one another only sluggishly.

On the other hand, in recent years experimental and theoretical evidence has been obtained that substantial amounts of certain high polymers show melting-point depressions because the free energy of certain portions of the solid is "abnormally" enhanced by effects not present in the resulting liquid. The principal such effects are believed to be crystal defects, other high-energy structural features such as chain folds, and especially the presence of platelike crystals so thin that their surface free energies are appreciable compared with their bulk free energies. A recent paper by Hoffman [19] discusses in detail these and other theoretical aspects of polyethylene and polychlorotrifluoroethylene. Such thin platelike crystals are known to be present in polytetrafluoroethylene too. It thus appears that the accelerated upturn in the heat-capacity curves of the solid forms of polytetrafluoroethylene, reported in the present paper and attributed to partial fusion, could be explained as being the result of the melting of thin crystals having a suitable distribution of thicknesses. (It should be noted, however, that each of these heat measurements was repeated with high reproducibility, so that it would be necessary to assume that the thin crystals were reformed in the same or an equivalent distribution upon subsequent cooling and recrystallization.)

It may well be that both ordinary "impurity" premelting (where the impurities affect the free energy of the liquid phase) and surface-free-energy effects (which affect the free energy of the crystalline phase) combine to cause the broad melting effect observed in polytetrafluoroethylene.

The authors are particularly indebted to C. A. Sperati, of E. I. du Pont de Nemours and Company, who carried out several tests on the sample of polytetrafluoroethylene used, and to John D. Hoffman, of the National Bureau of Standards, who reviewed the manuscript and made several helpful criticisms.

6. References

[1] C. A. Sperati and H. W. Starkweather, Jr., Fortschr. Hochpolym.-Forsch. **2,** 465 (1961) (in English).
[2] P. E. Thomas, J. F. Lontz, C. A. Sperati, and J. L. McPherson, J. Soc. Plastics Eng. **12,** 89 (1956).
[3] C. J. Speerschneider and C. H. Li, J. Appl. Phys. **33,** 1871 (1962).
[4] R. K. Eby and K. M. Sinnott, J. Appl. Phys. **32,** 1765 (1961).
[5] W. E. Hanford and R. M. Joyce, J. Am. Chem. Soc. **68,** 2082 (1946).
[6] N. K. J. Symons, J. Polymer Science **51,** S21 (1961).
[7] G. T. Furukawa, R. E. McCoskey, and G. J. King, J. Research NBS **49,** 273 (1952) RP2364.
[8] P. Marx and M. Dole, J. Am. Chem. Soc. **77,** 4771 (1955).
[9] P. L. McGeer and H. C. Duus, J. Chem. Phys. **20,** 1813 (1952).
[10] J. M. Lupton, 134th meeting of the Amer. Chem. Soc., Chicago, Ill., Sept. 1958. (See references [1], [11], and [18].)
[11] H. W. Starkweather, Jr., and R. H. Boyd, J. Phys. Chem. **64,** 410 (1960).
[12] W. Brandt, J. Chem. Phys. **26,** 262 (1957).
[13] Yu. Ya. Gotlib and I. V. Sochava, Dokl. Akad. Nauk SSSR **147,** 580 (1962).
[14] G. T. Furukawa, T. B. Douglas, R. E. McCoskey, and D. C. Ginnings, J. Research NBS **57,** 67 (1956) RP2694.
[15] D. C. Ginnings and R. J. Corruccini, J. Research NBS **38,** 593 (1947) RP1797.
[16] S. L. Madorsky, V. E. Hart, S. Strauss, and V. A. Sedlak, J. Res. NBS **51,** 327 (1953) RP2461.
[17] S. L. Madorsky and S. Strauss, J. Res. NBS **64A,** 513 (1960).
[18] J. C. Siegel, L. T. Muus, T. P. Lin, and H. A. Larsen, J. Polymer Science **2A,** 391 (1964).
[19] J. D. Hoffman, Trans. Soc. Plastic Eng. **4,** 315 (1964).

(Paper 69A2–336)

JOURNAL OF RESEARCH of the National Bureau of Standards—A. Physics and Chemistry
Vol. 69A, No. 2, March–April 1965

Anionic Polymerization of Isoprene at Low Concentrations of Polyisoprenyllithium

Lewis J. Fetters*

(December 13, 1964)

The kinetics of polymerization of isoprene with *n*-butyllithium initiator was investigated in *n*-hexane solution over an extended concentration range of poly-organolithium. The propagation reaction was found to be first-order with regard to monomer and half-order with respect to chain anion concentration. The degree of chain anion aggregation, in the association equilibrium between active single chains and inactive associated chains, was concurrently scrutinized. The evidence accrued from the studies indicates that the associated chains exist only as binary aggregates. These experimental findings are in concert with those results obtained at higher concentrations of polyorganolithium.

1. Introduction

The mechanism of anionic polymerization has received some elucidation from recent studies [1–31][1] of polymerization in homogeneous solution initiated by soluble organolithium compounds. The polymerization of such monomers as styrene in benzene and isoprene or butadiene in *n*-hexane or cyclohexane show a general absence of any termination or transfer reactions [5, 22–28, 31]. In other words, the growing chain anions retain their reactivity indefinitely. Furthermore, each initiating organolithium molecule generates one polymer chain [5, 11, 18, 22, 23].

Such homogeneous systems, therefore, have the special feature of leading to a very narrow molecular weight distribution (Poisson distribution), since all growing chains have equal probability of growth [32]. This is true only where the initiation step is not slow in comparison with the propagation reaction; otherwise a broadening of the distribution will occur. The slow occurrence of any irreversible termination during the course of the polymerization will also cause a considerable broadening of the molecular weight distribution [33–35]. This termination can result from a bimolecular reaction between an active chain-end and some monofunctional terminating impurity in the system, or from spontaneous unimolecular reactions such as a slow pseudo first-order reaction with solvent [23]. From the kinetics of the homo-polymerizations of butadiene and isoprene in benzene and concurrent molecular-weight studies [36], evidence has accrued that indicates the existence of facile transfer and termination steps. The exact nature of these reactions has not yet been elucidated fully.

It has been found that, in general, the polymer-lithium species in hydrocarbon solvents are associated in pairs [11, 15, 24, 27, 28]. This strong electrostatic association of chain anions is absent in ethers. As a result of these studies, it is possible to relate the kinetics of the systems with the nature of the polymerizing chain anions. Thus, in hydrocarbon media, the following equations best describe the chain growth mechanism:

$$(RM_jLi)_2 \overset{K_1}{\rightleftarrows} 2RM_jLi \tag{1}$$

$$RM_jLi + M \overset{k_p}{\rightarrow} RM_{j+1}Li \tag{2}$$

where RM_jLi denotes a polymer-lithium chain; and k_p is the velocity constant for the propagation reaction. Hence the rate controlling step for the propagation reaction is the dissociation of the chain pairs.

If the equilibrium constant, K_1, is small, then the observed rate of polymerization should be proportional to the half-power of the total chain anion concentration, both associated and dissociated. In other words the propagation reaction would show a nonintegral dependence upon the polymer-lithium concentration. This has been found to be the case [5,13,25,28]. Hence, the rate of polymerization can be given by the following:

$$\frac{d[M]}{dt} = k_p[RM_jLi][M] = k_pK_1^{1/2}[(RM_jLi)_2]^{1/2}[M] \tag{3}$$

This half-order dependence upon polymer-lithium concentration changes to first-order in ether solvents [25]. A notable exception to this trend is found in the polymerization of isoprene in *p*-dioxane by lithium catalysis. A half-order dependence of rate upon organolithium concentration is observed even though no polymer-lithium self-association has been found to exist. The kinetic behavior of this polymerization has been tentatively ascribed to solvation effects by the ether [37].

It should be pointed out that (3) is valid only when *the initiation reaction is complete*. Hence, it is imperative that the initiation reaction be completed prior to any investigation of the propagation step. From a kinetics standpoint, considerable complications can arise when the initiation and propagation reactions remain intertwined [5, 11, 19, 28, 38, 39, 40].

*National Academy of Sciences-National Research Council Postdoctoral Resident Research Associate.

[1] Figures in brackets indicate the literature references at the end of this paper.

These difficulties can be circumvented by pre-initiating [5, 22, 23, 25, 28] the polymerization with a small amount of monomer at a high temperature, e.g., 50 °C.

The lack of celerity in the initiation step is due, in part, to the ability of the initiating organolithium, e.g., ethyl- or *n*-butyllithium, to form associated species with polymer-lithium as well as with itself [11, 28, 41, 42]. Thus, the existence of these association, dissociation, and exchange equilibria of the organometallic species that are responsible for both initiation and propagation is of great importance. The polymer-lithium self-association is exemplified by equation (1). The self- and cross-associations involving the initiating organolithium and the polymer-lithium species are shown by the equilibria (4) and (5) as follows:

$$(RLi)_6 \overset{K_2}{\rightleftharpoons} (RLi)_{6-n} + nRLi \qquad (4)$$

$$(RM_jLi)_2 + (RLi)_6 \overset{K_3}{\rightleftharpoons} 2[RM_jLi \cdot xRLi] + (RLi)_{6-2x} \qquad (5)$$

where RLi denotes the initiating organolithium. The exact values of n and x are currently uncertain. However, kinetic data implies that the unassociated form of the initiating organolithium is the active species responsible for chain initiation [5, 19, 42] and that the above equilibria (1), (4), and (5) lie well over on the associated side over a wide concentration range.

Ethyl- and *n*-butyllithium are generally believed to be hexameric in hydrocarbon media [42], although some evidence points to lower degrees of association in some solvents [31, 43]. Iso-, secondary-, and tertiary-butyllithium can give faster rates of initiation than *n*-butyllithium [13]. This is apparently due to the different reactivities of the lithium-carbon bond and to lower degrees of association exhibited by these isomers of butyllithium [44].

In any case, it is necessary to complete the initiation step prior to the study of the propagation reaction in order to obviate the difficulties arising from the complex dimerization and mixed association equilibria. It might be added that in ether solvents, the initiation process is, for all practical purposes, instantaneous [18, 22–24, 26].

Using viscometric techniques [24, 27], it is possible to determine the concentrations of the species RM_jLi that are responsible for the propagation reaction. Hence, the calculation of the absolute value of the propagation rate constants is possible. For isoprene, in *n*-hexane, this was found [27] to be given by the expression:

$$k_p = 3.4 \times 10^3 \exp(-4100/RT) = 8.9\ LM^{-1}\text{sec}^{-1} \qquad (6)$$

at 60 °C. This compares with the expression found for styrene in benzene at the same temperature [26]:

$$k_p = 1.1 \times 10^4 \exp(-3800/RT) = 34\ LM^{-1}\text{sec}^{-1} \qquad (7)$$

The equilibrium constant, K_1, for the dissociation of the associated polyisoprenyl-lithium pairs, at 30 °C and over a concentration range of 10^{-2} to 10^{-3} moles l^{-1} is of the order of 5×10^{-7} [27]. The heat of dissociation of these associated pairs is about 37 kcals[3] $mole^{-1}$. The surprisingly high activation energy (22.6 kcals $mole^{-1}$ [25]) found for the propagation reaction includes, of course, one-half the heat of dissociation of the associated polyisoprenyl-lithium pairs.

In this same publication [27], several values of K_1 are recorded that are two orders of magnitude larger than the values reported above. These remarkably self-consistent values were obtained over a polyisoprenyl-lithium concentration range of 10^{-4} to 10^{-5} moles l^{-1}. These latter results were tentatively explained on the basis that fortuitous termination occurred, since such deleterious reactions are extremely difficult to avoid at these low concentrations. This, of course, could give rise to an apparent high value of K_1. On the other hand, these results could also be explained by assuming that the degree of chain-end association is appreciably concentration dependent within this polymer-lithium concentration range. Thus, a reexamination of the degree of polyisoprenyl-lithium self-association at very low polymer-lithium concentrations was undertaken in an attempt to resolve this question. Concurrently, kinetic measurements were also carried out. The results of this investigation are reported in this paper.

2. Experimental Methods

A detailed discussion of techniques and experimental procedures is available elsewhere [22, 23, 25, 27]. Experimental manipulations were accomplished with the aid of a high-vacuum apparatus at pressures of 10^{-5} to 10^{-6} mm Hg to ensure the absence of water, oxygen, and other impurities to which organolithium compounds are sensitive.

All monomer and solvent purifications, initiator preparations, and polymerization reactions were carried out either directly on the vacuum line, or in sealed evacuated vessels. All reaction vessels and flasks were constructed of Pyrex glass and were thoroughly flamed under high vacuum to remove adsorbed impurities. Evacuation time was 16 to 24 hr duration.

Isoprene (99 mole %) was purified by successive distillations into flasks coated with freshly sublimed sodium.

n-Hexane was purified by standing over concentrated sulfuric acid for a minimum of two weeks, distilling onto potassium/sodium amalgam, and finally distilling into a flask coated with freshly sublimed sodium.

The purity of the solvent was confirmed by running ultraviolet absorption spectrograms on the purified product. The tests indicated the absence of benzene and other impurities detectable by U. V. analysis.

[3] One kcal equals 4.184×10^3 J.

As a final precaution, both monomer and solvent were distilled from butyllithium into the reactor immediately prior to use.

Reaction rates were measured by standard dilatometric techniques. Starkweather and Taylor [45] have shown that the contraction of a polymerizing system is directly proportional to degree of conversion. Treloar has noted [46] that this finding may not necessarily apply to all systems. There is, however, no indication that Starkweather and Taylor's conclusions do not apply to the systems studied in this work. Pre-initiated polyisoprenyllithium was used to actuate the polymerizations with *n*-butyllithium used as the initiating organolithium.

By means of a specially constructed capillary flow viscometer [27], the flow times of the polymer solutions could be measured in vacuo at the conclusion of the polymerization, both before and after termination of the active chains. Termination was effected by the addition of a minute amount of methanol.

The magnitude of the viscosity change allows a calculation of the number of chains associated by means of the well-known equation for bulk viscosity [47, 48] (or concentrated solution viscosity at fixed concentration) in the "entanglement region", i.e.,

$$\eta = K(gM)^{3.4} \tag{8}$$

where η = bulk or concentrated solution viscosity
M = molecular weight
K = constant for a given polymer system
g = unity for linear chains, and less than unity for branched chains.

The value of "M," when measured for the active chain anions, will, of course, depend on the number of such chains associated. Since the latter number has not been found, so far, to exceed two, then the two chains thus associated at their active ends may be considered as linear, and "g" can be taken as unity.

Equation (8) is altered as follows for the calculation of the "association number", N:

$$\frac{\eta_a}{\eta_t} \text{ or } \frac{t_a}{t_t} = N^{3.4} \tag{9}$$

where t_a and t_t refer to the flow times of the active and terminated solutions, respectively.

It should be mentioned that care was taken to work with polymer solutions of sufficiently high concentrations where eq (8) would apply, i.e., where

$$v_2 M > 2M_e. \tag{10}$$

Here, v_2 denotes the volume fraction of polymer in solution, M the polymer molecular weight, and M_e the molecular weight of a polymer segment between the loci of entanglement. The validity of equation (8) at these concentrations has been demonstrated elsewhere [27, 49]. The value of M_e was taken as 7,000 [49].

The distribution of molecular weights of the linear molecules, which make up the composite, associated species, will influence the molecular weight distribution of the composite polymer chains. Therefore, since the flow behavior of these concentrated solutions is representative of the weight-average molecular weights, while in reality the number-averages are required, it is imperative to form macromolecules that closely approach the ideal monodisperse distribution in order to obtain a quantitative measure of the degree of ion-pair aggregation. Fortunately, as was previously noted, this polymerization system can lead to a very narrow distribution of chain-lengths, characterized by having a very low ratio of weight-average to number-average molecular weights, viz, $\overline{M}_w/\overline{M}_n \leqslant 1.15$ [23, 50–52]. Thus, care was continuously exercised to insure the rapid completion of the initiation step prior to the occurrence of the bulk of the propagation reaction. This technique is identical to the "two-stage" polymerization process of Wenger [53].

3. Results and Discussion

3.1. Polymer Association Phenomena

Table 1 contains the viscosity data, the resulting values of the association number, N, and the equilibrium constant, K_1. From the value of N the concentration of the dissociated polymer-lithium can be calculated readily. This method of computation is as follows:

Let $[RM_jLi]$ = concentration of dissociated polymer species;

$[(RM_jLi)_2]$ = concentration of associated polymer species; and

$[RM_jLi]_0$ = total concentration of all polymer species.

Hence, we have:

$$[RM_jLi]_0 = [RM_jLi] + 2[(RM_jLi)_2] \tag{11}$$

We may then let:

$$X = [(RM_jLi)_2]/[RM_jLi]$$

Thus:

$$X = (N-1)/2(2-N) \tag{12}$$

TABLE 1. *The association of polyisoprenyl-lithium in solution at 30 °C*

$[RM_iLi]_0$	Flow times (sec)		$[M]_0$	$v_2^{(1)}$	$N^{(2)}$	K_1x10^7
moles l^{-1}x10^4	active	terminated	moles $^{-1}$	x10^2		moles l^{-1}
2.10	1207	123.4	0.9	7.9	1.95	11.1
1.95	1745	175.1	.9	7.9	1.96	6.5
0.80	1291	134.0	.5	4.4	1.95	4.2
0.40	1554	172.8	.2	2.1	1.90	8.9

[1] v_2 was computed from the weight percent of polymer in solution.
[2] $N = M$ active/M terminated.

From the above relations, it is then possible to compute:

$$[RM_jLi]=[RM_jLi]_0/(2X+1) \quad (13)$$

$$[(RM_jLi)_2]=\{[RM_jLi]_0-[RM_jLi]\}/2. \quad (14)$$

In this fashion it is possible to calculate the equilibrium concentrations of both the associated species and the dissociated (active) species and hence the equilibrium constant, K_1.

$$K_1=[RM_jLi]^2/[(RM_jLi)_2].$$

As can be seen, the results reported in table 1 are consistent with those reported elsewhere [27] for the higher concentrations of $[RM_jLi]_0$. It therefore appears that the tentative reason presented previously to explain the high K_1 values was a correct one. Hence, it can be concluded that the active ion-pairs form aggregates made up of two macromolecules over a lithium concentration range of 10^{-2} to 10^{-5} moles l^{-1}.

In addition to measurements of the flow behavior of concentrated polymer-lithium solutions, dilute solution viscosity studies [28] and light scattering measurements [54] indicate that, in general, the polymer-lithium species are indeed associated in pairs in hydrocarbon media.

For a discussion of the type of bonding, i.e., multicenter electron-deficient bonds, believed to be responsible for the cluster formation of these organolithium species, the work of Coates [55] is suggested.

3.2. Polymerization Rate Measurements

The apparent near constancy of K_1 over the polyisoprenyl-lithium concentration range investigated indicates that the kinetics of the polymerization should likewise be self-consistent. The elucidation of this point shows this to be a valid assumption.

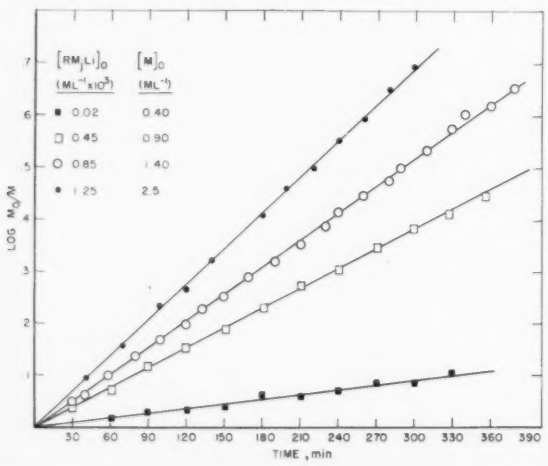

FIGURE 1. *First-order plots for isoprene in* n-*hexane (30 °C).*

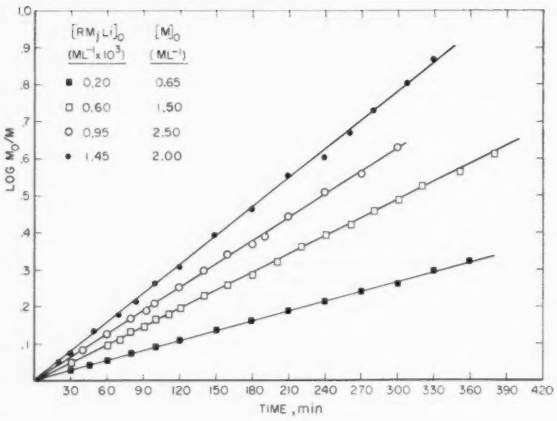

FIGURE 2. *First-order plots for isoprene in* n-*hexane (30) °C*

The dilatometric data are shown as first-order plots in figures 1 and 2, where M_0 refers to initial monomer concentration and M represents the concentration of monomer at any given time. It is apparent that this system shows good adherence to first-order kinetics with respect to monomer. No fall-off (or increase) in the first-order rates was detectable. These results are, of course, to be expected since the number of growing chains remains constant while the depletion of monomer is occurring. These data are recorded in table 2.

TABLE 2. *First-order propagation rate constants* (k_1) *(30° C)*

$[RM_jLi]_0$ moles $l^{-1}\times10^3$	[Monomer] moles l^{-1}	k_1 $min^{-1}\times10^3$
0.02	0.40	0.70
.20	.65	2.00
.45	.90	2.95
.60	1.50	3.75
.85	1.40	4.00
.95	2.5	4.80
1.25	2.5	5.30
1.45	2.0	6.00

As can be seen from figure 3, the apparent rates of propagation exhibit a half-order dependency on chain anion concentration. The introduction of the constant 0.707 is brought about in the following fashion. From eq (11) we have :

$$[RM_jLi]_0-[RM_jLi]-2[(RM_jLi)_2]=0. \quad (11')$$

Substitution in the equation for the associated species gives:

$$[RM_jLi]_0-[RM_jLi]-2K_1^{-1}[RM_jLi]^2=0. \quad (11')$$

Solving for $[RM_jLi]$ by use of the quadratic formula gives:

$$[RM_jLi]=\frac{-1\pm\sqrt{1+8K_1^{-1}[RM_jLi]_0}}{4K_1^{-1}}.$$

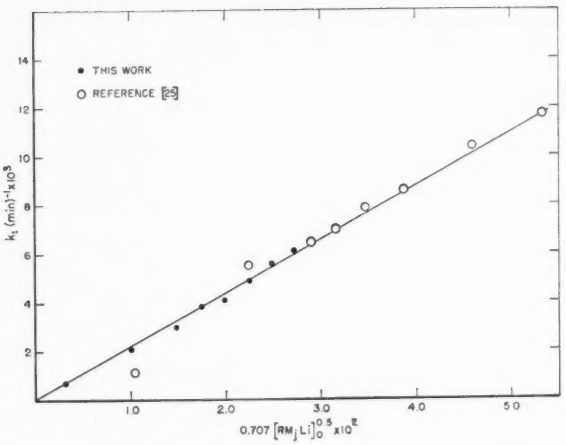

FIGURE 3. *Dependence of isoprene rate on isoprenyl-lithium concentration.*

Now since $K_i^{-1} >> 1$ one has:

$$[RM_jLi] = \sqrt{0.5K_i[RM_jLi]_0}.$$

Thus, by substitution in eq (3), we have:

$$\frac{-d[M]}{dt} = 0.707k_pK_i^{1/2}[RM_jLi]_0^{1/2}[M]. \qquad (3')$$

Hence, the slope in figure 3 is equivalent to $k_pK_i^{1/2}$ which, in this case, is equal to 0.21 liters$^{1/2}$ moles$^{-1/2}$ min^{-1}. No significant differences could be detected in the behavior of the propagation reaction over the polymer-lithium concentration range investigated in this work and that reported by Morton et al. [25]. These later results were corrected to 30 °C by utilizing the apparent energy of activation for the propagation reaction recorded elsewhere [25]. Thus, the kinetic data concur with the data pertaining to the degree of chain anion association over the same concentration range. Kuntz [13] has reported results that are in good accord with those presented herein.

At some variance with the results reported herein are the data of, among others, Spirin [16] and Sinn [30a, b, d, g]: both of whom studied the overall polymerization reaction. Spirin reported a rather complex dependency of the propagation rate of isoprene polymerization on the total concentration of organically-bonded lithium with heptane and toluene used as solvents. The proposed polymerization scheme assumes that the degree of ion-pair aggregation is concentration dependent. At low initiator concentrations (10^{-5} moles l^{-1}) the value assigned to the degree of chain-end association is two, while a value of six is applied to solutions with higher concentrations (10^{-2} moles l^{-1}) organolithium. Hence, such a solution would presumably consist of a mixture of linear (N=2) and star shaped (N=3 to 6) composite macromolecules. However, as Bueche has pointed out [48, 56], the existence of these star shaped macromolecules would be readily detectable since their presence would markedly influence the flow behavior of their concentrated, as well as dilute [56, 57], solutions. So far there has been no indication from physical measurements that any of these composite polymer chains, viz, polyisoprenyl-, polybutadienyl-, or polystyryl-lithium, possess degrees of association greater than two.

From an analysis of the experimental particulars of Spirin's work, it can be surmised that the results at high concentrations of organolithium were vitiated by incomplete initiation. It has been adumbrated [30 b], as well as conclusively demonstrated [28, 31], that the presence or residual initiating organolithium can serve to *depress* the polymerization rate in comparison to the rate of reaction obtained at an equivalent concentration of $[RM_jLi]_0$ when no initiating organolithium is present. In contradistinction to this effect is the behavior encountered when fluorenyllithium is added to an isoprene polymerization. The presence of this non-initiating organolithium effects a slight acceleration in the polymerization rate [15, 41].

This apparent alteration in the concentration of the active (dissociated) polymer-lithium species must be due to the cross-association existing within these systems. Thus, the concentration of the propagating polymer-lithium chains will be dependent upon the concentrations of the two organolithiums and on the respective equilibrium constants of the various and divers reactions, viz, eqs (1), (4), and (5). The concentration of the dissociated initiating organolithium would likewise be influenced in a similar fashion.

The existence of an equilibrium of the type shown in equation (5) is demonstrated by the decrease in the viscosity of polymer-lithium solutions on the addition of nonpolymeric organolithiums [28, 36, 41]. The polyisoprenyl- and polystyryl-lithium self-associated species are disrupted, albeit somewhat reluctantly, by organolithium compounds such as fluorenyl-, ethyl-, and *n*-butyllithium. The ability of these organolithiums to disrupt polyisoprenyl-lithium dimers changes in the following order: fluorenyl-$>>$, ethyl-$\geq$, *n*-butyllithium. A given amount of one of these organolithiums will disrupt the dimers of polystyryl-lithium with somewhat greater facility than those of polyisoprenyl-lithium. These data have been recorded, in part, elsewhere [11, 15]. The existence of these cross-associated species was initially forecast by Korotkov [2] and Tobolsky [4]. As might be expected dissimilar polymer-lithium species also form cross-associated composite macromolecules [36]. This behavior has its parallel in the formation of the cross-associated complexes resulting from the confluence of ethyl- and *t*-butyllithium [58].

At present it should not be assumed that the cross-associated aggregates, containing the polymeric and nonpolymeric organolithiums, consist of only one unique structure since various intermediates may also participate in the overall equilibrium. The same situation may also apply to the initiating

organolithium. Szwarc and Smid [59] have also called attention to this point.

It is perhaps pertinent to note that some evidence has accrued that indicates that the cross-associated species are made up exclusively of one polymer-lithium chain and one initiating organolithium molecule [28, 36, 41]. These complementary results [28, 36, 41] are based on the assumption that the initiating organolithium is completely dissociated at polymerization concentrations. Since this assumption contradicts the information concerning the apparent high degrees of association [31, 42, 60] exhibited by these initiating organolithiums at somewhat higher concentrations, a decision as to whether this relatively simple, and thus attractive, picture of a 1/1 ratio of components in the cross-associated composite species is a correct interpretation, must currently be left in abeyance.

In addition, it has been shown that chain initiation can yet be occurring during the period of the observed maximum in the polymerization reaction. This phenomenon has been observed in the polymerization of isoprene in hexane or cyclohexane [31] and for styrene in benzene [5, 19, 61]. Under certain conditions the polymerization can reach completion prior to the cessation of the initiation reaction [28, 31, 40]. This will be particularly true when the ratio of monomer to catalyst is low and the ratio of the apparent rates of propagation to initiation is high [40, 62]. Thus it must be emphasized that the attainment of a period of maximum rate in the polymerization reaction is not necessarily correlated with the completion of the initiation step. It is therefore apparent that the prime prerequisite for the attainment of meaningful kinetic data pertaining to the propagation process is the complete conversion of the initiating organolithium, e.g., ethyl- or *n*-butyllithium, to polymer-lithium. In this way it is possible to disentangle the individual steps of the overall process.

Sinn [30 a, b, g] has reported results similar to Spirin's for isoprene polymerization in heptane. The "overall rate" was found to be proportional to $[RLi]_0^{1/n}$ with n equal to 3 at low concentrations and equal to 6 at high catalyst levels and $[RLi]_0$ denoting the total concentration of organically bonded lithium. The range in concentration of $[RLi]_0$ was from 10^{-2} to 10^{-5} molar. Apparently the term "overall rate" was meant to signify the combined rates of both the initiation and propagation reactions. In order to account for these low orders of reaction, it has been proposed that the associated polyisoprenyl-lithium chain anoins exist as preponderantly trimeric and hexameric cruciform macromolecules [38].

At catalyst levels greater than 10^{-2} molar, Sinn has observed a virtual independence of polymerization rate with respect to organolithium concentration. Identical behavior has been reported by other workers for isoprene [2, 63] and styrene [61, 64] polymerizations in hydrocarbon media. Taylor [31] has unequivocally shown that this effect is due to the presence of residual initiating organolithium. The data of Kuntz [13] also lend credence to this interpretation.

Sinn has also studied [30d] the *n*-butyllithium initiated polymerization of isoprene, at 20 °C, at extreme dilutions of initiator, i.e., from 10^{-4} to 5×10^{-7} moles l^{-1}. A log-log plot of the "initial rate" versus $[RLi]_0$ results in a convex curve with the slope of its tangent equal to one at approximately 10^{-5} moles l^{-1} of $[RLi]_0$. At higher catalyst concentrations the value of the slope rapidly decreases whereas at concentrations less than 10^{-5} moles l^{-1} the slope increases, eventually becoming somewhat greater than two. Hence Sinn concludes that in this low catalyst range the order of the reaction exceeds two. To explain this phenomenon he has postulated that the propagation reaction involves an "activated" molecule formed by an association of a monomer unit with a dissociated chain anion. This species then reacts in turn with a pair of associated chain-ends to form a trimeric associate with the activated monomer then being incorporated into the chain with which it was originally associated. He therefore concludes that the rate determining step is the formation of the trimeric associate. This supposedly takes place only when the concentration of $[RM_jLi]\geqslant[(RM_jLi)_2]$. Utilizing the values of K_1 reported here and elsewhere [27] the condition of $[RM_jLi]\geqslant[(RM_jLi)_2]$ is meet, at 20 °C, when the concentration of $[RM_jLi]_0\leqslant10^{-6}$ moles l^{-1}.

It is possible that the high order of reaction observed at the extreme attenuations of added *n*-butyllithium may be an artifact. At these low concentrations a small amount of termination would lower the concentration of organically-bonded lithium. This would result in the appearance of anomalously slow rates of polymerization when compared to the rates of reaction obtained at higher catalyst concentrations. On the other hand, it is readily discernible that at successively greater dilutions of polymer-lithium the concentration of dissociated (active) macromolecular lithium will constitute an increasingly greater percentage of the total chain-anion concentration. Hence the dependency of the rate of polymerization on $[RM_jLi]_0$ will gradually approach first-order.

In order to reconcile the diverse kinetic results obtained at the various concentrations of *n*-butyllithium employed, Sinn et al. [38], developed a rather elaborate mathematical treatment. The frequency factor for propagation is found to have the somewhat bizarre value of $10^{14.2}$, and this is rationalized in terms of an entropy of solvation. This value of the temperature-independent factor A is markedly greater than that reported in eq (6).

Despite the explosive developments which have characterized the field of organolithium polymerization in the last decade, the elucidation of many features pertinent to the initiation and chain growth reaction is currently incomplete. In order to study the overall polymerization process in hydrocarbon media, it is necessary to be cognizant of such details as, for example, the value of the rate constant for the initiation reaction, the kinetic order of the initiation with reference to each reactant, the activation energy of the initiation, the nature of any

solvent effects, the effects of impurities resulting from the accidental destruction of the initiating organolithium, the association state of the organolithium species involved, and the nature of any cross-association between the various organolithiums in solution. Although these reactions occur in homogeneous medium, little is known about the actual nature of the dissociated "anionic" organolithium entities. Unlike the free radical systems, where the growing chain has been unequivocally identified as a free radical, the precise character of these organolitlium entities has yet to be fully elucidated. As a consequence, the question as to why lithium catalysis results in predominately cis-1,4 polyisoprene in hydrocarbon media [1] is not yet completely answered. The nature of the bonding responsible for the cluster formation of organolithiums is currently somewhat obscure. Further work is obviously necessary before truly adequate comment can be made concerning the field of organolithium polymerizations.

NOTE ADDED IN PROOF.—A study of the *n*-butyllithium initiated polymerization of isoprene in cyclohexane has appeared [65]. The order of the propagation reaction in organolithium was found to be one-quarter. This was correlated with a degree of association of four as ascertained by light scattering measurements. In contrast to these results are the findings of Francois [28] and Taylor [31]. Both groups reported an order of one-half in isoprenyllithium for the isolated propagation reaction when run in cyclohexane and degrees of chain end association close to two from viscosity measurements. Hsieh [66] reported an order for the propagation reaction in organolithium of one-half for $[RM_iLi]_0 > 10^{-2}$ molar and one-third when $[RM_iLi]_0$ was 10^{-4} to 10^{-2} molar. No attempt was made to ascertain the degree of carbanion association. Use [36] of 1,1-diphenyl-*n*-hexyllithium as an initiator indicates an order of one-half for the propagation reaction in cyclohexane with respect to isoprenyllithium.

4. References

[1] R. S. Stearns and L. E. Forman, J. Polymer Sci. **41,** 381 (1959).
[2] A. A. Korotkov, N. N. Chesnokova, and L. B. Truchmanova, Vysokomol. Soedin. **1,** 46 (1959); Rubber Chem. and Tech. **33,** 610 (1960).
[3] Yu. L. Spirin, A. R. Gantmakher, and S. S. Medvedev, Vysokomol. Soedin. **1,** 1258 (1959).
[4] K. F. O'Driscoll and A. V. Tobolsky, J. Polymer Sci. **35,** 259 (1959).
[5] D. J. Worsfold and S. Bywater, Can. J. Chem. **38,** 1891 (1960).
[6] Yu. L. Spirin, D. K. Polyakov, A. R. Gantmakher, and S. S. Medvedev, Vysokomol. Soedin. **2,** 1082 (1960).
[7] K. Kuwata, Bull. Chem. Soc. (Japan) **33,** 1091 (1960).
[8] R. C. P. Cubbon and D. Margerison, Proc. Chem. Soc. (London), 146 (1960).
[9] D. J. Worsfold and S. Bywater, J. Chem. Soc., 5234 (1960).
[10] E. N. Kopacheva, A. Dolgoplosk, and E. M. Kuznetsova, Doklady Akad. Nauk S.S.S.R. **130,** 1253 (1960).
[11] M. Morton, E. E. Bostick, and R. A. Livigni, Rubber and Plastics Age **42,** 397 (1961).
[12] J. Minoux, B. Francois, and C. Sadron, Makromol. Chem. **44,** 519 (1961).
[13] I. Kuntz, Polymer Preprints **2,** [2], 68 (1961); J. Polymer Sci. **2A,** 2827 (1964).
[14] C. E. Rogers, Polymer Preprints **2,** [2], 75 (1961).
[15] M. Morton, N. Calderon, L. J. Fetters, and J. F. Meier, Polymer Preprints **2,** [2], 310 (1961).
[16] Yu. L. Spirin, A. R. Gantmakher, and S. S. Medvedev, Doklady Akad. Nauk S.S.S.R. **146,** 368 (1962).
[17] Yu. L. Spirin, A. A. Arest-Yakubovich, D. K. Polyakov, A. R. Gantmakher, and S. S. Medvedev, J. Polymer Sci. **58,** 1181 (1962).
[18] S. Bywater and D. J. Worsfold, Can. J. Chem. **40,** 1564 (1962).
[19] R. C. P. Cubbon and D. Margerison, Proc. Roy. Soc. **268A,** 260 (1962).
[20] G. C. East, P. F. Lynch, and D. Margerison, Polymer **4,** 139 (1963).
[21] J. Minoux, Makromol. Chem. **61,** 22 (1963).
[22] M. Morton, A. A. Rembaum, and J. L. Hall, J. Polymer Sci. **1A,** 461 (1963).
[23] M. Morton, E. E. Bostick, and R. G. Clarke, J. Polymer Sci. **1A,** 475 (1963).
[24] M. Morton, L. J. Fetters, and E. E. Bostick, J. Polymer Sci., Part C, [1], 311 (1963).
[25] M. Morton, E. E. Bostick, R. A. Livigni, and L. J. Fetters, J. Polymer Sci. **1A,** 1735 (1963).
[26] M. Morton, L. J. Fetters, and J. F. Meier, 145th Am. Chem. Soc. Meeting, New York, September 1963.
[27] M. Morton and L. J. Fetters, J. Polymer Sci. **2A,** 3311 (1964).
[28] B. Francois, V. Sinn, and J. Parrod, J. Polymer Sci. Part C, [4], 375 (1964).
[29] S. S. Medvedev and A. R. Gantmakher, J. Polymer Sci. Part C, [4], 173 (1964).
[30] a. C. Lundborg and H. Sinn, Makromol. Chem. **41,** 242 (1960); b. H. Sinn and C. Lundborg, ibid. **47,** 86 (1961); c. H. Sinn and O. T. Onsager, ibid. **52,** 246 (1962); d. H. Sinn and O. T. Onsager, ibid. **55,** 167 (1962); e. H. Sinn and W. Hofmann, ibid. **56,** 234 (1962); f. H. Sinn and F. Bandermann, ibid. **62,** 134 (1963); and g. H. Sinn and F. Patat, Angew. Chem. **75,** 805 (1963).
[31] G. L. Taylor, Ph. D. Dissertation, University of Akron, 1964.
[32] P. J. Flory, Principles of polymer chemistry, p. 338 (Cornell University Press, Ithaca, New York, 1953).
[33] B. D. Coleman, F. Gornick, and G. Weiss, J. Chem. Phys. **39,** 3233 (1963).
[34] T. A. Orofino and F. Wenger, J. Chem. Phys. **35,** 532 (1961).
[35] M. Szware and M. Litt, J. Phys. Chem. **62,** 568 (1958).
[36] L. J. Fetters (unpublished results).
[37] J. F. Kenney, Ph. D. Dissertation, University of Akron, 1964.
[38] H. Sinn, C. Lundborg, and O. T. Onsager, Makromol. Chem. **70,** 222 (1964).
[39] L. Reich and S. Stivala, Makromol. Chem. **53,** 173 (1962).
[40] E. Bauer and M. Magat, J. Chim. Phys. **47,** 841 (1950).
[41] L. J. Fetters, Ph. D. Dissertation, University of Akron, 1962.
[42] D. Margerison and J. P. Newport, Trans. Faraday Soc. **59,** 2058 (1963) and references included therein.
[43] R. Piotrovski and M. Ronina, Doklady Akad. Nauk. S.S.S.R. **115,** 737 (1957).
[44] M. Weiner, G. Vogel, and R. West, Inorganic Chem. **1,** 654 (1962).
[45] H. Starkweather and G. B. Taylor, J. Am. Chem. Soc. **52,** 4708 (1930).
[46] F. E. Treloar, Polymer **1,** 513 (1960).
[47] T. G Fox, B. S. Gratch, and S. Loshaek, Rheology, Vol. 1, ed. F. Eirich, chap. 12, p. 443 (Academic Press, Inc., New York, 1956).
[48] F. Bueche, J. Chem. Phys. **40,** 484 (1964); J. Polymer Sci. **41,** 551 (1959).
[49] L. J. Fetters, J. Res. NBS **69A,** 33(1965).
[50] N. Calderon and K. W. Scott, J. Polymer Sci. **3A,** 551 (1965).
[51] S. E. Bresler, A. A. Korotkov, M. I. Mosevitsky, and I. Ya. Poddubnyi, Zhur. Tech. Fiz. **28,** 144 (1958).
[52] L. Gold, J. Chem. Phys. **28,** 91 (1958).
[53] F. Wenger, Makromol. Chem. **64,** 151 (1963).
[54] A. F. Johnson and D. J. Worsfold, J. Polymer Sic. **3A,** 449 (1965).
[55] G. E. Coates, Organometallic compounds, (2nd Ed., John Wiley & Sons, Inc., New York, N.Y., 1960).
[56] M. Morton, T. E. Helminiak, S. D. Gadkary, and F. Bueche, J. Polymer Sci. **57,** 471 (1962).

[57] T. A. Orofino and F. Wenger, J. Phys. Chem. **67,** 556 (1963).
[58] M. A. Weiner and R. West, J. Am. Chem. Soc. **85,** 485 (1963).
[59] M. Szwarc and J. Smid, Progress in reaction kinetics Vol. 2, chap. 5, p. 219 (Pergamon Press, Oxford, 1964).
[60] T. L. Brown, R. L. Gerteis, D. A. Bafus, and J. A. Ladd, J. Am. Chem. Soc. **86,** 2135 (1964).
[61] J. L. Hall, Ph. D. Dissertation, University of Akron, 1962.
[62] M. Szwarc, Fortschritte Hochpolymeren-Forschung **2,** 275 (1960).
[63] R. A. Livigni, Ph. D. Dissertation, University of Akron, 1961.
[64] F. J. Welch, J. Am. Chem. Soc. **81,** 1345 (1959).
[65] D. J. Worsfold and S. Bywater, Can. J. Chem. **42,** 2884 (1964).
[66] H. Hsieh, J. Polymer Sci. **3A,** 173 (1965).

(Paper 69A2–337)

JOURNAL OF RESEARCH of the National Bureau of Standards—A. Physics and Chemistry
Vol 69A, No. 2, March–April 1965

One Particle Transitions and Correlation in Quantum Mechanics

A. R. Ruffa

(October 9, 1964)

The quantum mechanical correlation problem, involving the evaluation of expectation values of many particle operators for a given eigenstate, is formulated, by means of the matrix sum rule, in terms of unobservable or virtual one particle transitions to other eigenstates of the system. This formulation is set forth for the two-fold purpose of both demonstrating the nature of the many particle correlations from the point of view of matrix mechanics, and making possible the derivation of sum rules which may be used in their analysis. The analysis shows that the transition integrals $<\alpha|\mathbf{A}_i|\alpha'>$ and $<\alpha|\mathbf{A}_j|\alpha'>$, where $\mathbf{A}_i$ and $\mathbf{A}_j$ are arbitrary one particle operators involving the ith and jth particles, respectively, are not necessarily equal, since such transitions can involve quantum states of different coordinate symmetry, i.e., the antisymmetric and symmetric states when $N=2$, and the states of mixed symmetry, in addition, when $N\geq 3$. The indistinguishability principle is demonstrated to require only that

$$\sum_{\alpha'}|<\alpha|\mathbf{A}_i|\alpha'>|^2=\sum_{\alpha'}|<\alpha|\mathbf{A}_j|\alpha'>|^2.$$

By detailed analysis of one particle transitions to states of various symmetries, the relationship between the various one particle transitions is determined. The expectation value for an antisymmetric state of the two particle operator $\sum_{i\neq j}\mathbf{A}_i\cdot\mathbf{A}_j$ is found to be

$$\sum_{i\neq j}<\alpha|\mathbf{A}_i\cdot\mathbf{A}_j|\alpha>=N(N-1)\sum_{\alpha_A'}|<\alpha|\mathbf{A}_1|\alpha_A'>|^2-N\sum_{\alpha_N'}|<\alpha_A|\mathbf{A}_1|\alpha_N'>|^2$$

where the sum α_A' is over all antisymmetric states, and the sum α_N' is over all the nonantisymmetric states. This equation is used to obtain an approximate relation between these expectation values and observable quantities.

From the Heisenberg commutation relations, the sum rule

$$\sum_{i=1}^{N}\sum_{\alpha'}(E_{\alpha'}-E_\alpha)|<\alpha|\mathbf{r}_i|\alpha'>|^2=3\hbar^2N/2m$$

is obtained and used to demonstrate some general properties of systems in the nonrelativistic approximation.

1. Introduction

Transitions in quantum mechanics usually refer to the change of an N particle system from one quantum state to another. Such a transition involving all the particles of the system is observable by radiative processes in principle if it is not prohibited by some selection rule. On the other hand, transitions not involving all the particles of the system have received little attention because they do not involve an observable property of the system. In the realm of scientific analysis, however, there are many occasions when it is desirable, if not expedient, to study a system in terms of properties which are not observable, but rather, are a product of the imagination—a method of inquiry analogous to a study of the rhinoceros by way of the properties of the unicorn and the dragon.

In line with this, the value of a discussion of such transitions lies in their connection with an unobservable property of the system, which nevertheless, because of its importance, has been the object of considerable interest. The property of interest concerns the effects resulting from the *correlations* of the particles of the system. The interest in these unobservable effects has arisen from the success of the relatively simple independent particle approximation in the description of the properties of a many particle system. While the independent particle model has proven to be an excellent first approximation, the limitations of this approach lie

mainly in its inability to properly evaluate the correlation effects. Consequently, the correlation problem concerns the attempt to arrive at a more accurate description of many particle systems.

From a mathematical point of view, the quantum mechanical correlation problem is associated with the evaluation of the expectation value, for a given quantum state, of any arbitrary many (two or more) particle operator—an expectation value which cannot be properly evaluated in the independent particle approximation. In the formalism of matrix mechanics, such an expectation value takes the form of a sum of products of matrix elements for the virtual one particle transitions. Consequently, in this article, the discussion of the one particle transitions is primarily intended to illustrate the nature of the many particle correlations from the matrix expansion point of view. In part 2, a detailed discussion of the requirements of the indistinguishability principle concerning the one particle transitions is included to elucidate some of their properties. Part 3 will demonstrate the detailed relationship between one particle transitions, while part 4 will give a discussion of the nature of two particle correlations in terms of the one particle transitions. Finally, in part 5, a sum rule which involves one particle transitions is obtained and used to demonstrate some general properties of systems in the nonrelativistic approximation. It is hoped that this somewhat different analysis of the correlation problem may introduce a fresh approach from which new ideas may evolve regarding this important topic.

2. Requirements of the Indistinguishability Principle in the Case of One Particle Transitions

If one considers the operator $\mathbf{A}=\sum_{i=1}^{N}\mathbf{A}_i$ for an N particle system where $\mathbf{A}_i$ operates on the ith particle, the principle of the indistinguishability of like particles requires that the expectation value

$$<\alpha|\mathbf{A}_i|\alpha>=\int\psi_\alpha^*(\mathbf{x}_1\mathbf{x}_2\ldots\mathbf{x}_N)\mathbf{A}_i\psi_\alpha(\mathbf{x}_1\mathbf{x}_2\ldots\mathbf{x}_N)d\mathbf{x}_1\ldots d\mathbf{x}_N$$

be equal to $<\alpha|\mathbf{A}_j|\alpha>$ where $i\neq j$. Here $\psi_\alpha(\mathbf{x}_1\mathbf{x}_2\ldots\mathbf{x}_N)$ is the N particle wave function describing the quantum state α of the N particle system. In the following discussion, this state will be assumed to refer to an electronic system, since this assumption involves no loss of generality. Therefore, as a consequence of the indistinguishability principle, the expectation value of $\mathbf{A}$ for a given state ψ_α is given by

$$<\alpha|\mathbf{A}|\alpha>=N<\alpha|\mathbf{A}_1|\alpha>. \tag{1}$$

The question may now be raised as to the relationship between $<\alpha|\mathbf{A}_i|\alpha'>$ and $<\alpha|\mathbf{A}_j|\alpha'>$ where the state $\psi_{\alpha'}$ differs from ψ_α. If, in analogy with the above discussion, one succumbs to the temptation of concluding that $<\alpha|\mathbf{A}_i|\alpha'>=<\alpha|\mathbf{A}_j|\alpha'>$, then one is immediately confronted with a contradiction in the evaluation of the expectation value of a many particle operator for a given quantum state.

This may be seen in the following manner. According to the sum rule for matrix multiplication, the expectation value for the two particle operator $\mathbf{A}_i\cdot\mathbf{A}_j$ evaluated for the state ψ_α is given by

$$<\alpha|\mathbf{A}_i\cdot\mathbf{A}_j|\alpha>=\sum_{\alpha'}<\alpha|\mathbf{A}_i|\alpha'><\alpha'|\mathbf{A}_j|\alpha> \tag{2}$$

where the sum is over all the eigenstates of the Hamiltonian. In the case when $i=j$, we are led to the relation

$$<\alpha|\mathbf{A}_i^2|\alpha>=\sum_{\alpha'}|<\alpha|\mathbf{A}_i|\alpha'>|^2 \tag{3}$$

since $\mathbf{A}_i$ is assumed to be Hermitian. If the relation $<|\mathbf{A}_i|\alpha'>=<\alpha|\mathbf{A}_j|\alpha'>$ is always correct, then comparison of (2) and (3) leads to the conclusion that $<\alpha|\mathbf{A}_i^2|\alpha>=<\alpha|\mathbf{A}_i\cdot\mathbf{A}_j|\alpha>$, which is not true in general. For example, the quantity $<\alpha|\mathbf{r}_i^2|\alpha>$ for the ground state of a free atom is proportional to its diamagnetic susceptibility, and is usually an order of magnitude greater than $<\alpha|\mathbf{r}_i\cdot\mathbf{r}_j|\alpha>$, a small quantity which vanishes for a free atom in the independent particle approximation. Similarly, the small quantity $<\alpha|\mathbf{p}_i\cdot\mathbf{p}_j|\alpha>$ vanishes for any bound state in the independent particle approximation, while $<\alpha|\mathbf{p}_i^2|\alpha>$, by the quantum mechanical virial theorem, is proportional to the total energy of the state ψ_α for any system described by a Hamiltonian which includes only Coulombic interactions. Consequently, the equality of the one particle transitions $<\alpha|\mathbf{A}_i|\alpha'>$ and $<\alpha|\mathbf{A}_j|\alpha'>$ would rule out the applicability of the matrix sum rule when applied to the determination of the expectation value of any two or more particle operator.

It is important to note that the indistinguishability principle, itself, does not require that $<\alpha|\mathbf{A}_i|\alpha'>$ equal $<\alpha|\mathbf{A}_j|\alpha'>$. This is easily demonstrated by using the sum rule for matrix multiplication which indicates that

$$<\alpha|\mathbf{A}_i^2|\alpha>=\sum_{\alpha'}|<\alpha|\mathbf{A}_i|\alpha'>|^2 \tag{3}$$

and

$$<\alpha_j|\mathbf{A}_j^2|\alpha>=\sum_{\alpha'}|<\alpha|\mathbf{A}_j|\alpha'>|^2. \tag{4}$$

According to the indistinguishability principle, the left hand sides of (3) and (4) are equal. Consequently, the indistinguishability principle requires only that

$$\sum_{\alpha'}|<\alpha|\mathbf{A}_j|\alpha'>|^2=\sum_{\alpha'}|<\alpha|\mathbf{A}_i|\alpha'>|^2. \tag{5}$$

3. Virtual One Particle Transitions Between States of Different Particle Coordinate Symmetry

The investigation into a more detailed relation between the $<\alpha|\mathbf{A}_i|\alpha'>$ and the $<\alpha|\mathbf{A}_j|\alpha'>$ than can be obtained from the indistinguishability principle leads immediately into a consideration of one particle transitions between states of different coordinate symmetry. As has been discussed before in some detail,[1] the eigenfunctions of an N particle Hamiltonian fall into three or more noncombining sets with different symmetry properties. The eigenfunctions of one set are antisymmetric with respect to particle interchanges, so that $\mathbf{P}_{ij}\,\psi_A=-\psi_A$, where $\mathbf{P}_{ij}$ is the permutation operator which interchanges the ith and jth electrons. Another set of eigenfunctions is symmetric, so that $\mathbf{P}_{ij}\psi_S=\psi_S$. In addition, when $N\geq 3$, there exist other mixed symmetry types ψ_M which are neither symmetric nor antisymmetric. It is evident that while the ψ_A and the ψ_S are eigenfunctions of all the $\mathbf{P}_{ij}$, the ψ_M are not since $\mathbf{P}^2{}_{ij}\psi=\psi$, and therefore if $\mathbf{P}_{ij}\psi=c\psi$, then $c=\pm 1$. However, mixed functions which are eigenfunctions of the $\mathbf{P}_{ij}$ individually can be constructed, since it is evident that $\psi_M+\mathbf{P}_{ij}\psi_M$ and $\psi_M-\mathbf{P}_{ij}\psi_M$ are symmetric and antisymmetric in the interchange of particles i and j, respectively. This property results from the fact that each $\mathbf{P}_{ij}$ commutes with the Hamiltonian, so that it is always possible to construct their simultaneous eigenfunctions.

In a real transition, i.e., one which is observable, at least in principle, in which the operator involved $\mathbf{A}=\sum_{i=1}^{N}\mathbf{A}_i$ is symmetric in all the particles, the matrix elements between states of different symmetry properties vanish. For an electronic system, it is well known that the wave functions belong to the antisymmetric set, so that real transitions can only occur between antisymmetric states. However, in a virtual one particle transition, this restriction

[1] E. Wigner, Z. Physik **40**, 492 (1927); **40**, 883 (1927); **43**, 624 (1927); F. Hund, Z. Physik **43**, 778 (1927); W. Heisenberg, Z. Physik **41**, 239 (1927); E. E. Witmer and J. P. Vinti, Phys. Rev. **47**, 538 (1935).

does not exist. In fact, as was seen above, a sum over all possible one particle transitions, i.e., those which involve transitions to *all* the eigenstates of the Hamiltonian, can only be meaningful if it includes transitions between states of different symmetry. This means that for an electronic system, one must consider, in addition to transitions to antisymmetric states, for which $\langle\alpha_A|\mathbf{A}_i|\alpha'_A\rangle$ and $\langle\alpha_A|\mathbf{A}_j|\alpha'_A\rangle$ are equal, transitions of the type $\langle\alpha_A|\mathbf{A}_i|\alpha'_S\rangle$ and, for the case when $N\geq 3$, transitions of the type $\langle\alpha_A|\mathbf{A}_i|\alpha'_M\rangle$ as well.[2] It is apparent from this discussion that the expectation value for an antisymmetric state of a two particle operator cannot be completely defined in terms of one particle transitions between antisymmetric eigenstates of the Hamiltonian alone.

It is now necessary to analyze in detail the relationship between one particle transitions involving states of different symmetry. Since the cases $N=2$ and $N\geq 3$ are somewhat different, they will be studied separately.

3.1. One Particle Transitions for Two Electron Systems

In the case of a two particle system, the eigenfunctions of the Hamiltonian are either symmetric or antisymmetric. We assume a two electron system to be in the antisymmetric state ψ_α. If one considers the transition element $\langle\alpha|\mathbf{A}_1|\alpha'\rangle$ and then applies the permutation operator P_{12} to the integral, one obtains $\langle-\alpha|\mathbf{A}_2|-\alpha'\rangle=\langle\alpha|\mathbf{A}_2|\alpha'\rangle$ if the state $\psi_{\alpha'}$ is also antisymmetric. However, one obtains $\langle-\alpha|\mathbf{A}_2|\alpha'\rangle=-\langle\alpha|\mathbf{A}_2|\alpha'\rangle$ if the state $\psi_{\alpha'}$ is symmetric. Since the integral must be invariant under interchanges of the dummy indices 1 and 2, we conclude for a two electron system that

$$\langle\alpha_A|\mathbf{A}_1|\alpha'_A\rangle=\langle\alpha_A|\mathbf{A}_2|\alpha'_A\rangle \tag{6}$$

and

$$\langle\alpha_A|\mathbf{A}_1|\alpha'_S\rangle=-\langle\alpha_A|\mathbf{A}_2|\alpha'_S\rangle \tag{7}$$

for one electron transitions between two antisymmetric states and between an antisymmetric state and a symmetric state, respectively.[3]

3.2. One Particle Transitions for Systems of Three or more Electrons

For systems of three or more electrons, an analysis similar to that made above indicates that for one particle transitions between antisymmetric states only, $\langle\alpha_A|\mathbf{A}_i|\alpha'_A\rangle=\langle\alpha_A|\mathbf{A}_j|\alpha'_A.\rangle$, while the one particle transition integrals between symmetric and antisymmetric states vanish. The validity of the latter statement may be seen by considering transitions between symmetric and antisymmetric states involving the operators $\mathbf{A}_i$, $\mathbf{A}_j$, and $\mathbf{A}_k$, where i, j, and k are different indices. We note that[3a]

$$\mathbf{P}_{ij}\langle\alpha_A|\mathbf{A}_i|\alpha'_S\rangle=\langle\alpha_A|\mathbf{A}_i|\alpha'_S\rangle=-\langle\alpha_A|\mathbf{A}_j|\alpha'_S\rangle \tag{8}$$

$$\mathbf{P}_{ik}\langle\alpha_A|\mathbf{A}_i|\alpha'_S\rangle=\langle\alpha_A|\mathbf{A}_i|\alpha'_S\rangle=-\langle\alpha_A|\mathbf{A}_k|\alpha'_S\rangle \tag{9}$$

$$\mathbf{P}_{jk}\langle\alpha_A|\mathbf{A}_j|\alpha'_S\rangle=\langle\alpha_A|\mathbf{A}_j|\alpha'_S\rangle=-\langle\alpha_A|\mathbf{A}_k|\alpha'_S\rangle. \tag{10}$$

The only possible way for (8), (9), and (10) to be simultaneously correct is if

$$\langle\alpha_A|\mathbf{A}_i|\alpha'_S\rangle=\langle\alpha_A|\mathbf{A}_j|\alpha'_S\rangle=\langle\alpha_A|\mathbf{A}_k|\alpha'_S\rangle=0. \tag{11}$$

---

[2] For a system of Bosons, which are described by symmetric wave functions, one must consider in addition to the $\langle\alpha_s|\mathbf{A}_i|\alpha'_S\rangle$, transitions of the type $\langle\alpha_s|\mathbf{A}_i|\alpha'_A\rangle$ and $\langle\alpha_s|\mathbf{A}_i|\alpha'_M\rangle$.

[3] If one were discussing a system of two Bosons, the above rules would hold in reverse order, i.e., one particle transition integral between two symmetric states would be equal, while one particle transition integral between a symmetric and an antisymmetric state would have opposite signs.

[3a] The operation $\mathbf{P}_{ij}\langle\alpha|A_i|\alpha'\rangle$ is equivlent to the transformation $\langle\alpha|\mathbf{P}_{ij^2}A_i\mathbf{P}_{ij^2}|\alpha'\rangle$ since it is evident that $\langle\alpha|\mathbf{P}_{ij}^{-1}A_i\mathbf{P}_{ij}|\alpha'\rangle=\langle\alpha|\mathbf{P}_{ij}A_i\mathbf{P}_{ij}|\alpha'\rangle=\langle\alpha|A_i|\alpha'\rangle$.

By allowing the indices i, j, and k to take on all possible combinations of values from 1 to N, one may see that all the one electron transitions between an antisymmetric and a symmetric state vanish.

There now remains for analysis the case of the virtual one particle transitions between the antisymmetric and the mixed states ψ_M. Since, as was seen above, there are no one particle transitions between antisymmetric and symmetric states when $N \geq 3$, the transitions between the antisymmetric and mixed states are decisive in providing a meaningful application of the sum rule for matrix multiplication as used in eqs (2), (3), and (4). However, because the mixed states are not eigenfunctions of the permutation operator, there is no simple relationship connecting the transition elements involving the operators $\mathbf{A}_i$ and $\mathbf{A}_j$. This may be demonstrated by noting that since the permutation and Hamiltonian operators commute, then

$$\mathbf{P}_{ij}(\mathbf{H}\psi_{M\alpha}) = \mathbf{H}(\mathbf{P}_{ij}\psi_{M\alpha}) = E_\alpha(\mathbf{P}_{ij}\psi_{M\alpha}).$$

Consequently, $\mathbf{P}_{ij}\psi_{M\alpha}$ is also an eigenfunction of the Hamiltonian having the same energy as $\psi_{M\alpha}$, so that $\mathbf{P}_{ij}\psi_{M\alpha}$ must be some linear combination of the degenerate eigenfunctions of the energy level E_α. Because of this equivalence degeneracy, which cannot be removed by any perturbation symmetric in all the electrons, the relationship between transition integrals involving the operators $\mathbf{A}_i$ and $\mathbf{A}_j$ is not a simple proportionality, but instead, involves linear combinations of transition integrals to the various degenerate states.

It is, however, possible to derive a relationship between these transition integrals which is more detailed than that given by the indistinguishability principle in eq (5). That the interchange of two particles in a $\psi_{M\alpha}$ yields a linear combination of mixed wave functions which are degenerate with $\psi_{M\alpha}$ may be expressed in the following way:

$$\mathbf{P}_{ij}\psi_{M\alpha l} = \sum_{l'} t_{ll'}\psi_{M\alpha l'} \tag{12}$$

where the sum is over all the states of the l-fold degenerate level E_α. Equation (12) in matrix notation is

$$\mathbf{P}_{ij}(\psi_{M\alpha l}) = (\psi_{M\alpha l})\mathbf{T} \tag{13}$$

where $(\psi_{M\alpha l})$ is the $1 \times l$ row vector composed of the linearly independent $\psi_{M\alpha l}$. That the $l \times l$ matrix $\mathbf{T}$ is nonsingular, and is, in fact, its own inverse is easily seen since

$$\mathbf{P}_{ij}^2(\psi_{M\alpha l}) = (\psi_{M\alpha l}) = (\psi_{M\alpha l})\mathbf{TT} \tag{14}$$

or

$$\mathbf{TT} = \mathbf{1}. \tag{15}$$

Moreover, because $\mathbf{T}^2$ is real, $\mathbf{T}$ must also be real.

We now construct the $1 \times l$ row matrix composed on the one particle transitions between the antisymmetric state $\psi_{A\alpha}$ and the mixed states of the l-fold degenerate energy level $E_{\alpha'}$, i.e., $(\langle\alpha_A|\mathbf{A}_i|\alpha'_{M_1}\rangle \ldots \langle\alpha_A|\mathbf{A}_i|\alpha'_{M_l}\rangle)$. From (13), it is evident that

$$\begin{aligned}
&\mathbf{P}_{ij}(\langle\alpha_A|\mathbf{A}_i|\alpha'_{M_1}\rangle \ldots \langle\alpha_A|\mathbf{A}_i|\alpha'_{M_l}\rangle) \\
&= (\langle\alpha_A|\mathbf{A}_i|\alpha'_{M_1}\rangle \ldots \langle\alpha_A|\mathbf{A}_i|\alpha'_{M_l}\rangle) \\
&= (\langle\alpha_A|\mathbf{A}_j|\alpha'_{M_1}\rangle \ldots \langle\alpha_A|\mathbf{A}_j|\alpha'_{M_l}\rangle)\mathbf{T}.
\end{aligned} \tag{16}$$

The complex conjugate of the matrix $(\langle\alpha_A|\mathbf{A}_i|\alpha'_{M_1}\rangle \ldots \langle\alpha_A|\mathbf{A}_i|\alpha'_{M_l}\rangle)$ is the $l \times 1$ column matrix

$$\begin{pmatrix} \langle\alpha'_{M_1}|\mathbf{A}_i|\alpha_A\rangle \\ \vdots \\ \langle\alpha'_{M_l}|\mathbf{A}_i|\alpha_A\rangle \end{pmatrix}.$$

From (16), one may see that

$$\mathbf{P}_{ij}\begin{pmatrix}\langle\alpha'_{M_1}|\mathbf{A}_i|\alpha_A\rangle\\ \vdots\\ \langle\alpha'_{M_l}|\mathbf{A}_i|\alpha_A\rangle\end{pmatrix}=\begin{pmatrix}\langle\alpha'_{M_1}|\mathbf{A}_i|\alpha_A\rangle\\ \vdots\\ \langle\alpha'_{M_l}|\mathbf{A}_i|\alpha_A\rangle\end{pmatrix}=-\mathbf{T}\begin{pmatrix}\langle\alpha'_{M_1}|\mathbf{A}_i|\alpha_A\rangle\\ \vdots\\ \langle\alpha'_{M_l}|\mathbf{A}_j|\alpha_A\rangle\end{pmatrix}. \tag{17}$$

Taking the inner or scalar product of $(\langle\alpha_A|\mathbf{A}_i|\alpha'_{M_1}\ldots\langle\alpha_A|\mathbf{A}_i|\alpha'_{M_l}\rangle)$ and its complex conjugate, and using (16) and (17), one obtains

$$(\langle\alpha_A|\mathbf{A}_i|\alpha'_{M_1}\rangle\ldots\langle\alpha_A|\mathbf{A}_i|\alpha'_{M_l}\rangle)\begin{pmatrix}\langle\alpha'_{M_1}|\mathbf{A}_i|\alpha_A\rangle\\ \vdots\\ \langle\alpha'_{M_l}|\mathbf{A}_i|\alpha_A\rangle\end{pmatrix}$$

$$=(\langle\alpha_A|\mathbf{A}_j|\alpha'_{M_1}\rangle\ldots\langle\alpha_A|\mathbf{A}_j|\mathbf{A}\alpha'_{M_l}\rangle)\,\mathbf{TT}\begin{pmatrix}\langle\alpha'_{M_1}|\mathbf{A}_j|\alpha_A\rangle\\ \vdots\\ \langle\alpha'_{M_l}|\mathbf{A}_j|\alpha_A\rangle\end{pmatrix} \tag{18'}$$

or

$$\sum_l\langle\alpha_A|\mathbf{A}_i|\alpha'_{M_l}\rangle\langle\alpha'_{M_l}|\mathbf{A}_i|\alpha_A\rangle=\sum_l\langle\alpha_A|\mathbf{A}_j|\alpha'_{M_l}\rangle\langle\alpha'_{M_l}|\mathbf{A}_j|\alpha_A|\rangle. \tag{18}$$

Consequently, the sum of the square moduli of the one particle transition integrals involving $\mathbf{A}_i$ and $\mathbf{A}_j$ between an antisymmetric state and the degenerate states of mixed symmetry are equal.

In summary, the relationship between one particle transitions for systems of three or more electrons are[4]

$$\langle\alpha_A|\mathbf{A}_i|\alpha'_A\rangle=\langle\alpha_A|\mathbf{A}_j|\alpha'_A\rangle$$

$$\langle\alpha_A|\mathbf{A}_i|\alpha'_S\rangle=\langle\alpha_A|\mathbf{A}_j|\alpha'_S\rangle=0$$

$$\sum_l|\langle\alpha_A|\mathbf{A}_i|\alpha'_{Ml}\rangle|^2=\sum_l|\langle\alpha_A|\mathbf{A}_j|\alpha'_{M_l}\rangle|^2.$$

4. Nature of Two Particle Correlations in Terms of One Particle Transitions

It will be assumed in this discussion that any many-particle operator of interest can be expanded in products of one particle operators. Since the main features of the matrix sum expansion of the expectation value of a product of one particle operators is illustrated by the expansion of a product of two one particle operators, the following discussion will center its attention on the two particle operator $\mathbf{A}_i\cdot\mathbf{A}_j$.

For a two electron system, the discussion of the previous section indicates that

$$\begin{aligned}\langle\alpha|\mathbf{A}_1\cdot\mathbf{A}_2|\alpha\rangle&=\sum_{\alpha'_A}\langle\alpha_A|\mathbf{A}_1|\alpha'_A\rangle\langle\alpha'_A|\mathbf{A}_2|\alpha_A\rangle\\&\quad+\sum_{\alpha'_S}\langle\alpha_A|\mathbf{A}_1|\alpha'_S\rangle\langle\alpha'_S|\mathbf{A}_2|\alpha_A\rangle\\&=\sum_{\alpha'_A}|\langle\alpha_A|\mathbf{A}_1|\alpha'_A\rangle|^2-\sum_{\alpha'_S}|\langle\alpha_A|\mathbf{A}_1|\alpha'_S\rangle|^2\end{aligned} \tag{19}$$

where the sum α'_A is over the antisymmetric states and the sum α'_S is over the symmetric states. It is apparent that for the expectation value of $\mathbf{A}_1\cdot\mathbf{A}_2$ to be zero, the sums of the square moduli of the transitions involving $\mathbf{A}_1$ over all antisymmetric states must equal the sum over all symmetric states. This is not the case in general, unless the electrons are isolated and do not interact. Moreover, it is apparent that the sign of the expectation value is dependent upon which of the two sums is larger in magnitude.

[4] For a system of Bosons, the above rules would be $\langle\alpha_S|\mathbf{A}_i|\alpha'_S\rangle=\langle\alpha_S|\mathbf{A}_j|\alpha'_S\rangle$, $\langle\alpha_S|\mathbf{A}_i|\alpha'_A\rangle=\langle\alpha_S|\mathbf{A}_j|\alpha'_A\rangle=0$, and $\Sigma|\langle\alpha_S|\mathbf{A}_i|\alpha'_{M_l}\rangle|^2=\Sigma|\langle\alpha_S|\mathbf{A}_j|\alpha'_{M_l}\rangle|^2$.

In the case of three or more electrons, one considers the operator $\sum_{i\neq j}\mathbf{A}_i\cdot\mathbf{A}_j$. The expectation value of this operator is given by

$$\sum_{i\neq j}\langle\alpha|\mathbf{A}_i\cdot\mathbf{A}_j|\alpha\rangle=\sum_{i\neq j}\sum_{\alpha_A'}\langle\alpha_A|\mathbf{A}_i|\alpha_A'\rangle\langle\alpha_A'|\mathbf{A}_j|\alpha_A\rangle$$
$$+\sum_{i\neq j}\sum_{\alpha_M'}\langle\alpha_A|\mathbf{A}_i|\alpha_M'\rangle\langle\alpha_M'|\mathbf{A}_j|\alpha_A\rangle. \tag{20}$$

If one notes that $\langle\alpha_M'|\sum_{j=1}^{N}\mathbf{A}_j|\alpha_A\rangle=0$, then $\langle\alpha_M'|\sum_{j\neq i}\mathbf{A}_j|\alpha_A\rangle=-\langle\alpha_M'|\mathbf{A}_i|\alpha_A\rangle$. Consequently, (20) may be written:

$$\sum_{i\neq j}\langle\alpha|\mathbf{A}_i\cdot\mathbf{A}_j|\alpha\rangle=N(N-1)\sum_{\alpha_A'}|\langle\alpha_A|\mathbf{A}_1|\alpha_A'\rangle|^2-N\sum_{\alpha_M'}|\langle\alpha_A|\mathbf{A}_1|\alpha_M'\rangle|^2 \tag{21}$$

It may be seen that the magnitude and sign of the expectation value of $\sum_{i\neq j}\mathbf{A}_i\cdot\mathbf{A}_j$ is dependent upon the relative magnitudes of the sums

$$\sum_{\alpha_M'}|\langle\alpha_A|\mathbf{A}_1|\alpha_M'\rangle|^2 \text{ and } (N-1)\sum_{\alpha_A'}|\langle\alpha_A|\mathbf{A}_1|\alpha_A'\rangle|^2.$$

Equations (19) and (21) may be combined to read for the general case

$$\sum_{i\neq j}\langle\alpha|\mathbf{A}_i\cdot\mathbf{A}_j|\alpha\rangle=N(N-1)\sum_{\alpha_A'}|\langle\alpha|\mathbf{A}_1|\alpha_A'\rangle|^2-N\sum_{\alpha_N'}|\langle\alpha_A|\mathbf{A}_1|\alpha_N'\rangle|^2 \tag{22}$$

where the sum α_N' is over all the non-antisymmetric states.

We are now in a position to discuss the physical nature of the two particle correlations. From a conceptional point of view, the expectation value $\langle\alpha|\mathbf{A}_i\cdot\mathbf{A}_j|\alpha\rangle$ may be given a geometrical meaning. If $\mathbf{A}_i$ and $\mathbf{A}_j$ are represented as vector quantities, then the above expectation value may be represented as their scalar product $|\mathbf{A}_i|\ |\mathbf{A}_j|\cos\gamma$, where $|\mathbf{A}_i|$ and $|\mathbf{A}_j|$ are the average magnitudes of the vectors given by $|\mathbf{A}_i|^2=\langle\alpha|\mathbf{A}_{ix}^2+\mathbf{A}_{iy}^2+\mathbf{A}_{iz}^2|\alpha\rangle$ and γ is the average angle between them. Since the average values of the magnitudes of $\mathbf{A}_i$ and $\mathbf{A}_j$ are equal because of the indistinguishability principle, the scalar product reduces to $|\mathbf{A}_1|^2\cos\gamma$.

The above discussion may now be applied to the derivation of an important approximate relation between the ratios $\langle\alpha|\mathbf{A}_i^2|\alpha\rangle/\langle\alpha|\mathbf{B}_i^2|\alpha\rangle$ and $\langle\alpha|\mathbf{A}_i\cdot\mathbf{A}_j|\alpha\rangle/\langle\alpha|\mathbf{B}_i\cdot\mathbf{B}_j|\alpha\rangle$, where the $\mathbf{A}_i$ and $\mathbf{B}_i$ refer to two different operators. Beginning with the assumption $\langle\alpha|\mathbf{A}_i^2|\alpha\rangle\gg\langle\alpha|\mathbf{A}_i\cdot\mathbf{A}_j|\alpha\rangle$, for any $\mathbf{A}_i$, we make the approximation

$$\frac{\langle\alpha|\mathbf{A}_1^2|\alpha\rangle}{\langle\alpha|\mathbf{B}_1^2|\alpha\rangle}\approx\frac{\langle\alpha|(\sum_i\mathbf{A}_i)^2|\alpha\rangle}{\langle\alpha|(\sum_i\mathbf{B}_i)^2|\alpha\rangle}. \tag{23}$$

Now

$$\frac{\langle\alpha|\mathbf{A}_1^2|\alpha\rangle}{\langle\alpha|\mathbf{B}_1^2|\alpha\rangle}=\frac{Q+T}{S+P} \tag{24}$$

where

$$Q=\sum_{\alpha_N'}|\langle\alpha|\mathbf{A}_1|\alpha_A'\rangle|^2$$

$$T=\sum_{\alpha_N'}|\langle\alpha|\mathbf{A}_1|\alpha_N'\rangle|^2$$

$$S=\sum_{\alpha_A'}|\langle\alpha|\mathbf{B}_1|\alpha_A'\rangle|^2$$

$$P=\sum_{\alpha_N'}|\langle\alpha|\mathbf{B}_1|\alpha_N'\rangle|^2$$

On the other hand, it is evident that $(\sum_i\mathbf{A}_i)^2$ and $(\sum_i\mathbf{B}_i)^2$ are symmetric operators so that in the

expansion of their expectation values, only transitions to antisymmetric states need be considered. Consequently:

$$\frac{\langle\alpha|(\sum_i \mathbf{A}_i)^2|\alpha\rangle}{\langle\alpha|(\sum_i \mathbf{B}_i)^2|\alpha\rangle} = \frac{\sum_{\alpha_A'} |\langle\alpha|(\sum_i \mathbf{A}_i)|\alpha_A'\rangle|^2}{\sum_{\alpha_A'} |\langle\alpha|(\sum_i \mathbf{B}_i)|\alpha_A'\rangle|^2}$$

$$= \frac{\sum_{\alpha_A'} |\langle\alpha|N\mathbf{A}_1|\alpha_A'\rangle|^2}{\sum_{\alpha_A'} |\langle\alpha|N\mathbf{B}_1|\alpha_A'\rangle|^2} = \frac{Q}{S}. \tag{25}$$

We now consider the ratio of the two particle correlation terms. The use of eq (22) yields

$$\frac{\sum_{i\neq j}\langle\alpha|\mathbf{A}_i\cdot\mathbf{A}_j|\alpha\rangle}{\sum_{i\neq j}\langle\alpha|\mathbf{B}_i\cdot\mathbf{B}_j|\alpha\rangle} = \frac{N(N-1)Q-NT}{N(N-1)S-NP} \tag{26}$$

which upon application of the indistinguishability principle becomes

$$\frac{\langle\alpha|\mathbf{A}_1\cdot\mathbf{A}_2|\alpha\rangle}{\langle\alpha|\mathbf{B}_1\cdot\mathbf{B}_2|\alpha\rangle} = \frac{(N-1)Q-T}{(N-1)R-P}. \tag{27}$$

It is apparent from (23), (24), and (25) that in this approximation:

$$\frac{Q+T}{S+P} \approx \frac{Q}{S}$$

from which we obtain

$$T \approx \frac{QP}{S}. \tag{28}$$

Substitution of this result in eq (27) yields the result:

$$\frac{\langle\alpha|\mathbf{A}_1\cdot\mathbf{A}_2|\alpha\rangle}{\langle\alpha|\mathbf{B}_1\cdot\mathbf{B}_2|\alpha\rangle} \approx \frac{(N-1)\mathbf{Q}-\dfrac{QP}{S}}{(N-1)S-P} = \frac{Q}{S} \tag{29}$$

from which we conclude

$$\frac{\langle\alpha|\mathbf{A}_1^2|\alpha\rangle}{\langle\alpha|\mathbf{B}_1^2|\alpha\rangle} \approx \frac{\langle\alpha|\mathbf{A}_1\cdot\mathbf{A}_2|\alpha\rangle}{\langle\alpha|\mathbf{B}_1\cdot\mathbf{B}_2|\alpha\rangle}. \tag{30}$$

An equivalent relation is

$$\frac{\sum_i\langle\alpha|\mathbf{A}_i^2|\alpha\rangle}{\sum_i\langle\alpha|\mathbf{B}_i^2|\alpha\rangle} \approx \frac{\sum_{i\neq j}\langle\alpha|\mathbf{A}_i\mathbf{A}_j|\alpha\rangle}{\sum_{i\neq j}\langle\alpha|\mathbf{B}_i\mathbf{B}_j|\alpha\rangle} \approx \frac{\langle\alpha|(\sum_i \mathbf{A}_i)^2|\alpha\rangle}{\langle\alpha|(\sum_i \mathbf{B}_i)^2|\alpha\rangle}. \tag{31}$$

In the limit when the ratios $\langle\alpha|\mathbf{A}_1\cdot\mathbf{A}_2|\alpha\rangle/\langle\alpha|\mathbf{A}_1^2|\alpha\rangle$ and $\langle\alpha|\mathbf{B}_1\cdot\mathbf{B}_2|\alpha\rangle/\langle\alpha|\mathbf{B}_1^2|\alpha\rangle$ both approach zero, the above approximate relations (30) and (31) become exact. One may conclude from equation (30) that in this limit, the correlation angles involving the two operators under consideration are equal. These relations are important in that they equate the ratio of two correlation terms to ratios of quantities which are observables, at least in principle.

Because of the importance of these relations, a few remarks regarding their applicability and range of validity are pertinent. The derivation of eqs (30) and (31) establishes the equality of the correlation angles associated with all two particle operators of the type $\mathbf{A}_1\cdot\mathbf{A}_2$ when correlation effects are very small. Such a situation occurs in systems consisting of very weakly interacting particles. This result is not trivial since a weak interaction only necessarily implies that the quantities $\cos\gamma$ for different operators are small, and not that there is necessarily any relationship between them in the limit of vanishing interaction.

It is now of value to analyze the applicability of these relations to a system where the interparticle interactions are not necessarily small. One might expect, in this case, that a more realistic assumption upon which to base the above derivation is that $<\alpha|\mathbf{A}_i^2|\alpha>$ must be very large compared to $(N-1)<\alpha|\mathbf{A}_i\cdot\mathbf{A}_j|\alpha>$ for an N particle system, since there are N terms of the first type and $N(N-1)$ terms of the second type. The factor $(N-1)$ would introduce an order of magnitude increase in the size of the small quantity and would, of course, place some doubt upon the validity of the initial assumption.

For most real systems, however, this consideration does not present a serious problem, primarily because the particles of a system generally arrange themselves in groups which are not strongly correlated. An example of this is the electronic shells of atoms. Consequently, the correlation terms do not generally become more important for systems with large numbers of particles than for systems containing few particles.

A check on this conclusion is possible in the case when the operators $\mathbf{A}_i$ involved are the radius vectors $\mathbf{r}_i$ of the electrons in an atom or molecule. Kirkwood and Vinti,[5] using different techniques, independently derived an approximate expression relating the electric and diamagnetic susceptibilities of closed shell atoms and molecules. However, Kirkwood's expression neglects the contribution due to the correlation term $\sum_{i\neq j}<\alpha|\mathbf{r}_i\cdot\mathbf{r}_j|\alpha>$. Since Kirkwood's calculated diamagnetic susceptibilities for several rare gases and diatomic hydrogen do not differ from the observed values by more than a few percent, it appears safe to conclude that $\sum_i<\alpha|\mathbf{r}_i^2|\alpha>$ is generally at least an order of magnitude greater than $\sum_{i\neq j}<\alpha|\mathbf{r}_i\cdot\mathbf{r}_j|\alpha>$.

The question still remains as to whether this ratio is great enough to insure the validity of eqs (30) and (31) when applied to most systems. In order to arrive at a definitive answer to this question, one must first recognize that the fundamental assumption (23) involved in the derivation of these equations is valid not only in the limit of vanishing correlation, but also in the case when the correlation angles involved are equal or do not differ greatly in magnitude. Since we have already established that the correlation angles are equal for vanishingly small correlation, it is reasonable to conclude that the correlation angles are very nearly (if not actually) equal in the case when $\sum_{i\neq j}<\alpha|\mathbf{A}_i\cdot\mathbf{A}_j|\alpha>$ is an order of magnitude smaller than $\sum_i<\alpha|\mathbf{A}_i^2|\alpha>$. Consequently, we may conclude that in most cases, the approximation (23) is a good one, and equations (30) and (31) are valid. This conclusion is of great practical value, since these equations enable one to calculate the value of any correlation term, given the appropriate observables, once any one such term is evaluated either indirectly or by direct theoretical calculation. An example of such a calculation will be discussed in the next section.

5. Derivation and Application of a Sum Rule for One Particle Transitions

Sum rules, in general, are useful in providing information about a system without a detailed knowledge of its wave functions or energy levels. In the case of sum rules which involve one particle transitions, information can be obtained regarding the relative magnitudes of one particle transitions as well as the relative energy separations of the various quantum states (observable or unobservable) of the system. In some cases, information can be obtained regarding the expectation value of many-particle operators.

One useful sum rule of this type follows from the N electron nonrelativistic Hamiltonian

$$\mathbf{H}=(1/2m)\sum_i\mathbf{p}_i^2+V(\mathbf{r}_1\mathbf{r}_2\ldots\mathbf{r}_N) \tag{32}$$

and the Heisenberg commutation relations

$$\mathbf{r}_i\mathbf{p}_j-\mathbf{p}_j\mathbf{r}_i=3i\hbar\delta_{ij}, \tag{33}$$

[5] J. G. Kirkwood, Phys. Zeits. **33**, 57 (1932); J. P. Vinti, Phys. Rev. **41**, 813 (1932).

$$\mathbf{r}_i\mathbf{r}_j-\mathbf{r}_j\mathbf{r}_i=0 \tag{34}$$

$$\mathbf{p}_i\mathbf{p}_j-\mathbf{p}_j\mathbf{p}_i=0 \tag{35}$$

From (32), (33), (34), and (35), it follows that

$$\mathbf{p}_i=-(im/\hbar)(\mathbf{r}_i\mathbf{H}-\mathbf{H}\mathbf{r}_i) \tag{36}$$

so that the matrix components of $\mathbf{p}_i$ in terms of those of $\mathbf{r}_i$ are

$$<\alpha|\mathbf{p}_i|\alpha'>=-\frac{im}{\hbar}E_{\alpha'\alpha}<\alpha|\mathbf{r}_i|\alpha'> \tag{37}$$

where $E_{\alpha'\alpha}=E_{\alpha'}-E_{\alpha}$. Since $<\alpha|\mathbf{r}_i\mathbf{p}_i-\mathbf{p}_i\mathbf{r}_i|\alpha>=3i\hbar$, then

$$\sum_{\alpha'}E_{\alpha'\alpha}|<\alpha|\mathbf{r}_i|\alpha'>|^2=3\hbar^2/2m. \tag{38}$$

Since the sum is the same for all the N particles, we conclude that

$$\sum_{i=1}\sum_{\alpha'}E_{\alpha'\alpha}|<\alpha|\mathbf{r}_i|\alpha'>|^2=3\hbar^2N/2m. \tag{39}$$

It is apparent that these sum rules confirm the result (18) for the special case when $\mathbf{A}_i=\mathbf{r}_i$, since they can only be correct, in general, if the sum of the square moduli of the transitions involving $\mathbf{r}_i$ and $\mathbf{r}_j$ to degenerate states are equal.

The sum rules (38) and (39) resemble the well-known Thomas-Kuhn-Reiche [6] sum rule for real transitions

$$\sum_{\alpha'}E_{\alpha'\alpha}|<|\alpha|\mathbf{R}|\alpha'>|^2=3\hbar^2N/2m \tag{40}$$

where $\mathbf{R}=\sum_{i=1}^{N}\mathbf{r}_i$. This sum rule may be obtained by summing eq (37) over all the electrons and noting that $<\alpha|\mathbf{RP}-\mathbf{PR}|\alpha>=3Ni\hbar$, where $\mathbf{P}=\sum_{i=1}^{N}\mathbf{p}_i$.

Comparison of (39) and (40) confirms the fact that transitions to unobservable quantum states are decisive in validating sums which involve one particle transitions. If the sum (39) only involved transitions to antisymmetric states, it would differ from the sum (40) by a factor of N. From equation (40), it is evident that

$$\sum_{i=1}^{N}\sum_{\alpha_A'}E_{\alpha_A'\alpha_A}|<\alpha_A|\mathbf{r}_i|\alpha_A'>|^2=3\hbar^2/2m. \tag{41}$$

where the sum in (41) is over one particle transitions to antisymmetric states only. As a result, one may conclude that

$$\sum_{i=1}^{2}\sum_{\alpha_S'}E_{\alpha_S'\alpha_A}|<\alpha_A|\mathbf{r}_i|\alpha_S'>|^2=3\hbar^2/2m \tag{42}$$

for a two electron system, where the sum (42) is over transitions to symmetric states only, while

$$\sum_{i=1}^{N}\sum_{\alpha_M'}E_{\alpha_M'\alpha_A}|<\alpha_A|\mathbf{r}_i|\alpha_M'>|^2=(N-1)3\hbar^2/2m \tag{43}$$

for a three or more electron system, where the sum (43) is over transitions to mixed states only.

If one subtracts (39) from (40) one finds that

$$\sum_{i\neq j}\sum_{\alpha'}E_{\alpha'\alpha}<\alpha|\mathbf{r}_i|\alpha'><\alpha'|\mathbf{r}_j|\alpha>=0. \tag{44}$$

---

[6] W. Thomas, Naturwissenschaften **13**, 627 (1925); W. Kuhn, Z. Physik **33**, 408 (1925); F. Reiche and W. Thomas, Z. Physik **34**, 510 (1925).

This result would appear to be paradoxical if one sums (44) by means of an average energy $\overline{E}$ such that (44) becomes

$$\overline{E}\sum_{\alpha'}\sum_{i\neq j}{}'\langle\alpha|\mathbf{r}_i|\alpha'\rangle\langle\alpha'|\mathbf{r}_j|\alpha\rangle=\overline{E}\sum_{i\neq j}{}'\langle\alpha|\mathbf{r}_i\cdot\mathbf{r}_j|\alpha\rangle.$$

Since $\langle\alpha|\sum_{i\neq j}\mathbf{r}_i\cdot\mathbf{r}_j|\alpha\rangle$ is not equal to zero in general, this result indicates that $\overline{E}$ always vanishes. Although the invariably null value of the average energy difference seems to be a strange result, the correctness of the sum (44) can be directly demonstrated from the commutation relations. By application of (37), one may see that

$$\sum_{i\neq j}\sum_{\alpha'}E_{\alpha'\alpha}\langle\alpha|\mathbf{r}_i|\alpha'\rangle\langle\alpha'|\mathbf{r}_j|\alpha\rangle=-\frac{\hbar}{2im}\sum_{i\neq j}\sum_{\alpha'}\langle\alpha|\mathbf{r}_i|\alpha'\rangle\langle\alpha'|\mathbf{p}_j|\alpha\rangle$$
$$+\frac{\hbar}{2im}\sum_{i\neq j}\sum_{\alpha'}\langle\alpha|\mathbf{p}_j|\alpha'\rangle\langle\alpha'|\mathbf{r}_i|\alpha\rangle \quad (45)$$

where in the second sum, the dummy indices i and j have been interchanged. The right hand side of (45) is simply, from the sum rule for matrix multiplication $-\frac{\hbar}{2im}\sum_{i\neq i}\langle\alpha|\mathbf{r}_i\cdot\mathbf{p}_j-\mathbf{p}_j\cdot\mathbf{r}_i|\alpha\rangle$ which is zero as a result of the commutation relation (33).[7]

The origin of the vanishing average energy difference can be demonstrated if one rewrites the sum (44) in the following manner:

$$\sum_{i\neq j}\Big(\sum_{\alpha'_A}E_{\alpha'_A\alpha_A}\langle\alpha|\mathbf{r}_i|\alpha'_A\rangle\langle\alpha'_A|\mathbf{r}_j|\alpha_A\rangle+\sum_{\alpha'_N}E_{\alpha'_N\alpha_A}\langle\alpha_A|\mathbf{r}_i|\alpha'_N\rangle\langle\alpha'_N|\mathbf{r}_j|\alpha_A\rangle\Big) \quad (46)$$

where the sum α'_N is over all the states which are not antisymmetric, i.e., the symmetric states for $N=2$, and the mixed states for $N\geq 3$. The sum (46) can be written in the form

$$\sum_i\Big((N-1)\overline{E}_A\sum_{\alpha'_A}|\langle\alpha_A|\mathbf{r}_i|\alpha'_A\rangle|^2-\overline{E}_N\sum_{\alpha'_N}|\langle\alpha_A|\mathbf{r}_i|\alpha'_N\rangle|^2\Big)$$
$$=N(N-1)\overline{E}_A\sum_{\alpha'_A}|\langle\alpha_A|\mathbf{r}_1|\alpha'_A\rangle|^2-N\overline{E}_N\sum_{\alpha'_N}|\langle\alpha_A|\mathbf{r}_1|\alpha'_N\rangle|^2 \quad (47)$$

where $\overline{E}_A$ and $\overline{E}_N$ are the average energy differences between the ground state and the antisymmetric states, and the ground state and the non-antisymmetric states, respectively.

For the special case, when $\langle\alpha|\mathbf{r}_i\cdot\mathbf{r}_j|\alpha\rangle=0$, i.e., when the electrons are uncorrelated and the system has no electric dipole moment, then $N(N-1)\sum|\langle\alpha_A|\mathbf{r}_1|\alpha'_A|^2-N\sum|\langle\alpha_A|\mathbf{r}_1|\alpha'_N\rangle|^2=0$ and $\overline{E}_A$ and $\overline{E}_N$ must be equal. In all other cases, however, these two quantities are not equal, but, instead, their values are adjusted so that $N(N-1)\,\overline{E}_A\sum_{\alpha_A}|\langle\alpha_A|\mathbf{r}_1|\alpha'_A\rangle|^2$ always equals $N\overline{E}_N\sum_{\alpha_N}|\langle\alpha_A|\mathbf{r}_1|\alpha'_A\rangle|^2$. As seen in this light, the vanishing total average energy difference results from the fact that it is a composite of average energy differences involving virtual one particle transitions to states of different symmetry. This special relationship that exists in the nonrelativistic approximation between these weighted mean energy differences and the transition integrals of the type $\langle\alpha_A|\mathbf{r}_1|\alpha'_A\rangle$ and $\langle\alpha_A|\mathbf{r}_1|\alpha'_N\rangle$ is a restriction on all systems, regardless of their detailed properties, which is imposed by the nature of the Schrodinger representation, which in turn follows from the commutation relations.

The sum rules (38) and (39) have immediate application in a demonstration of an approximate relationship between the diamagnetic susceptibility and the total energy of a system in the nonrelativistic approximation. If one assumes that the ground state of the system does

[7] The author is indebted to Dr. J. P. Vinti for clarifying this point.

not have an electric dipole moment, i.e., that

$$<\alpha|X|\alpha>=N<\alpha|x_1|\alpha>=0=<\alpha|y_i|\alpha>=<\alpha|z_i|\alpha>$$

then (38) may be written

$$\overline{E}_{r_i}\sum_{\alpha}|<\alpha|\mathbf{r}_i|\alpha'>|^2=\overline{E}_{r_i}<\alpha|\mathbf{r}_i^2|\alpha>=3\hbar^2/2m. \tag{48}$$

On the other hand, (48) may be rewritten in the following fashion by making use of (37):

$$\sum_{\alpha'}E_{\alpha'\alpha}|<\alpha|\mathbf{r}_i|\alpha'>|^2=3\hbar^2/2m=\left(\frac{\hbar}{m}\right)^2\sum_{\alpha'}\frac{|<\alpha|\mathbf{p}_i|\alpha'>|^2}{E_{\alpha'\alpha}}. \tag{49}$$

Equation (49) may now be written as

$$1/\overline{E}_{p_i}\left(\frac{\hbar}{m}\right)^2\sum_{\alpha'}|<\alpha|\mathbf{p}_i|\alpha'>|^2=1/\overline{E}_{p_i}\left(\frac{\hbar}{m}\right)^2<\alpha|\mathbf{p}_i^2|\alpha>=3\hbar^2/2m \tag{50}$$

since $\sum_i<\alpha|\mathbf{p}_i|\alpha>$vanishes for any bound state. Comparison of (48) and (50) reveals that if the approximation $\overline{E}_{p_i}=\overline{E}_{r_i}$ is made, then the simple relationship

$$<\alpha|\mathbf{r}_i^2|\alpha><\alpha|\mathbf{p}_i^2|\alpha>=(3\hbar/2)^2 \tag{51}$$

results. One may note the similarity between (51) and the well known expression for the uncertainty principle.

When eqs (48) and (50) are summed over all the electrons, the following equations are obtained:

$$\overline{E}_{r_i}\sum_{i=1}^{N}<\alpha|\mathbf{r}_i^2|\alpha>=3N\hbar^2/2m \tag{52}$$

$$1/\overline{E}_{p_i}\sum_{i=1}^{N}<\alpha|\mathbf{p}_i^2|\alpha>=3N\,m/2. \tag{53}$$

Using the expression for the diamagnetic susceptibility[8]

$$\chi_{\text{dia}}=-\frac{e^2}{6mc^2}\sum_{i=1}^{N}<\alpha|\mathbf{r}_i^2|\alpha>, \tag{54}$$

eq (42) becomes:

$$\chi_{\text{dia}}=-\frac{N\hbar^2e^2}{4m^2c^2}\frac{1}{\overline{E}_{r_i}}. \tag{55}$$

Since the nonrelativistic Hamiltonian (32) contains only Coulombic interactions, by the virial theorem, the total energy of the system W_0 is equal to the negative of its kinetic energy $1/2m\sum_{=1}^{N}<\alpha|\mathbf{p}_i^2|\alpha>$. Making use of this fact, (53) becomes

$$W_0=-\frac{3N}{4}\overline{E}_{p_i}. \tag{56}$$

Combining (55) and (56), and again making use of the approximation $\overline{E}_{p_i}=\overline{E}_{r_i}$, one obtains the simple relation between χ_{dia} and W_0:

$$\chi_{\text{dia}}W_0=K^2 \tag{57}$$

where

$$K=\frac{\sqrt{3}N\hbar e}{4mc}.$$

[8] J. H. Van Vleck, Theory of Electric and Magnetic Susceptibilities (Oxford Univ. Press, 1932).

We are now in a position to examine the observable manifestations of the two particle correlations in the special case when the operators involved are the coordinates and moment of the particles. The expectation values of the operators $\sum_{i\neq j} \mathbf{r}_i \cdot \mathbf{r}_j$ and $\sum_{i\neq j} \mathbf{p}_i \cdot \mathbf{p}_j$ can be considered to be observable since they can be expressed as the difference between two quantities which are observable at least in principle. The first operator is equal to $\left(\sum_i \mathbf{r}_i\right)^2 - \sum_i \mathbf{r}_i^2$; the expectation value of the first quantity is equal to the square of the extension of the system while, as discussed above, the expectation value of the second is proportional to the diamagnetic susceptibility of the system. Unfortunately, neither of these quantities is easy to determine with any degree of accuracy by experimental techniques except under special conditions. The diamagnetic susceptibility can be experimentally observed only if other magnetic effects, which would normally be dominant, vanish as is the case in closed shell atoms and molecules. The extension of the system is not easily observable, experimentally, although it is related to the electric polarizability (see footnote 5). The second operator is equal to $\left(\sum_i \mathbf{p}_i\right)^2 - \sum_i \mathbf{p}_i^2$ which is again the difference between two observable quantities. A term proportional to the first operator, added to the Hamiltonian, exactly expresses the effect of the nuclear motion upon the energy of an atomic system.[9] Consequently, the expectation value of this term gives, in first order perturbation theory, the shift in energy levels due to the nuclear motion. This can be observed directly in the relative shifts of the energy levels of different isotopes of a given atom. The expectation value of the second operator is, as discussed above, proportional to the total energy of the system.

We may now derive simplified relations for the ratio $\sum_{i\neq j} \langle\alpha|\mathbf{p}_i \cdot \mathbf{p}_j|\alpha\rangle / \sum_{i\neq j} \langle\alpha|\mathbf{r}_i \cdot \mathbf{r}_j|\alpha\rangle$. It is evident from the approximate relations (30)and (31) that

$$\frac{\sum_{i\neq j} \langle\alpha|\mathbf{p}_i \cdot \mathbf{p}_j|\alpha\rangle}{\sum_{i\neq j} \langle\alpha|\mathbf{r}_i \cdot \mathbf{r}_j|\alpha\rangle} \approx \frac{\sum_i \langle\alpha|\mathbf{p}_i^2|\alpha\rangle}{\sum_i \langle\alpha|\mathbf{r}_i^2|\alpha\rangle} = \frac{e^2}{3c^2} \frac{W_0}{\chi_{\text{dia}}}. \tag{58}$$

Although W_0 and χ_{dia} may be obtained experimentally or from the available wavefunction, a further simplification of this expression is useful. From eq (51), it may be seen that

$$\frac{\sum_i \langle\alpha|\mathbf{p}_i^2|\alpha\rangle}{\sum \langle\alpha|\mathbf{r}_i^2|\alpha\rangle} \approx \frac{N^2(3\mathrm{h}/2)^2}{\left(\sum_i \langle\alpha|\mathbf{r}_i^2|\alpha\rangle\right)^2}. \tag{59}$$

Consequently

$$\sum_i \langle\alpha|\mathbf{p}_j \cdot \mathbf{p}_j|\alpha\rangle \approx (3\mathrm{h}/2)^2 N^2 \frac{\sum_{i\neq j} \langle\alpha|\mathbf{r}_i \cdot \mathbf{r}_j|\alpha\rangle}{\left(\sum_i \langle\alpha|\mathbf{r}_i^2|\alpha\rangle\right)^2}. \tag{60}$$

Though approximate, this relation offers a considerable advantage in the calculation of the contribution of $\sum_{i\neq j} \langle\alpha|\mathbf{p}_i \cdot \mathbf{p}_j|\alpha\rangle$ to the isotope shift of atomic energy levels since it does not involve multiple differentiation of complicated wavefunctions.

Finally, it may be remarked that the sum rule [10] for atomic transition probabilities

$$\left(\frac{m}{h}\right)^2 \sum_{\alpha'} E_{\alpha'\alpha}^2 |\langle\alpha|\sum_i \mathbf{r}_i|\alpha\rangle|^2 = 2mW_0 + \sum_{i\neq j} \langle\alpha|\mathbf{p}_i \cdot \mathbf{p}_j|\alpha\rangle \tag{61}$$

once again displays $\sum_{i\neq j} \langle\alpha|\mathbf{p}_i \cdot \mathbf{p}_j|\alpha\rangle$ as the difference between two observable quantities. The simplified formula (60) can be used to advantage in calculating its contribution to the sum.

[9] D. S. Hughes and C. Eckart, Phys. Rev. **36**, 694 (1930).
[10] J. P. Vinti, Phys. Rev. **41**, 432 (1932).

For example, in the case of the helium atom, use of a wavefunction due to Hylleraas which gives the energy correct to one part in 3000 gives for $\sum_{i\neq j} <\alpha|\mathbf{r}_i\cdot\mathbf{r}_j|\alpha>$ the value $-0.146a_0^2$ and for $\sum_i <\alpha|\mathbf{r}_i^2|\alpha>$, the value $+2.34a_0^2$. From (60), it is easily found that $\sum_{i\neq j} <\alpha|\mathbf{p}_i\cdot\mathbf{p}_j|\alpha>$ is $-.24\hbar^2/a_0$. This is about four percent of the value of $2mW_0$ determined with the same wavefunction, so that this term amounts to a four percent correction in the value of the sum expressed in eq (61).

It may be further observed from the above discussion that $\sum_{i\neq j} <\alpha|\mathbf{p}_i\cdot\mathbf{p}_j|\alpha>$ and $\sum_{i\neq j} <\alpha|\mathbf{r}_i\cdot\mathbf{r}_j|\alpha>$ have the same sign. Since the electrons repel each other, one would expect the average angle between two radius vectors $\mathbf{r}_i$ and $\mathbf{r}_j$ to be greater than $\pi/2$ in a spherically symmetric system so that $\sum_{i\neq j} <\alpha|\mathbf{r}_i\cdot\mathbf{r}_j|\alpha>$ is negative as was determined above for He. Consequently, one may conclude, in general, that $\sum_{i\neq j} <\alpha|\mathbf{p}_i\cdot\mathbf{p}_j|\alpha>$ is negative also under the same conditions.

6. Conclusion

The main purpose of this article has been to demonstrate the nature of the many particle correlations in a system in terms of expansions involving unobservable one particle transitions between states of different symmetry. This conceptional approach has been explored and used to derive relations for some two particle operators which are of use in various types of calculations. However, the ultimate value of this approach lies in the application of sum rules which involve one particle transitions in an attempt to obtain information regarding the many particle correlations which has been largely intractable by other approximation schemes. This method of analysis will be explored in future publications.

The author is indebted to Dr. J. P. Vinti for several stimulating discussions regarding sum rules which involve virtual one particle transitions.

(Paper 69A2–338)

JOURNAL OF RESEARCH of the National Bureau of Standards—A. Physics and Chemistry
Vol. 69A, No. 2, March–April 1965

Disaccommodation of Magnetic Spectra of Two Manganese Zinc Ferrites

A. L. Rasmussen

(October 19, 1964)

Disaccommodation of the complex susceptibility (time change after demagnetization) of two manganese zinc ferrite materials of the composition $Mn_{0.597}Zn_{0.265}Fe_{2.07}O_4$ and $Mn_{0.584}Zn_{0.353}Fe_{2.08}O_4$ was studied in response to demagnetizing frequency and rate, temperature, frequencies of ~20 kHz to ~2000 kHz, and rf magnetic field intensities of $\sim 10^{-4}$ oersted and $\sim 10^{-2}$ oersted. Precise susceptibility spectra near −10.0 °C show that the resonance maxima shift to higher frequency and decrease in magnitude with increasing time after demagnetization and that the disaccommodation rate varies considerably and changes sign with frequency. Activation energies of the order of 0.8 electron volt were computed at 100 kHz.

Definitions by Symbols

f, ω = Frequency, angular frequency.
κ' = Real component of relative permittivity.
κ'' = Imaginary component of relative permittivity.
χ' = Real component of the relative susceptibility.
χ'' = Imaginary component of the relative susceptibility.
χ'_{max} = Maximum of the real component of the relative susceptibility.
$f_{\chi'_{max}}$ $\omega_{\chi'_{max}}$ = Frequency, angular frequency corresponding to χ'_{max}.
$\chi'_{LF\ min}$ = Low frequency minimum of the real component of the relative susceptibility.
$\chi(t)$ = χ' at a time, t, after demagnetization.
χ_0 = χ' at time = 0 after demagnetization.
χ_∞ = χ' at time = ∞ after demagnetization.
E = Activation energy.
κ = Boltzmann constant.
T = Temperature, degrees Kelvin.
E_1 = Activation energy corresponding to τ_1 values.
E_2 = Activation energy corresponding to τ_2 values.
E_0 = Mean of E_1 and E_2.

1. Introduction

Disaccommodation [1] is defined as time change of the magnetic susceptibility after demagnetization. It is described as a wall phenomenon in which the domain walls move less freely in narrowing potential wells. The referenced literature yields information concerning disaccommodation at low and very low frequencies. Nowhere does it describe disaccommodation through the susceptibility resonance spectra. Disaccommodation of the imaginary component of susceptibility is also not mentioned, probably because the losses were small at the frequencies measured. This paper attempts to partially fill these gaps.

The literature [2-8] shows that the intensity of disaccommodation of ferrite materials in the temperature range of −200 to +400 °C and the order of 100 kHz varies considerably with temperature and can be classified into intensity bands which have been attributed to various diffusion and migration processes [1, 9–15] operating upon domain walls. In a given band, the disaccommodation curve, the reciprocal of the susceptibility versus time, may be represented by an equation with a logarithmic distribution of time constants [11, 16].

Most disaccommodation measurements in this work were made near −10.0 °C. At these temperatures and 100 kHz the materials exhibited large disaccommodation and curves approximating a logarithmic distribution of time constants. Figures 1 and 2 illustrate the wide variation of disaccommodation with temperature. Lower temperatures were not available with the equipment used. Time constants and activation energies were calculated using data from these figures.

Disaccommodation as determined from the complex susceptibility of two manganese zinc ferrite materials was studied in response to demagnetizing frequency and rate, temperature, frequencies of ~20 kHz to ~2000 kHz, and rf magnetic field intensities of $\sim 10^{-4}$ oersted and $\sim 10^{-2}$ oersted.

Precise susceptibility spectra near −10.0 °C show that the resonance maxima shift to higher frequency and decrease in magnitude with increasing time after demagnetizing and that the disaccommodation rate varies considerably and changes sign with frequency. Activation energies of the order of 0.8 electron volt were computed at 100 kHz.

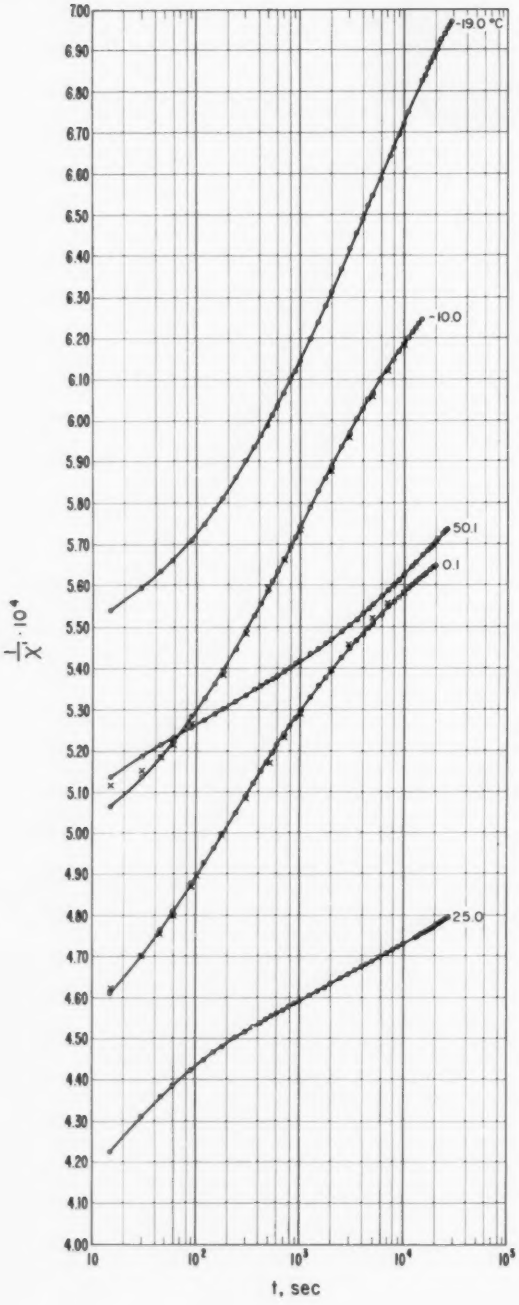

FIGURE 1. *Material A. 100 kHz disaccommodation data at various temperatures, $1/\chi'$ versus time after the completion of 20 kHz a-c field demagnetization.*

H_{rf}=8.4×10⁻⁵ oersted. The points marked with x's are calculated values using eq (4) of section 5.

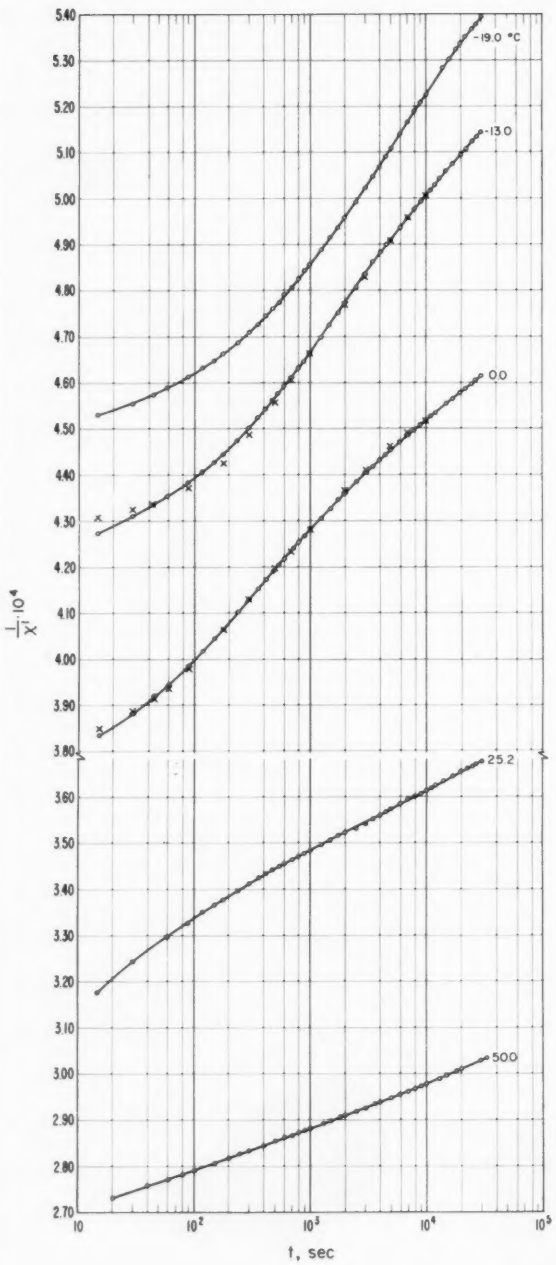

FIGURE 2. *Material B. 100 kHz disaccommodation data at various temperatures, $1/\chi'$ versus time after the completion of 20 kHz a-c field demagnetization.*

H_{rf}=8.5×10⁻⁵ oersted. The points marked with x's are calculated values using eq (4) of section 5.

2. Materials

The materials were commercial manganese zinc composition, chosen for study because of their extreme instability in susceptibility. Their chemical composition is

Material	Composition	Density
		g/cm^3
A	$Mn_{0.507}Zn_{0.265}Fe_{2.07}O_4$	4.83
B	$Mn_{0.584}Zn_{0.353}Fe_{2.05}O_4$	4.80

3. Measurement Techniques

The following are discussed: temperature equipment, demagnetization procedure, stray and radio-frequency fields, measurement details, precision and accuracy, and permittivity and resistivity of the materials.

The temperature equipment, figure 3, was designed to avoid mechanically shocking the sample and to maintain temperatures within ± 0.10 °C. These precautions were necessary to obtain precise data. An antifreeze solution was pumped at the desired temperature through the brass tubing coil inside the Dewar. Temperature was monitored by a thermoelement near the sample and adjusted by a thermostat in the antifreeze bath. Fiberglass insulation was supplied where needed. A drying agent was used in the Dewar.

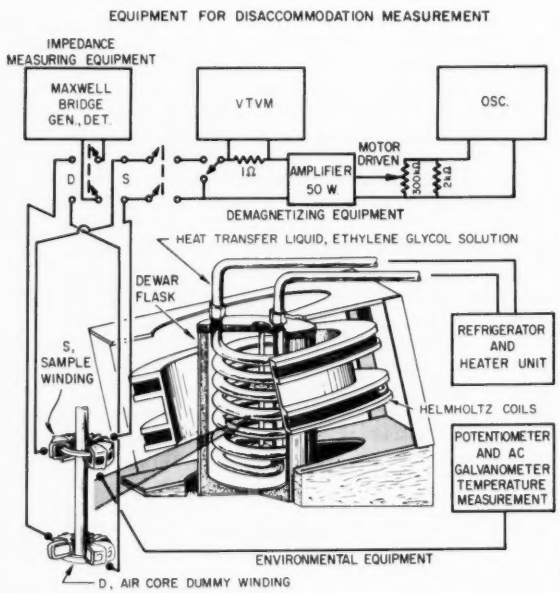

FIGURE 3. *Diagram of equipment used in obtaining experimental data.*

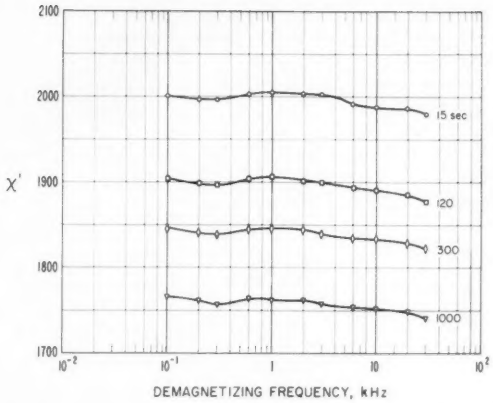

FIGURE 4. *Material A. 100 kHz susceptibility versus demagnetizing frequency at given times after the completion of a-c field demagnetization.*

$H_{rf}=8.4\times10^{-3}$ oersted. Temperature = −10.0 °C.

Since disaccommodation varies considerably with temperature, thermal demagnetization was considered impractical in this work. A-c field demagnetization in the direction of the applied rf field and of the circumference of the toroidal specimen was used [17]. A demagnetizing field of 20 kHz was applied decreasing uniformly from ~ 10 oersteds to $\sim 10^{-4}$ oersted in 0.28 second. The sample winding was switched to a rf bridge immediately afterwards. Figure 4 shows the susceptibility is a slowly varying function of the demagnetizing frequency. Increasing the demagnetizing time 2 and 3 times 0.28 second yields the same curves. The demagnetizing field did not overheat the sample; and, in the region near −10 °C, it yielded to a close approximation the same susceptibility-time curve for increments of the order of ± 33 percent in its initial value. With increments larger than +33 percent, the temperature of the sample rose because of the power dissipated in the demagnetizing winding. The susceptibility was thus changed. If the field is decreased more than 33 percent, lower susceptibility values resulted, presumably because the sample was not completely demagnetized.

The stray field was reduced to $\sim 10^{-2}$ oersted in the vicinity of the sample by using helmholtz coils, figure 3. This prevented partial magnetization of the sample. Subsequent measurements indicated this special precaution unnecessary. Values of rf magnetic field were $\sim 10^{-4}$ oersted for all measurements except for one disaccommodation magnetic spectra of material A where fields $\sim 10^{-2}$ oersted were used. Here a low pass filter was attached to the rf bridge generator at each frequency to prevent the sample from exhibiting an impedance at harmonics of the generator. Disaccommodation data at any given frequency were not affected by connecting or disconnecting the sample winding from the rf bridge or making disaccommodation measurements at other frequencies in the interim.

Impedance measurements, figure 3, of wound forms with and without the sample were made using a high precision, hf Maxwell impedance bridge at very low power levels. The sample and dummy windings were made as nearly alike as possible and had a low capacity. The winding to measure the impedance was also used to demagnetize the sample. The susceptibility was calculated [18] as follows:

$$\chi' - j\chi'' = \frac{L_{\text{sample}} - L_{\text{dummy}}}{(N_{\text{turns}})^2 L_{\text{air inductance of sample}}}$$

$$- j \frac{R_{\text{sample}} - R_{\text{dummy}}}{\omega (N_{\text{turns}})^2 L_{\text{air inductance of sample}}}.$$

In summary, to measure the sample the following procedure was used:

(1) The wound sample and the wound dummy were allowed to reach thermal equilibrium in a Dewar at the desired temperature.
(2) The field in the sample was adjusted to the desired value.
(3) The impedance of the dummy winding was measured using the bridge.
(4) The sample was demagnetized at a given frequency, generally 20 kHz, in ~0.28 second except where mentioned otherwise in the text.
(5) The sample winding was switched to the bridge operating at the desired frequency.
(6) The impedance of the sample was measured at the desired times after demagnetization while maintaining all field and temperature conditions.

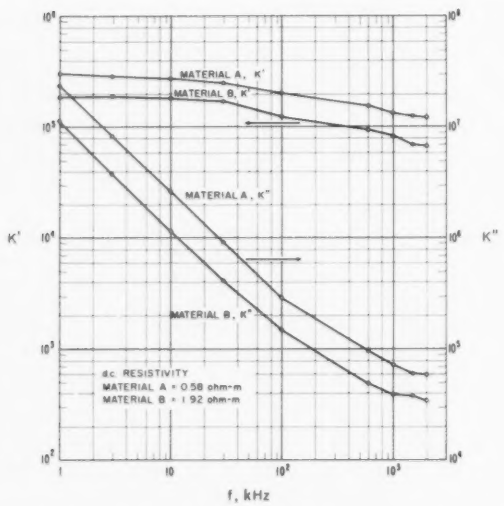

FIGURE 5. *Materials A and B. Relative complex permittivity versus frequency and d-c resistivity at ambient temperature of 23 °C.*

Repeatability of all impedance data was approximately ±0.1 percent except occasionally at the initial portion of the disaccommodation curve it was the order of ±0.2 percent. Precision was approximately ±0.05 percent to ±0.1 percent. The errors of L and R from the winding capacity were evaluated to be ~1 percent or less at 2000 kHz.

In evaluating the susceptibility error, consideration was given to dimensional effects resulting from the high permittivities of the materials [19]. Toroidal samples used to measure susceptibility were OD 2.49 cm, ID 2.24 cm and height 0.127 cm yielding a 0.127 cm × 0.127 cm square cross section. Disk and bar samples used to measure permittivity were (1) OD ~0.25 cm and height ~0.25 cm and (2) length 1.5 cm and 0.5 cm × 0.5 cm square cross section, respectively. Two terminal techniques were used to measure the properties of the disk samples, and four terminal techniques to measure the bars at lower frequencies. The two methods yielded comparable results where the data overlapped. The bars were also used to measure d-c resistivity. Data are shown in figure 5. The error in χ' and χ'' for the materials at 2000 kHz and 23 °C was estimated to be the order of 1 and 5 percent, respectively, using equations found in [19]. It is estimated the error is the same order at lower temperatures.

4. Disaccommodation Spectra Data

A description is given of disaccommodation spectra data appearing in figures 6 through 13. The various times appearing in the figures refer to the time lapsed after completion of 20 kHz demagnetization process described in section 3.

Susceptibility-temperature curves at several times, figures 6 and 7, show (1) the susceptibility of material A has a maximum at 25 °C which decreases with time and (2) the susceptibility of material B, initially linear, develops a curvature with time.

Complex susceptibility frequency spectra at the given times, figures 8 through 10, show (a) the resonance maxima shift to higher frequency, decrease in magnitude and remain left of the retreating high frequency side of the spectra; the resonance peaks broaden considerably with some reduction in magnitude when H_{rf} is increased a hundred times for material A shown in figure 9; and (b) values of the variable, $\Delta\chi' = (\chi'_{\max} - \chi'_{\text{LF min}})$, increase with time.

The real susceptibility versus time curves at various frequencies, figure 11, show that with positive increments of frequency the mean slope gradually decreases, then increases and becomes positive. The imaginary component follows a similar pattern to the region where measurements ceased. The disaccommodation varies considerably over the frequency range, the real component increasing with time at the high frequency end. These variations are observed as changes with time in the susceptibility frequency spectra. Disaccommodation data are not affected by making disaccommodation measurements at other frequencies in the interim of measurements at a given frequency.

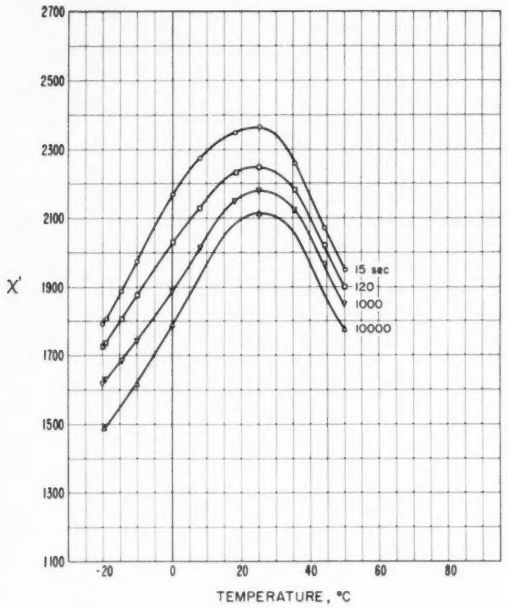

FIGURE 6. *Material A. 100 kHz disaccommodation data, χ' versus temperature at given times after the completion of 20 kHz a-c field demagnetization.*

H_{tf}=8.4×10⁻⁵ oersted.

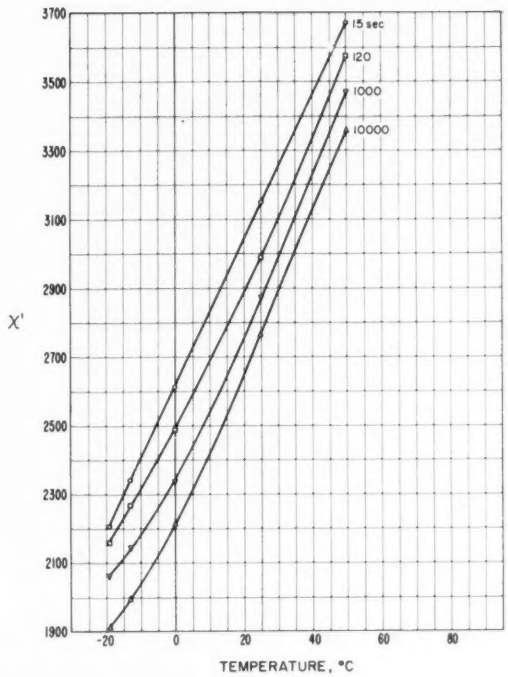

FIGURE 7. *Material B. 100 kHz disaccommodation data, χ' versus temperature at given times after the completion of 20 kHz a-c field demagnetization.*

H_{tf}=8.5×10⁻⁵ oersted.

The reciprocal of the complex susceptibility or the complex reluctivity, $\chi'/(\chi'^2+\chi''^2)$ and $\chi''/(\chi'^2+\chi''^2)$, versus time curves at various frequencies, figure 12 for material A, shows that the real component curves have positive slope tending toward zero at higher frequencies and the imaginary component, negative slope. These expressions may be useful in defining disaccommodation for the user of materials.

Disaccommodation of ferrite materials has been attributed to a domain wall related mechanism [1, 9–15, 20–22]. If the resonance found in the susceptibility spectra is predominately from domain wall motion, it was thought that the application of the domain wall equation to the data may help in understanding the disaccommodation mechanism. The spectra of these materials at room temperature show only one resonance to 100 MHz. With high zinc content it is possible that the wall resonance frequency and the rotation resonance frequency, if both exist, are close together or coalesce [23–25] Indirect evidence that domain wall motion may contribute a major role to the susceptibility are the low porosity [23], the high susceptibility, the high temperature coefficient of susceptibility [25], the large disaccommodation of the materials [14], the low resonance frequencies [23, 25], and the sharpness and magnitude of the resonance. For these reasons, the domain wall motion equation was applied to the experimental data.

The motion of an average wall under the influence of an alternating field is [23–26]

$$m\frac{d^2x}{dt^2}+\beta\frac{dx}{dt}+\alpha x=NM_sH_0\exp(j\omega t) \qquad (1)$$

where

x=the displacement of the wall from its equilibrium position;
$m=N_m/\gamma^2\delta$=wall inertia or apparent mass per unit area of wall;
$\beta=N_\beta\lambda/\gamma^2\delta$=opposing force or damping coefficient;
α=restoring force;
M_s=saturation magnetization;
$H_0\exp(j\omega t)$=applied field;
N, N_m and N_β=constants depending on the type of domain wall;
γ=magneto-mechanical ratio of an electron;
λ=relaxation frequency or damping factor from Landau Lifshitz equation of motion;
δ=Domain wall thickness.

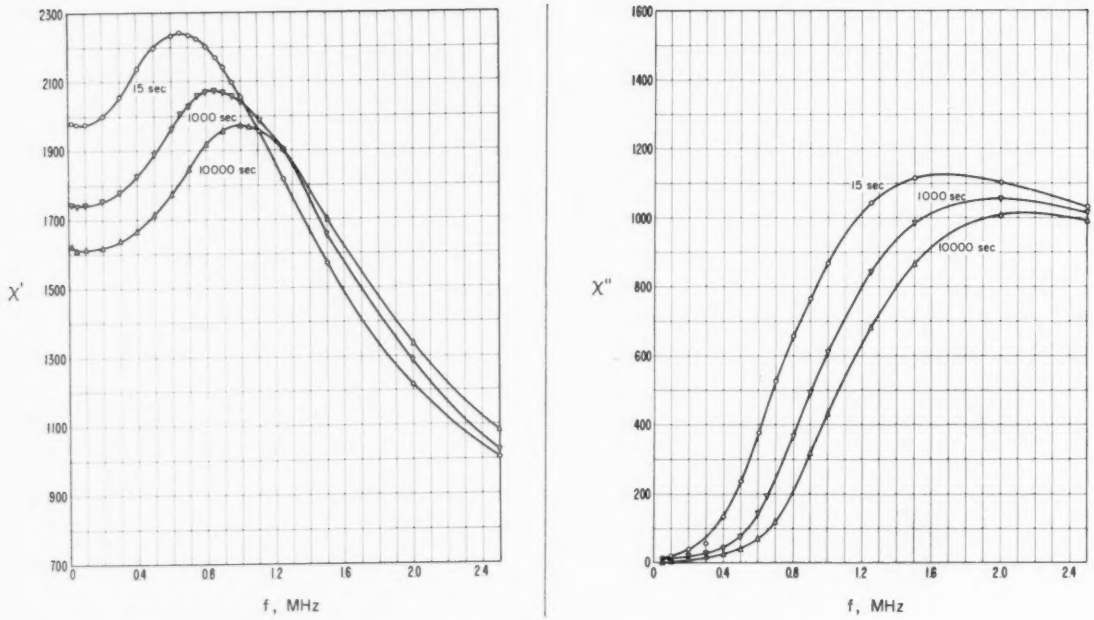

FIGURE 8. *Material A. Disaccommodation, χ' and χ'' versus frequency at given times after the completion of 20 kHz a-c field demagnetization.*

H_{rf}=8.4×10^{-5} oersted. Temperature=−10.0 °C.

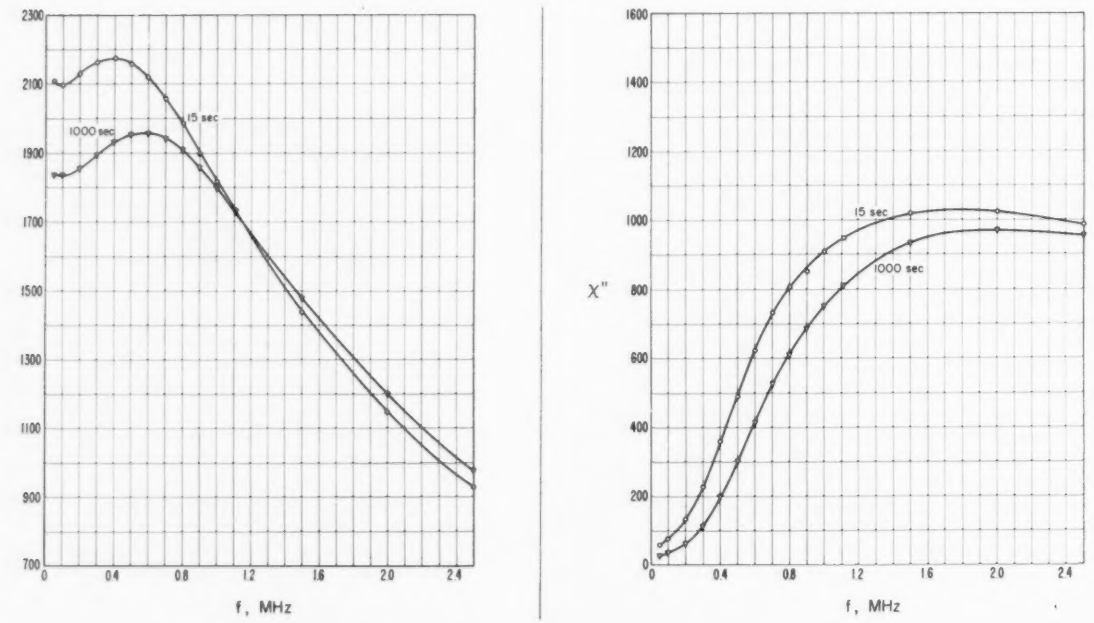

FIGURE 9. *Material A. Disaccommodation, χ' and χ'' versus frequency at given times after the completion of 20 kHz a-c field demagnetization.*

H_{rf}=8.4×10^{-3} oersted (100 times value of fig. 8). Temperature=−10.0 °C.

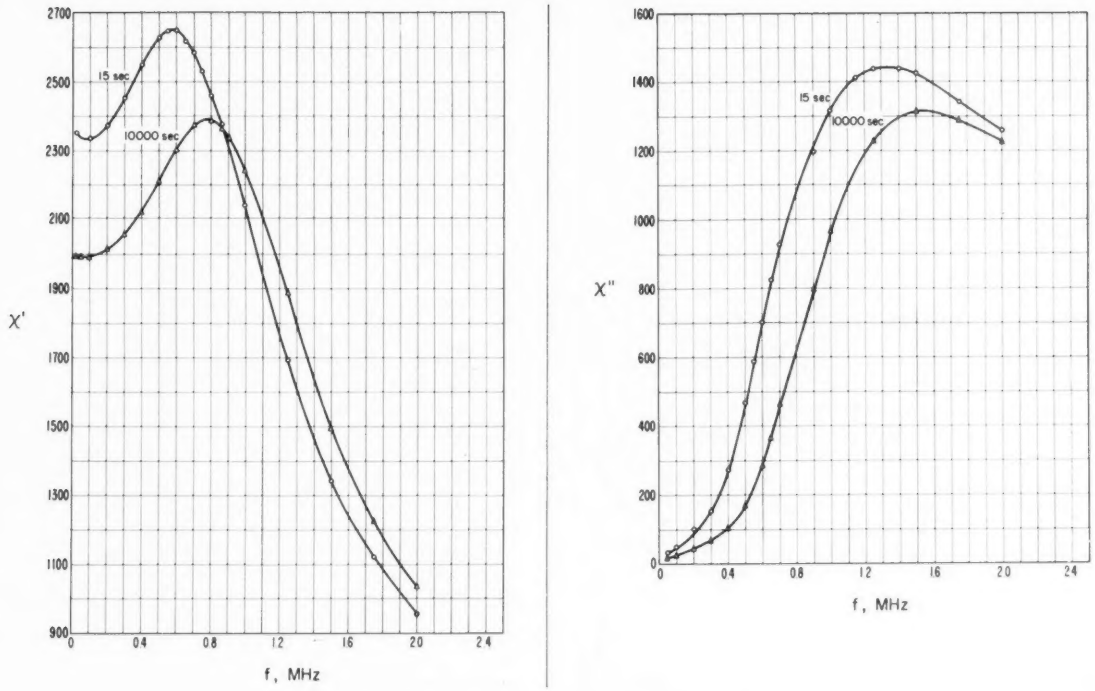

FIGURE 10. *Material B. Disaccommodation, χ' and χ'' versus frequency at given times after the completion of 20 kHz a-c field demagnetization.*

$H_{rf}=8.5\times10^{-3}$ oersted. Temperature $=-13.0$ °C.

It can be shown that [24]

$$\chi'-j\chi''=\frac{[1-(\omega/\omega_0)^2]\chi_s}{[1-(\omega/\omega_0)^2]^2+(\omega/\omega_c)^2}-j\frac{(\omega/\omega_c)\chi_s}{[1-(\omega/\omega_0)^2]^2+(\omega/\omega_c)^2} \quad (2)$$

where

$\omega_0^2=\alpha/m$

$\omega_c=\alpha/\beta$

$\chi_s=NM_s^2/\alpha d$, relative static susceptibility and

$d=$domain thickness.

Application of eq (2) to the data leads to the conclusion that the relaxation frequency, λ, and the ratio of domain wall thickness to domain thickness, δ/d, are increasing with time. If the anisotropy energy (discussed in the literature in relation to disaccommodation mechanism [13–15, 21, 22, 27–29]) is changing by a sufficiently large amount with time, the domain structure may be affected. However, any conclusions drawn from the wall equation are uncertain because it poorly fits the data. A more quantitative analysis of the data may require separating domain wall and domain rotation susceptibilities and using a distribution of ω_0 and ω_c values Other data may also be necessary. An explanation remains to be given of the changes with time in the magnetic spectra where the maxima and low frequency minima values of susceptibility are decreasing and the resonant frequencies are increasing after the demagnetization process.

5. Calculation of Time Constants and Activation Energies

The susceptibility and time relation for domain wall motion may empirically be expressed as [11, 16, 30, 31]

$$\frac{1}{\chi(t)}=\frac{1}{\chi_0}+\left(\frac{1}{\chi_\infty}-\frac{1}{\chi_0}\right)\left\{1+\frac{1}{\ln\frac{\tau_2}{\tau_1}}\left[Ei\left(-\frac{t}{\tau_2}\right)-Ei\left(-\frac{t}{\tau_1}\right)\right]\right\}. \quad (3)$$

The function in braces is designated $G(t)$ and represents a logarithmic distribution of time constants where τ_1 is the shortest and τ_2 is the longest time

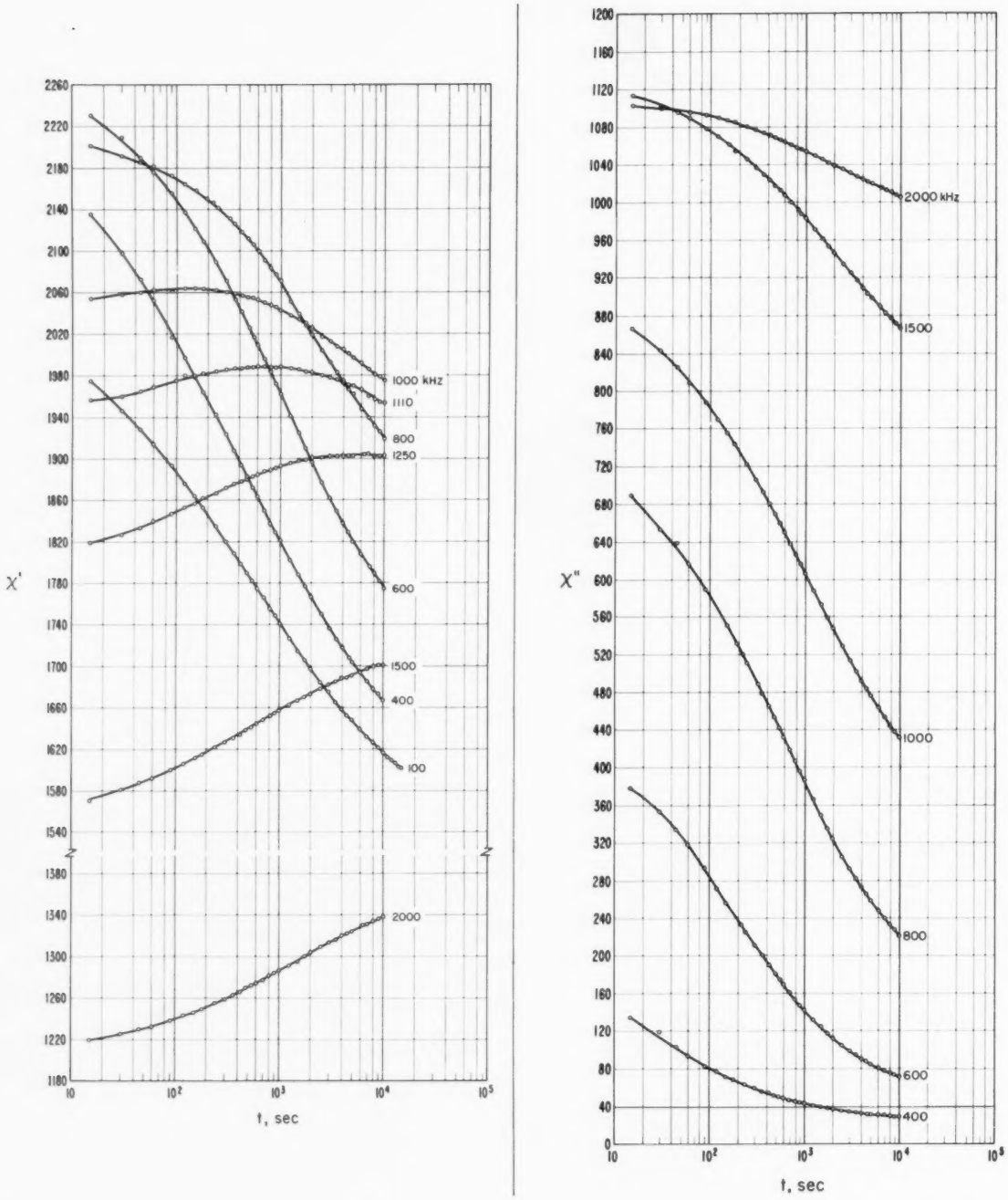

FIGURE 11. *Material A. Disaccommodation data at various frequencies, χ' and χ" versus time after the completion of 20 kHz a-c field demagnetization.*

H_{rf}=8.4×10⁻³ oersted. Temperature=−10.0 °C.

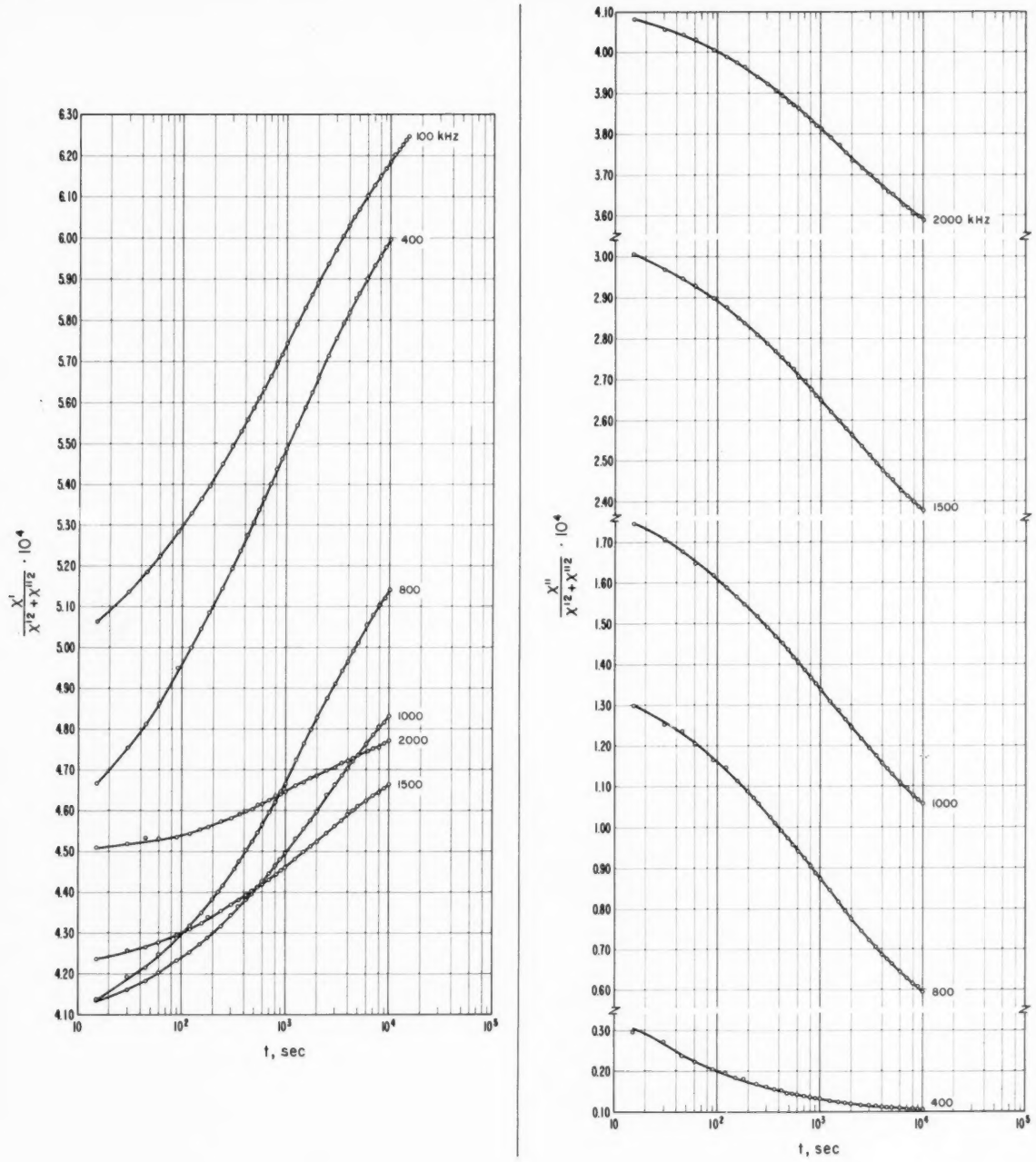

FIGURE 12. *Material A. Disaccommodation data at various frequencies, $\chi'/(\chi'^2+\chi''^2)$ and $\chi''/(\chi'^2+\chi''^2)$ versus time after the completion of 20 kHz a-c field demagnetization.*

H_{rf}=8.4×10⁻⁵ oersted. Temperature=−10.0 °C.

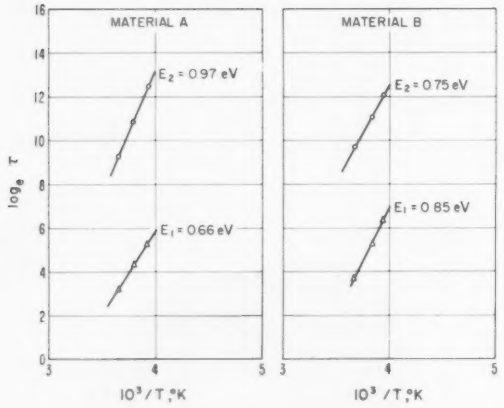

FIGURE 13. *Materials A and B. 100 kHz time constant (τ) and activation energy (E) data.*

(Equations and more data are described in section 5 and table 1 of the text.)

constant. $G(t)$ was used by Richter [32], Becker [33], and Néel [31] and may be expressed as

$$\frac{1}{\ln \tau_2/\tau_1}\int_{\tau_1}^{\tau_2}(1-e^{-t/\tau})\frac{d\tau}{\tau}.$$

It will be seen that the experimental results fit eq (3) very well.

Equation (3) may be expressed as [11]

$$\frac{1}{\chi(t)}=\frac{1}{\chi_\infty}+B\left[Ei\left(-\frac{t}{\tau_2}\right)-Ei\left(-\frac{t}{\tau_1}\right)\right] \quad (4)$$

where

$$B=\left(\frac{1}{\chi_\infty}-\frac{1}{\chi_0}\right)\frac{1}{\ln\frac{\tau_2}{\tau_1}}=\frac{1}{\chi_1}\frac{1}{\ln\frac{\tau_2}{\tau_1}}. \quad (5)$$

When $\tau_1 \ll t_B \ll \tau_2$, it can be shown that

$$\frac{1}{\chi(t_B)}=\frac{1}{\chi_\infty}+B\left(\gamma+\ln\frac{t_B}{\tau_2}\right)$$

$$=A+B\ln t_B \quad (6)$$

where $\gamma=0.5772\ldots$ The time t_B is taken from the reluctance versus $\log_{10} t$ curve in a linear region. $B\times 2.303$ is its slope and B may be expressed as

$$B=\frac{\frac{1}{\chi(t_C)}-\frac{1}{\chi(t_D)}}{2.303\,(\log_{10} t_C-\log_{10} t_D)} \quad (7)$$

where t_C and t_D are two time values chosen to obtain the slope of the linear portion of the curve.

When $t>>\tau_1$.

$$\frac{1}{\chi(t)}=\frac{1}{\chi_\infty}+BEi\left(-\frac{t}{\tau_2}\right). \quad (8)$$

Hence the following expression is derived to obtain τ_2 through successive approximations

$$Ei\left(-\frac{t}{\tau_2}\right)+\ln\tau_2=\frac{\frac{1}{\chi(t)}-\frac{1}{\chi(t_B)}}{B}+\gamma+\ln t_B. \quad (9)$$

In the data of this paper $t=10^4$ seconds has been used in eq (9).

It can also be shown that for $\tau_1<<t_B<<\tau_2$

$$\frac{1}{\chi(t_B)}=\frac{1}{\chi_0}+B\left(\gamma+\ln\frac{t_B}{\tau_1}\right) \quad (10)$$

and at a time $t_A<<t_B$

$$\frac{1}{\chi(t_A)}=\frac{1}{\chi_0}+B\left(\gamma+\ln\frac{t_A}{\tau_1}-Ei\left(-\frac{t_A}{\tau_1}\right)\right). \quad (11)$$

From eqs (10) and (11), the following is derived to find τ_1

$$-Ei\left(-\frac{t_A}{\tau_1}\right)=\frac{\frac{1}{\chi(t_A)}-\frac{1}{\chi(t_B)}+B\ln\frac{t_B}{t_A}}{B}. \quad (12)$$

The activation energy may be determined from Arrhenius' relationship

$$\tau=\tau_\infty e^{E/\kappa T} \quad (13)$$

and

$$\tau_1=\tau_{\infty 1}e^{E_1/\kappa T}$$

$$\tau_2=\tau_{\infty 2}e^{E_2/\kappa T}.$$

The activation energy equals the slope of the $\ln\tau$ versus $10^3/T(°K^{-1})$ curve $\times\kappa$. See figure 13 and table 1.

Calculated data, $(1/\chi')$ versus time, from eq (4) are compared to experimental data in figures 1 and 2.

TABLE 1. *Materials A and B*

Activation energies and time constants at 100 kHz computed by method described in section 5

Material	Temperature	τ_1	τ_2	E_1	E_2	E_0
	°C	sec	sec	eV	eV	eV
A	−10.0	76.6	4.8×10^4	0.66	0.97	0.82
B	−13.0	174	5.9×10^4	.85	.75	.80

The author thanks R. S. Yoshida for making many measurements, calculations and figures, for winding samples, and for making instrumentation

improvements; J. L. Ivey for the arrangement of the Helmholtz coils and the demagnetizing equipment and for his helpful suggestions; R. D. Harrington for his astute observations and suggestions; M. B. Lindell for constructing instruments; J. L. Dalke for his encouragement; and H. C. Leistner and A. J. Pannone for preparing samples.

6. References

[1] Snoek, J. L., New developments in ferromagnetic materials, Elsevier Publ. Co., New York, N.Y., 2d ed., 139 pp. (1949).

[2] Marais, A., and Merceron, Th., Disaccommodation of the permeability of nickel-zinc ferrites, C. R. Acad. Sci. **248,** 2976–2978 (May 25, 1959) (In French).

[3] Marais, A., and Merceron, Th., Disaccommodation of the permeability of nickel-zinc ferrites, C. R. Acad. Sci. **249,** 2511–2513 (Dec. 9, 1959) (In French).

[4] Krupička, S., and Vilim, F., Magnetic relaxation spectrum of ferrites $Mn_zFe_{3-z}O_{4+\gamma}$, Czech. J. Phys. **B11,** No. 1, 10–17 (1961).

[5] Krupička, S., A note on magnetic after-effect in iron rich ferrites, Czech. J. Phys. **B11,** No. 1, 457–459 (1961).

[6] Okada, T., and Yamadaya, T., Role of cation vacancies in disaccommodation of manganese ferrite, J. Phys. Soc. Japan **17,** 1799 (1962).

[7] Krupička, S., Study of relaxation spectrum of $Mn_zFe_{3-z}O_{4+\gamma}$ ferrites, J. Phys. Soc. Japan **17,** Suppl. B–1, 304–308 (1962).

[8] Braginski, A., Marais, A., and Merceron, Th., Magnetic after-effect in solid solutions of Mn and Ni ferrites with magnetite, J. Phys. Soc. Japan **17,** Suppl. B–1, 300–303 (1962).

[9] Enz, U., Relations between disaccommodation and magnetic properties of manganese-ferrous ferrite, Physica **XXIV,** 609–624 (1958).

[10] Ohta, K., Time decrease of magnetic permeability in some mixed ferrites, J. Phys. Soc. Japan **16,** No. 2, 250–258 (Feb. 1961).

[11] Krupička, S., Study of magnetic after-effect in magnesium manganese ferrite, Czech. J. Phys. **10,** No. 11, 782–810 (1960).

[12] Iida, S., Mechanism of disaccommodation in ferrites, J. Phys. Soc. Japan **17,** No. 1, 123–127 (Jan. 1962).

[13] Yanase, A., Mechanism of disaccommodation in ferrite, J. Phys. Soc. Japan **17,** No. 6, 1005–1011 (June 1962).

[14] Ohta, K., and Yamadaya, T., Induced magnetic anisotropy and disaccommodation of manganese-zinc ferrites, J. Phys. Soc. Japan **17,** Suppl. B–1, 291–295 (1962).

[15] Braginski, M., and Merceron, Th., Influence of walls on after-effect phenomena, J. Phys. Radium **23,** No. 10, 876–877 (1962) (In French).

[16] Brissonneau, P., Magnetism—On the determination of the time constants of the magnetic after-effect from diffusion, Comp. Rend. Acad, Sci. **244,** 1174–1177 (Feb. 25, 1957) (In French).

[17] Rathenau, G. W., and Fast, J. F., Initial permeabilities of sintered ferrites, Physica **XXI,** 964–970 (1955).

[18] Harrington, R. D., and Danielson, B. L., A technique for reducing errors in permeability measurements with coils, Proc. IRE **48,** No. 3, 365–366 (March 1960).

[19] Brockman, F. W., Dowling, P. H., and Steneck, W. G., Dimensional effects resulting from a high dielectric constant found in a ferromagnetic ferrite, Phys. Rev. **77,** No. 1, 85–93 (1950).

[20] Krupička, S., and Gerber, R., A contribution to studying the mechanism of permeability disaccommodation in ferrites, Czech. J. Phys. **10,** No. 2, 158–160 (1960).

[21] Schnettler, F. J., and Gyorgy, E. M., Origin of the induced magnetic anisotropy in nickel ferrite, J. Appl. Phys. **35,** No. 2, 330–334 (Feb. 1964).

[22] Gyorgy, E. M., and Schnettler, F. M., Induced anisotropy in YIG and Si and Mn additions, J. Appl. Phys, **35,** No. 3, Part 2, 1067–1068 (March 1964).

[23] Pippin, J. E., and Hogan, C. L., Initial permeability spectra in ferrites and garnets, Scientific Report No. 1. Contract AF 19 (604)–1084, Gordon McKay Laboratory, Harvard University, 39 pp. (April 1959).

[24] Rado, G. T., Wright, R. W., and Emerson, W. H., Ferromagnetism at very high frequencies III. Two mechanisms of dispersion in a ferrite, Phys. Rev. **80,** No. 2, 273–280 (Oct. 1950).

[25] Rado, G. T., Magnetic spectra of ferrites, Rev. Mod. Phys. **25,** No. 1, 81–89 (Jan. 1953).

[26] Rado, G. T., On the inertia of oscillating ferromagnetic domain walls, Phys. Rev. **83,** No. 4, 821–826 (Aug. 1951).

[27] Kubota, B., Yanase, A., Taward, Y , and Neichi, Y., Induced anisotropy in iron rich nickel ferrite with a small cobalt substitution, J. Phys. Soc. Japan **17,** Suppl. B–1, 296–299 (1962).

[28] Iida, S., and Inoue, T., Theoretical and experimental study of the induced anisotropy in iron cobalt ferrites and disaccommodation phenomena in ferrites, J. Phys. Soc. Japan **17,** Suppl. B–1, 281–287 (1962).

[29] Ohta, K., Magnetocrystalline anisotropy and magnetic permeability of Mn-Zn-Fe ferrites, J. Phys. Soc. Japan **18,** No. 5, 685–690 (May 1963).

[30] Brissonneau, P., Contribution a l'etude quantitative du traînage magnétique de diffusion du carbone dans le fer α, J. Phys. Chem. Solids **7,** 22–51 (Feb. 1958).

[31] Neel, M. L., Théorie Du traînage magnétique de diffusion, J. Phys. Radium **13,** No. 5, 249–264, (May 1952).

[32] Richter, G., Über die magnetische Nachwirkung am carbony Leisen, Ann. Physik **29,** 605–635 (1937).

[33] Becker, R., and Döring, W., Ferromagnetismus, Verlag von Julius Springer, Berlin (1939); Photo Lithoprint Reproduction, Edwards Brothers, Inc., Ann Arbor, Mich. (1943).

(Paper 69A2–339)

JOURNAL OF RESEARCH of the National Bureau of Standards—A. Physics and Chemistry
Vol. 69A, No. 2, March–April, 1965

Splitting of a Set of Equivalent Sites in Centrosymmetric Space Groups Into Subsets Under Homogeneous Stress

J. B. Wachtman, Jr., and H. S. Peiser

(November 18, 1964)

It is assumed that the symmetry operations possessed by a homogeneously stressed crystal will be those common to the crystal and to the macroscopic state of stress. Application of stress either leaves a space group unaltered or lowers it to a subgroup. Such lowering can always be considered to take place in successive steps each of which leaves no group intermediate between the starting group and the subgroup. Each such step can be accomplished by a uniaxial stress; for the centrosymmetric space groups, all but one of the symmetry reductions consisting of two or more successive steps can also be accomplished by a uniaxial stress. A set of sites all of which are equivalent in the unstrained crystal may split into two or more subsets under stress. For each space group all possibilities are taken into account by considering the behavior of the general position (most general set of symmetry related sites) because the behavior of each special position can easily be derived by specializing the description of the general position. The splitting of the general position under homogeneous stress is tabulated for all possibilities for each centrosymmetric space group.

1. Introduction

The reduction of the symmetry of crystals and the accompanying introduction of inequivalence of sites within crystals is not only a subject of interest for its own sake, but is also important in several areas of solid state physics. The present writers became interested from the standpoint of internal friction studies. In such studies, stress is applied to a crystal to lower its symmetry and cause a partial ordering of defects. This subject has been developed extensively [1–5] [1] and other possible applications of stress-induced symmetry lowering have also been discussed [6]. The present paper is limited to a tabulation of the splitting of sets of initially equivalent sites into subsets under homogeneous stress.

2. Specification of Stress or Strain

It is possible to formulate the present paper in terms of either stress or strain, but stress appears to be somewhat more appropriate as we shall subsequently point out in connection with Curie's principle. We restrict consideration to homogeneous stress; i.e., to stress which varies with location slowly enough that it may be assumed constant over a number of unit cells.

Stress is a second-rank, symmetric tensor [7] and therefore has six independent components in an arbitrary rectangular Cartesian coordinate system. For any given state of stress, a rotated coordinate system (called the principal axis system and designated X, Y, Z) can be found in which the stress can be described by at most three nonzero components; i.e., the stress tensor is diagonalized. The six independent components are thus specified by three angles giving the orientation of the principal axis system and three diagonal components in this system. Any state of homogeneous stress can then be characterized as being uniaxial, biaxial, or triaxial according to the number of nonzero components in the principal axis system. This specification of the six quantities describing stress (or any other symmetric second-rank tensor) can be visualized in terms of the orientation, shape, and size of the representation quartic. If σ_{ij} denotes the components of the stress in a set of rectangular Cartesian coordinates x_i and if we define a surface made up of points (x_1, x_2, x_3) satisfying

$$\sum_{i,j=1}^{3} \sigma_{ij} x_i x_j = 1 \qquad (1)$$

we obtain a surface called the representation quartic. If we transform the stress to the principal axis system, all cross terms vanish. It is then easy to see that, if the three components of stress in the principal axis system are all larger than zero, the surface is an ellipsoid. Cases where one, two, or all three of the principal stresses are negative correspond respectively to a hyperboloid of one sheet, a hyperboloid of two sheets, and to an imaginary ellipsoid [7]. It is, however, not necessary to consider negative stress components in this paper because we are concerned only with the symmetry of the stress and this symmetry is unchanged if one or more of the principal stresses change sign.

We can thus describe any triaxial stress by giving the shape, size, and orientation of an ellipsoid. This description has the advantage of ease of visualization, but requires us to specialize to fewer dimensions for biaxial or uniaxial stress; the appropriate figures are an ellipse and the two ends of a straight line segment respectively. We can retain the advantage of easy visualization and deal only with three-dimensional figures by introducing the modified stress ellipsoid

[1] Figures in brackets indicate the literature references at the end of this paper.

which is the figure obtained by adding an arbitrary value of isostatic stress to the state of stress being considered. This addition is permissible in dealing with symmetry changes caused by stress because an isostatic stress should cause no change of crystal symmetry. The modified stress ellipsoid for uniaxial stress is thus an ellipsoid of revolution with its unique axis pointing in the direction of the uniaxial stress. The modified stress ellipsoid for biaxial stress is one with three unequal axes as is the modified stress ellipsoid for triaxial stress; these two ellipsoids can be distinguished only by comparing the size of the principal axes with the value of the assumed isostatic stress. The fact that one cannot distinguish between biaxial and triaxial stress from the shape of the modified stress ellipsoid alone causes no difficulty in the present application because any reduction of crystal symmetry that can be caused by stress can be accomplished by biaxial stress. Isostatic stress can lead to mechanical relaxation by changing the degree of inequivalence of sites that are already inequivalent. This is illustrated, for example, by the isostatic relaxation modes discussed by Franklin [8]. Such cases do not concern us here because we are restricting consideration to inequivalence of sites that are equivalent in the absence of stress.

Stresses applied to a given crystal can be classified into three types depending on the effect on the symmetry of the crystal. First, and most highly specialized, is stress that causes no reduction of symmetry. This is the type in which the modified stress ellipsoid has all of the symmetry elements of the crystal and has them in the same orientation as the crystal. Examples are isostatic stress applied to any crystal or uniaxial stress applied parallel to the unique axis of a tetragonal, hexagonal, or trigonal crystal. Second, and less specialized, is stress that causes a minimum step of symmetry lowering; that is, symmetry lowering such that there is no space group which is a stress-induced subgroup of the original group, which is also a supergroup of the final group, and which is distinct from both initial and final groups. Third, and least specialized, is stress that causes a compound step of symmetry lowering, i.e., which does leave one or more distinct space groups intermediate between the initial and final space groups. In this paper, we specify the stress for all the possible minimum steps and compound steps that can be caused by homogeneous stress.

In specifying stress, we need only specify (1) whether two of the axes X, Y, Z of the modified stress ellipsoid are equal (if so, Z is taken as the unique axis) and (2) the orientation of these axes. In giving these specifications, we adopt the convention that there is no equality of axes and no specialization of orientation unless explicitly stated. Our intention in this paper is to give the most general (i.e., least specialized) stress that will accomplish each symmetry reduction. From an experimental point of view, one might wish to know what is the most highly specialized stress that can be used, because it is easier to apply uniaxial stress than biaxial stress. We shall leave detailed treatment of this subject to a subsequent paper and simply state the result that any minimum step can be done by uniaxial stress. For the centrosymmetric space groups, any compound step can also be done by uniaxial stress, with the exception that biaxial stress is required to reach space groups associated with one of the two nonequivalent orientations in which mmm occurs as a subgroup of m3m.

The strain can be specified by an ellipsoid in exactly the same way as the stress and a modified strain ellipsoid can be introduced to correspond to the modified stress ellipsoid. For an elastically isotropic body, the principal axes of the modified strain ellipsoid have the same orientation as the principal axes of the modified stress ellipsoid. Crystals are usually elastically anisotropic, however, and the principal axes of the two modified ellipsoids need not be parallel. The lowering of crystal symmetry can, if desired, be discussed in terms of the modified stress ellipsoid without error because we are concerned only with the retention of symmetry by the stressed crystal. To be retained a symmetry element must belong to the unstressed crystal and the modified stress ellipsoid (Curie's principle [6]); it must therefore also be possessed by the strain ellipsoid. We could thus use the modified strain ellipsoid in our discussion, but it is conceptually simpler to use the modified stress ellipsoid.

3. Effect of Symmetry Lowering on Space Groups

3.1. Reduction of Point-Group Symmetry

The point groups are discussed in this paper primarily because the stress required to lower a given space group to a subgroup can be specified completely in terms of the corresponding point group, i.e., the specification is the same for any space-group reduction corresponding to the reduction from one point group to another. This permits the space-group results to be collected into tables, each of which consists of all transitions from one space group to another associated with reduction from a given point group to another. The stress can thus be described once for each table provided the specification is given in terms of axes that are fixed with respect to the point group. For two space groups associated with the same point group the axes used in the International Tables [9] are not always taken in the same orientation relative to the point groups. In the centrosymmetric space goups this complication arises only for $\bar{3}$m. For all tables other than table 8 each specification of stress is the same for all of the space groups in that table.

As noted in the preceding section, we are giving the most general specification of stress, despite the fact that more specialized stresses may be of interest in some applications. Such specializations can be discussed in terms of the point groups alone and so are being left for treatment in a paper devoted to point groups.

3.2. Reduction of Space-Group Symmetry

In considering the subgroup reached from a given space group, we again assume that the subgroup has the symmetry common to the starting group and the stress. For the symmorphic space groups (those which contain their point groups), we can again take the symmetry of the stress to be that of the modified stress ellipsoid, but for the nonsymmorphic space groups, we must extend our understanding of "symmetry of the stress" to include all glide planes parallel to mirror planes of the modified stress ellipsoid and all screw axes parallel to rotation axes of the same order possessed by the modified stress ellipsoid. The possible stress-induced reductions of space groups have been tabulated [6].

3.3. Mapping of General Positions

A general position (set of symmetry-related but unspecialized sites) in a starting space group must remain a general position in a subgroup because no symmetry can be gained by application of stress. The number of sites in the general position per lattice point in the starting space group is equal to the order, N, of the point group associated with the starting space group. In going to a subgroup with associated point group of order n, this set of N sites must split into N/n subsets, each of which contains n sites and is a general position of the final space group. Table 1 through 12 give the coordinates (referred to the axes of the starting space group) of these subsets. In these tables, we have used the coordinates of the International Tables [9]; where a choice of origin is given, we have taken the origin at a center of symmetry in order to permit coordinates with $\pm$ prefix to indicate a pair of sites. For the rhombohedral space groups, we have used hexagonal axes despite the resulting triple cell, because hexagonal axes seem to be preferred by most workers.

To illustrate the use of tables 1 through 12 consider, for example, space group P2/m associated with point group 2/m, which goes to space group $P\bar{1}$ associated with point group $\bar{1}$ under the action of a stress that is not specially oriented to preserve the 2/m symmetry. In P2/m, the general site (x, y, z) is carried by the symmetry operations into the equivalent sites $(-x, -y, -z)$, $(+x, -y, +z)$, and $(-x, +y, -z)$. Under the action of the symmetry operations remaining in $P\bar{1}$, the site (x, y, z) is carried only into $(-x, -y, -z)$ and these two sites form a general position in $P\bar{1}$. The site $(+x, -y, +z)$ is equivalent to $(-x, +y, -z)$ and these two together also form a general position in $P\bar{1}$. This mapping of the complete set of four equivalent sites making up a general position in P2/m onto two distinct subsets each of which composes a general position in $P\bar{1}$ is indicated in the tables by listing the sites making up a general position for P2/m in the two subsets $\{\pm(x, y, z)\}$ and $\{\pm(x, \overline{y}, z)\}$.

Note that the coordinates (x, y, z) of a site have one set of values (x_1, y_1, z_1) in the first subset and another set of values (x_2, y_2, z_2) in the second subset. This is true throughout the tables; whenever a set of equivalent sites splits into subsets, the coordinates of any site in the stressed crystal are related by symmetry to those of the other sites in the same subset, but are not so related to the coordinates of sites in other subsets, and are distinct from the original coordinates in the unstressed crystal. This distinction is brought out in the tables by keeping the coordinates of sites in different subsets in different columns rather than by using subscripts.

A given point group may occur in more than one orientation as a subgroup of an initial point group. These two settings may be equivalent (i.e., one is generated from the other by a symmetry operation of the initial point group) or inequivalent. Equivalent settings of subgroups of point groups correspond to equivalent settings of subgroups of space groups and need not be considered separately. Inequivalent settings correspond to physically distinct symmetry lowerings and are listed separately in the tables. See, for example, the two inequivalent ways in which mmm can occur as a subgroup of 4/mmm (both given in one table, 6, by use of top and bottom captions) and the three ways 2/m can result from mmm. The occurrence of two or more inequivalent settings of a subgroup can be shown by two or more parallel tie lines on a decomposition chart, as was done for the point groups by the Internationale Tabellen [10].

A second example will illustrate both the possibility of alternative space groups associated with the same point group and the situation which arises when the number of lattice points per cell changes: consider the behavior of Cmmm under a stress oriented to lower mmm to 2/m. This reduction can be done by letting one axis of the modified stress ellipsoid coincide with any one of the three diad axes in mmm. We use the convention of the International Tables [9] and take our x, y, z axes in the same orientation relative to the space group operations, i.e., x and y axes in the plane of the diagram as shown in the International Tables with origin at upper left-hand corner. The positive direction of the x axis is downward in the page and that of the y axis is to the right in the page, the interaxial angle is determined by the symmetry. The positive z axis points upward from the page; its angular relations to the other two axes are determined by symmetry. If one axis of the modified stress ellipsoid is taken parallel to either the x or y axis of Cmmm and otherwise unspecialized the space group C2/m is obtained. If, however, an axis of the modified stress ellipsoid is taken parallel to z, the space group P2/m is obtained. We have gone from a face-centered cell with two lattice points per cell to a cell with one lattice point. This causes no difficulty in the tables, however, because we list the sites associated with a lattice point rather than a cell. Thus, the set of general sites in Cmmm splits into the subsets $\{\pm(x, y, z), \pm(x, y, \overline{z})\}$ and $\{\pm(x, \overline{y}, \overline{z}), \pm(x, \overline{y}, z)\}$. Each of these subsets must map onto the set of sites making up the general position of

TABLE 1. *Reduction from m3m to 4/mmm*

Space group of unstrained crystal order 48 per lattice point		If stressed so that $X=Y$, $z \| Z$			Space group of strained crystal order 16 per lattice point	
		Coordinates referred to axes of unstrained crystal				
No.	Symbol	1st Subset	2d Subset	3d Subset	No.	Symbol
221	Pm3m	$\pm(x, y, z)\pm(x, y, \bar{z})$ $\pm(x, \bar{y}, z)\pm(x, \bar{y}, \bar{z})$ $\pm(y, x, z)\pm(y, x, \bar{z})$ $\pm(y, \bar{x}, z)\pm(y, \bar{x}, \bar{z})$	$\pm(y, z, x)\pm(y, z, \bar{x})$ $\pm(y, \bar{z}, x)\pm(y, \bar{z}, \bar{x})$ $\pm(z, y, x)\pm(z, y, \bar{x})$ $\pm(z, \bar{y}, x)\pm(z, \bar{y}, \bar{x})$	$\pm(z, x, y)\pm(z, x, \bar{y})$ $\pm(z, \bar{x}, y)\pm(z, \bar{x}, \bar{y})$ $\pm(x, z, y)\pm(x, z, \bar{y})$ $\pm(x, \bar{z}, y)\pm(x, \bar{z}, \bar{y})$	123	P4/mmm
222	Pn3n	$\pm(x, y, z)\pm(\frac{1}{2}+x, \frac{1}{2}+y, \bar{z})$ $\pm(\frac{1}{2}+x, \bar{y}, \frac{1}{2}+z)\pm(x, \frac{1}{2}-y, \frac{1}{2}-z)$ $\pm(\frac{1}{2}+y, \frac{1}{2}+x, \frac{1}{2}+z)\pm(y, x, \frac{1}{2}-z)$ $\pm(y, \frac{1}{2}-x, z)\pm(\frac{1}{2}+y, \bar{x}, \bar{z})$	$\pm(y, z, x)\pm(\frac{1}{2}+y, \frac{1}{2}+z, \bar{x})$ $\pm(\frac{1}{2}+y, \bar{z}, \frac{1}{2}+x)\pm(y, \frac{1}{2}-z, \frac{1}{2}-x)$ $\pm(\frac{1}{2}+z, \frac{1}{2}+y, \frac{1}{2}+x)\pm(z, y, \frac{1}{2}-x)$ $\pm(z, \frac{1}{2}-y, x)\pm(\frac{1}{2}+z, \bar{y}, \bar{x})$	$\pm(z, x, y)\pm(\frac{1}{2}+z, \frac{1}{2}+x, \bar{y})$ $\pm(\frac{1}{2}+z, \bar{x}, \frac{1}{2}+y)\pm(z, \frac{1}{2}-x, \frac{1}{2}-y)$ $\pm(\frac{1}{2}+x, \frac{1}{2}+z, \frac{1}{2}+y)\pm(x, z, \frac{1}{2}-y)$ $\pm(x, \frac{1}{2}-z, y)\pm(\frac{1}{2}+x, \bar{z}, \bar{y})$	126	P4/nnc
223	Pm3n	$\pm(x, y, z)\pm(x, y, \bar{z})$ $\pm(x, \bar{y}, z)\pm(x, \bar{y}, \bar{z})$ $\pm(\frac{1}{2}+y, \frac{1}{2}+x, \frac{1}{2}+z)\pm(\frac{1}{2}+y, \frac{1}{2}+x, \frac{1}{2}-z)$ $\pm(\frac{1}{2}+y, \frac{1}{2}-x, \frac{1}{2}+z)\pm(\frac{1}{2}+y, \frac{1}{2}-x, \frac{1}{2}-z)$	$\pm(y, z, x)\pm(y, z, \bar{x})$ $\pm(y, \bar{z}, x)\pm(y, \bar{z}, \bar{x})$ $\pm(\frac{1}{2}+z, \frac{1}{2}+y, \frac{1}{2}+x)\pm(\frac{1}{2}+z, \frac{1}{2}+y, \frac{1}{2}-x)$ $\pm(\frac{1}{2}+z, \frac{1}{2}-y, \frac{1}{2}+x)\pm(\frac{1}{2}+z, \frac{1}{2}-y, \frac{1}{2}-x)$	$\pm(z, x, y)\pm(z, x, \bar{y})$ $\pm(z, \bar{x}, y)\pm(z, \bar{x}, \bar{y})$ $\pm(\frac{1}{2}+x, \frac{1}{2}+z, \frac{1}{2}+y)\pm(\frac{1}{2}+x, \frac{1}{2}+z, \frac{1}{2}-y)$ $\pm(\frac{1}{2}+x, \frac{1}{2}-z, \frac{1}{2}+y)\pm(\frac{1}{2}+x, \frac{1}{2}-z, \frac{1}{2}-y)$	131	$P4_2/mmc$
224	Pn3m	$\pm(x, y, z)\pm(\frac{1}{2}+x, \frac{1}{2}+y, \bar{z})$ $\pm(\frac{1}{2}+x, \bar{y}, \frac{1}{2}+z)\pm(x, \frac{1}{2}-y, \frac{1}{2}-z)$ $\pm(y, x, z)\pm(\frac{1}{2}+y, \frac{1}{2}+x, \bar{z})$ $\pm(\frac{1}{2}+y, \bar{x}, \frac{1}{2}+z)\pm(y, \frac{1}{2}-x, \frac{1}{2}-z)$	$\pm(y, z, x)\pm(\frac{1}{2}+y, \frac{1}{2}+z, \bar{x})$ $\pm(\frac{1}{2}+y, \bar{z}, \frac{1}{2}+x)\pm(y, \frac{1}{2}-z, \frac{1}{2}-x)$ $\pm(z, y, x)\pm(\frac{1}{2}+z, \frac{1}{2}+y, \bar{x})$ $\pm(\frac{1}{2}+z, \bar{y}, \frac{1}{2}+x)\pm(z, \frac{1}{2}-y, \frac{1}{2}-x)$	$\pm(z, x, y)\pm(\frac{1}{2}+z, \frac{1}{2}+x, \bar{y})$ $\pm(\frac{1}{2}+z, \bar{x}, \frac{1}{2}+y)\pm(z, \frac{1}{2}-x, \frac{1}{2}-y)$ $\pm(x, z, y)\pm(\frac{1}{2}+x, \frac{1}{2}+z, \bar{y})$ $\pm(\frac{1}{2}+x, \bar{z}, \frac{1}{2}+y)\pm(x, \frac{1}{2}-z, \frac{1}{2}-y)$	134	$P4_2/nnm$
225	Fm3m	$\pm(x, y, z)\pm(x, y, \bar{z})$ $\pm(x, \bar{y}, z)\pm(x, \bar{y}, \bar{z})$ $\pm(y, x, z)\pm(y, x, \bar{z})$ $\pm(y, \bar{x}, z)\pm(y, \bar{x}, \bar{z})$	$\pm(y, z, x)\pm(y, z, \bar{x})$ $\pm(y, \bar{z}, x)\pm(y, \bar{z}, \bar{x})$ $\pm(z, y, x)\pm(z, y, \bar{x})$ $\pm(z, \bar{y}, x)\pm(z, \bar{y}, \bar{x})$	$\pm(z, x, y)\pm(z, x, \bar{y})$ $\pm(z, \bar{x}, y)\pm(z, \bar{x}, \bar{y})$ $\pm(x, z, y)\pm(x, z, \bar{y})$ $\pm(x, \bar{z}, y)\pm(x, \bar{z}, \bar{y})$	139	I4/mmm
226	Fm3c	$\pm(x, y, z)\pm(x, y, \bar{z})$ $\pm(x, \bar{y}, z)\pm(x, \bar{y}, \bar{z})$ $\pm(y, x, \frac{1}{2}+z)\pm(y, x, \frac{1}{2}-z)$ $\pm(y, \bar{x}, \frac{1}{2}+z)\pm(y, \bar{x}, \frac{1}{2}-z)$	$\pm(y, z, x)\pm(y, z, \bar{x})$ $\pm(y, \bar{z}, x)\pm(y, \bar{z}, \bar{x})$ $\pm(z, y, \frac{1}{2}+x)\pm(z, y, \frac{1}{2}-x)$ $\pm(z, \bar{y}, \frac{1}{2}+x)\pm(z, \bar{y}, \frac{1}{2}-x)$	$\pm(z, x, y)\pm(z, x, \bar{y})$ $\pm(z, \bar{x}, y)\pm(z, \bar{x}, \bar{y})$ $\pm(x, z, \frac{1}{2}+y)\pm(x, z, \frac{1}{2}-y)$ $\pm(x, \bar{z}, \frac{1}{2}+y)\pm(x, \bar{z}, \frac{1}{2}-y)$	140	I4/mcm

| | | |

TABLE 2. *Reduction from m3m to $\bar{3}m$*

Space group unstrained crystal order 48 per lattice point		If stressed so that $X=Y$, $[111] \parallel Z$				Space group unstrained crystal order 12 per lattice point	
		Coordinates referred to axes of unstrained crystal					
No.	Symbol	1st Subset	2d Subset	3d Subset	4th Subset	No.	Symbol
221	Pm3m	$\pm(x,y,z)\pm(y,x,z)$ $\pm(y,z,x)\pm(z,y,x)$ $\pm(z,x,y)\pm(x,z,y)$	$\pm(x,\bar{z},y)\pm(z,\bar{x},\bar{y})$ $\pm(z,\bar{y},\bar{x})\pm(y,\bar{z},x)$ $\pm(y,x,\bar{z})\pm(x,y,\bar{z})$	$\pm(x,\bar{y},\bar{z})\pm(y,\bar{x},z)$ $\pm(y,z,\bar{x})\pm(z,y,\bar{x})$ $\pm(z,\bar{x},y)\pm(x,\bar{z},\bar{y})$	$\pm(x,z,\bar{y})\pm(z,x,\bar{y})$ $\pm(z,\bar{y},x)\pm(y,\bar{z},\bar{x})$ $\pm(y,\bar{x},\bar{z})\pm(x,\bar{y},z)$	166	R$\bar{3}$m
222	Pn3n	$\pm(x,y,z)\pm(\frac{1}{2}+y,\frac{1}{2}+x,\frac{1}{2}+z)$ $\pm(y,z,x)\pm(\frac{1}{2}+z,\frac{1}{2}+y,\frac{1}{2}+x)$ $\pm(z,x,y)\pm(\frac{1}{2}+x,\frac{1}{2}+z,\frac{1}{2}+y)$	$\pm(x,\frac{1}{2}-z,y)\pm(z,\frac{1}{2}-x,\frac{1}{2}-y)$ $\pm(\frac{1}{2}+z,\bar{y},\bar{x})\pm(\frac{1}{2}+y,\bar{z},\frac{1}{2}+x)$ $\pm(y,x,\frac{1}{2}-z)\pm(\frac{1}{2}+x,\frac{1}{2}+y,\bar{z})$	$\pm(x,\frac{1}{2}-y,\frac{1}{2}-z)\pm(y,\frac{1}{2}-x,z)$ $\pm(\frac{1}{2}+y,\frac{1}{2}+z,\bar{x})\pm(z,y,\frac{1}{2}-x)$ $\pm(\frac{1}{2}+z,\bar{x},\frac{1}{2}+y)\pm(\frac{1}{2}+x,\bar{z},\bar{y})$	$\pm(x,z,\frac{1}{2}-y)\pm(\frac{1}{2}+z,\frac{1}{2}+x,\bar{y})$ $\pm(z,\frac{1}{2}-y,x)\pm(y,\frac{1}{2}-z,\frac{1}{2}-x)$ $\pm(\frac{1}{2}+y,\bar{x},\bar{z})\pm(\frac{1}{2}+x,\bar{y},\frac{1}{2}+z)$	167	R$\bar{3}$c
223	Pm3n	$\pm(x,y,z)\pm(\frac{1}{2}+y,\frac{1}{2}+x,\frac{1}{2}+z)$ $\pm(y,z,x)\pm(\frac{1}{2}+z,\frac{1}{2}+y,\frac{1}{2}+x)$ $\pm(z,x,y)\pm(\frac{1}{2}+x,\frac{1}{2}+z,\frac{1}{2}+y)$	$\pm(\frac{1}{2}+x,\frac{1}{2}-z,\frac{1}{2}+y)\pm(z,\bar{x},\bar{y})$ $\pm(\frac{1}{2}+z,\frac{1}{2}-y,\frac{1}{2}-x)\pm(y,\bar{z},x)$ $\pm(\frac{1}{2}+y,\frac{1}{2}+x,\frac{1}{2}-z)\pm(x,y,\bar{z})$	$\pm(x,\bar{y},\bar{z})\pm(\frac{1}{2}+y,\frac{1}{2}-x,\frac{1}{2}+z)$ $\pm(y,z,\bar{x})\pm(\frac{1}{2}+z,\frac{1}{2}+y,\frac{1}{2}-x)$ $\pm(z,\bar{x},y)\pm(\frac{1}{2}+x,\frac{1}{2}-z,\frac{1}{2}-y)$	$\pm(\frac{1}{2}+x,\frac{1}{2}+z,\frac{1}{2}-y)\pm(z,x,\bar{y})$ $\pm(\frac{1}{2}+z,\frac{1}{2}-y,\frac{1}{2}+x)\pm(y,\bar{z},\bar{x})$ $\pm(\frac{1}{2}+y,\frac{1}{2}-x,\frac{1}{2}-z)\pm(x,\bar{y},z)$	167	R$\bar{3}$c
224	Pn3m	$\pm(x,y,z)\pm(y,x,z)$ $\pm(y,z,x)\pm(z,y,x)$ $\pm(z,x,y)\pm(x,z,y)$	$\pm(\frac{1}{2}+x,\bar{z},\frac{1}{2}+y)\pm(z,\frac{1}{2}-x,\frac{1}{2}-y)$ $\pm(z,\frac{1}{2}-y,\frac{1}{2}-x)\pm(\frac{1}{2}+y,\bar{z},\frac{1}{2}+x)$ $\pm(\frac{1}{2}+y,\frac{1}{2}+x,\bar{z})\pm(\frac{1}{2}+x,\frac{1}{2}+y,\bar{z})$	$\pm(x,\frac{1}{2}-y,\frac{1}{2}-z)\pm(\frac{1}{2}+y,\bar{x},\frac{1}{2}+z)$ $\pm(\frac{1}{2}+y,\frac{1}{2}+z,\bar{x})\pm(\frac{1}{2}+z,\frac{1}{2}+y,\bar{x})$ $\pm(\frac{1}{2}+z,\bar{x},\frac{1}{2}+y)\pm(x,\frac{1}{2}-z,\frac{1}{2}-y)$	$\pm(\frac{1}{2}+x,\frac{1}{2}+z,\bar{y})\pm(\frac{1}{2}+z,\frac{1}{2}+x,\bar{y})$ $\pm(\frac{1}{2}+z,\bar{y},\frac{1}{2}+x)\pm(y,\frac{1}{2}-z,\frac{1}{2}-x)$ $\pm(y,\frac{1}{2}-x,\frac{1}{2}-z)\pm(\frac{1}{2}+x,\bar{y},\frac{1}{2}+z)$	166	R3m
225	Fm3m	$\pm(x,y,z)\pm(y,x,z)$ $\pm(y,z,x)\pm(z,y,x)$ $\pm(z,x,y)\pm(x,z,y)$	$\pm(x,\bar{z},y)\pm(z,\bar{x},\bar{y})$ $\pm(z,\bar{y},\bar{x})\pm(y,\bar{z},x)$ $\pm(y,x,\bar{z})\pm(x,y,\bar{z})$	$\pm(x,\bar{y},\bar{z})\pm(y,\bar{x},z)$ $\pm(y,z,\bar{x})\pm(z,y,\bar{x})$ $\pm(z,\bar{x},y)\pm(x,\bar{z},\bar{y})$	$\pm(x,z,\bar{y})\pm(z,x,\bar{y})$ $\pm(z,\bar{y},x)\pm(y,\bar{z},\bar{x})$ $\pm(y,\bar{x},\bar{z})\pm(x,\bar{y},z)$	166	R3m
226	Fm3c	$\pm(x,y,z)\pm(y,x,\frac{1}{2}+z)$ $\pm(y,z,x)\pm(z,y,\frac{1}{2}+x)$ $\pm(z,x,y)\pm(x,z,\frac{1}{2}+y)$	$\pm(x,\bar{z},\frac{1}{2}+y)\pm(z,\bar{x},\bar{y})$ $\pm(z,\bar{y},\frac{1}{2}-x)\pm(y,\bar{z},x)$ $\pm(y,x,\frac{1}{2}-z)\pm(x,y,\bar{z})$	$\pm(x,\bar{y},\bar{z})\pm(y,\bar{x},\frac{1}{2}+z)$ $\pm(y,z,\bar{x})\pm(z,y,\frac{1}{2}-x)$ $\pm(z,\bar{x},y)\pm(x,\bar{z},\frac{1}{2}-y)$	$\pm(x,z,\frac{1}{2}-y)\pm(z,x,\bar{y})$ $\pm(z,\bar{y},\frac{1}{2}+x)\pm(y,\bar{z},\bar{x})$ $\pm(y,\bar{x},\frac{1}{2}-z)\pm(x,\bar{y},z)$	167	R3c
227	Fd3m	$\pm(x,y,z)\pm(y,x,z)$ $\pm(y,z,x)\pm(z,y,x)$ $\pm(z,x,y)\pm(x,z,y)$	$\pm(\frac{3}{4}+x,\bar{z},\frac{3}{4}+y)\pm(z,\frac{1}{4}-x,\frac{1}{4}-y)$ $\pm(z,\frac{1}{4}-y,\frac{1}{4}-x)\pm(\frac{3}{4}+y,\bar{z},\frac{3}{4}+x)$ $\pm(\frac{3}{4}+y,\frac{3}{4}+x,\bar{z})\pm(\frac{3}{4}+x,\frac{3}{4}+y,\bar{z})$	$\pm(x,\frac{1}{4}-y,\frac{1}{4}-z)\pm(\frac{3}{4}+y,\bar{x},\frac{3}{4}+z)$ $\pm(\frac{3}{4}+y,\frac{3}{4}+z,\bar{x})\pm(\frac{3}{4}+z,\frac{3}{4}+y,\bar{x})$ $\pm(\frac{3}{4}+z,\bar{x},\frac{3}{4}+y)\pm(x,\frac{1}{4}-z,\frac{1}{4}-y)$	$\pm(\frac{3}{4}+x,\frac{3}{4}+z,\bar{y})\pm(\frac{3}{4}+z,\frac{3}{4}+x,\bar{y})$ $\pm(\frac{3}{4}+z,\bar{y},\frac{3}{4}+x)\pm(y,\frac{1}{4}-z,\frac{1}{4}-x)$ $\pm(y,\frac{1}{4}-x,\frac{1}{4}-z)\pm(\frac{3}{4}+x,\bar{y},\frac{3}{4}+z)$	166	R3m
228	Fd3c	$\pm(x,y,z)\pm(y,x,\frac{1}{2}+z)$ $\pm(y,z,x)\pm(z,y,\frac{1}{2}+x)$ $\pm(z,x,y)\pm(x,z,\frac{1}{2}+y)$	$\pm(\frac{1}{4}+x,\bar{z},\frac{3}{4}+y)\pm(z,\frac{1}{4}-x,\frac{1}{4}-y)$ $\pm(z,\frac{1}{4}-y,\frac{3}{4}-x)\pm(\frac{3}{4}+y,\bar{z},\frac{3}{4}+x)$ $\pm(\frac{3}{4}+y,\frac{1}{4}+x,\bar{z})\pm(\frac{3}{4}+x,\frac{3}{4}+y,\bar{z})$	$\pm(x,\frac{1}{4}-y,\frac{1}{4}-z)\pm(\frac{1}{4}+y,\bar{x},\frac{3}{4}+z)$ $\pm(\frac{3}{4}+y,\frac{3}{4}+z,\bar{x})\pm(\frac{3}{4}+z,\frac{1}{4}+y,\bar{x})$ $\pm(\frac{3}{4}+z,\bar{x},\frac{3}{4}+y)\pm(x,\frac{1}{4}-z,\frac{3}{4}-y)$	$\pm(\frac{3}{4}+x,\frac{1}{4}+z,\bar{y})\pm(\frac{3}{4}+z,\frac{3}{4}+x,\bar{y})$ $\pm(\frac{1}{4}+z,\bar{y},\frac{3}{4}+x)\pm(y,\frac{1}{4}-z,\frac{1}{4}-x)$ $\pm(y,\frac{1}{4}-x,\frac{3}{4}-z)\pm(\frac{3}{4}+x,\bar{y},\frac{3}{4}+z)$	167	R3c
229	Im3m	$\pm(x,y,z)\pm(y,x,z)$ $\pm(y,z,x)\pm(z,y,x)$ $\pm(z,x,y)\pm(x,z,y)$	$\pm(x,\bar{z},y)\pm(z,\bar{x},\bar{y})$ $\pm(z,\bar{y},\bar{x})\pm(y,\bar{z},x)$ $\pm(y,x,\bar{z})\pm(x,y,\bar{z})$	$\pm(x,\bar{y},\bar{z})\pm(y,\bar{x},z)$ $\pm(y,z,\bar{x})\pm(z,y,\bar{x})$ $\pm(z,\bar{x},y)\pm(x,\bar{z},\bar{y})$	$\pm(x,z,\bar{y})\pm(z,x,\bar{y})$ $\pm(z,\bar{y},x)\pm(y,\bar{z},\bar{x})$ $\pm(y,\bar{x},\bar{z})\pm(x,\bar{y},z)$	166	R3m
230	Ia3d	$\pm(x,y,z)\pm(\frac{1}{4}+y,\frac{1}{4}+x,\frac{1}{4}+z)$ $\pm(y,z,x)\pm(\frac{1}{4}+z,\frac{1}{4}+y,\frac{1}{4}+x)$ $\pm(z,x,y)\pm(\frac{1}{4}+x,\frac{1}{4}+z,\frac{1}{4}+y)$	$\pm(\frac{3}{4}+x,\frac{3}{4}-z,\frac{1}{4}+y)\pm(\frac{1}{2}+z,\frac{1}{2}-x,\bar{y})$ $\pm(\frac{3}{4}+z,\frac{1}{4}-y,\frac{3}{4}-x)\pm(y,\frac{1}{2}-z,\frac{1}{2}+x)$ $\pm(\frac{1}{4}+y,\frac{3}{4}+x,\frac{3}{4}-z)\pm(\frac{1}{2}+x,y,\frac{1}{2}-z)$	$\pm(\frac{1}{2}+x,\frac{1}{2}-y,\bar{z})\pm(\frac{3}{4}+y,\frac{3}{4}-x,\frac{1}{4}+z)$ $\pm(\frac{1}{2}+y,z,\frac{1}{2}-x)\pm(\frac{1}{4}+z,\frac{3}{4}+y,\frac{3}{4}-x)$ $\pm(z,\frac{1}{2}-x,\frac{1}{2}+y)\pm(\frac{3}{4}+x,\frac{1}{4}-z,\frac{3}{4}-y)$	$\pm(\frac{1}{4}+x,\frac{3}{4}+z,\frac{3}{4}-y)\pm(\frac{1}{2}+z,x,\frac{1}{2}-y)$ $\pm(\frac{3}{4}+z,\frac{3}{4}-y,\frac{1}{4}+x)\pm(\frac{1}{2}+y,\frac{1}{2}-z,\bar{x})$ $\pm(\frac{3}{4}+y,\frac{1}{4}-x,\frac{3}{4}-z)\pm(x,\frac{1}{2}-y,\frac{1}{2}+z)$	167	R$\bar{3}$c

TABLE 3. *Reduction from m3 to mmm*

Space group of unstrained crystal order 24 per lattice point		If stressed so that $x, y, z \parallel X, Y, Z$, any permutation			Space group of strained crystal order 8 per lattice point	
		Coordinates referred to axes of unstrained crystal				
No.	Symbol	1st Subset	2d Subset	3d Subset	No.	Symbol
200	Pm3	$\pm(x, y, z)$ $\pm(x, \bar{y}, \bar{z})$ $\pm(x, \bar{y}, z)$ $\pm(x, y, \bar{z})$	$\pm(y, z, x)$ $\pm(y, \bar{z}, \bar{x})$ $\pm(y, \bar{z}, x)$ $\pm(y, z, \bar{x})$	$\pm(z, x, y)$ $\pm(z, \bar{x}, \bar{y})$ $\pm(z, \bar{x}, y)$ $\pm(z, x, \bar{y})$	47	Pmmm
201	Pn3	$\pm(x, y, z)$ $\pm(x, \frac{1}{2}-y, \frac{1}{2}-z)$ $\pm(\frac{1}{2}+x, \bar{y}, \frac{1}{2}+z)$ $\pm(\frac{1}{2}+x, \frac{1}{2}+y, \bar{z})$	$\pm(y, z, x)$ $\pm(y, \frac{1}{2}-z, \frac{1}{2}-x)$ $\pm(\frac{1}{2}+y, \bar{z}, \frac{1}{2}+x)$ $\pm(\frac{1}{2}+y, \frac{1}{2}+z, \bar{x})$	$\pm(z, x, y)$ $\pm(z, \frac{1}{2}-x, \frac{1}{2}-y)$ $\pm(\frac{1}{2}+z, \bar{x}, \frac{1}{2}+y)$ $\pm(\frac{1}{2}+z, \frac{1}{2}+x, \bar{y})$	48	Pnnn
202	Fm3	$\pm(x, y, z)$ $\pm(x, \bar{y}, \bar{z})$ $\pm(x, \bar{y}, z)$ $\pm(x, y, \bar{z})$	$\pm(y, z, x)$ $\pm(y, \bar{z}, \bar{x})$ $\pm(y, \bar{z}, x)$ $\pm(y, z, \bar{x})$	$\pm(z, x, y)$ $\pm(z, \bar{x}, \bar{y})$ $\pm(z, \bar{x}, y)$ $\pm(z, x, \bar{y})$	69	Fmmm
203	Fd3	$\pm(x, y, z)$ $\pm(x, \frac{1}{4}-y, \frac{1}{4}-z)$ $\pm(\frac{3}{4}+x, \bar{y}, \frac{3}{4}+z)$ $\pm(\frac{3}{4}+x, \frac{3}{4}+y, \bar{z})$	$\pm(y, z, x)$ $\pm(y, \frac{1}{4}-z, \frac{1}{4}-x)$ $\pm(\frac{3}{4}+y, \bar{z}, \frac{3}{4}+x)$ $\pm(\frac{3}{4}+y, \frac{3}{4}+z, \bar{x})$	$\pm(z, x, y)$ $\pm(z, \frac{1}{4}-x, \frac{1}{4}-y)$ $\pm(\frac{3}{4}+z, \bar{x}, \frac{3}{4}+y)$ $\pm(\frac{3}{4}+z, \frac{3}{4}+x, \bar{y})$	70	Fddd
204	Im3	$\pm(x, y, z)$ $\pm(x, \bar{y}, \bar{z})$ $\pm(x, \bar{y}, z)$ $\pm(x, y, \bar{z})$	$\pm(y, z, x)$ $\pm(y, \bar{z}, \bar{x})$ $\pm(y, \bar{z}, x)$ $\pm(y, z, \bar{x})$	$\pm(z, x, y)$ $\pm(z, \bar{x}, \bar{y})$ $\pm(z, \bar{x}, y)$ $\pm(z, x, \bar{y})$	71	Immm
205	Pa3	$\pm(x, y, z)$ $\pm(\frac{1}{2}+x, \frac{1}{2}-y, \bar{z})$ $\pm(x, \frac{1}{2}-y, \frac{1}{2}+z)$ $\pm(\frac{1}{2}+x, y, \frac{1}{2}-z)$	$\pm(y, z, x)$ $\pm(\frac{1}{2}+y, \frac{1}{2}-z, \bar{x})$ $\pm(y, \frac{1}{2}-z, \frac{1}{2}+x)$ $\pm(\frac{1}{2}+y, z, \frac{1}{2}-x)$	$\pm(z, x, y)$ $\pm(\frac{1}{2}+z, \frac{1}{2}-x, \bar{y})$ $\pm(z, \frac{1}{2}-x, \frac{1}{2}+y)$ $\pm(\frac{1}{2}+z, x, \frac{1}{2}-y)$	61	Pbca
206	Ia3	$\pm(x, y, z)$ $\pm(x, \bar{y}, \frac{1}{2}-z)$ $\pm(\frac{1}{2}+x, \bar{y}, z)$ $\pm(x, \frac{1}{2}+y, \bar{z})$	$\pm(y, z, x)$ $\pm(y, \bar{z}, \frac{1}{2}-x)$ $\pm(\frac{1}{2}+y, \bar{z}, x)$ $\pm(y, \frac{1}{2}+z, \bar{x})$	$\pm(z, x, y)$ $\pm(z, \bar{x}, \frac{1}{2}-y)$ $\pm(\frac{1}{2}+z, \bar{x}, y)$ $\pm(z, \frac{1}{2}+x, \bar{y})$	73	Ibca

$z)$, $\pm(x, y, \bar{z})\}$ becomes the twofold stress-induced subset $\pm(x, y, 0)$ of a special position. Similarly, $\{\pm(x, \bar{y}, z), \pm(x, \bar{y}, \bar{z})\}$ becomes $(\pm x, \bar{y}, 0)$ so that the set of four special sites with Wyckoff symbol p in Cmmm split into two subsets of special sites.

This process of specialization can be applied to obtain the stress-induced splitting of any set of special positions in any space group. Three types of behavior occur separately or at the same time:

(1) Two or more of the subsets resulting from the set making up the general position may become indistinguishable when the position is specialized. This can lead to unequal splitting such as the splitting of a set of six sites composing a special position into subsets of two and four. Unequal splitting always results in fewer subsets than splitting of a general position. The extreme case of this behavior occurs when all of the subsets resulting from the set of sites in the general positions become indistinguishable when the position is specialized. Thus many special positions do not split into subsets even though general positions always split into subsets when the space group symmetry is lowered. For unequal splitting to result from a minimum step of symmetry lowering a three-fold axis must be lost; unequal splitting can result from a compound step if a four-fold axis is lost.

(2) Sites in the same subset may become identical in clusters of two or more each. The subset then composes a special position in the stressed crystal.

(3) The number of degrees of freedom in a subset may exceed that in the original set because of loss of relevance of the restriction relative to the remaining symmetry.

An example that illustrates all three of these types of behavior at once is provided by specializing the general position in space group $P\bar{3}m1$, to the special position with point symmetry m and considering the splitting of this set of sites making up this special position into subsets under a stress that reduces $P\bar{3}m1$ to C2/m. Under tensile stress along [110], the general position splits into three subsets $\{\pm(x, y, z),$

TABLE 4. *Reduction from m3 to* $\bar{3}$

Space group of unstrained crystal order 24 per lattice point		If stressed so that $X=Y$, $[111]\|\|Z$				Space group of strained crystal order 6 per lattice point	
		Coordinates referred to axes of unstrained crystal					
No.	Symbol	1st Subset	2d Subset	3d Subset	4th Subset	No.	Symbol
200	Pm3	$\pm(x, y, z)$ $\pm(y, z, x)$ $\pm(z, x, y)$	$\pm(x, \bar{y}, \bar{z})$ $\pm(y, z, \bar{x})$ $\pm(z, \bar{x}, y)$	$\pm(x, \bar{y}, z)$ $\pm(y, \bar{z}, \bar{x})$ $\pm(z, x, \bar{y})$	$\pm(x, y, \bar{z})$ $\pm(y, \bar{z}, x)$ $\pm(z, \bar{x}, \bar{y})$	148	$R\bar{3}$
201	Pn3	$\pm(x, y, z)$ $\pm(y, z, x)$ $\pm(z, x, y)$	$\pm(x, \frac{1}{2}-y, \frac{1}{2}-z)$ $\pm(\frac{1}{2}+y, \frac{1}{2}+z, \bar{x})$ $\pm(\frac{1}{2}+z, \bar{x}, \frac{1}{2}+y)$	$\pm(\frac{1}{2}+x, \bar{y}, \frac{1}{2}+z)$ $\pm(y, \frac{1}{2}-z, \frac{1}{2}-x)$ $\pm(\frac{1}{2}+z, \frac{1}{2}+x, \bar{y})$	$\pm(\frac{1}{2}+x, \frac{1}{2}+y, \bar{z})$ $\pm(\frac{1}{2}+y, \bar{z}, \frac{1}{2}+x)$ $\pm(z, \frac{1}{2}-x, \frac{1}{2}-y)$	148	$R\bar{3}$
202	Fm3	$\pm(x, y, z)$ $\pm(y, z, x)$ $\pm(z, x, y)$	$\pm(x, \bar{y}, \bar{z})$ $\pm(y, z, \bar{x})$ $\pm(z, \bar{x}, y)$	$\pm(x, \bar{y}, z)$ $\pm(y, \bar{z}, \bar{x})$ $\pm(z, x, \bar{y})$	$\pm(x, y, \bar{z})$ $\pm(y, \bar{z}, x)$ $\pm(z, \bar{x}, \bar{y})$	148	$R\bar{3}$
203	Fd3	$\pm(x, y, z)$ $\pm(y, z, x)$ $\pm(z, x, y)$	$\pm(x, \frac{1}{4}-y, \frac{1}{4}-z)$ $\pm(\frac{3}{4}+y, \frac{3}{4}+z, \bar{x})$ $\pm(\frac{3}{4}+z, \bar{x}, \frac{3}{4}+y)$	$\pm(\frac{3}{4}+x, \bar{y}, \frac{3}{4}+z)$ $\pm(y, \frac{1}{4}-z, \frac{1}{4}-x)$ $\pm(\frac{3}{4}+z, \frac{3}{4}+x, \bar{y})$	$\pm(\frac{3}{4}+x, \frac{3}{4}+y, \bar{z})$ $\pm(\frac{3}{4}+y, \bar{z}, \frac{3}{4}+x)$ $\pm(z, \frac{1}{4}-x, \frac{1}{4}-y)$	148	$R\bar{3}$
204	Im3	$\pm(x, y, z)$ $\pm(y, z, x)$ $\pm(z, x, y)$	$\pm(x, \bar{y}, \bar{z})$ $\pm(y, z, \bar{x})$ $\pm(z, \bar{x}, y)$	$\pm(x, \bar{y}, z)$ $\pm(y, \bar{z}, \bar{x})$ $\pm(z, x, \bar{y})$	$\pm(x, y, \bar{z})$ $\pm(y, \bar{z}, x)$ $\pm(z, \bar{x}, \bar{y})$	148	$R\bar{3}$
205	Pa3	$\pm(x, y, z)$ $\pm(y, z, x)$ $\pm(z, x, y)$	$\pm(\frac{1}{2}+x, \frac{1}{2}-y, \bar{z})$ $\pm(\frac{1}{2}+y, z, \frac{1}{2}-x)$ $\pm(z, \frac{1}{2}-x, \frac{1}{2}+y)$	$\pm(x, \frac{1}{2}-y, \frac{1}{2}+z)$ $\pm(\frac{1}{2}+y, \frac{1}{2}-z, \bar{x})$ $\pm(\frac{1}{2}+z, x, \frac{1}{2}-y)$	$\pm(\frac{1}{2}+x, y, \frac{1}{2}-z)$ $\pm(y, \frac{1}{2}-z, \frac{1}{2}+x)$ $\pm(\frac{1}{2}+z, \frac{1}{2}-x, \bar{y})$	148	$R\bar{3}$
206	Ia3	$\pm(x, y, z)$ $\pm(y, z, x)$ $\pm(z, x, y)$	$\pm(x, \bar{y}, \frac{1}{2}-z)$ $\pm(y, \frac{1}{2}+z, \bar{x})$ $\pm(\frac{1}{2}+z, \bar{x}, y)$	$\pm(\frac{1}{2}+x, \bar{y}, z)$ $\pm(y, \bar{z}, \frac{1}{2}-x)$ $\pm(z, \frac{1}{2}+x, \bar{y})$	$\pm(x, \frac{1}{2}+y, \bar{z})$ $\pm(\frac{1}{2}+y, \bar{z}, x)$ $\pm(z, \bar{x}, \frac{1}{2}-y)$	148	$R\bar{3}$

TABLE 5. *Reduction from 6/mmm to mmm*

Space group of unstrained crystal order 24 per lattice point		If stressed so that z and y $\|\|$ any two of X, Y, Z			Space group of strained crystal order 8 per lattice point	
		Coordinates referred to axes of unstrained crystal				
No.	Symbol	1st Subset	2d Subset	3d Subset	No.	Symbol
191	P6/mmm	$\pm(x, y, z)$ $\pm(x, y, \bar{z})$ $\pm(x, x-y, z)$ $\pm(x, x-y, \bar{z})$	$\pm(y, x, z)$ $\pm(y, x, \bar{z})$ $\pm(y, y-x, z)$ $\pm(y, y-x, \bar{z})$	$\pm(x-y, x, z)$ $\pm(x-y, x, \bar{z})$ $\pm(x-y, \bar{y}, z)$ $\pm(x-y, \bar{y}, \bar{z})$	65	Cmmm
192	P6/mcc	$\pm(x, y, z)$ $\pm(x, y, \bar{z})$ $\pm(x, x-y, \frac{1}{2}+z)$ $\pm(x, x-y, \frac{1}{2}-z)$	$\pm(y, x, \frac{1}{2}+z)$ $\pm(y, x, \frac{1}{2}-z)$ $\pm(y, y-x, z)$ $\pm(y, y-x, \bar{z})$	$\pm(x-y, x, z)$ $\pm(x-y, x, \bar{z})$ $\pm(x-y, \bar{y}, \frac{1}{2}+z)$ $\pm(x-y, \bar{y}, \frac{1}{2}-z)$	66	Cccm
193	$P6_3/mcm$	$\pm(x, y, z)$ $\pm(x, y, \frac{1}{2}-z)$ $\pm(x, x-y, \frac{1}{2}+z)$ $\pm(x, x-y, \bar{z})$	$\pm(y, x, z)$ $\pm(y, x, \frac{1}{2}-z)$ $\pm(y, y-x, \frac{1}{2}+z)$ $\pm(y, y-x, \bar{z})$	$\pm(x-y, x, \frac{1}{2}+z)$ $\pm(x-y, x, \bar{z})$ $\pm(x-y, \bar{y}, z)$ $\pm(x-y, \bar{y}, \frac{1}{2}-z)$	63	Cmcm
194	$P6_3/mmc$	$\pm(x, y, z)$ $\pm(x, y, \frac{1}{2}-z)$ $\pm(x, x-y, z)$ $\pm(x, x-y, \frac{1}{2}-z)$	$\pm(y, x, \frac{1}{2}+z)$ $\pm(y, x, \bar{z})$ $\pm(y, y-x, \frac{1}{2}+z)$ $\pm(y, y-x, \bar{z})$	$\pm(x-y, x, \frac{1}{2}+z)$ $\pm(x-y, x, \bar{z})$ $\pm(x-y, \bar{y}, \frac{1}{2}+z)$ $\pm(x-y, \bar{y}, \bar{z})$	63	Cmcm

TABLE 6. *Reduction from 4/mmm to mmm*

Space group of unstrained crystal order 16 per lattice point		If stressed so that $x, y, z \parallel X, Y, Z$, any permutation				Space group of strained crystal order 8 per lattice point			
		Coordinates referred to axes of unstrained crystal							
No.	Symbol	1st Subset		2d Subset		No.	Symbol		
123	P4/mmm	$\pm(x, y, z)$ $\pm(x, y, \bar{z})$	$\pm(x, \bar{y}, z)$ $\pm(x, \bar{y}, \bar{z})$	$\pm(y, x, z)$ $\pm(y, x, \bar{z})$	$\pm(y, \bar{x}, z)$ $\pm(y, \bar{x}, \bar{z})$	47	Pmmm	65	Cmmm
124	P4/mcc	$\pm(x, y, z)$ $\pm(x, y, \bar{z})$	$\pm(x, \bar{y}, \frac{1}{2}+z)$ $\pm(x, \bar{y}, \frac{1}{2}-z)$	$\pm(y, x, \frac{1}{2}+z)$ $\pm(y, x, \frac{1}{2}-z)$	$\pm(y, \bar{x}, z)$ $\pm(y, \bar{x}, \bar{z})$	49	Pccm	66	Cccm
125	P4/nbm	$\pm(x, y, z)$ $\pm(\frac{1}{2}+x, \frac{1}{2}+y, \bar{z})$	$\pm(\frac{1}{2}+x, \bar{y}, z)$ $\pm(x, \frac{1}{2}-y, \bar{z})$	$\pm(\frac{1}{2}+y, \frac{1}{2}+x, z)$ $\pm(y, x, \bar{z})$	$\pm(y, \frac{1}{2}-x, z)$ $\pm(\frac{1}{2}+y, \bar{x}, \bar{z})$	50	Pban	67	Cmma
126	P4/nnc	$\pm(x, y, z)$ $\pm(\frac{1}{2}+x, \frac{1}{2}+y, \bar{z})$	$\pm(\frac{1}{2}+x, \bar{y}, \frac{1}{2}+z)$ $\pm(x, \frac{1}{2}-y, \frac{1}{2}-z)$	$\pm(\frac{1}{2}+y, \frac{1}{2}+x, \frac{1}{2}+z)$ $\pm(y, x, \frac{1}{2}-z)$	$\pm(y, \frac{1}{2}-x, z)$ $\pm(\frac{1}{2}+y, \bar{x}, \bar{z})$	48	Pnnn	68	Ccca
127	P4/mbm	$\pm(x, y, z)$ $\pm(x, y, \bar{z})$	$\pm(\frac{1}{2}+x, \frac{1}{2}-y, z)$ $\pm(\frac{1}{2}+x, \frac{1}{2}-y, \bar{z})$	$\pm(\frac{1}{2}+y, \frac{1}{2}+x, z)$ $\pm(\frac{1}{2}+y, \frac{1}{2}+x, \bar{z})$	$\pm(y, \bar{x}, z)$ $\pm(y, \bar{x}, \bar{z})$	55	Pbam	65	Cmmm
128	P4/mnc	$\pm(x, y, z)$ $\pm(x, y, \bar{z})$	$\pm(\frac{1}{2}+x, \frac{1}{2}-y, \frac{1}{2}+z)$ $\pm(\frac{1}{2}+x, \frac{1}{2}-y, \frac{1}{2}-z)$	$\pm(\frac{1}{2}+y, \frac{1}{2}+x, \frac{1}{2}+z)$ $\pm(\frac{1}{2}+y, \frac{1}{2}+x, \frac{1}{2}-z)$	$\pm(y, \bar{x}, z)$ $\pm(y, \bar{x}, \bar{z})$	58	Pnnm	66	Cccm
129	P4/nmm	$\pm(x, y, z)$ $\pm(\frac{1}{2}+x, \frac{1}{2}+y, \bar{z})$	$\pm(x, \frac{1}{2}-y, z)$ $\pm(\frac{1}{2}+x, \bar{y}, \bar{z})$	$\pm(y, x, z)$ $\pm(\frac{1}{2}+y, \frac{1}{2}+x, \bar{z})$	$\pm(y, \frac{1}{2}-x, z)$ $\pm(\frac{1}{2}+y, \bar{x}, \bar{z})$	59	Pmmn	67	Cmma
130	P4/ncc	$\pm(x, y, z)$ $\pm(\frac{1}{2}+x, \frac{1}{2}+y, \bar{z})$	$\pm(x, \frac{1}{2}-y, \frac{1}{2}+z)$ $\pm(\frac{1}{2}+x, \bar{y}, \frac{1}{2}-z)$	$\pm(y, x, \frac{1}{2}+z)$ $\pm(\frac{1}{2}+y, \frac{1}{2}+x, \frac{1}{2}-z)$	$\pm(y, \frac{1}{2}-x, z)$ $\pm(\frac{1}{2}+y, \bar{x}, \bar{z})$	56	Pccn	68	Ccca
131	$P4_2/mmc$	$\pm(x, y, z)$ $\pm(x, y, \bar{z})$	$\pm(x, \bar{y}, z)$ $\pm(x, \bar{y}, \bar{z})$	$\pm(y, x, \frac{1}{2}+z)$ $\pm(y, x, \frac{1}{2}-z)$	$\pm(y, \bar{x}, \frac{1}{2}+z)$ $\pm(y, \bar{x}, \frac{1}{2}-z)$	47	Pmmm	66	Cccm
132	$P4_2/mcm$	$\pm(x, y, z)$ $\pm(x, y, \bar{z})$	$\pm(x, \bar{y}, \frac{1}{2}+z)$ $\pm(x, \bar{y}, \frac{1}{2}-z)$	$\pm(y, x, z)$ $\pm(y, x, \bar{z})$	$\pm(y, \bar{x}, \frac{1}{2}+z)$ $\pm(y, \bar{x}, \frac{1}{2}-z)$	49	Pccm	65	Cmmm
133	$P4_2/nbc$	$\pm(x, y, z)$ $\pm(\frac{1}{2}+x, \frac{1}{2}+y, \bar{z})$	$\pm(\frac{1}{2}+x, \bar{y}, z)$ $\pm(x, \frac{1}{2}-y, \bar{z})$	$\pm(\frac{1}{2}+y, \frac{1}{2}+x, \frac{1}{2}+z)$ $\pm(y, x, \frac{1}{2}-z)$	$\pm(y, \frac{1}{2}-x, \frac{1}{2}+z)$ $\pm(\frac{1}{2}+y, \bar{x}, \frac{1}{2}-z)$	50	Pban	68	Ccca
134	$P4_2/nnm$	$\pm(x, y, z)$ $\pm(\frac{1}{2}+x, \frac{1}{2}+y, \bar{z})$	$\pm(\frac{1}{2}+x, \bar{y}, \frac{1}{2}+z)$ $\pm(x, \frac{1}{2}-y, \frac{1}{2}-z)$	$\pm(\frac{1}{2}+y, \frac{1}{2}+x, z)$ $\pm(y, x, \bar{z})$	$\pm(y, \frac{1}{2}-x, \frac{1}{2}+z)$ $\pm(\frac{1}{2}+y, \bar{x}, \frac{1}{2}-z)$	48	Pnnn	67	Cmma
No.	Symbol	1st Subset	2d Subset	1st Subset	2d Subset			No.	Symbol
Space group of unstrained crystal order 16 per lattice point		Coordinates referred to axes of unstrained crystal						Space group of strained crystal order 8 per lattice point	
		If stressed so that $[1\bar{1}0]$, $[110]$, $z \parallel X, Y, Z$, any permutation							

(Continued on next page)

TABLE 6. *Reduction from 4/mmm to mmm*—Continued

Space group of unstrained crystal order 16 per lattice point		If stressed so that $x, y, z \parallel X, Y, Z$, any permutation				Space group of strained crystal order 8 per lattice point			
		Coordinates referred to axes of unstrained crystal							
No.	Symbol	1st Subset		2d Subset		No.	Symbol		
135	$P4_2/mbc$	$\pm(x, y, z)$ $\pm(x, y, \bar{z})$	$\pm(\frac{1}{2}+x, \frac{1}{2}-y, z)$ $\pm(\frac{1}{2}+x, \frac{1}{2}-y, \bar{z})$	$\pm(\frac{1}{2}+y, \frac{1}{2}+x, \frac{1}{2}+z)$ $\pm(\frac{1}{2}+y, \frac{1}{2}+x, \frac{1}{2}-z)$	$\pm(y, \bar{x}, \frac{1}{2}+z)$ $\pm(y, \bar{x}, \frac{1}{2}-z)$	55	Pbam	66	Ccem
136	$P4_2/mnm$	$\pm(x, y, z)$ $\pm(x, y, \bar{z})$	$\pm(\frac{1}{2}+x, \frac{1}{2}-y, \frac{1}{2}+z)$ $\pm(\frac{1}{2}+x, \frac{1}{2}-y, \frac{1}{2}-z)$	$\pm(y, x, z)$ $\pm(y, x, \bar{z})$	$\pm(\frac{1}{2}+y, \frac{1}{2}-x, \frac{1}{2}+z)$ $\pm(\frac{1}{2}+y, \frac{1}{2}-x, \frac{1}{2}-z)$	58	Pnnm	65	Cmmm
137	$P4_2/nmc$	$\pm(x, y, z)$ $\pm(\frac{1}{2}+x, \frac{1}{2}+y, \bar{z})$	$\pm(x, \frac{1}{2}-y, z)$ $\pm(\frac{1}{2}+x, \bar{y}, \bar{z})$	$\pm(y, x, \frac{1}{2}+z)$ $\pm(\frac{1}{2}+y, \frac{1}{2}+x, \frac{1}{2}-z)$	$\pm(y, \frac{1}{2}-x, \frac{1}{2}+z)$ $\pm(\frac{1}{2}+y, \bar{x}, \frac{1}{2}-z)$	59	Pmmn	68	Ccca
138	$P4_2/ncm$	$\pm(x, y, z)$ $\pm(\frac{1}{2}+x, \frac{1}{2}+y, \bar{z})$	$\pm(x, \frac{1}{2}-y, \frac{1}{2}+z)$ $\pm(\frac{1}{2}+x, \bar{y}, \frac{1}{2}-z)$	$\pm(y, x, z)$ $\pm(\frac{1}{2}+y, \frac{1}{2}+x, \bar{z})$	$\pm(y, \frac{1}{2}-x, \frac{1}{2}+z)$ $\pm(\frac{1}{2}+y, \bar{x}, \frac{1}{2}-z)$	56	Pccn	67	Cmma
139	$I4/mmm$	$\pm(x, y, z)$ $\pm(x, y, \bar{z})$	$\pm(x, \bar{y}, z)$ $\pm(x, \bar{y}, \bar{z})$	$\pm(y, x, z)$ $\pm(y, x, \bar{z})$	$\pm(y, \bar{x}, z)$ $\pm(y, \bar{x}, \bar{z})$	71	Immm	69	Fmmm
140	$I4/mcm$	$\pm(x, y, z)$ $\pm(x, y, \bar{z})$	$\pm(x, \bar{y}, \frac{1}{2}+z)$ $\pm(x, \bar{y}, \frac{1}{2}-z)$	$\pm(y, x, \frac{1}{2}+z)$ $\pm(y, x, \frac{1}{2}-z)$	$\pm(y, \bar{x}, z)$ $\pm(y, \bar{x}, \bar{z})$	72	Ibam	69	Fmmm
141	$I4_1/amd$	$\pm(x, y, z)$ $\pm(x, \frac{1}{2}+y, \bar{z})$	$\pm(x, \frac{1}{2}-y, z)$ $\pm(x, \bar{y}, \bar{z})$	$\pm(\frac{1}{4}+y, \frac{1}{4}+x, \frac{3}{4}+z)$ $\pm(\frac{1}{4}+y, \frac{3}{4}+x, \frac{1}{4}-z)$	$\pm(\frac{1}{4}+y, \frac{1}{4}-x, \frac{3}{4}+z)$ $\pm(\frac{1}{4}+y, \frac{3}{4}-x, \frac{1}{4}-z)$	74	Imma	70	Fddd
142	$I4_1/acd$	$\pm(x, y, z)$ $\pm(x, \frac{1}{2}+y, \bar{z})$	$\pm(x, \frac{1}{2}-y, \frac{1}{2}+z)$ $\pm(x, \bar{y}, \frac{1}{2}-z)$	$\pm(\frac{1}{4}+y, \frac{1}{4}+x, \frac{1}{4}+z)$ $\pm(\frac{1}{4}+y, \frac{3}{4}+x, \frac{3}{4}-z)$	$\pm(\frac{1}{4}+y, \frac{1}{4}-x, \frac{3}{4}+z)$ $\pm(\frac{1}{4}+y, \frac{3}{4}-x, \frac{1}{4}-z)$	73	Ibca	70	Fddd
No.	Symbol	1st Subset	2d Subset	1st Subset	2d Subset			No.	Symbol
Space group of unstrained crystal order 16 per lattice point		Coordinates referred to axes of unstrained crystal						Space group of strained crystal order 8 per lattice point	
		If stressed so that $[1\bar{1}0]$, $[110]$, $z \parallel X, Y, Z$, any permutation							

TABLE 7. *Reduction from 6/m to 2/m*

Space group of unstrained crystal order 12 per lattice point		If stressed so that $z \parallel X$, Y, or Z			Space group of strained crystal order 4 per lattice point	
		Coordinates referred to axes of unstrained crystal				
No.	Symbol	1st Subset	2d Subset	3d Subset	No.	Symbol
175	P6/m	$\pm(x, y, z)$ $\pm(x, y, \bar{z})$	$\pm(x-y, x, z)$ $\pm(x-y, x, \bar{z})$	$\pm(y, y-x, z)$ $\pm(y, y-x, \bar{z})$	10	P2/m
176	$P6_3/m$	$\pm(x, y, z)$ $\pm(x, y, \frac{1}{2}-z)$	$\pm(x-y, x, \frac{1}{2}+z)$ $\pm(x-y, x, \bar{z})$	$\pm(y, y-x, \frac{1}{2}+z)$ $\pm(y, y-x, \bar{z})$	11	$P2_1/m$

TABLE 8. *Reduction from $\bar{3}m$ to 2/m*

Space group of unstrained crystal order 12 per lattice point		If stressed so that	Coordinates referred to axes of unstrained crystal			Space group of strained crystal order 4 per lattice point	
No.	Symbol		1st Subset	2d Subset	3d Subset	No.	Symbol
162	$P\bar{3}1m$	$[1\bar{1}0] \parallel X$, Y, or Z	$\pm(x, y, z)$ $\pm(y, x, z)$	$\pm(x, x-y, \bar{z})$ $\pm(x-y, x, \bar{z})$	$\pm(y, y-x, \bar{z})$ $\pm(x-y, \bar{y}, z)$	12	C2/m
163	$P\bar{3}1c$	$[1\bar{1}0] \parallel X$, Y, or Z	$\pm(x, y, z)$ $\pm(y, x, \frac{1}{2}+z)$	$\pm(x, x-y, \frac{1}{2}-z)$ $\pm(x-y, x, \bar{z})$	$\pm(y, y-x, \bar{z})$ $\pm(x-y, \bar{y}, \frac{1}{2}+z)$	15	C2/c
164	$P\bar{3}m1$	$[110] \parallel X$, Y, or Z	$\pm(x, y, z)$ $\pm(y, x, \bar{z})$	$\pm(x, x-y, z)$ $\pm(x-y, x, \bar{z})$	$\pm(y, y-x, \bar{z})$ $\pm(x-y, \bar{y}, \bar{z})$	12	C2/m
165	$P\bar{3}c1$	$[110] \parallel X$, Y, or Z	$\pm(x, y, z)$ $\pm(y, x, \frac{1}{2}-z)$	$\pm(x, x-y, \frac{1}{2}+z)$ $\pm(x-y, x, \bar{z})$	$\pm(y, y-x, \bar{z})$ $\pm(x-y, \bar{y}, \frac{1}{2}-z)$	15	C2/c
166	$R\bar{3}m$ hex. axes	$[110] \parallel X$, Y, or Z	$\pm(x, y, z)$ $\pm(y, x, \bar{z})$	$\pm(x, x-y, z)$ $\pm(x-y, x, \bar{z})$	$\pm(y, y-x, \bar{z})$ $\pm(x-y, \bar{y}, \bar{z})$	12	C2/m
167	$R\bar{3}c$ hex. axes	$[110] \parallel X$, Y, or Z	$\pm(x, y, z)$ $\pm(y, x, \frac{1}{2}-z)$	$\pm(x, x-y, \frac{1}{2}+z)$ $\pm(x-y, x, \bar{z})$	$\pm(y, y-x, \bar{z})$ $\pm(x-y, \bar{y}, \frac{1}{2}-z)$	15	C2/c

TABLE 9. *Reduction from 4/m to 2/m*

Space group of unstrained crystal order 8 per lattice point		If stressed so that $z \parallel X$, Y, or Z		Space group of strained crystal order 4 per lattice point	
		Coordinates referred to axes of unstrained crystal			
No.	Symbol	1st Subset	2d Subset	No.	Symbol
83	P4/m	$\pm(x, y, z)$ $\pm(x, y, \bar{z})$	$\pm(y, \bar{x}, z)$ $\pm(y, \bar{x}, \bar{z})$	10	P2/m
84	$P4_2/m$	$\pm(x, y, z)$ $\pm(x, y, \bar{z})$	$\pm(y, \bar{x}, \frac{1}{2}+z)$ $\pm(y, \bar{x}, \frac{1}{2}-z)$	10	P2/m
85	P4/n	$\pm(x, y, z)$ $\pm(\frac{1}{2}+x, \frac{1}{2}+y, \bar{z})$	$\pm(y, \frac{1}{2}-x, z)$ $\pm(\frac{1}{2}+y, \bar{x}, \bar{z})$	13	P2/c
86	$P4_2/n$	$\pm(x, y, z)$ $\pm(\frac{1}{2}+x, \frac{1}{2}+y, \bar{z})$	$\pm(\frac{1}{2}+y, \bar{x}, \frac{1}{2}+z)$ $\pm(y, \frac{1}{2}-x, \frac{1}{2}-z)$	13	P2/c
87	I4/m	$\pm(x, y, z)$ $\pm(x, y, \bar{z})$	$\pm(y, \bar{x}, z)$ $\pm(y, \bar{x}, \bar{z})$	12	C2/m
88	$I4_1/a$	$\pm(x, y, z)$ $\pm(x, \frac{1}{2}+y, \bar{z})$	$\pm(\frac{1}{4}+y, \frac{1}{4}-x, \frac{1}{4}+z)$ $\pm(\frac{1}{4}+y, \frac{3}{4}-x, \frac{3}{4}-z)$	15	C2/c

TABLE 10. *Reduction from mmm to 2/m*

Space group of unstrained crystal order 8 per lattice point		If stressed so that $x \parallel X$, Y, or Z		Space group of strained crystal order 4 per lattice point		If stressed so that $y \parallel X$, Y, or Z		Space group of strained crystal order 4 per lattice point		If stressed so that $z \parallel X$, Y, or Z		Space group of strained crystal order 4 per lattice point	
		Coordinates referred to axes of unstrained crystal				Coordinates referred to axes of unstrained crystal				Coordinates referred to axes of unstrained crystal			
No.	Symbol	1st Subset	2d Subset	No.	Symbol	1st Subset	2d Subset	No.	Symbol	1st Subset	2d Subset	No.	Symbol
47	Pmmm	$\pm(x, y, z)$ $\pm(x, \bar{y}, \bar{z})$	$\pm(x, y, \bar{z})$ $\pm(x, \bar{y}, z)$	10	P2/m	$\pm(x, y, z)$ $\pm(x, \bar{y}, z)$	$\pm(x, y, \bar{z})$ $\pm(x, \bar{y}, \bar{z})$	10	P2/m	$\pm(x, y, z)$ $\pm(x, y, \bar{z})$	$\pm(x, \bar{y}, \bar{z})$ $\pm(x, \bar{y}, z)$	10	P2/m
48	Pnnn	$\pm(x, y, z)$ $\pm(x, \frac{1}{2}-y, \frac{1}{2}-z)$	$\pm(\frac{1}{2}+x, \frac{1}{2}+y, \bar{z})$ $\pm(\frac{1}{2}+x, \bar{y}, \frac{1}{2}+z)$	13	P2/c	$\pm(x, y, z)$ $\pm(\frac{1}{2}+x, \bar{y}, \frac{1}{2}+z)$	$\pm(\frac{1}{2}+x, \frac{1}{2}+y, \bar{z})$ $\pm(x, \frac{1}{2}-y, \frac{1}{2}-z)$	13	P2/c	$\pm(x, y, z)$ $\pm(\frac{1}{2}+x, \frac{1}{2}+y, \bar{z})$	$\pm(x, \frac{1}{2}-y, \frac{1}{2}-z)$ $\pm(\frac{1}{2}+x, \bar{y}, \frac{1}{2}+z)$	13	P2/c
49	Pccm	$\pm(x, y, z)$ $\pm(x, \bar{y}, \frac{1}{2}-z)$	$\pm(x, y, \bar{z})$ $\pm(x, \bar{y}, \frac{1}{2}+z)$	13	P2/c	$\pm(x, y, z)$ $\pm(x, \bar{y}, \frac{1}{2}+z)$	$\pm(x, y, \bar{z})$ $\pm(x, \bar{y}, \frac{1}{2}-z)$	13	P2/c	$\pm(x, y, z)$ $\pm(x, y, \bar{z})$	$\pm(x, \bar{y}, \frac{1}{2}-z)$ $\pm(x, \bar{y}, \frac{1}{2}+z)$	10	P2/m
50	Pban	$\pm(x, y, z)$ $\pm(x, \frac{1}{2}-y, \bar{z})$	$\pm(\frac{1}{2}+x, \frac{1}{2}+y, \bar{z})$ $\pm(\frac{1}{2}+x, \bar{y}, z)$	13	P2/c	$\pm(x, y, z)$ $\pm(\frac{1}{2}+x, \bar{y}, z)$	$\pm(\frac{1}{2}+x, \frac{1}{2}+y, \bar{z})$ $\pm(x, \frac{1}{2}-y, \bar{z})$	13	P2/c	$\pm(x, y, z)$ $\pm(\frac{1}{2}+x, \frac{1}{2}+y, \bar{z})$	$\pm(x, \frac{1}{2}-y, \bar{z})$ $\pm(\frac{1}{2}+x, \bar{y}, z)$	13	P2/c
51	Pmma	$\pm(x, y, z)$ $\pm(\frac{1}{2}+x, \bar{y}, \bar{z})$	$\pm(\frac{1}{2}+x, y, \bar{z})$ $\pm(x, \bar{y}, z)$	11	P2₁/m	$\pm(x, y, z)$ $\pm(x, \bar{y}, z)$	$\pm(\frac{1}{2}+x, y, \bar{z})$ $\pm(\frac{1}{2}+x, \bar{y}, \bar{z})$	10	P2/m	$\pm(x, y, z)$ $\pm(\frac{1}{2}+x, y, \bar{z})$	$\pm(x, \bar{y}, \bar{z})$ $\pm(x, \bar{y}, z)$	13	P2/c
52	Pnna	$\pm(x, y, z)$ $\pm(x, \frac{1}{2}-y, \frac{1}{2}-z)$	$\pm(\frac{1}{2}+x, y, \bar{z})$ $\pm(\frac{1}{2}+x, \frac{1}{2}-y, \frac{1}{2}+z)$	13	P2/c	$\pm(x, y, z)$ $\pm(\frac{1}{2}+x, \frac{1}{2}-y, \frac{1}{2}+z)$	$\pm(\frac{1}{2}+x, y, \bar{z})$ $\pm(x, \frac{1}{2}-y, \frac{1}{2}-z)$	14	P2₁/c	$\pm(x, y, z)$ $\pm(\frac{1}{2}+x, y, \bar{z})$	$\pm(x, \frac{1}{2}-y, \frac{1}{2}-z)$ $\pm(\frac{1}{2}+x, \frac{1}{2}-y, \frac{1}{2}+z)$	13	P2/c
53	Pmna	$\pm(x, y, z)$ $\pm(x, \bar{y}, \bar{z})$	$\pm(\frac{1}{2}+x, y, \frac{1}{2}-z)$ $\pm(\frac{1}{2}+x, \bar{y}, \frac{1}{2}+z)$	10	P2/m	$\pm(x, y, z)$ $\pm(\frac{1}{2}+x, \bar{y}, \frac{1}{2}+z)$	$\pm(\frac{1}{2}+x, y, \frac{1}{2}-z)$ $\pm(x, \bar{y}, \bar{z})$	13	P2/c	$\pm(x, y, z)$ $\pm(\frac{1}{2}+x, y, \frac{1}{2}-z)$	$\pm(x, \bar{y}, \bar{z})$ $\pm(\frac{1}{2}+x, \bar{y}, \frac{1}{2}+z)$	14	P2₁/c
54	Pcca	$\pm(x, y, z)$ $\pm(\frac{1}{2}+x, \bar{y}, \frac{1}{2}-z)$	$\pm(\frac{1}{2}+x, y, \bar{z})$ $\pm(x, \bar{y}, \frac{1}{2}+z)$	14	P2₁/c	$\pm(x, y, z)$ $\pm(x, \bar{y}, \frac{1}{2}+z)$	$\pm(\frac{1}{2}+x, y, \bar{z})$ $\pm(\frac{1}{2}+x, \bar{y}, \frac{1}{2}-z)$	13	P2/c	$\pm(x, y, z)$ $\pm(\frac{1}{2}+x, y, \bar{z})$	$\pm(\frac{1}{2}+x, \bar{y}, \frac{1}{2}-z)$ $\pm(x, \bar{y}, \frac{1}{2}+z)$	13	P2/c
55	Pbam	$\pm(x, y, z)$ $\pm(\frac{1}{2}+x, \frac{1}{2}-y, \bar{z})$	$\pm(x, y, \bar{z})$ $\pm(\frac{1}{2}+x, \frac{1}{2}-y, z)$	14	P2₁/c	$\pm(x, y, z)$ $\pm(\frac{1}{2}+x, \frac{1}{2}-y, z)$	$\pm(x, y, \bar{z})$ $\pm(\frac{1}{2}+x, \frac{1}{2}-y, \bar{z})$	14	P2₁/c	$\pm(x, y, z)$ $\pm(x, y, \bar{z})$	$\pm(\frac{1}{2}+x, \frac{1}{2}-y, \bar{z})$ $\pm(\frac{1}{2}+x, \frac{1}{2}-y, z)$	10	P2/m
56	Pccn	$\pm(x, y, z)$ $\pm(\frac{1}{2}+x, \bar{y}, \frac{1}{2}-z)$	$\pm(\frac{1}{2}+x, \frac{1}{2}+y, \bar{z})$ $\pm(x, \frac{1}{2}-y, \frac{1}{2}+z)$	14	P2₁/c	$\pm(x, y, z)$ $\pm(x, \frac{1}{2}-y, \frac{1}{2}+z)$	$\pm(\frac{1}{2}+x, \frac{1}{2}+y, \bar{z})$ $\pm(\frac{1}{2}+x, \bar{y}, \frac{1}{2}-z)$	14	P2₁/c	$\pm(x, y, z)$ $\pm(\frac{1}{2}+x, \frac{1}{2}+y, \bar{z})$	$\pm(\frac{1}{2}+x, \bar{y}, \frac{1}{2}-z)$ $\pm(x, \frac{1}{2}-y, \frac{1}{2}+z)$	13	P2/c
57	Pbcm	$\pm(x, y, z)$ $\pm(x, \frac{1}{2}-y, \bar{z})$	$\pm(x, y, \frac{1}{2}-z)$ $\pm(x, \frac{1}{2}-y, \frac{1}{2}+z)$	13	P2/c	$\pm(x, y, z)$ $\pm(x, \frac{1}{2}-y, \frac{1}{2}+z)$	$\pm(x, y, \frac{1}{2}-z)$ $\pm(x, \frac{1}{2}-y, \bar{z})$	14	P2₁/c	$\pm(x, y, z)$ $\pm(x, y, \frac{1}{2}-z)$	$\pm(x, \frac{1}{2}-y, \bar{z})$ $\pm(x, \frac{1}{2}-y, \frac{1}{2}+z)$	11	P2₁/m
58	Pnnm	$\pm(x, y, z)$ $\pm(\frac{1}{2}+x, \frac{1}{2}-y, \frac{1}{2}-z)$	$\pm(x, y, \bar{z})$ $\pm(\frac{1}{2}+x, \frac{1}{2}-y, \frac{1}{2}+z)$	14	P2₁/c	$\pm(x, y, z)$ $\pm(\frac{1}{2}+x, \frac{1}{2}-y, \frac{1}{2}+z)$	$\pm(x, y, \bar{z})$ $\pm(\frac{1}{2}+x, \frac{1}{2}-y, \frac{1}{2}-z)$	14	P2₁/c	$\pm(x, y, z)$ $\pm(x, y, \bar{z})$	$\pm(\frac{1}{2}+x, \frac{1}{2}-y, \frac{1}{2}-z)$ $\pm(\frac{1}{2}+x, \frac{1}{2}-y, \frac{1}{2}+z)$	10	P2/m
59	Pmmn	$\pm(x, y, z)$ $\pm(\frac{1}{2}+x, \bar{y}, \bar{z})$	$\pm(\frac{1}{2}+x, \frac{1}{2}+y, \bar{z})$ $\pm(x, \frac{1}{2}-y, z)$	11	P2₁/m	$\pm(x, y, z)$ $\pm(x, \frac{1}{2}-y, z)$	$\pm(\frac{1}{2}+x, \frac{1}{2}+y, \bar{z})$ $\pm(\frac{1}{2}+x, \bar{y}, \bar{z})$	11	P2₁/m	$\pm(x, y, z)$ $\pm(\frac{1}{2}+x, \frac{1}{2}+y, \bar{z})$	$\pm(\frac{1}{2}+x, \bar{y}, \bar{z})$ $\pm(x, \frac{1}{2}-y, z)$	13	P2/c
60	Pbcn	$\pm(x, y, z)$ $\pm(\frac{1}{2}+x, \frac{1}{2}-y, \bar{z})$	$\pm(\frac{1}{2}+x, \frac{1}{2}+y, \frac{1}{2}-z)$ $\pm(x, \bar{y}, \frac{1}{2}+z)$	14	P2₁/c	$\pm(x, y, z)$ $\pm(x, \bar{y}, \frac{1}{2}+z)$	$\pm(\frac{1}{2}+x, \frac{1}{2}+y, \frac{1}{2}-z)$ $\pm(\frac{1}{2}+x, \frac{1}{2}-y, \bar{z})$	13	P2/c	$\pm(x, y, z)$ $\pm(\frac{1}{2}+x, \frac{1}{2}+y, \frac{1}{2}-z)$	$\pm(\frac{1}{2}+x, \frac{1}{2}-y, \bar{z})$ $\pm(x, \bar{y}, \frac{1}{2}+z)$	14	P2₁/c

61	Pbca	$\pm(x, y, z)$ $\pm(\frac{1}{2}+x, \frac{1}{2}-y, \bar{z})$	$\pm(\frac{1}{2}+x, y, \frac{1}{2}-z)$ $\pm(x, \frac{1}{2}-y, \frac{1}{2}+z)$	14	$P2_1/c$	$\pm(x, y, z)$ $\pm(x, \frac{1}{2}-y, \frac{1}{2}+z)$	$\pm(\frac{1}{2}+x, y, \frac{1}{2}-z)$ $\pm(\frac{1}{2}+x, \frac{1}{2}-y, \bar{z})$	14	$P2_1/c$	$\pm(x, y, z)$ $\pm(\frac{1}{2}+x, y, \frac{1}{2}-z)$	$\pm(\frac{1}{2}+x, \frac{1}{2}-y, \bar{z})$ $\pm(x, \frac{1}{2}-y, \frac{1}{2}+z)$	14	$P2_1/c$
62	Pnma	$\pm(x, y, z)$ $\pm(\frac{1}{2}+x, \frac{1}{2}-y, \frac{1}{2}-z)$	$\pm(\frac{1}{2}+x, y, \frac{1}{2}-z)$ $\pm(x, \frac{1}{2}-y, z)$	14	$P2_1/c$	$\pm(x, y, z)$ $\pm(x, \frac{1}{2}-y, z)$	$\pm(\frac{1}{2}+x, y, \frac{1}{2}-z)$ $\pm(\frac{1}{2}+x, \frac{1}{2}-y, \frac{1}{2}-z)$	11	$P2_1/m$	$\pm(x, y, z)$ $\pm(\frac{1}{2}+x, y, \frac{1}{2}-z)$	$\pm(\frac{1}{2}+x, \frac{1}{2}-y, \frac{1}{2}-z)$ $\pm(x, \frac{1}{2}-y, z)$	14	$P2_1/c$
63	Cmcm	$\pm(x, y, z)$ $\pm(x, \bar{y}, \bar{z})$	$\pm(x, y, \frac{1}{2}-z)$ $\pm(x, \bar{y}, \frac{1}{2}+z)$	12	C2/m	$\pm(x, y, z)$ $\pm(x, \bar{y}, \frac{1}{2}+z)$	$\pm(x, y, \frac{1}{2}-z)$ $\pm(x, \bar{y}, \bar{z})$	15	C2/c	$\pm(x, y, z)$ $\pm(x, y, \frac{1}{2}-z)$	$\pm(x, \bar{y}, \bar{z})$ $\pm(x, \bar{y}, \frac{1}{2}+z)$	11	$P2_1/m$
64	Cmca	$\pm(x, y, z)$ $\pm(x, \bar{y}, \bar{z})$	$\pm(x, \frac{1}{2}+y, \frac{1}{2}-z)$ $\pm(x, \frac{1}{2}-y, \frac{1}{2}+z)$	12	C2/m	$\pm(x, y, z)$ $\pm(x, \frac{1}{2}-y, \frac{1}{2}+z)$	$\pm(x, \frac{1}{2}+y, \frac{1}{2}-z)$ $\pm(x, \bar{y}, \bar{z})$	15	C2/c	$\pm(x, y, z)$ $\pm(x, \frac{1}{2}+y, \frac{1}{2}-z)$	$\pm(x, \bar{y}, \bar{z})$ $\pm(x, \frac{1}{2}-y, \frac{1}{2}+z)$	14	$P2_1/c$
65	Cmmm	$\pm(x, y, z)$ $\pm(x, \bar{y}, \bar{z})$	$\pm(x, y, \bar{z})$ $\pm(x, \bar{y}, z)$	12	C2/m	$\pm(x, y, z)$ $\pm(x, \bar{y}, z)$	$\pm(x, y, \bar{z})$ $\pm(x, \bar{y}, \bar{z})$	12	C2/m	$\pm(x, y, z)$ $\pm(x, y, \bar{z})$	$\pm(x, \bar{y}, \bar{z})$ $\pm(x, \bar{y}, z)$	10	P2/m
66	Cccm	$\pm(x, y, z)$ $\pm(x, \bar{y}, \frac{1}{2}-z)$	$\pm(x, y, \bar{z})$ $\pm(x, \bar{y}, \frac{1}{2}+z)$	15	C2/c	$\pm(x, y, z)$ $\pm(x, \bar{y}, \frac{1}{2}+z)$	$\pm(x, y, \bar{z})$ $\pm(x, \bar{y}, \frac{1}{2}-z)$	15	C2/c	$\pm(x, y, z)$ $\pm(x, y, \bar{z})$	$\pm(x, \bar{y}, \frac{1}{2}-z)$ $\pm(x, \bar{y}, \frac{1}{2}+z)$	10	P2/m
67	Cmma	$\pm(x, y, z)$ $\pm(x, \bar{y}, \bar{z})$	$\pm(\frac{1}{2}+x, y, \bar{z})$ $\pm(\frac{1}{2}+x, \bar{y}, z)$	12	C2/m	$\pm(x, y, z)$ $\pm(\frac{1}{2}+x, \bar{y}, z)$	$\pm(\frac{1}{2}+x, y, \bar{z})$ $\pm(x, \bar{y}, \bar{z})$	12	C2/m	$\pm(x, y, z)$ $\pm(\frac{1}{2}+x, y, \bar{z})$	$\pm(x, \bar{y}, \bar{z})$ $\pm(\frac{1}{2}+x, \bar{y}, z)$	13	P2/c
68	Ccca	$\pm(x, y, z)$ $\pm(\frac{1}{2}+x, \bar{y}, \frac{1}{2}-z)$	$\pm(x, \frac{1}{2}+y, \bar{z})$ $\pm(\frac{1}{2}+x, \frac{1}{2}-y, \frac{1}{2}+z)$	15	C2/c	$\pm(x, y, z)$ $\pm(\frac{1}{2}+x, \frac{1}{2}-y, \frac{1}{2}+z)$	$\pm(x, \frac{1}{2}+y, \bar{z})$ $\pm(\frac{1}{2}+x, \bar{y}, \frac{1}{2}-z)$	15	C2/c	$\pm(x, y, z)$ $\pm(x, \frac{1}{2}+y, \bar{z})$	$\pm(\frac{1}{2}+x, \bar{y}, \frac{1}{2}-z)$ $\pm(\frac{1}{2}+x, \frac{1}{2}-y, \frac{1}{2}+z)$	13	P2/c
69	Fmmm	$\pm(x, y, z)$ $\pm(x, \bar{y}, \bar{z})$	$\pm(x, y, \bar{z})$ $\pm(x, \bar{y}, z)$	12	C2/m	$\pm(x, y, z)$ $\pm(x, \bar{y}, z)$	$\pm(x, y, \bar{z})$ $\pm(x, \bar{y}, \bar{z})$	12	C2/m	$\pm(x, y, z)$ $\pm(x, y, \bar{z})$	$\pm(x, \bar{y}, \bar{z})$ $\pm(x, \bar{y}, z)$	12	C2/m
70	Fddd	$\pm(x, y, z)$ $\pm(x, \frac{1}{4}-y, \frac{1}{4}-z)$	$\pm(\frac{1}{4}+x, \frac{1}{4}+y, \bar{z})$ $\pm(\frac{1}{4}+x, \bar{y}, \frac{1}{4}+z)$	15	C2/c	$\pm(x, y, z)$ $\pm(\frac{1}{4}+x, \bar{y}, \frac{1}{4}+z)$	$\pm(\frac{1}{4}+x, \frac{1}{4}+y, \bar{z})$ $\pm(x, \frac{1}{4}-y, \frac{1}{4}-z)$	15	C2/c	$\pm(x, y, z)$ $\pm(\frac{1}{4}+x, \frac{1}{4}+y, \bar{z})$	$\pm(x, \frac{1}{4}-y, \frac{1}{4}-z)$ $\pm(\frac{1}{4}+x, \bar{y}, \frac{1}{4}+z)$	15	C2/c
71	Immm	$\pm(x, y, z)$ $\pm(x, \bar{y}, \bar{z})$	$\pm(x, y, \bar{z})$ $\pm(x, \bar{y}, z)$	12	C2/m	$\pm(x, y, z)$ $\pm(x, \bar{y}, z)$	$\pm(x, y, \bar{z})$ $\pm(x, \bar{y}, \bar{z})$	12	C2/m	$\pm(x, y, z)$ $\pm(x, y, \bar{z})$	$\pm(x, \bar{y}, \bar{z})$ $\pm(x, \bar{y}, z)$	12	C2/m
72	Ibam	$\pm(x, y, z)$ $\pm(x, \bar{y}, \frac{1}{2}-z)$	$\pm(x, y, \bar{z})$ $\pm(x, \bar{y}, \frac{1}{2}+z)$	15	C2/c	$\pm(x, y, z)$ $\pm(x, \bar{y}, \frac{1}{2}+z)$	$\pm(x, y, \bar{z})$ $\pm(x, \bar{y}, \frac{1}{2}-z)$	15	C2/c	$\pm(x, y, z)$ $\pm(x, y, \bar{z})$	$\pm(x, \bar{y}, \frac{1}{2}-z)$ $\pm(x, \bar{y}, \frac{1}{2}+z)$	12	C2/m
73	Ibca	$\pm(x, y, z)$ $\pm(x, \bar{y}, \frac{1}{2}-z)$	$\pm(x, \frac{1}{2}+y, \bar{z})$ $\pm(\frac{1}{2}+x, \bar{y}, z)$	15	C2/c	$\pm(x, y, z)$ $\pm(\frac{1}{2}+x, \bar{y}, z)$	$\pm(x, \frac{1}{2}+y, \bar{z})$ $\pm(x, \bar{y}, \frac{1}{2}-z)$	15	C2/c	$\pm(x, y, z)$ $\pm(x, \frac{1}{2}+y, \bar{z})$	$\pm(x, \bar{y}, \frac{1}{2}-z)$ $\pm(\frac{1}{2}+x, \bar{y}, z)$	15	C2/c
74	Imma	$\pm(x, y, z)$ $\pm(x, \bar{y}, \bar{z})$	$\pm(x, \frac{1}{2}+y, \bar{z})$ $\pm(x, \frac{1}{2}-y, z)$	12	C2/m	$\pm(x, y, z)$ $\pm(x, \frac{1}{2}-y, z)$	$\pm(x, \frac{1}{2}+y, \bar{z})$ $\pm(x, \bar{y}, \bar{z})$	12	C2/m	$\pm(x, y, z)$ $\pm(x, \frac{1}{2}+y, \bar{z})$	$\pm(x, \bar{y}, \bar{z})$ $\pm(x, \frac{1}{2}-y, z)$	15	C2/c

TABLE 11. *Reduction from $\bar{3}$ to $\bar{1}$*

Space group of unstrained crystal order 6 per lattice point		No specialization of stress			Space group of strained crystal order 2 per lattice point	
		Coordinates referred to axes of unstrained crystal				
No.	Symbol	1st Subset	2d Subset	3d Subset	No.	Symbol
147	$P\bar{3}$	$\pm(x, y, z)$	$\pm(y, y-x, \bar{z})$	$\pm(x-y, x, \bar{z})$	2	$P\bar{1}$
148	$R\bar{3}$ hex. axes	$\pm(x, y, z)$	$\pm(y, y-x, \bar{z})$	$\pm(x-y, x, \bar{z})$	2	$P\bar{1}$

TABLE 12. *Reduction from 2/m to $\bar{1}$*

Space group of unstrained crystal order 4 per lattice point		No specialization of stress		Space group of strained crystal order 2 per lattice point	
		Coordinates referred to axes of unstrained crystal (2 || y)			
No.	Symbol	1st Subset	2d Subset	No.	Symbol
10	P2/m	$\pm(x, y, z)$	$\pm(x, \bar{y}, z)$	2	$P\bar{1}$
11	$P2_1/m$	$\pm(x, y, z)$	$\pm(x, \frac{1}{2}-y, z)$	2	$P\bar{1}$
12	C2/m	$\pm(x, y, z)$	$\pm(x, \bar{y}, z)$	2	$P\bar{1}$
13	P2/c	$\pm(x, y, z)$	$\pm(x, \bar{y}, \frac{1}{2}+z)$	2	$P\bar{1}$
14	$P2_1/c$	$\pm(x, y, z)$	$\pm(x, \frac{1}{2}-y, \frac{1}{2}+z)$	2	P.
15	C2/c	$\pm(x, y, z)$	$\pm(x, \bar{y}, \frac{1}{2}+z)$	2	$P\bar{1}$

TABLE 13. *Most general stress consistent with a reduction of a centrosymmetric point group to any one of its stress-induced subgroups (hexagonal axes used for trigonal groups)*

Initial group \ Subgroup	m3m	m3	6/mmm	6/m	4/mmm	4/m	$\bar{3}$m	$\bar{3}$	mmm	2/m	$\bar{1}$
m3m	$X=Y=Z$	...	...	...	$X=Y$, $z\|\|Z$	...	$X=Y$, $[111]\|\|Z$	...	$x, y, z\|\|X, Y, Z$ any permutation; or $[110], [1\bar{1}0], z\|\|X, Y, Z$ any permutation	$x\|\|X, Y,$ or Z; or $[110]\|\|X, Y,$ or Z	Any
m3		$X=Y=Z$	...	...	...	...	...	$X=Y$, $[111]\|\|Z$	$x, y, z\|\|X, Y, Z$ any permutation	$x\|\|X, Y,$ or Z	Any
6/mmm			$X=Y$, $z\|\|Z$	...	...	...	...	...	$z, y\|\|$any two of X, Y, Z	y, $[1\bar{1}0]$, or z $\|\|X, Y,$ or Z	Any
6/m				$X=Y$, $z\|\|Z$	...	...	...	...	...	$z\|\|X, Y,$ or Z	Any
4/mmm					$X=Y$, $z\|\|Z$	...	...	...	$x, y, z\|\|X, Y, Z$ any permutation; or $[110], [1\bar{1}0], z\|\|X, Y, Z$ any permutation	x, $[110]$, or z $\|\|X, Y,$ or Z	Any
4/m						$X=Y$, $z\|\|Z$	...	...	...	$z\|\|X, Y,$ or Z	Any
$\bar{3}$m							$X=Y$, $z\|\|Z$	...	...	For $\bar{3}$m1: $[110]\|\|X, Y,$ or Z; for $\bar{3}$1m: $[1\bar{1}0]\|\|X, Y,$ or Z	Any
$\bar{3}$								$X=Y$, $z\|\|Z$	...	...	Any
mmm									$x, y, z\|\|X, Y, Z$ any permutation	$x, y,$ or z $\|\|X, Y,$ or Z	Any
2/m(2||y)										$y\|\|X, Y,$ or Z	Any
$\bar{1}$											Any

Subgroups to the right of boundary indicated by dashed line are reached by compound steps.

$\pm(y, x, \bar{z})\}$, $\{\pm(x, x-y, z), \pm(x-y, x, \bar{z})\}$, and $\{\pm(y, y-x, \bar{z}), \pm(x-y, \bar{y}, \bar{z})\}$ as the tables show. The special position with point symmetry m in P3m1 is designated by Wyckoff symbol i in the International Tables and can be generated from the point (x, x, z). We then take $y=x$ throughout the three subsets and examine the resulting types of behavior. Type 1 is shown by subsets two and three because each site in one becomes identical to a site in the other. The resulting subset is $\{\pm(x, 2x, z), \pm(2x, x, z)\}$. Type 2 is shown by the first subset in which pairs of sites become identical resulting in the subset $\{\pm(x, \bar{x}, z)\}$. The two sites in this last subset lie on the mirror plane remaining in C2/m and so constitute a set of special positions in the stressed crystal. In contrast, the sites in the subset resulting from the original second and third subsets do not lie on any symmetry element of C2/m so the site $(x, 2x, z)$ should be written (x, y, z) because there is no longer any symmetry constraining y to equal $2x$ and the subset becomes $\{\pm(x, y, z), \pm(y, x, z)\}$ which composes a general position in C2/m. In this example of type 3 behavior, four of the sites of a special position with two degrees of freedom map onto the general position and so gain an additional degree of freedom. Mapping onto a general position occurs if and only if the number in a subset equals the order of the point group of the stressed crystal.

The authors are indebted to Dr. J. D. H. Donnay for having read this paper in manuscript and made several pertinent suggestions.

4. References

[1] B. S. Berry, Review of internal friction due to point defects, Acta. Met. **10**, 271 (1962).
[2] J. B. Wachtman, Jr., and H. S. Peiser, Symmetry conditions for internal friction caused by jumping of point defects in crystals, Appl. Phys. Letters **1**, 20 (1962).
[3] A. S. Nowick and W. R. Heller, Anelasticity and stress induced ordering of point defects in crystals, Adv. in Phys. (Phil. Mag. supplement) **12**, 251 (1963).
[4] J. B. Wachtman, Jr., H. S. Peiser, and E. P. Levine, Symmetry splitting of equivalent sites in oxide crystals and related mechanical effects, J. Res. NBS **67A**, 281 (1963).
[5] A. S. Nowick and W. R. Heller, Criteria for occurrence of internal friction due to point defects in crystals, Bull. Am. Phys. Soc. **8**, 236 (1963).
[6] H. S. Peiser, J. B. Wachtman, Jr., and R. W. Dickson, Reduction of space groups to subgroups by homogeneous strain, J. Res. NBS **67A**, 395 (1963).
[7] J. F. Nye, Physical properties of crystals, Oxford University Press (1957).
[8] A. D. Franklin, Relaxation modes for trapped crystal point defects, J. Res. NBS **67A**, 291 (1963).
[9] International Tables for X-ray Crystallography, Vol. I. Edited by N. F. M. Henry and K. Lonsdale, Kynoch Press (Birmingham, 1952).
[10] Internationale Tabellen zur Bestimmung von Kristallstrukturen, Erster Band, Gruppentheoretische Tafeln xii + 452 pp. Gebrueder Borntraeger, Berlin (1935), (Reprinted with corrigenda by Edwards Brothers. Inc., Ann Arbor, Mich., 1944.)

(Paper 69A2–340)

JOURNAL OF RESEARCH of the National Bureau of Standards—A. Physics and Chemistry
Vol. 69A, No. 2, March–April, 1965

Publications of the National Bureau of Standards*

Selected Abstracts

Construction of a Michelson interferometer for Fourier spectroscopy, H. N. Rundle, *J. Res. NBS* **69C** (*Engr. and Instr.*), *No. 1* (*Jan.–Mar. 1964*).
A brief outline is presented of the theory of the use of a double beam interferometer as applied to Fourier spectroscopy. A Michelson interferometer is described which is suitable for use in Fourier spectroscopy in the 1 to 10 micron region. The instrument can be used at any resolving power up to about 10^5.

The National Bureau of Standards gas thermometer II. Measurement of capacitance to a grounded surface with a transformer ratio-arm bridge, L. A. Guildner and R. E. Edsinger, *J. Res. NBS* **69C** (*Eng. and Instr.*), *No. 1* (*Jan.–Mar. 1964*).
A modification of the conventional transformer ratio-arm capacitance bridge was made to measure the values of three lead capacitors having one of the plates grounded. With this ground point it is necessary to use tri-axial cable with solid shields. A troublesome capacitance coupling between the primary and secondary shields of the transformer was neutralized by means which still enable one to attain the extremely high precision and accuracy characteristic of this type of bridge. The modified bridge was developed initially for highly accurate determinations of the locations of the grounded mercury menisci of the National Bureau of Standards precision manometer. Other applications are readily thought of and one interesting example is presented.

An adiabatic calorimeter for the range, 10 to 360 K., K. F. Sterrett, D. H. Blackburn, A. B. Bestul, S. S. Chang, and J. Horman, *J. Res. NBS* **69C** (*Eng. and Instr.*), *No. 1*, (*Jan.–Mar. 1965*).
A low-temperature adiabatic calorimeter and cryostat assembly is described for measuring heat capacities in the temperature range 10 to 360° K. A combination of dewar and tank system is used as refrigerant containers. The temperature of the adiabatic shield is automatically controlled to within a millidegree of that of the calorimeter vessel. This apparatus offers facilities for rapid cooling to about 55 °K and long term adiabatic control for conditioning of a sample and, thus, is especially suitable for measurements on glass, where long equilibration time is sometimes involved.
Data on the empty calorimeter vessel and on the Calorimetry Conference standard sample of synthetic sapphire are presented as a measure of the precision and the accuracy of the apparatus.

Effect of electron collisions on the formulas of magneto ionic theory, K. G. Budden, *Radio Sci. J. Res. NBS/USNC-URSI, Vol.* **69D,** *No. 2* (*Feb. 1965*).
In the standard simple treatment of magneto ionic theory the effect of collisions is allowed for by assuming that an electron experiences a retarding force proportional to its velocity, and the two complex refractive indices of an ionized medium are then given by the Appleton-Hartree formula. Experiments have shown, however, that the collision frequency is approximately proportional to the square of the electron's velocity, and proper allowance for this, using the Boltzmann equation, leads to a modification of the Appleton-Hartree formula which was given by Sen and Wyller. In this tutorial paper the same modified formula is derived, but by a different method which, it is hoped, can be followed by readers not intimately familiar with the previous literature. Some numerical results are presented in which the modified and unmodified formulae are compared. It is concluded that the standard Appleton-Hartree formula can be used without modification for nearly all radio propagation problems in the ionosphere, provided that the correct effective value of the collision frequency is used. The modifications may be important, however, in the theory of wave interaction and for waves of very low frequency whose wave normals are perpendicular to the earth's magnetic field.

Discussion of basic equations with source terms in compressive plasmas, Kun-Mu Chen, *Radio Sci. J. Res. NBS/USNC–URSI, Vol.* **69D,** *No. 2* (*Feb. 1965*).
It is shown that the same set of basic equations with source terms can and should be applied to both a compressive and an incompressive isotropic plasma. In a compressive plasma, an electric source can excite an electroacoustic wave. In an incompressive plasma, however, this electroacoustic wave reduces to an accumulation of charges shielding the electric source. The physical meaning of the dielectric constant of an incompressive plasma is discussed and the physical model of an incompressive plasma is re-examined.

The electrical properties of aluminum for cryogenic electromagnets, R. J. Corruccini, *NBS Tech. Note 218* (*Aug. 30, 1964*), *30 cents.*
The published data for the ideal resistivity and the magnetoresistivity of aluminum have been correlated. It is shown that both properties can be calculated for the limited ranges of temperature and purity that are of importance for aluminum cryogenic electromagnets from the residual resistivity ratio alone. Empirical functions are given for these properties, and sample calculations are given of the figure of merit for a particular aluminum solenoid relative to the same solenoid using water-cooled copper.

Demagnetizing factors for oblate spheroids used in ferrimagnetic resonance measurements, L. B. Schmidt, W. E. Case, and R. D. Harrington, *NBS Tech. Note 221* (*Sept. 4, 1964*), *20 cents.*
Demagnetizing factors for oblate spheroids magnetized along the short axis are given for aspect ratios from 25.0 to 35.0 in increments of 0.1, from 35.0 to 55.0 in increments of 0.2, from 55.0 to 80.0 in increments of 0.5, from 80.0 to 129.0 in increments of 1.0. The values of all demagnetizing factors given in the tables have been rounded off to 6 decimal places and are accurate to ± 5 units in the seventh place. The tables are presented in a form convenient for use in ferrimagnetic resonance measurements on disk shaped samples. A brief discussion of the effect of accuracy of demagnetizing factors on measurements of this type is included.

Survey of magnetic thin film materials, G. W. Reimherr, *NBS Tech. Note 247* (*Sept. 25, 1964*), *40 cents.*
This survey lists the materials reportedly made as a magnetic thin film, along with some of their properties and potential applications. Research activity using the less-frequently mentioned magnetic film materials is noted. About 200 references are cited.

Electronic energy bands in strontium titanate, A. H. Kahn and A. J. Leyendecker, *Phys. Rev.* **135,** *No. 5A, 1321–1225* (*Aug. 31, 1964*).
A theoretical examination of the electronic energy bands of cubic strontium titanate has been performed by application of the LCAO (linear combination of atomic orbitals) method. Diagonal energies were determined from ionization potentials

and crystalline fields based on a point charge model for the ions. The ionic charges were adjusted to give agreement with the observed energy gap. Overlap integrals were estimated from free ion wave functions. For the crystals studied, the calculations led to filled valence bands derived primarily from oxygen $2p$ orbitals and empty conduction bands derived predominantly from titanium $3d$ orbitals. In cubic strontium and barium titanates, there are six lowest conduction band ellipsoids lying along (100) directions of k-space with minima probably at the edges of the Brillouin zone. The longitudinal mass is about 20–50 m_o and the transverse mass about 1 m_o. Spin-orbit splitting removes degeneracy at $k=0$ and leads to additional conduction bands several hundredths of an ev above the lowest conduction band.
Comparison is made with experimental data on conductivity, Hall effect, thermoelectric power, reflectivity, and soft X-ray emission. Results are in substantial agreement with experiment.

Experiments on self-ionizing shock waves in a magnetic field, Y. Nakagawa and K. B. Earnshaw, *Book, Comptes Rendus de la VI^e Conference Internationale sur les Phenomenes D'Ionisation dans les Gaz, ed. P. Hubert and E. Cremieu-Alcan, IV, 303–309 (S.E.R.M.A., Paris, France, 1963).*
The structure of a self-ionizing shock wave in He of 50 μ Hg has been studied experimentally. The shock wave was produced by means of an electric discharge and part of the shock tube was placed in a transverse magnetic field. By varying the strength of this magnetic field, it was possible to study the variation of the structure of the shock as well as the state of ionization behind the shock in the range of Mach number from 40 to 99.5 and of Magnetic Mach number (shock velocity/Alfvén velocity 0.18 to 20. It was found that ionization behind the shock wave can be best explained in terms of streams of electrons and ions produced by the discharge.

Refractivities of the rare earth oxides, E. M. Levin, *(Proc. Third Rare Earth Research Conf., Apr. 2–24, 1963), Book, Rare Earth Research, Chapter on Magnetic and Optical Studies, pp. 339–350 (Gordon and Breach, Science Publ., Inc., New York, N.Y., May 1964).*
Index of refraction and density data obtained for a number of rare earth borates (ABO_3) and aluminates and gallates ($A_2B_2O_{12}$) permitted the calculation of the specific refractivities (by the Gladstone and Dale formula) of the rare earth sesquioxides. This was done using the additive rule between the products of the specific refractivities and the weight fractions of the constituent oxides. The specific refractivity values decreased with decreasing ionic radius of the cation, ranging from 0.148 for La_2O_3 to 0.107 for Dy_2O_3 to 0.090 for Lu_2O_3, and include the lowest values ever reported for oxides. Specific refractivities and molar refractivities (Lorentz-Lorenz formula) were calculated also from data on crystal fragments of the cubic rare earth oxides, obtained from two sources. Specific refractivities decreased from a value of 0.120 for Dy_2O_3 to 0.099 for Lu_2O_3, and were 10 to 13% higher than those calculated from the binary oxide compounds. Molar refractivities (Lorentz-Lorenz) of the pure oxides varied from 22.5 for Dy_2O_3 to 20.2 for Lu_2O_3 and were in good agreement with reported data.

Vibration-rotation bands of deuterium cyanide and hydrogen cyanide, A. G. Maki, E. K. Plyler, and R. Thibault, *J. Opt. Soc. Am.* **54,** *No. 7, 869–876 (July 1964).*
Six vibration-rotation bands of DCN between 2 and 6 microns have been analyzed. All the rotational constants have been obtained through the terms quadratic in vibrational quantum numbers. Two quadratic and seven cubic vibrational anharmonic constants have been obtained explicitly. Seven combinations of quadratic and cubic vibrational constants have also been obtained. Data are given on the analysis of the two parallel fundamental bands of $DC^{13}N$, as well as the ν_3 bands of DCN^{15}, $HC^{13}N$, and HCN^{15}. Δ-Δ transitions of both DCN and HCN in the ν_3 fundamental regions have been analyzed. The splitting of the Δ levels was clearly observed for the first time and is in agreement with the l-type resonance calculations. The line structure of the Q branches of both π-π and $\Delta\nu\Delta$ "hot bands" has also been resolved. By means of the Ritz principle the levels $2\nu_2^0$, $2\nu_2^2$, and ν_2^1 of DCN and $2\nu_2^2$ of HCN have been determined.

Ellipsometry in the measurement of surfaces and thin films, Symposium Proceedings Washington 1963, ed. E. Passaglia, R. R. Stromberg, and J. Kruger, *NBS Misc. Publ. 256 (Sept. 15, 1964), $2.25.*
A symposium on the Ellipsometer and its Use in the Measurement of Surfaces was held at the National Bureau of Standards in September 1963. This volume contains 19 of the papers included in the program, together with any discussions which followed oral presentation. Topics covered include historical review, theory, computational techniques, measurement techniques, and the use of ellipsometry in measuring metal surface oxide films and organic films.

Research on cyrstal growth and characterization at the National Bureau of Standards January to June 1964, ed. H. F. McMurdie, *NBS Tech. Note 251 (Oct. 19, 1964), 45 cents.*
The National Bureau of Standards with partial support from the Advanced Research Projects Agency of the Department of Defense is continuing a wide program of studies involving crystalline materials. These include investigation of methods and theory of growth, study of detection and effects of defects, determination of physical properties, refinement of chemical analysis, and determination of stability relations and atomic structure. The types of materials range from organic compounds, through metals, and inorganic salts to refractory oxides. This Technical Note, the fourth in the series, summarizes the progress of these various projects from January to June, 1964, and lists the related publications and participating scientists.

Procedures for precise determination of thermal radiation properties November 1962 to October 1963, J. C. Richmond, D. P. DeWitt, and W. D. Hayes, Jr., *NBS Tech. Note 252 (Nov. 20, 1964), 40 cents.*
The preliminary design of an intergrating-sphere reflectometer, utilizing a helium-neon continuous-wave gas laser as the source, for measuring the reflectance of specimens at high temperature, was completed. Development work on an ellipsoidal mirror reflectometer for measuring spectral reflectance in the wavelength range of 2 to 15 microns of specimens at room temperature was continued. The study of equations relating spectral emissivity of metals to other properties was continued. Platinum-13% rhodium and oxidized Inconel working standards of normal spectral emittance were calibrated over the wavelength range of 1 to 15 microns at temperatures of 800, 1100 and 1300 °K. Several modifications of the normal spectral emittance equipment were made to permit operation in the 15–35 micron range.

Franck-Condon factors for the ionization of CO, NO, and O_2, M. E. Wacks, *J. Chem Phys.* **41,** *No. 4, 930–936 (Aug. 1964).*
Calculated values of the vibrational overlap integrals for the following transitions are given:

a) $CO(X^1\Sigma^+, v''=0) \rightarrow CO^+(X^2\Sigma^+, v'=0\rightarrow 10)$; $(A^2\pi_i, v'=0\rightarrow 10)$; $(B^2\Sigma^+, v'=0\rightarrow 10)$.
b) $NO(X^2\pi, v''=0) \rightarrow NO^+(X^1\Sigma^+, v'=0\rightarrow 10)$; $(A^1\pi, v'=0\rightarrow 10)$.
c) $O^2(X^3\Sigma^-_g, v''=0,1) \rightarrow O_2^+(X^2\pi_g, v'=0\rightarrow 10)$; $(a^4\pi_u, v'=0\rightarrow 15)$; $(A^2\pi_u, v'=0\rightarrow 20)$; $(b^4\Sigma^-_g, v'=0\rightarrow 10)$.

These probabilities are used to construct theoretical ionization efficiency curves assuming an energy dependence for the electronic transition integral for both photoionization and ionization by electron impact. Previously published experimental data are discussed in terms of the theoretically calculated Franck-Condon probabilities.

Versatile Stark waveguide for microwave spectroscopy, D. R. Lide, Jr., *Rev. Sci. Instr.* **35,** *No. 9, 1226 (Sept. 1964).*
A simple waveguide design for Stark-modulation microwave spectrometers is described. The guide provides a homogeneous Stark field which is perpendicular to the microwave

electric field. The design has been used successfully in spectrometers operating at high frequencies, high temperatures, and for other special purposes.

Alkaline earth cation distributions in various borates, S. Block and G. J. Piermarini, *Phys. and Chem. of Glasses* **5,** *No. 5, 138–144 (Oct. 1964).*
X-ray scattering curves of two different strontium borate glasses have been measured and from these curves, electron radial distribution functions have been calculated. The resulting distribution curves are compared with earlier work on barium borate, barium borosilicate, and cadmium borate. The curves are found to be all strikingly similar which indicates a corresponding similarity in the short-range order of the heavy cations for each glass. An analysis of the distribution curves based on the random packing of hard spheres suggests that the heavy cations occupy characteristic positions in the overall glass structure. These positions are governed to a certain extent by crystal chemical restraints as is demonstrated by a correlation between distribution curves obtained both from the glass and corresponding polycrystalline material.

Microwave spectroscopy, D. R. Lide, Jr., *Ann. Rev. Phys. Chem.* **15,** *225–250 (1964).*
This article is a critical review of research in microwave spectroscopy of gasses during the past several years. The major topics covered are accurate structure determinations, structures of new or unusual molecules, internal rotation, vibrational information, high temperature spectroscopy, and instrumentation. A bibliography of the most important publications is included.

Growth spirals on $NiBr_2$ platelets, E. N. Sickafus and D. R. Winder, *J. Appl. Phys.* **35,** *No. 8, 2541–2545 (Aug. 1964).*
Platelets of $NiBr_2$ have been grown by sublimation in an atmosphere of water vapor and helium. Several crystal habits were observed including dendrites, platelets, and whiskers. Platelets and dendrites grow in the region of substrate temperatures greater than 500 °C and although these crystals are anhydrous the presence of water vapor greatly enhances the growth rate. The crystals are deliquescent. In the early stages of water adsorption the surface is not wetted but water droplets form at surface imperfections. The resultant decoration of surface morphology exhibits an anisotropy related to the surface structure. Photomicrographs are presented of concentric growth spirals occurring on the isolated faces of the same crystal platelet. These structures are demonstrated via direct observation of the opposite sides of the crystal, superposition of the opposite sides in thin regions of growth, and with the aid of Fizeau interferograms.

Infrared spectrum of CF_2, D. E. Milligan, D. E. Mann, and M. E. Jacox, *J. Chem. Phys.* **41,** *No. 5, 1199–1203 (Sept. 1, 1964).*
A low temperature infrared study of the photolysis products of CF_2N_2 in inert matrices has yielded the three vibrational fundamentals of the species CF_2, at 668, 1102, and 1222 cm^{-1}. Supplementary ultraviolet observations have confirmed the presence of CF_2 in high concentration. Detection of the stretching fundamentals of $C^{13}F_2$, present in natural abundance, has permitted an estimate of the FCF angle. The thermodynamic properties of CF_2 have also been estimated. CF_2 appears not to react with CO or with CO_2 in a matrix environment.

Change in the heat capacity of boron trioxide during the glass transformation, S. S. Chang and A. B. Bestul, *J. Phys. Chem.* **68,** *3082 (1964).*
A previous compilation showed that for B_2O_3 the change in heat capacity during the glass transformation, Δc_p, is only about one fifth of the "universal" value which applies to most glass-forming substances. A computational error has been found in the value for B_2O_3 in the above-mentioned compilation. The correct value of Δc_p for B_2O_3 is 2.65 cal. deg.$^{-1}$ per "bead", which agrees very well with Wunderlich's "universal" Δc_p value of 2.7 ± 0.5 cal. deg.$^{-1}$. Thus B_2O_3 in fact behaves like other glass-forming substances in this respect, rather than being exceptional.

The structure of the triclinic form of sodium tetrametaphosphate tetrahydrate, H. M. Ondik, *Acta Cryst.* **17,** *No. 9, 1139–1145 (Sept. 1964)*
The cell dimensions of triclinic sodium tetrametaphosphate tetrahydrate, $Na_4P_4O_{12}{\cdot}4H_2O$, are $a=6.652\pm0.001$, $b=9.579\pm0.002$, $c=6.320\pm0.001$Å, $\alpha=103°24'\pm1'$, $\beta=106°59'\pm1'$, $\gamma=93°17\pm1'$, space group $P\bar{1}$, $V=1$.
The structure was determined from a three-dimensional Patterson function, and refined by complete matrix least squares. The R value for 1335 observed non-zero reflections is 0.086.
The tetrametaphosphate ring is on the center of symmetry at the origin of the unit cell. One of the two crystallographically different Na ions is five-fold coordinated and the other is six-fold coordinated.
The five-fold coordinated Na ion links the rings along *c*, the six-fold coordinated ion links the rings along *a*. There are some similarities between the structures of the monoclinic and triclinic forms of this salt but the differences are too great to permit a transition between the two forms in the solid state. Such a transition, reported by other workers, has not been confirmed by this investigator.

Standards of electromotive force, W. J. Hamer, *J. Wash. Acad. Sci.* **54,** *297–315 (1964).*
The history of the unit of electromotive force (emf) as maintained in the United States is reviewed. The method by which the unit is maintained by standard cells is discussed. Characteristics of standard cells are briefly considered. Data on the units of emf, as maintained in various countries, are given for the international comparisons made since 1948. Brief discussions of voltage ranges, ac voltages, and zener diodes are included as they relate to emf standards.

Experimental transition probabilities for six oxygen multiplets, J. E. Solarski and W. L. Wiese, *Phys. Rev.* **135,** *No. 5A, A1236–A1241 (Aug. 31, 1964).*
The transition probabilities of six oxygen I multiplets in the visible and near infrared region have been measured in a wall stabilized high current arc operating either in pure oxygen or in a nitrogen-oxygen mixture. Temperatures were obtained from intensity measurements of an oxygen or nitrogen line of known transition probability and by applying the arc equilibrium and conservation equations. Several independent runs were carried out. The results agree usually within 20% with those of other experimental and theoretical methods.

Electrochemical calorimetry III. Thermal effects of nickel-cadmium batteries, W. H. Metzger, Jr., and J. M. Sherfey, *Electrochem. Technology* **2,** *No. 9–10, 285–289 (Sept.–Oct. 1964).*
This paper reports some interesting sidelights obtained while making calorimetric measurements during various charge-discharge cycles of nickel-cadmium cells proposed as satellite power sources by the National Aeronautics and Space Administration (NASA). Typical curves of heat changes as a function of time during operation are shown and discussed. The heat of reaction of oxygen with the constituents of the cell was measured and close agreement was obtained with the literature value for the heat of formation of cadmium oxide.

Electrochemical calorimetry. IV. Measurement of the Peltier heat and voltage attending the passage of current across a liquid junction, A. Brenner and S. L. Gray, *J. Electrochem. Soc.* **111,** *No. 11, 1225–1230 (Nov. 1964).*
The experiments involved the measurement of the temperature change resulting from the passage of current across the interface of two electrolytes. Measurements were made at various distances from the junction so as to yield a temperature profile of the effect. The total heat effect was calculated from the integrated area under the curve of temperature profile. The coefficient obtained by dividing the total heat effect in joules by the current in coulombs was reported as a voltage equivalent.
The following values were obtained for three systems of electrolytes and are probably correct to within about 7 mv:

0.04 *M* hydrochloric acid and 0.4 *M* hydrochloric acid, 30 mv. 0.90 *M* hydrochloric acid and 3.0 *M* potassium chloride, 80 mv. 1.15*M* hydrochloric acid and 1.21 *M* lithium chloride, 80 mv.

A hypothesis was advanced to relate the voltage equivalent of the heat effects to the diffusion liquid junction potentials and to the Peltier effect.

The National Bureau of Standards tritiated water standards, W. B. Mann, *J. Appl. Rad. and Isotopes* **15,** *628, Pergamon Press Ltd. (1964).*
This letter notes the very close agreement obtained by Euratom and the National Bureau of Standards in their calibration, by gas counting, of the National Bureau of Standards tritiated water standard.

Diffusion in a polymer with lamellar morphology, polyethylene, R. K. Eby, *J. Appl. Phys.* **35,** *No. 9, 2720–2724 (Sept. 1964).*
Data for the diffusion of ethane in polyethylene are presented together with the results of optical microscopy and x-ray diffraction for the same samples. These data support the hypothesis that diffusion in polymers with a lamellar morphology occurs in the lamellar boundaries and that, therefore, lamellar orientation is an important parameter. Lamellar thickness and perfection are also important.

Lasers for length measurement, A. G. McNish, *Science* **146,** *No. 3541, 177–182 (Oct. 1964).*
CW lasers will find extensive use in length measurement because of the high coherence and intensity of the light they produce.

Infrared spectrum and structure of gaseous Al_2O, M. J. Linevsky, D. White, and D. E. Mann, *J. Chem. Phys.* **41,** *No. 2, 542–545 (July 15, 1964).*
The infrared absorption spectrum of Al_2O trapped in solid argon and krypton matrices has been observed. It is possible from the observed spectra and isotope shifts for Al_2O^{16} and Al_2O^{18} to conclude that the molecular symmetry of Al_2O is C_{2v} and that the Al–O–Al angle is probably not far from 145°. Force constants and the bending frequency ν_2 have been calculated. Reanalysis of the ultraviolet spectra of exploding aluminum wires provides additional support both for the bent structure and for the calculated value of ν_2. The Al-O bond distance is estimated to be 1.66 A. The 3 fundamental frequencies for Al_2O^{16} in an argon matrix are (in cm^{-1}): ν_1=715, ν_2=[238]; ν_3=994.

High resolution infrared spectra of $C_2^{12}H_2$, $C^{12}C^{13}H_2$ and $C_2^{13}H_2$, W. J. Lafferty and R. J. Thibault, *J. Mol. Spectry.* **14,** *No. 1, 79–96 (Sept. 1964).*
Two parallel bands in Fermi resonance, ν_3 and $\nu_2+\nu_4{}^1+\nu_5{}^1$, have been studied in the 3200–3400 cm^{-1} region of $C_2{}^{12}H_2$. The calculated unperturbed frequencies for ν_3 and $\nu_2+\nu_4{}^1+\nu_5{}^1$ are 3288.66 cm^{-1} and 3288.11 cm^{-1}, respectively. The assignment of ν_3 to the higher frequency transition is confirmed by the study of this diad in $C^{13}C^{12}H_2$ and $C_2{}^{13}H_2$. In addition the absorption spectra of $C^{13}C^{12}$ $R_2$and $C_2{}^{13}H_2$ have been obtained in the 2600–2800 cm^{-1}, 3300–3400, and 6400–6600 cm^{-1} spectral regions. The unperturbed vibrational frequencies have been obtained for $C^{13}C^{12}H_2$, and a few of these frequencies have been calculated for $C_2{}^{13}H_2$. Equilibrium B values have been obtained for the isotopic carbon molecules, and these values have been used to calculate accurate r_e distances for acetylene. The "substitution structure" has also been calculated.

Rotation-vibration interaction and other corrections to the spin doublet separation in $^2\Pi$ diatomic molecules, T. C. James, *J. Chem. Phys.* **41,** *No. 3, 631–641 (Aug. 1, 1964).*
The effect of rotation-vibration interaction on the spin doublet separation in $^2\Pi$ states of diatomic molecules is treated. Almy and Horsfall's refinement of Hill and Van Vleck's treatment is questioned and an alternative approach making use of Dunham's treatment of $^1\Sigma$ diatomic molecules is used. The J dependence of the spin-orbit coupling constants is included in the discussion. Vibrational wave functions (including rotation-vibration interaction) and matrix elements are discussed. Additional corrections arising from the Λ doubling and from the spin-rotation interaction Γ $N{\cdot}S$ are briefly considered. A comparison of the results of this work with experimental spin doublet separation leads to better agreement between theory and experiment for the examples treated.

Other NBS Publications

J. Res. NBS 69B (Math. and Math. Phys.), No. 1 (Jan.–Mar. 1965), 75 cents.
Lectures on matroids. W. T. Tutte.
Menger's theorem for matroids. W. T. Tutte.
Single-element extensions of matroids. H. H. Crapo.
Minimum partition of a matroid into independent subsets. J. Edmonds.
Lehman's switching game and a theorem of Tutte and Nash-Williams. J. Edmonds.
Character subgroups of *F*-groups. M. I. Knopp and M. Newman.
A note on multipliers of difference sets. R. A. Brualdi.
Modification of Edmonds' maximum matching algorithm. C. Witzgall and C. T. Zahn, Jr.
On measurable sets and functions. A. J. Goldman.
Characteristic formulation for nonperiodic solutions of Mathieu's equation. T. Tamir and H. C. Wang.
On the surface duality of linear graphs. J. Edmonds.
Maximum matching and a polyhedron with 0,1-vertices. J. Edmonds.

J. Res. NBS 69C (Eng. and Instr.), No. 1 (Jan.–Mar. 1965), 75 cents.
Two picnometers of increased convenience and precision. A. Johnson.
Construction of a Michelson interferometer for Fourier spectroscopy. H. N. Rundle. (See above abstracts.)
The National Bureau of Standards gas thermometer II. Measurement of capacitance to a grounded surface with a transformer ratio-arm bridge. L. A. Guildner and R. E. Edsinger. (See above abstracts.)
An adiabatic calorimeter for the range, 10 to 360 °K. K. F. Sterrett, D. H. Blackburn, A. B. Bestul, S. S. Chang, and J. Horman. (See above abstracts.)
A rugged null-type pressure transducer of high reproducibility for accurate gas phase PVT measurements. M. Waxman and W. T. Chen.
Detection and damping of thermal-acoustic oscillations in low-temperature measurements. D. A. Ditmars and G. T. Furukawa.
NBS free-air chamber for measurement of 10 to 60 kV x rays. P. J. Lamperti and H. O. Wyckoff.
A compensated solenoid giving a uniform magnetic field over a large volume. C. Snow and R. L. Driscoll.
Evaluation of a microwave phase measurement system. D. A. Ellerbruch.
Polarographic analysis of titantium (IV)—EDTA complex: application to paint pigments. H. W. Berger and B. C. Cadoff.
Soil resistivity as related to underground corrosion and cathodic protection. W. J. Schwerdtfeger.

Radio Sci. J. Res. NBS/USNC–URSI, 69D, No. 2 (Feb. 1965). $1.00.
Electromagnetic wave penetration of reentry plasma sheaths. M. P. Bachynski.
On the use of refractive index diagrams for source-excited anisotropic regions. L. B. Felsen.
Surface waves along a perfectly conducting plane covered with semi-infinite magneto-plasma. S. Adachi and Y. Mushiake.
On the point of emergence of a microwave beam entering a linearly graded plasma. A. L. Cullen.
Self and mutual admittances of waveguides radiating into plasma layers. J. Galejs.
Effect of electron collisions on the formulas of magneto-ionic theory. K. G. Budden. (See above abstracts.)

Momentum transfer collisions in oxygen for thermal electrons. M. H. Mentzoni.
Experimental studies of perturbations in ionospheric plasma. L. H. Heisler.
Electromagnetic scattering by gyrotropic cylinders with axial magnetic fields. W. C. Y. Lee, L. Peters, Jr., and C. H. Walter.
Radar cross sections of plasma bodies at the plasma frequency. L. Peters, Jr.
Electroacoustic waves excited by a space vehicle in ionized atmosphere and its effect on radar return. K.-M. Chen.
Discussion on basic equations with source terms in compressive plasmas. K.-M. Chen. (See above abstracts.)
Scattering of electromagnetic and electroacoustic waves by a cylindrical object in a compressible plasma. J. R. Wait.
Multiphase periodic very-low-frequency emissions. N. Brice.
Radio studies of the high-latitude ionosphere during the solar eclipse of 20 July 1963. R. D. Hunsucker.
VLF and LF fields propagating near and into a rough sea. R. M. Lerner and J. Max.
Insulated and loaded loop antenna immersed in a conducting medium. R. H. Williams.
Capacitance of biconical antennas in magneto-ionic media; elliptic cone capacitance. V. P. Pyati and H. Weil.
Calculations of the bistatic scattering cross section of a sphere with an impedance boundary condition. J. R. Wait and C. M. Jackson.
Concept of differential reflectivity as applied to the reflection of beam-limited radiation by a convex body. A. Erteza, J. A. Doran, and D. H. Lenhert.

Radio Sci. J. Res. NBS/USNC–URSI, 69D, No. 3 (Mar. 1965), $1.00.

Propagation in nonuniform gyrotropic media. S. H. Gross and L. B. Felsen.
Geometrical optics for gyrotropic bodies. W. C. Y. Lee, L. Peters, Jr., and C. H. Walter.
Attenuation of hydromagnetic waves in the ionosphere. S.-I. Akasofu.
Self distortion of radio signals in the *D* region. L. R. Megill.
Atmospheric gravity waves: a new toy for the wave theorist. C. O. Hines.
Electromagnetic fluctuations in an equilibrium plasma. R. E. Burgess.
A generalized hydromagnetic wave in an inhomogeneous, cylindrical plasma. C. K. McLane and T. Tsukishima.
Angular dependence of the refractive index in the ionosphere. G. A. Deschamps.
Electrodynamics of moving anisotropic media: the first-order theory. C. T. Tai.
Study of the phenomenon of whistler echoes. T. Laaspere, W. C. Johnson, and J. F. Walkup.
Multiple-frequency investigations of radio wave absorption during the dawn-breakup phase of auroras. R. Parthasarathy, and F. T. Berkey.
Sferic excitation of a two-layer conducting medium. Martin B. Kraichman.
Currents, charges, and near fields of cylindrical antennas. R. W. P. King and T. T. Wu.
A note on the radiation conductance of an axial slot on a cylinder. C. M. Knop and C. T. Swift.
Analytical formulas for radio paths in spherically stratified ionospheres. E. Woyk (Chvojkova).

A complete mode sum for LF, VLF, ELF terrestrial radio wave fields, J. R. Johler and L. A. Berry, NBS Mono. 78 (Oct. 1, 1964), 20 cents.
A study of lunar surface radio communication, L. E. Vogler, NBS Mono. 85 (Sept. 14, 1964), 70 cents.
Standard Reference Materials: Preparation of NBS copper-base spectrochemical standards, R. E. Michaelis, L. L. Wyman, and R. Flitsch, NBS Misc. Publ. 260–2 (Oct. 15, 1964), 35 cents.
Quarterly radio noise data June, July, August, 1963, W. Q. Crichlow, R. T. Disney, and M. A. Jenkins, NBS Tech. Note 18–19 (Aug. 21, 1964), 50 cents.
Some modifications in methods of calibration of universal ratio sets, D. Ramaley, NBS Tech. Note 220 (Aug. 30, 1964), 25 cents.
Concerning the theory of radiation from a slotted conducting plane in a plasma environment, J. R. Wait, NBS Tech. Note 223 (Sept 28, 1964), 20 cents.
Bibliography on the measurement of bulk resistivity of semiconductor materials for electron devices, J. C. French, NBS Tech. Note 232 (Oct. 21, 1964), 60 cents.
A nomogram for computing $\frac{a+jb}{c+jd}$ and a nomogram for computing $\left|\frac{a+jb}{c+jd}\right|$, H. S. Bowman, NBS Tech. Note 250 (Oct. 2, 1964), 15 cents.
Standards and measurement of attenuation, impedance and phase shift, R. W. Beatty, Proc. URSI XIVth General Assembly, Tokyo, Japan, Sept. 1963, XIII, 80–92 (1964).
Vapour pressure, G. T. Armstrong, Encyclopaedic Dictionary of Physics **7,** 586–587 (Pergamon Press Inc., New York, N.Y., 1962).
Analysis of a differential phase shifter, D. A. Ellerbruch, IEEE Trans. Microwave Theory Tech. **MTT–12,** No. 4, 453–459 (July 1964).
Exterior corrosion of cast-iron pipe, M. Romanoff, J. Am. Water Works Assoc. **56,** No. 9, 1129–1143 (Sept. 1964).
The energy loss of electrons in solids, A. M. Rauth and J. A. Simpson, Radiation Res. **22,** No. 4, 643–661 (Aug. 1964).
Coherence theories of tropospheric radio propagation, J. R. Wait, IEEE Trans. Ant. Prop. **AP–12,** No. 5, 649–651 (Sept. 1964).
Solar activity, J. V. Lincoln, IQSY Instruction Manual. No. 2, Report of sudden ionospheric disturbances, Suppl., pp. 1–11 (IQSY Secretariat, London, England, 1963).
Comparison calibration of inductive voltage dividers, R. V. Lisle and T. L. Zapf, ISA Trans. **3,** No. 3, 238–242 (July 1964).
IQSY Instruction Manual. No. 1. World days, A. H. Shapley, 32 pages, IQSY Secretariat, London, England (July 1963).
Heater lead problem in calorimetry, D. C. Ginnings and E. D. West, Rev. Sci. Instr. **35,** No. 8, 965–967 (Aug. 1964).
Aspects of the National Bureau of Standards instrumentation literature reference file, J. F. Mayo-Wells (ISA 19th Annual Conf. and Exhibit, New York, N.Y., Oct. 12–15, 1964), ISA Preprint 20.6–5–64 (1964).
Influence of the refractive index profile in VHF reflection from a tropospheric layer, J. R. Wait and C. M. Jackson, IEEE Trans. Ant. Prop. **AP–12,** No. 4, 512–513 (July 1964).
Photometric observations of the airglow during the IQSY, F. E. Roach, IQSY Instruction Manual. No. 5: Airglow, Pt. I, 1–24 (IQSY Secretariat, London, England, 1963).
Correlation matrix for radio waves in the troposphere, E. C. Barrows (Proc. Symp. Electromagnetic Theory and Antennas, Copenhagen, 1962), Monograph, Electromagnetic Theory and Antennas 2, Sec. C, 743–746 (Macmillan and Co., Ltd., London, England, 1963).
Frequency and time broadcast services of the National Bureau of Standards, A. H. Morgan, Proc. ISA 17th Annual Automation Conf. and Exhibit, New York, N.Y., Oct. 15–18, 1962, Pt. I, Paper 1.1.62, 9 pages (1962).
Frostbite: signs, prevention, and treatment, J. R. Meyer-Arendt, Trail and Timberline, p. 3 (Jan. 1964).
Formation of an electron depleted region in the ionosphere by chemical releases, D. Golomb, N. W. Rosenberg, J. W. Wright, and R. A. Barnes (Proc. 4th Intern. Space Science Symp., Warsaw, June 4–10, 1963), Book, Space Research, ed. P. Muller, IV, 389–398 (North Holland Publ. Co., Amsterdam, The Netherlands, 1964).
The ionosphere, A. H. Shapley, U.S. Information Agency Voice of America Forum Series on Space Science, Lecture No. 7, 6 pages (1963).
Infrared spectroscopy of weak charge-transfer complexes, E. E. Ferguson, J. Chem. Phys. **61,** 257–262 (1964).
Quarterly radio noise data September, October, November 1963, W. Q. Crichlow, R. T. Disney, and M. A. Jenkins, NBS Tech. Note 18–20 (Oct. 23, 1964), 50 cents.
Calculation of sunrise and sunset times at ionospheric heights along a great circle path, A. H. Brady and D. D. Crombie, NBS Tech. Note 209 (Nov. 8, 1964), 20 cents.

A program for plotting circles of constant overpressure around targeted points, M. L. Joel and D. D. Lottridge, NBS Tech. Note 249 (Oct. 28, 1964), 40 cents.

Weights and measures—a challenge to industry, M. W. Jensen, Proc. 50th Mid-Year Meeting Chemical Specialties Manufacturers Assoc., Chicago, Ill., May 18–20, 1964, pp. 24–26 (Chem. Specialties Mfg. Assoc. Inc., New York, N.Y., 1964).

Interpretation of potentiometric titrations of weak acids in methanol-water solvents, K. C. Ong, R. A. Robinson, and R. G. Bates, Anal. Chem. **36,** 1971–1972 (Sept. 1964).

Fluctuations in ionospheric absorption events at conjugate stations, J. K. Hargreaves and H. J. A. Chivers, Nature **203,** No. 4948, 963–964 (Aug. 29, 1964).

RF and microwave power measurements, G. F. Engen, Proc. URSI XIVth General Assembly, Tokyo, Japan, Sept. 1963, XIII, 77–80 (1964).

LF–VLF frequency and time services of the National Bureau of Standards, D. H. Andrews (Proc. 19th Annual ISA Conf. and Exhibit, New York, N.Y., Oct. 12–15, 1964), ISA Preprint 21. 3–2–64 (1964).

Fresnel zone diffraction effects at 50 Gc/sec. determined from measured aperture field data, R. C. Baird, Program and Digest 1963 IEEE Prof. Group Ant. and Prop. Symp. Space Telecommunications, July 9–11, 1963, Boulder, Colo., pp. 171–173 (1963).

Computer interpretation of English text and picture patterns, R. A. Kirsch, IEEE Trans. Electron. Computers **EC–13,** No. 4, 363–376 (Aug. 1964).

On the implication of diurnal, seasonal and geographical variations in composition of high atmosphere from *F*-region measurements, J. W. Wright (Proc. NATO Advanced Study Institute, Sheikampen, Norway, Apr. 17–26, 1963), Book, Electron Density Distribution in the Ionosphere and Exosphere, pp. 186–198 (North Holland Publ. Co., Amsterdam, The Netherlands, 1964).

Ionospheric winds: motions into night and sporadic *E* correlations, N. W. Rosenberg, H. D. Edwards, and J. W. Wright (Proc. 4th Intern. Space Science Symp., Warsaw, June 4–10, 1963), Book, Space Research, ed. P. Muller, IV, 171–181 (North Holland Publ. Co., Amsterdam, The Netherlands, 1964).

Oblique incidence pulse measurement at 100 kc, R. H. Dougherty, AGARDograph 74, Propagation of Radio Waves at Frequencies below 300 KC, pp. 133–148 (Pergamon Press Inc., New York, N.Y., 1963).

Nonresonant absorption and collision diameters in the foreign-gas broadening of symmetric top molecules, G. Birnbaum and A. A. Maryott, J. Chem. Phys. **41,** No. 1, 154–157 (July 1, 1964).

Methods of calibration of airglow photometers at Fritz Peak Observatory, L. L. Smith and R. B. Alexander, IQSY Instruction Manual No. 5: Airglow, Pt. II, pp. 25–36 (IQSY Secretariat, London, England, 1963).

Electromagnetic cross sections for electron and nuclear research, H. W. Koch, Nucl. Instr. Methods **28,** 199–204 (1964).

Exclusion of parity unfavored transitions in forward scattering collisions, U. Fano, Phys. Rev. **135,** No. 3B, B863–B864 (Aug. 10, 1964).

Microscopic-astrophysics and the development of astrophysical-laboratories, R. N. Thomas, Bull. Centre Intern. d'Astrophysique de l'Observatoire de Nice, No. 1, pp. 7–16 (Nice, France, 1964).

Alouette ionic, magnetic-field and plasma studies, W. Calvert, H. Rishbeth, and T. E. VanZandt, IG Bull. No. 83, 16–19 (May 1964); Trans. AGU **45,** No. 2, 398–401 (June 1964).

Ozonation of asphalt flux, P. G. Campbell and J. R. Wright, I. E. C. Prod. Res. and Devel. **3,** 186–194 (Sept. 1964).

Propagation of radio waves past a coast line with a gradual change of surface impedance, J. R. Wait and K. P. Spies, IEEE Trans. Ant. Prop. **AP–12,** No. 5, 570–575 (Sept. 1964).

On the propagation of long wave-length terrestrial radio waves—two theoretical techniques, J. R. Johler and L. A. Berry, AGARDograph 74, Propagation of Radio Waves below 300 KC, pp. 101–129 (Pergamon Press Inc., New York, N.Y., 1963).

On the validity of the Einstein-Smoluchowski theory light scattering, R. Zwanzig, J. Am. Chem. Soc. **86,** 3489–3493 (Mar. 30, 1964).

Microwave propagation in an overdense bounded magneto-plasma, B. Wieder, Phys. Fluids **7,** 964–972 (July 1964).

Pulsed and CW sinusoidal voltage and current measurements, M. C. Selby, Proc. URSI XIVth General Assembly, Tokyo, Japan, Sept. 1963, XIII, 92–100 (1964).

Thermodynamic data compilation and review at the National Bureau of Standards, G. T. Armstrong, Svensk Kem. Tidskr. **76,** No. 8, 419–427 (1964).

Ionosonde studies of some chemical releases in the ionosphere, J. W. Wright (Proc. NATO Advanced Study Institute, Sheikampen, Norway, Apr. 17–26, 1963), Book, Electron Density Distribution in the Ionosphere and Exosphere, pp. 116–137 (North Holland Publ. Co., Amsterdam, The Netherlands, 1964).

Standard nuclear instrument modules, L. Costrell, U.S. Atomic Energy Commission TID Report 20893, 12 pages (July 1964).

Charge-transfer absorption spectra of NO in Kr and CH_3OH solutions, E. E. Ferguson and H. P. Broida, J. Chem. Phys. **40,** No. 12, 3715–3716 (June 15, 1964).

Ionospheric storms, S. Matsushita, Proc. URSI XIVth General Assembly, Tokyo, Japan, Sept. 1963, XIII, 169–180 (1964).

Symplectic modulary groups, M. Newman and J. R. Smart, Acta Arithmetica **IX,** 83–89 (1964).

Propagation of a reflected shock wave in a transverse magnetic field, Y. Boublil and K. B. Earnshaw, Phys. Fluids **7,** No. 6, 876–881 (June 1964).

Behavior of coaxial cable connectors for pulses with nanosecond risetimes, R. B. Schwartz and A. C. B. Richardson, Nuclear Instruments and Methods **29,** 83–88, North-Holland Publ. Co. (1964).

Theory of boil-off calorimetry, R. B. Jacobs, Rev. Sci. Instr. **35,** No. 7, 828–832 (July 1964).

"Thumbtack" accelerometer for the 1.5–150 kc range, P. Hertelendy and P. Reynard, Rev. Sci. Instr. **35,** No. 10, 1305–1306 (Oct. 1964).

The application of Archimedes' principle to determination of the apparent volume of leather, J. R. Kanagy, J. Am. Leather Chem. Assoc. **LIX,** No. 11, 636–649 (Nov. 1964).

On the twilight sodium emission—1: Observations from a southern hemisphere station, M. Gadsden, Ann. Geophys. **20,** No. 3, 261–272 (1964).

Spectra tristimulus values for the CIE (u, v, w) uniform spacing system, I. Nimeroff, J. Opt. Soc. Am. (Letter to Editor) **54,** No. 11, 1365–1367 (Nov. 1964).

Proton-transfer reactions between H_3^+ and saturated hydrocarbons, P. Ausloos and S. G. Lias, J. Chem. Phys. **40,** No. 12, 3599–3605 (June 15, 1964).

Resinography with 8-Å X-rays, S. B. Newman, Symp. on Resinographic Methods, ASTM Spec. Tech. Publ. No. 348, (1963).

Microwave spectrum of the SO radical, F. X. Powell and D. R. Lide, Jr., J. Chem. Phys. **41,** No. 5, 1413–1419 (Sept. 1964).

Resonances of a spherical void in a compressible isotropic plasma, J. R. Wait, J. Geophys. Res. **69,** No. 19, 4189–4191 (Oct. 1, 1964).

Evaluating computer systems analysis and design work in the Federal Government, W. H. Gammon, Book, Ideas for Management, Systems and Procedures 1964, 319–322 (1964).

Some remarks on microgrammars, W. C. Watt, Proc. Wash. Linguistics Club **2,** No. 1, 13–17, (Oct. 26, 1964).

Microwave and high-frequency calibration services of the National Bureau of Standards, W. E. Larson, IEEE Trans. Microwave Theory Tech. **M TT–12,** No. 4, 480–482 (July 1964).

Determination of the propagation constants for ultrasonic waves in melting and molten polyethylene, R. K. Eby, J. Acoust. Soc. Am. **36,** No. 8, 1485–1487 (Aug. 1964).

Radiation from sources immersed in compressible plasma media, J. R. Wait, Can. J. Phys. **42,** 1760–1780 (Sept. 1964).

Conductance of copper *m*-benedisulfonate hexahydrate in *N*-methylpropionamide from 20 to 40°, T. B. Hoover, J. Phys. Chem. **68,** No. 10, 3003–3008 (Oct. 1964).

Polarized electrons and positrons by tagging technique, H. Olsen and L. C. Maximon, Phys. Rev. Letters **13,** No. 3, 112–114 (July 20, 1964).

Theory of whisker growth and evaporation, J. A. Simmons, R. L. Parker, and R. E. Howard, J. Appl. Phys. **35,** No. 7, 2271–2272 (July 1964).

Mass spectrometric study of the production of methylamine from azomethane, M. E. Wacks, J. Phys. Chem. **68,** No. 9, 2725–2726 (Sept. 1964).

Gaussian correlation functions: Two-electron systems, W. A. Lester, Jr., J. Chem. Phys. **41,** No. 5, 1407–1413 (Sept. 1, 1964).

Nonspattering solder flux, W. R. Bjorklund, Rev. Sci. Instr. **35,** No. 10, 1369–1370 (Oct. 1964).

Use of the index of refraction as a means for study of plasma configurations, E. G. Johnson, Phys. Fluids **7,** 1551–1552 (Sept. 1964).

Application of the theory of absorbing Markov chains to the statistical thermodynamics of polymer chains in a lattice, J. Mazur, J. Chem. Phys. **41,** No. 8, 2256–2266 (Oct. 15, 1964).

A combinatorial problem and a simple decoding method for cyclic codes, M. Nesenbergs, IEEE Trans. Inform. Theory **IT-10,** 250–252 (July 1964).

Observed line shapes of collective excitations in Al, Be, and Ge, N. Swanson, J. Opt. Soc. Am. **54,** No. 9, 1130–1133 (Sept. 1964).

Flash-photolysis spectroscopy of matrices, L. J. Schoen and D. E. Mann, J. Chem. Phys. **41,** No. 5, 1514 (Sept. 1964).

**Publications for which a price is indicated are available by purchase from the Superintendent of Documents, U.S. Government Printing Office, Washington, D.C. 20402 (foreign postage, one-fourth additional). Reprints from outside journals and the NBS Journal of Research may often be obtained directly from the authors.*

UNIVERSITY MICROFILMS
313 NORTH FIRST STREET
ANN ARBOR, MICHIGAN
SJR-A-OCT

UNITED STATES
GOVERNMENT PRINTING
DIVISION OF PUBLIC DOCUMENTS
WASHINGTON, D.C. 20402

OFFICIAL BUSINESS

PENALTY FOR PRIVATE USE TO AVOID
PAYMENT OF POSTAGE, $300
(GPO)

JOURNAL OF RESEARCH of the National Bureau of Standards
A. Physics and Chemistry

Vol. 69A, No. 2 March–April 1965

Contents

Page

Radiolysis of $N^{15}N^{14}O$. R. Gorden, Jr., and P. Ausloos. 79

Oscillator strengths for lines of Ni I. Charles H. Corliss. 87

More wavelengths from thorium lamps. William F. Meggers and Robert W. Stanley. 109

Phase equilibria in the system vanadium oxide-niobium oxide. J. L. Waring and R. S. Roth. 119

Thermodynamics of the ternary system: water-glycine-potassium chloride at 25 °C from vapor pressure measurements. V. E. Bower and R. A. Robinson. 131

Heat of formation of aluminum fluoride by direct combination of the elements. Eugene S. Domalski and George T. Armstrong. 137

Relative enthalpy of polytetrafluoroethylene from 0 to 440 °C. Thomas B. Douglas and Ann W. Harman. 149

Anionic polymerization of isoprene at low concentrations of polyisoprenyllithium. Lewis J. Fetters. 159

One particle transitions and correlation in quantum mechanics. A. R. Ruffa. 167

Disaccommodation of magnetic spectra of two mangenese zinc ferrites. A. L. Rasmussen. 181

Splitting of a set of equivalent sites in centrosymmetric space groups into subsets under homogeneous stress. J. B. Wachtman, Jr., and H. S. Peiser. 193

Publications of the National Bureau of Standards. 209

Library of Congress Catalog Card Number: 62–37059

For sale by the Superintendent of Documents, U.S. Government Printing Office, Washington, D.C., 20402. Price 70 cents (single copy)
Subscription price: $4 a year; 75 cents additional for foreign mailing
UNITED STATES GOVERNMENT PRINTING OFFICE, WASHINGTON : 1965